中国气象科学研究院年报

ANNUAL REPORT OF CAMS

2016

中国气象科学研究院

Chinese Academy of Meteorological Sciences

中国气象科学研究院年报
ANNUAL REPORT OF CAMS

2016

中国气象科学研究院
Chinese Academy of Meteorological Sciences

目　　次

Contents

灾害天气
Severe Weather

灾害天气研究进展

1 灾害天气监测

1.1 华南云降水微物理结构观测和综合分析

在2016年华南暴雨外场试验期间，利用Ka波段云雷达、C波段连续波雷达和激光云高仪等设备，获取了华南云降水垂直结构综合数据；利用X波段相控阵天气雷达和X波段双线偏振雷达，获取了强对流三维结构数据，这些数据在云降水机理研究方面得到应用。分析了云雷达、C波段连续波雷达和激光云高仪探测能力，提出了3种数据的融合方法，形成了数据融合数据，利用这些数据分析和改进了华南夏季云降水的统计特征，包括云底和云底高度日变化、不同高度云发生频次变化、不同高度云和降水分类的回波强度概率分布等（图1）。（刘黎平，阮征，崔哲虎）

1.2 雷达成果的集成和业务应用

（1）与中国气象局数值预报中心等合作，研发了适应于雷达数据模式同化的新一代天气雷达质量控制软件系统，通过了中国气象局预报与网络司组织的评估。同时，研发了涵盖所有型号新一代天气雷达（包括上海WSR-88D双线偏振雷达）的质量控制软件系统，实现了全部的新一代天气雷达质量控制，为雷达数据同化提供技术支撑。(王红艳，刘黎平，李丰)

（2）建立风廓线雷达质控软件系统，在广州市气象局业务运行为短临预报提供支持，该系统在中国气象局气象探测中心业务试运行，提交中国气象局数值预报中心进行模式试验，并在中国气象科学研究院业务系统中运行，提供面向科研的支撑（图2）。（阮征，李丰）

（3）集成实验室多年的双线偏振雷达质量控制、降水估测、相态识别、短临预报等成果，研发了北京市气象局X波段双线偏振雷达数据处理和短临预报系统，实现了试运行。(刘黎平，胡志群，王红艳)

（4）与河南电力研究院合作，研发的新一代天气雷达飑线和对流系统识别软件系统成功应用于河南、浙江和新疆电力部门。（刘黎平，王红艳）

1.3 多种观测设备在多个科研项目上开展的外场试验

在"华南暴雨RDP外场试验"和"第3次青藏高原大气科学试验——边界层和对流层观测"项目中，云雷达、激光雷达、X波段相控阵天气雷达和C波段偏振雷达数据应用于云降水微物理和动力结构观测，形成了多种遥感手段反演高原和华南对流系统空气上升速度、云水/云冰/雨水/雪水的垂直廓线的反演方法。（刘黎平，胡志群）

2 青藏高原研究

2.1 青藏高原感热、潜热通量对湍流、对流结构的影响

基于第3次青藏高原大气科学试验11个站点的观测结果，分析了青藏高原和周边地区大气近地层

陆面参数和湍流特征。大涡模拟试验表明，青藏高原近地层感热、潜热通量可影响湍流和对流结构，也可显著影响对流云中液态水含量异常变化。数值模拟可揭示出青藏高原特殊的"爆米花"对流云特征可能的成因。（王寅钧，徐祥德）

2.2 基于高原试验获取的高原西部自动探空观测资料和"内插猜估"插值方案的新资料变分同化试验

基于高原试验获取的高原西部申扎、改则、狮泉河3站自动探空观测资料，设计了"内插猜估"探空观测资料的插值构造方案，并将"内插猜估"后得到的新探空数据同化到数值模式当中。数值试验中降水分析结果表明，将青藏高原西部有限探空观测数据以及经过"内插猜估"后的探空数据进行同化后，降水的TS评分均得到提高，其中"内插猜估"试验中，降水的TS评分提高更为明显。（张胜军，徐祥德）

2.3 青藏高原对流结构及其与下游暴雨过程的关联性

基于高原地区独特情况，建立了一个新的高原对流系统（TCS）提取方法，从而剔除了高原卷云和卷层云的影响。对TCS的季节变化特征进行了统计分析，发现各季节高原对流对青藏高原及其下游地区降水都具有重要贡献。通过暴雨过程及其前期水汽输送通量、涡度、散度三维结构综合相关分析，揭示了长江流域大范围持续暴雨发生、发展过程中青藏高原上游势–流函数场动力系统三维结构"强信号"特征。（胡亮，徐祥德）

2.4 青藏高原大气水分循环的势–流函数解析

基于青藏高原大地形热力、动力效应引起的绕流、爬流特征，采用大气运动场的流函数与势函数场，以更清晰地描述青藏高原热力驱动相关联的区域–全球多尺度环流特征。通过势函数风结构揭示出青藏高原大地形区域水汽流入、流出与辐散–辐合综合物理图像。另外，通过流函数场剖析大气环流动力结构特征，以凸显青藏高原热力驱动下的高层反气旋、低层气旋性耦合环流动力结构，并探讨此类高原特殊动力结构在大地形与大气环流系统、波流相互作用中的贡献，揭示高原热力、动力过程对东亚、全球大气水分循环的影响及其水汽交换输送多尺度源–汇结构（图3）。（徐祥德）

2.5 中国东部暴雨水汽输送结构综合相关模型

中国东部暴雨频数分布状态呈东南高频区向西北方向的大地形边缘带逐步递减，这与中国3阶梯大地形与梅雨边缘带走向一致，其也反映出东部暴雨频数分布与梅雨带季节性演变、水汽输送强弱及其与大地形动力、热力影响等因素存在某种相关关系。研究表明了中国东部整层水汽输送结构及其环流型特征与中国东部暴雨极端事件发生频数亦显著相关。（徐祥德）

2.6 三江源区大气的水汽来源、输送途径及其空间结构特征

夏季三江源区短时输送的水汽主要来自于青藏高原以及其西北侧陆地区域，而更长时间（8～10天）的来源可追踪到阿拉伯海和孟加拉湾等远距离海洋区域；水汽输送通道主要有2支，第1支为沿着索马里海到阿拉伯海的跨赤道水汽输送，第2支为在西风控制下从中亚乃至西亚地区向三江源区的输送（图4）。（陈斌）

2.7 青藏高原与太平洋/大西洋热力作用对北半球陆地夏季风年际变化的协同影响

青藏高原加热可以调整高原与太平洋之间的垂直环流，进而调节太平洋地区的凝结潜热加热和干绝热加热，导致该地区对流层中上层的温度异常，最终对夏季亚洲–太平洋涛动（APO）的年际变化产生重要影响。夏季亚洲季风区降水与北美中纬度降水存在显著负相关，形成洲际间的降水异常型，而与北美季风降水存在正相关，这种降水异常型与春夏季欧亚（包括青藏高原）和北美陆地加热及热

带中东太平洋海温的异常有密切联系。（刘舸，赵平，陈军明）

3 暴雨研究

3.1 华南季风降水试验进展

灾害天气国家重点实验室暴雨研究团队自2013年以来牵头推进世界气象组织（WMO）世界天气研究计划（WWRP）"华南季风降水试验"（SCMREX 2013—2018）研究发展项目，SCMREX旨在通过外场观测以及物理机制和对流可分辨模拟研究提高华南前汛期强降水预报水平。其实施内容含4个组成部分：外场观测，资料管理，强降水事件物理机制研究，以及包括资料同化影响、模式物理过程表达方案检验与改进、集合预报试验等对流可分辨数值试验。2016年利用比2013—2015年更多的先进设备开展了华南暴雨外场观测试验，加密观测期（IOP）从2017年5月1日连续运行至6月15日。已经收集了试验期间的业务观测网和移动设备观测资料，并纳入了SCMREX资料库。进行了SCMREX数据库和网站的维护和升级，并改进了SCMREX网站（http://scmrec.cma.gov.cn）。SCMREX网站上添加了往年加密观测期间主要强降水事件的文字描述以及雷达、卫星、闪电等图形，并且在机理研究、资料同化影响、模式云降水微物理过程参数化方案检验和改进、集合预报试验等各方面取得了新的进展。2016年10月SCMREX首席科学家罗亚丽研究员向WMO热带气象研究工作组汇报了最新进展，得到包括WMO季风委员会主席Chie-Pei Chang教授在内的工作组专家的高度肯定。暴雨团队牵头全面总结了SCMREX 2013—2015年的进展，形成的综述性论文发表在《美国气象学会通报》（BAMS）（罗亚丽）。

3.2 华南前汛期暴雨机理研究

暴雨研究团队利用SCMREX获取的最新综合性观测资料，研究发现华南前汛期沿海极端强降水是由长生命史的中尺度对流系统（MCS）产生的，这些MCS的维持时间、组织结构、准静止等特点与前汛期的环境大气热动力条件密切相关：这些MCS发生在盛行的低层西南气流中，即使没有低空急流也能输送足够的水汽，华南复杂的下垫面特征（如海陆对比、海岸线附近和内陆都分布着山脉）有利于持续的对流初生，MCS的一系列反馈作用（如，对流产生的冷出流边界处常常发生连续对流初生）。图5给出了如何基于雷达观测和地面中尺度分析来估计中尺度冷出流边界的厚度。分析了华南前汛期降水日变化特征，指出华南前汛期日变化存在3种传播模态：（i）发生在华南西部上午的东传或东南传降水日变化模态，这种模态主要与增强的低空西南急流及其造成的低空辐合有关；（ii）发生在午后华南东部与局地暖湿环境有关的准静止模态；（iii）发生在日间沿海向内陆传播的与海陆风有关的降水日变化模态，这种模态在季风爆发后更为显著（图5）。（罗亚丽，宝兴华，姜智娜）

3.3 我国极端小时降水研究

综合分析自动气象站雨量计观测、天气图、组合雷达反射率等资料，利用客观和人工判断相结合的天气背景识别方法，分析了从海南岛至东北地区的我国东部广大地区的极端小时降水的天气背景。小时降水（＞0.1 mm/h）的季节变化显示降水发生频次和强度具有复杂的区域特征，因此采用99.9百分位定义各个台站的极端小时降水的阈值。极端降水在华南沿海和华北平原最强，1981—2013年期间，77%的极端小时降水发生在夏季，峰值（30.4%）出现在7月。根据天气背景类型将2011—2015年大约5800个极端小时降水分为4种类型：低涡／切变型、弱天气尺度强迫型、地面锋面型、热带气旋型，它们分别占总频次的39.1%、39.0%、13.9%和8.0%，并且具有各自不同的区域分布及日变化和季节变化特征。热带气旋型在东南和华南沿海最为频繁，深入内陆锐减；地面锋面型在104°E以东分布比较均匀；低涡／切变线型在四川盆地有一个显著的高频中心，从这个中心朝着东南和东北方向伸展出2个高频带；弱天气尺度强迫型在东南、西南和华北以及东北的最东部地区发生比较频繁。中尺度对流

系统与更小尺度的系统对弱天气尺度强迫型的发生频次的贡献相当，但是二者发生频次较高的地点有所差异。（罗亚丽）

3.4　我国中东部地闪统计特征及其与降水的关系

利用我国6年地闪观测资料和TRMM观测资料，对我国中东部地区的地闪时空活动规律进行了统计研究，并对比分析了其与降水的关系。结果表明，地闪频次在夏季（冬季）最高（最低），且正地闪比例最低（最高）。华北地区夏季地闪频发，而冬季地闪多发生在长江流域。最大地闪活动中心位于广东中部地区，地闪密度达9次/（km²·a），珠江三角洲北部年平均闪电日达70天以上，其次是长江中下游地区和四川盆地及周边地区。在地形复杂的华北地区和四川盆地及周边地区，其西部的高山区雷暴日数大于东部平原（盆地）区，但地闪密度明显小于后者，这与高山地区频发的短时午后雷暴有关。地闪频次在8月最高，而对流性降水在5月或7月达到峰值。四川盆地及其周边山区暖季降水峰值出现在夜间，而除此以外的我国东部平原地区暖季降水日变化存在2个峰值，其中午后的峰值对应着地闪频次的峰值；而夜间到清晨的降水峰值对应的闪电活动较少，缘于此阶段层状降水比例增大。（夏茹娣）

3.5　海南岛降水时空分布规律

基于5年高分辨率地面和探空观测资料的统计分析和数值试验，开展海南岛降水时空分布规律原因探究，揭示了环境条件对降水时间分布规律的影响和环境风、地形和海风环流对降水空间分布的综合作用机理。结果表明，4—9月的高湿度和有效位能、低自由对流高度和弱垂直切变使该时期为海南岛的显著降水时期。弱环境风速、低地形和海风环流共同作用使得强降水容易在背风坡海岸生成，并在不同环境风向下产生不同传播特点。（梁钊明）

3.6　华南飑线精细结构分析

利用双多普勒风场反演技术，研究了2007年4月24日影响广东省的一次飑线的形成机理和三维结构，给出了此次飑线的三维结构概念模型。相对风暴的自后向前的干冷气流从层状云3 km的低层进入飑线；相对风暴的自前向后的气流从对流线中低层进入飑线内部，在7.5 km高度分成2支气流，一支流向前部，另一支则流向层状云区。（周海光）

4　台风研究

4.1　海温对热带气旋（TC）加强的影响

利用1988—2014年北大西洋热带气旋（TC）最佳路径资料及全球再分析资料研究发现，TC所处的海温不仅决定TC最大可能强度（MPI），还决定了TC最大可能加强速度（MPIR），海温和MPIR之间存在指数关系。研究发现，随着海温增加，TC的加强速度和MPIR也增大，当海温大于27 ℃时，MPIR随海温增加迅速增大。而且，TC的加强速度在高海温低垂直切变的区域会更大，这也说明虽然海温可以决定MPIR，但是实际的TC加强速度还受着环境因素的影响，比如环境垂直风切变。本项研究不仅提出了很好的台风加强研究思路，同时也为业务预报提供了较好的理论依据。（徐晶，王玉清）

4.2　西北太平洋高空冷涡（UTCL）对热带气旋（TC）活动的影响

利用中国气象局最佳路径资料与全球再分析格点数据，对2000—2012年西北太平洋热带气旋（TC）及其间高空冷涡（UTCL）的活动以及它们的相互关系进行统计分析。结果表明，346个TC中73%在其生命史存在UTCL活动，其中21%与UTCL中心相对距离小于15经/纬距，即二者可能发生相

互作用。进一步分析发现，该距离内 UTCL 对 TC 运动和强度变化均存在一定影响。与整个太平洋 TC 运动状况相比，尽管 UTCL 的存在从整体上并没有增加 TC 移向的突变比例，但对于特定方位角和相对距离，UTCL 对 TC 运动的影响是显著的，比如 5 经/纬距内 TC 易发生突然左折。UTCL 对强度变化的影响主要发生在 TC 的发生和初期发展时期，当二者进入相互作用距离，在 12 h 内约 45% 的 TC 强度增强，38% 维持，仅有 17% 强度减弱。增强 TC 主要位于 UTCL 的南侧，减弱主要位于其北侧。对于 TC 强度的迅速变化，迅速加强（RI）容易在 UTCL 东东南象限和南西南象限发生。TC 迅速减弱（RW）的样本则大多出现在 UTCL 的西侧（图 6）。（李英，魏娜，张大林）

5　雷电研究

5.1　青藏高原闪电活动与对流云结构的关系

基于自主研制的地基全天空云观测系统观测并分析了高原日喀则地区的云量、云状等分布特征，发现日喀则地区的云量和云状都呈现明显的季节分布。基于 TRMM 卫星降水特征（PFs）资料，分析了高原产生闪电的对流云和没有产生闪电的云结构特征及差异性。研究表明，产生闪电的 PFs 的面积比无闪电发生的 PFs 的面积要大一个量级。高原东北部（青海地区）产生闪电的 PFs 尺度普遍在 1400 km^{2}以上。高原东南部（中心 29° N、97° E 附近）产生闪电的 PFs 尺度最小，极小值在 500 km^{2}以下。高原上产生闪电的 PFs 的云高要比没有产生闪电的 PFs 的云高 2 ～ 4 km。高原上产生闪电的 PFs 的云顶高度在中南部最高，可到 12 km 以上，藏南附近区域最低，低于 10 km。高原产生闪电的 PFs 的 20 dBz 最大高度与分布于喜马拉雅山以南的平原相当但略小，而 40 dBz 的最大高度大于喜马拉雅山以南地区。产生闪电的 PFs 的平均闪电密度在高原的西部和东北部地区较大。（张义军，郑栋，吕伟涛，孟青，杨俊，姚雯，马颖，王飞）

5.2　特种观测资料同化及雷电灾害天气系统的监测预警方法

（1）利用水汽混合比与闪电频数、霰混合比的经验关系式，建立了 SAFIR3000 全闪辐射源资料与相对湿度的经验关系，并在 WRF-3DVar 同化系统中实现对全闪定位资料的连续循环同化。利用基于 WRF-Electric 模式搭建的雷电活动短时预报平台，连续开展 2 个汛期的雷电活动预报试验，并对试验结果进行初步检验。初步完成利用雷电临近预警系统与中尺度起放电模式相耦合实现 0 ～ 12 h 雷电预报方法的方案设计，以弥补原有仅靠外推算法时效性短的缺陷，进而提升雷电的预警预报效果（图 7）。（徐良韬，姚雯，张荣）

（2）对 10 次中尺度对流系统雷达和地闪数据的综合分析发现，层云地闪首次回击电流峰值通常要大于对流地闪首次回击的电流峰值。层云地闪一般在最大反射率核心（≥ 30 dBz）分布在 3 ～ 6 km 高度的区域边缘或者围绕该区域接地。这一区域的反射率特征与回波亮带特征具有一致性，表明亮带区域的电荷结构对层云闪电的激发或者传播可能具有重要影响。这一结果为研究亮带和层云地闪之间的关系提供了一个重要证据，也为层云地闪预警方法的研究提供了一条理论依据（图 8）。（王飞）

5.3　闪电初始阶段特征与雷暴结构的时空配置关系

进一步完善了低频电场变化探测阵列（LFEDA）的方法和技术，并在广东进行了闪电活动观测试验，获取了大量雷暴过程的闪电放电探测数据，初步完成了对 LFEDA 的性能评估。基于位于 LFEDA 站网内的人工触发闪电的评估表明其具有良好的探测性能，对触发闪电和回击的探测效率分别达到了 100% 和 95%，平均定位误差达到 102 m。将雷暴演变过程中 LFEDA 的三维总闪定位结果与雷达回波结合也表明 LFEDA 具有可靠的探测能力。此外，基于 LFEDA 数据分析了一次云闪个例和一次地闪个例先导过程的通道发展特征，获得了与通道发展的一些相关参量，这些分析表明 LFEDA 具有描述闪电三

维通道的能力。

研究分析了一次超级单体组合体过程的闪电起始特征。发现闪电起始位置主要被霰、干雪、小雹和冰晶4类粒子主导，对应的闪电起始占总闪电的比例分别为44.3%、44.1%、8.0%和3.0%。在南部超级单体发生龙卷的阶段，与霰粒子对应的闪电起始主导超级单体的主体区域以及它的右侧和前侧；与干雪对应的闪电起始主导前侧云砧、右侧云砧和后侧云砧的外围区域；与小雹对应的闪电起始则主要集中在上升气流区的周围，更偏向主上升气流区的前侧。高密度的闪电起始对应差分反射率弧的位置和右侧云砧的区域。平均闪电起始高度的分布呈现自后侧向前侧和自右侧到左侧逐渐降低的趋势，同时，从闪电起始位置高度分布范围看，其最大范围出现在上升气流区的前侧。研究表明，起始自前侧云砧区域的闪电尺度最大，然后是那些起始自上升气流区前侧和接近差分反射率弧的区域。研究支持了关于电荷口袋的概念，并进一步推测在右侧云砧区的电荷口袋分布量最大和最为紧凑，所有导致该区域频繁的闪电起始，但对应闪电尺度小，闪电起始的垂直范围浅薄。（郑栋，张阳，张义军，孟青，张文娟，徐良韬，黄治钢）

5.4 雷暴上升运动与起电和放电活动关系的模拟

利用一个三维起电放电数值模式，研究了上升运动与雷暴中主要的起电活动和放电活动的关系。结果发现，上升运动在对闪电活动的发展（在此以闪电活动中和电荷率表征）起到主要促进作用的同时，还对闪电活动的增强起着抑制作用。上升运动有利于非感应起电活动的发生，但过强的上升运动则不利于非感应起电效率的进一步提高。模拟个例中具有较高起电效率的非感应起电活动基本发生在上升速度小于20 m/s的上升运动区内。此外，上升速度中心的高度在闪电活动的多数时间里与反转温度的高度基本保持一致，可以用来区分霰粒子非感应起电获得不同极性电荷区域的分界。（王飞）

5.5 雷电重大灾害天气系统的动力过程和演变规律

利用多种观测资料和高分辨率数值模式，对2个发生在不利大尺度背景下的局地雷暴过程进行研究，重点分析了触发过程。研究表明，北京地区周边雷暴系统的冷池出流、局地地形和北京城市复杂下垫面特征等均会对局地雷暴的发生产生重要影响。对2015年7月中旬京津冀地区持续性夜间雷雨天气开展了初步分析，发现傍晚到夜间的低层上升运动更强，水汽输送和辐合更充分，层结更不稳定，均有利于降水在傍晚和夜间发生。对多雨多闪、多雨少闪和少雨多闪等3类事件的背景环流合成分析表明，多雨多闪和多雨少闪事件均发生在高层有异常正辐散、中层槽和低层有西南气流输送水汽的背景下，而少雨多闪事件主要是由山区地面加热作用引起，中高层天气尺度强迫较弱；多雨多闪事件的环境场拥有相对高的对流有效位能（CAPE）和LI以及较小的对流抑制能量（CIN），而多雨少闪事件多发生在夜间，CAPE和CIN值较小；少雨多闪事件发生在相对中等强度的CAPE和0～6 km垂直风切变环境场中。

明确了超级单体中闪电起始对应水成物粒子类型、闪电起始密度、高度、垂直范围等特征。构建了闪电起始特征与超级单体结构的关系模型。发现大、小电流地闪气候活动在自身特性和时空分布上存在显著差异性，这种差异性随季节和下垫面而变化。（张大林）

5.6 雷电物理过程研究、雷电探测技术发展和外场观测试验

继续开展广东闪电综合观测试验，在人工触发闪电实现、放电过程精细化观测、雷暴的全闪探测以及雷电物理过程研究等方面获得了显著进展。（1）成功人工触发闪电13次，触发闪电成功率约72%，无论是触发次数还是成功率，都保持了较高的水平。（2）发展了连续干涉仪精细化定位技术，建设了3天线阵列的观测系统，实现了触发闪电和自然闪电全放电过程通道发展的高时间分辨率、精细化描绘。（3）进一步完善了闪电低频电场探测阵列并开展观测，获取了6—11月从化地区雷暴过程的云闪、地闪及NBE事件的脉冲放电信息，实现了闪电放电通道初步可分辨的全闪三维定位。此外，

开展了高原地区低频电场探测阵列的站点考察，并完成 2 个子站的建设。（4）获得了对先导始发先驱脉冲、不规则先导发展特征及物理过程的新认识，并发现了大电荷转移过程 M 分量、连续电流及回击的相关性。（5）广州高建筑物雷电观测大幅提升了先导过程的高速光学观测能力及不同强度的电磁场辐射信号的完整记录能力，得到了先导梯级发展的精细化特征，给出了负极性地闪连接过程中下行负先导和上行连接先导的 2 种基本的连接行为（图9）。（吕伟涛，张阳，郑栋，张义军，姚雯，马颖，黄治钢，徐良韬，齐奇）

6 模式关键技术和再分析资料研究

6.1 天气气候一体化模式关键技术研究

在模式动力框架方面，在广泛调研当今国际趋势的基础上，建立了正二十面体网格生成器，并基于该网格建立了球面平流方程求解器和浅水方程求解器；在正二十面体网格上建立了正定的两步保形平流方案，测试显示该方案目前可以很好地运行于正二十面体网格，计算效果与之前在经纬度网格上的效果相当。在物理过程方面，为改善该耦合模式中大气顶辐射收支不平衡问题，引入一个新的云辐射方案（BCC_RAD），显著改善了大气顶辐射收支的平衡状况，并显著改善东亚层云区冷季短波云辐射强迫的模拟。在模式耦合技术方面，本年度基于美国国家大气研究中心（NCAR）的 CESM 模式以及耦合器 CPL7，替换大气和海洋分量模式，逐步建立一个新分量的海–陆–气–冰耦合系统，由此掌握高分辨率耦合模拟的耦合技术；实现耦合模式和 MPI-M 水文模式耦合，径流通过水文模块进入海洋，完成了全球水量循环的闭合，模式具备气候系统模式所需的完备分量。在耦合模式同化方面，基于中国气象科学研究院现有的耦合气候系统模式版本，引进了中国科学院大气物理研究所发展的 EnOI-IAU同化方法，基于耦合模式同化海洋温盐廓线资料（弱耦合同化），并开展了年代际气候预测回报试验（图10～11）。（张祎，陈昊明，容新尧，李建）

6.2 东亚区域大气再分析攻关任务

完成了东亚区域大气再分析系统搭建并进行初步测试。对 2014 年 7 月进行了试验（不同化观测资料），并进一步优化模式参数组合。开展了 2014 年 6—8 月的模拟，并基于模拟结果进行了背景误差协方差的统计计算和与默认背景协方差矩阵初步的对比。完善了同化流程，开展了再分析同化试验。为了突出东亚区域再分析特色，开展关键资料的分析研究，即对未参加国际交换的探空资料、地基GPS/Met、卫星导风、雷达资料等资料进行了同化试验。结合观测试验开展观测试验资料同化试验，通过与高原试验项目的联合开展了高原试验资料同化试验并完成 1 个月资料的同化运行；通过与华南季风观测试验团队的合作，基于华南观测试验资料开展了模式云物理过程的比对与优化。（梁旭东，尹金方，陈锋，刘英，何会中，周海波，郝世峰）

7 信息网络支撑

完成中国气象科学研究院重点工作"科研数据共享平台"项目建设，在此基础上整合了华南季风降水试验数据共享网站和第 3 次青藏高原大气科学试验项目网站。2016 年汛期开始向中国气象科学研究院内部用户开放使用。承担完成了网络信息安全检查工作 10 多项，完成了院网站挂标和集约化网站群建设。升级和扩容了高性能存储系统，增强了数据服务的支持能力。完成中国气象科学研究院信息系统运维管理与技术支持，保证对外服务网站全年无安全事故（图12）。（高梅，张文华，李斌，李丰，赵盛华，朱孔驹）
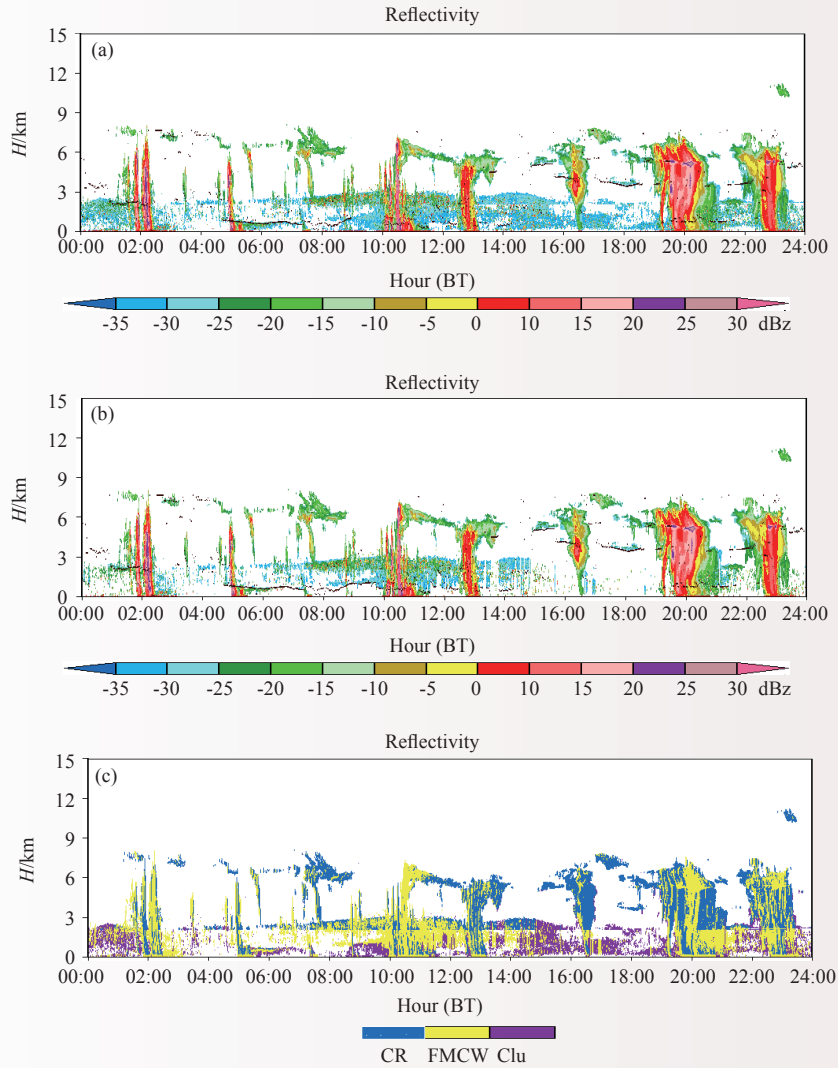
图 1　2016年7月10日在广东龙门观测的回波强度的时间高度图：(a)Ka波段云雷达（CR）、C波段调频连续波（FMCW）垂直观测雷达（CVPR）和激光云高仪（CEIL）融合的回波强度；(b)剔除杂波后的回波强度；(c)融合数据的资料来源。（(a)(b)中黑点为激光云高仪观测的云底，(c)中蓝色和黄色分别表示云雷达和C波段调频连续波垂直观测雷达观测数据，紫色为杂波）

Fig. 1　Time-height cross-sections of reflectivity on 10 July 2016 in Longmen, Guangdong: (a) the merged reflectivity from Ka band cloud radar, C band frequency modulated continuous wave (FMCW) vertical pointing radar (CVPR) and a laser ceilometer (CEIL); (b) reflectivity after removing clutters; (c) data resources of reflectivity. The black dots in (a) and (b) indicate the CEIL-derived cloud-base heights. In (c), data from CR and CVPR, and clutters are shaded in blue, yellow and purple, respectively

图 2 风廓线雷达质控软件系统及同化试验结果
Fig. 2 Wind profiler radar (WPR) data quality control (QC) scheme and numerical assimilation experiment
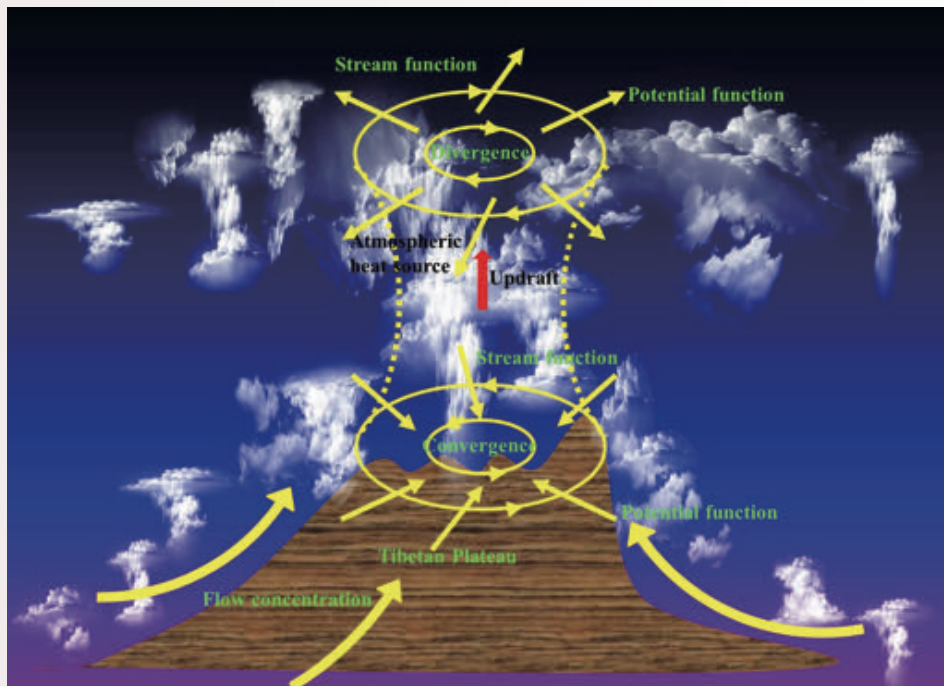
图 3 青藏高原热力驱动区域-全球水分循环多尺度特征
Fig. 3 Regional to global multi-scale characteristics of the heat-induced atmospheric water tower over the Tibetan Plateau
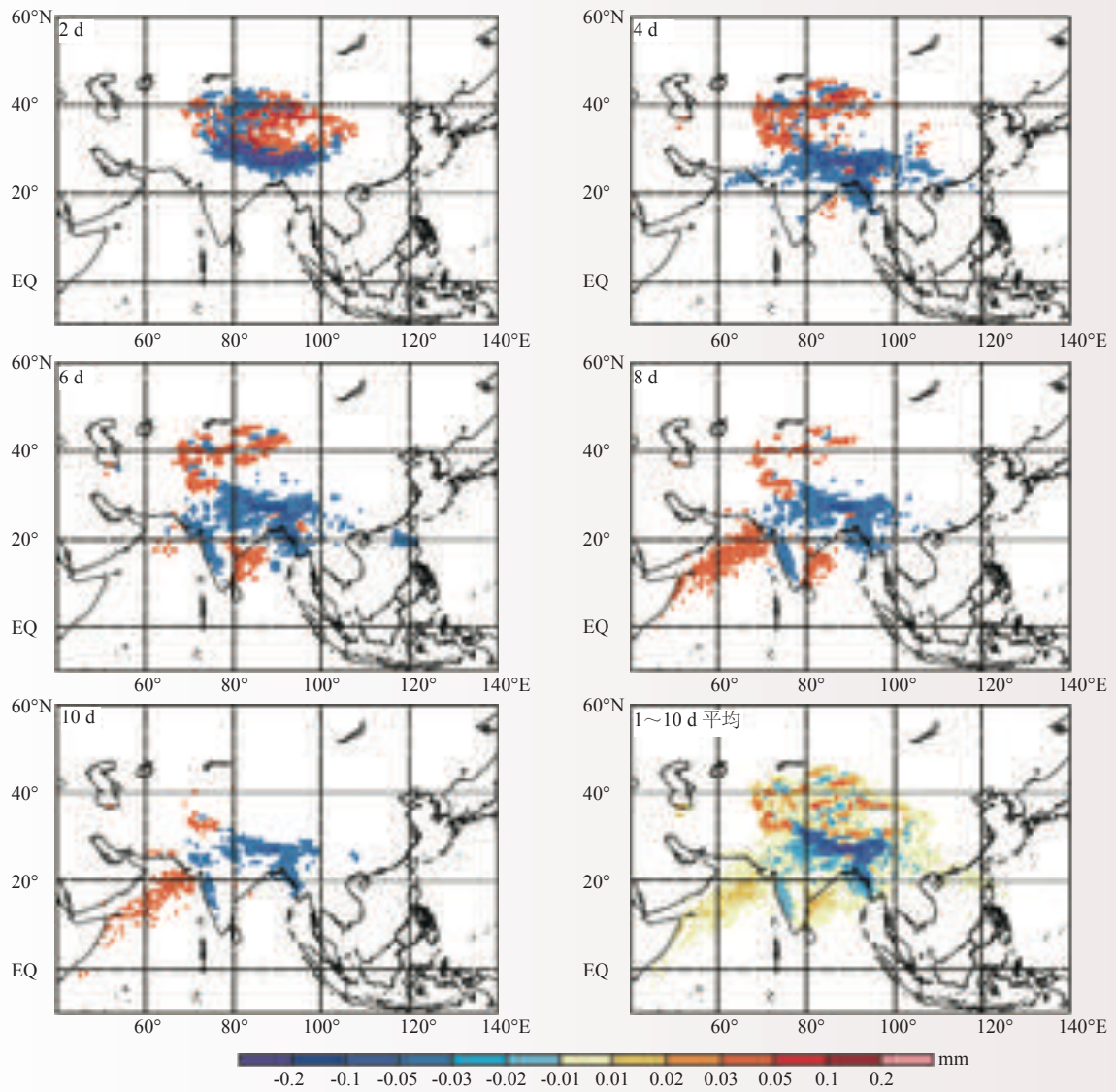
图 4　夏季（6－8月）到达三江源空气块诊断的E-P场

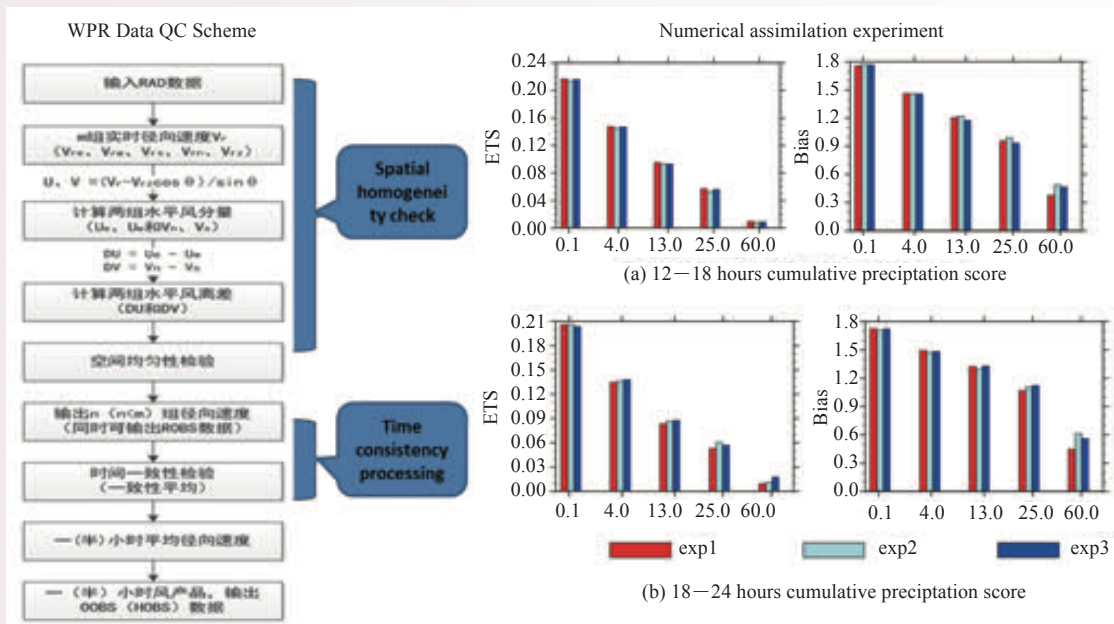Fig. 4　The summer seasonal mean (July-August) of E-P calculated using all air parcels reaching the TRHR
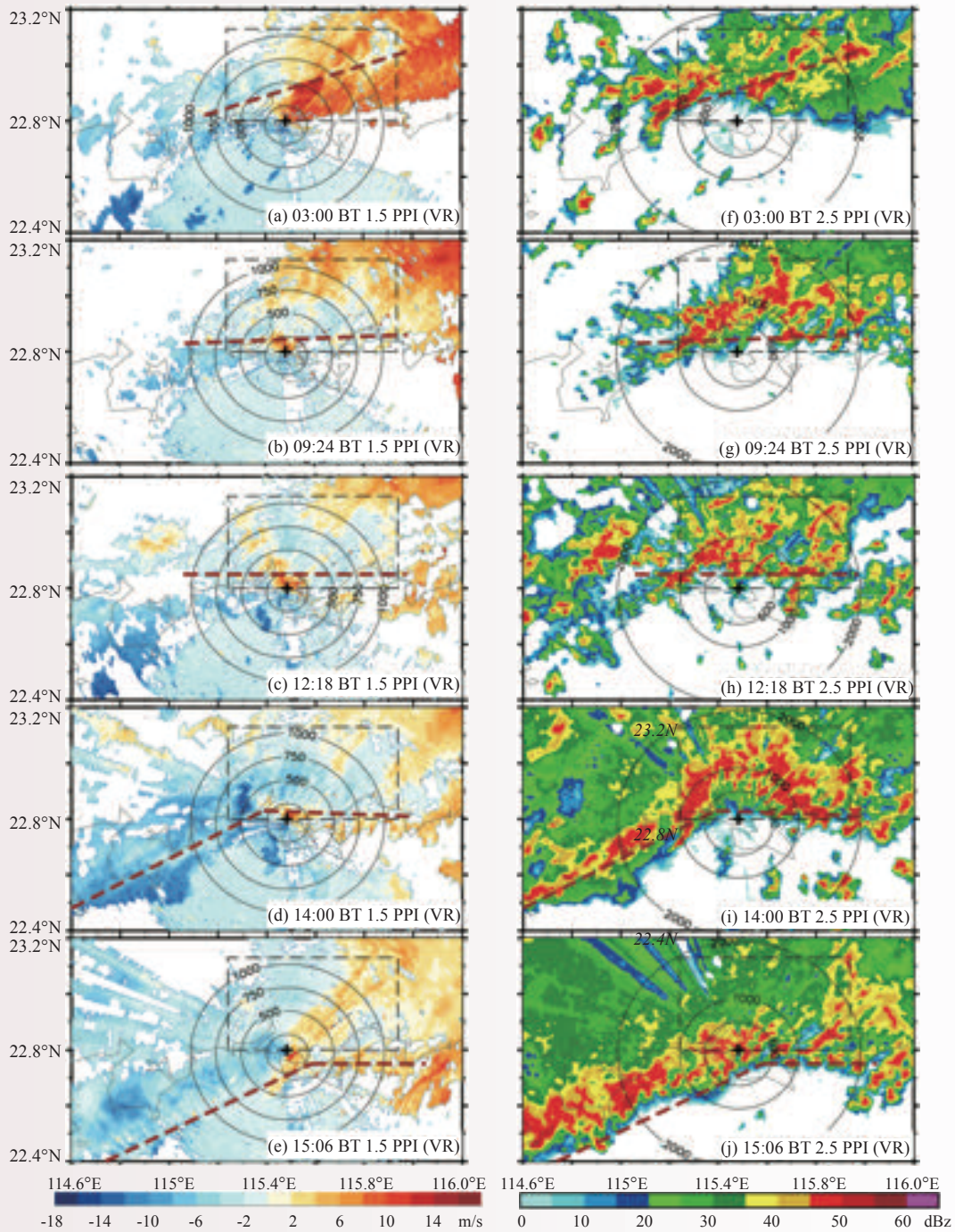
图 5　2015年5月20日5个时刻汕尾S波段雷达的PPI图（其中：(a～e)为仰角1.5°的径向风速度，黑色圆圈代表距地高度250 m、500 m、750 m和1000 m；(f～j)为仰角2.5°的雷达回波反射率，黑色圆圈代表距地高度600 m、1000 m和2000 m。黑色虚线框为关键区，棕色虚线表示根据地面自动站观测估计的中尺度边界的大致位置）

Fig. 5　PPI analysis of Shanwei S-band radar at 5 selected times on 20 May 2015: (a-e) the radical velocity at 1.5° elevation (m s^{-1}), with the black circles denoting the height of 250 m, 500 m, 750 m and 1000 m MSL, respectively; (f-j) the reflectivity at 2.5° elevation (dBz), with the black circles denoting the height of 600 m, 1000 m and 2000 m MSL, respectively, with the black rectangle box representing the control region with extreme accumulated rainfall, the brown dashed lines representing the approximate locations of the surface mesoscale boundary based on the surface observations
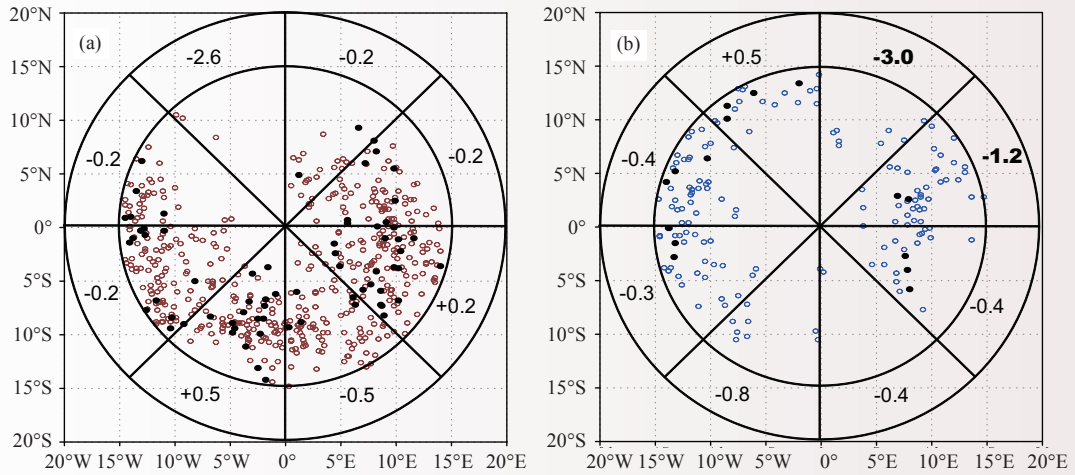
图 6　12 h加强(a)和12 h减弱(b)热带气旋（TC）中心相对于高空冷涡（UTCL）中心（0点）空间分布（黑色点显示快速增强/减弱TC位置）

Fig. 6　The spatial frequency distribution of TCs within a 15° distance from the composite UTCL center during the subsequent (a) 12 h intensifying, (b) 12 h weakening. Black dots denote the locations of TCs experiencing rapid intensity changes

Lightning density/(flashes/(km$^2 \cdot$ 6h))
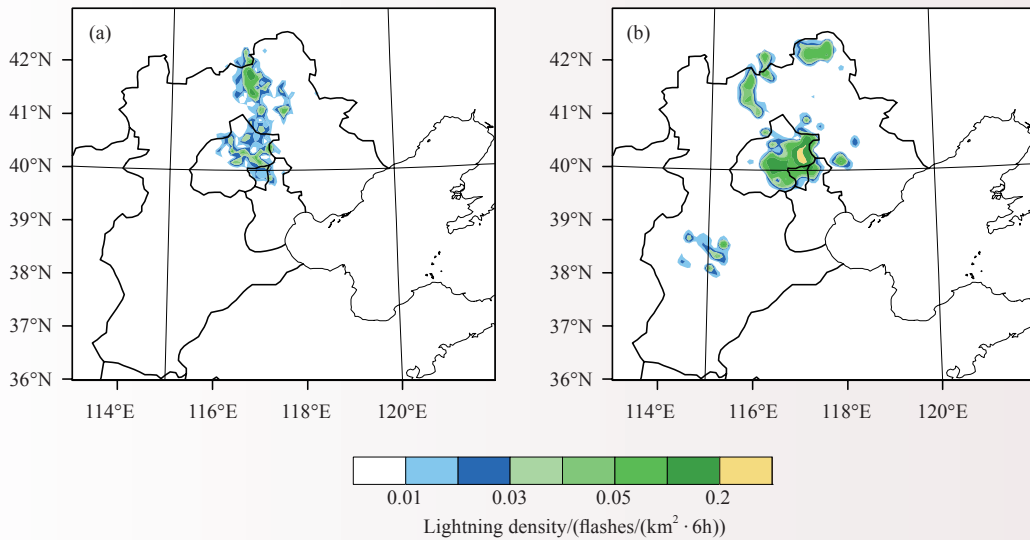
图 7　观测和模拟的6 h闪电活动分布

Fig. 7　The observed and simulated 6-hour accumulated lightning
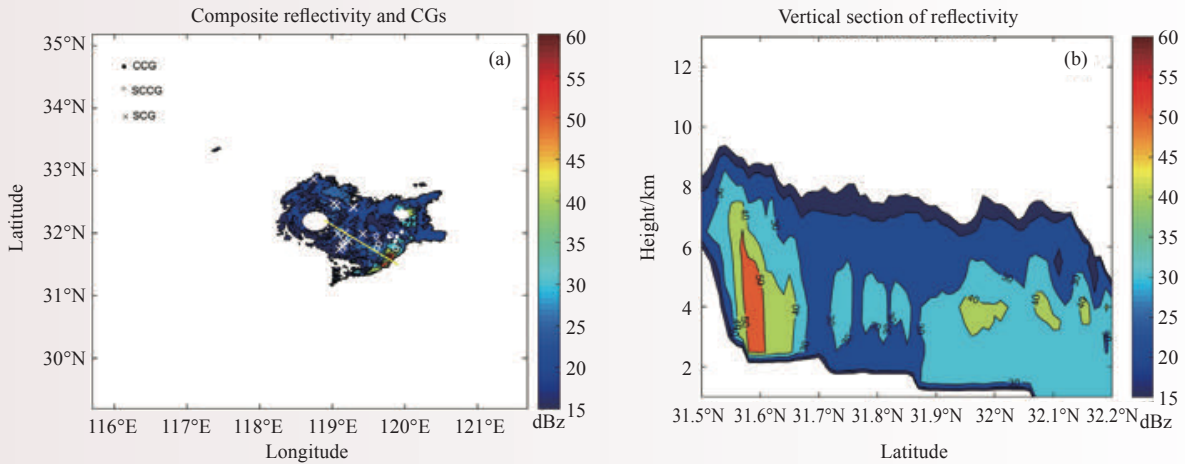
图 8 雷达组合反射率与对流地闪（白色实心●）、层云–对流地闪（○）和层云地闪（×）的接地位置（a）及图（a）中黄色实线位置的雷达反射率垂直剖面（b）

Fig. 8 (a) Composite radar reflectivity, overlain with the return stroke points of CCGs (white dots), SCCGs (○) and SCGs (×); (b) Vertical reflectivity profile along the yellow segment in (a)
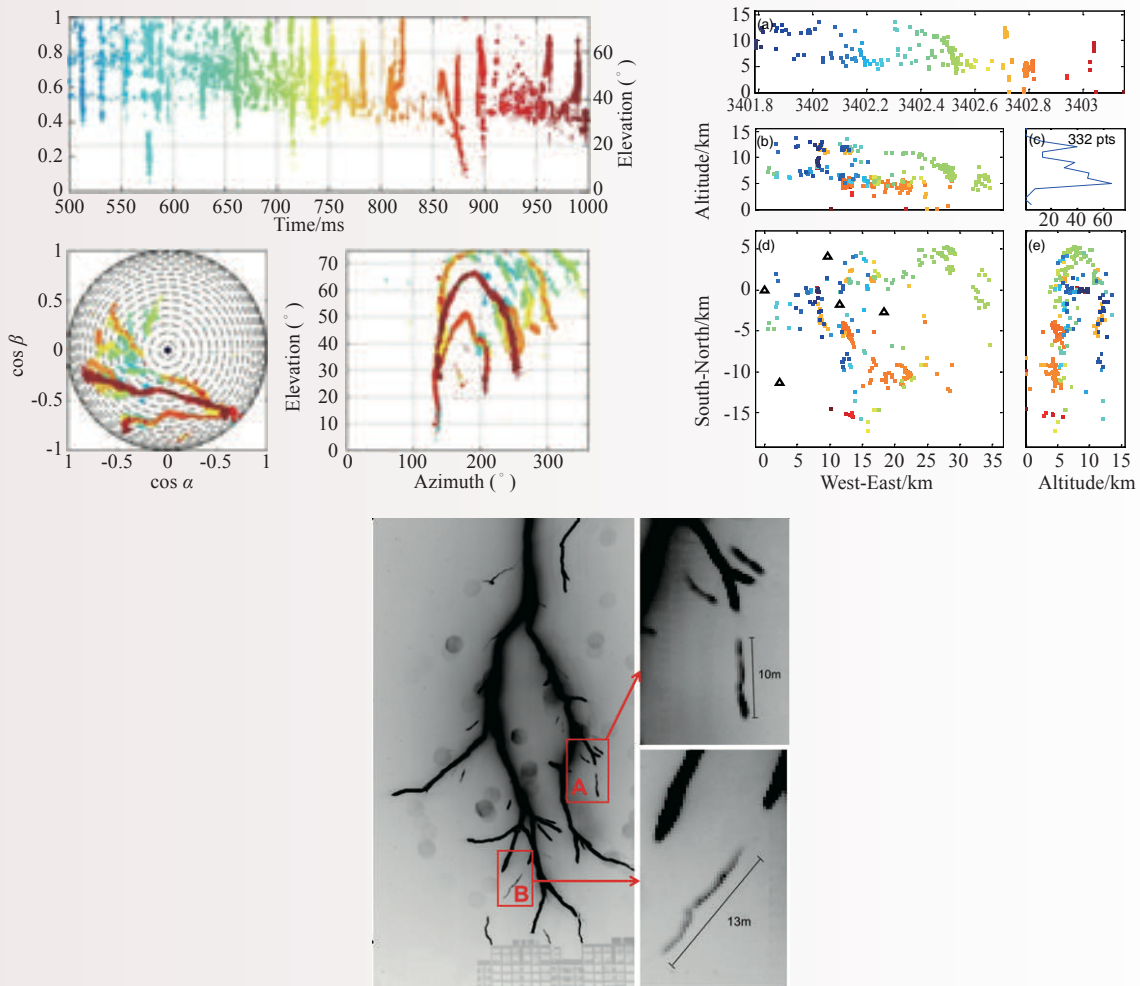
图 9 连续干涉仪甚高频定位结果（左）、LFEDA低频定位结果（右）和下行先导图像（下）
Fig. 9 VHF location of continuous INTF (left), LF location of LFEDA (right) and image of downward leader (below)
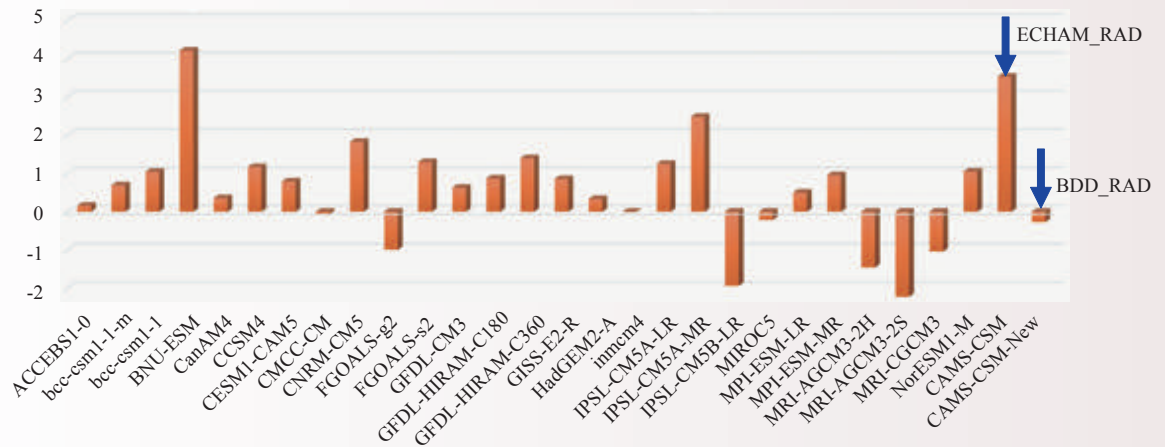
图 10　气候模式模拟的全球平均大气顶净能量收支（从左至右分别为27个参加CMIP5的模式及CAMS_CSM和采用BCC_RAD方案的CAMS_CSM的结果）

Fig. 10　Global annual mean residual energy (unit: W/m²) at the model top in 27 CMIP5 models and CAMS_CSM with different radiation schemes
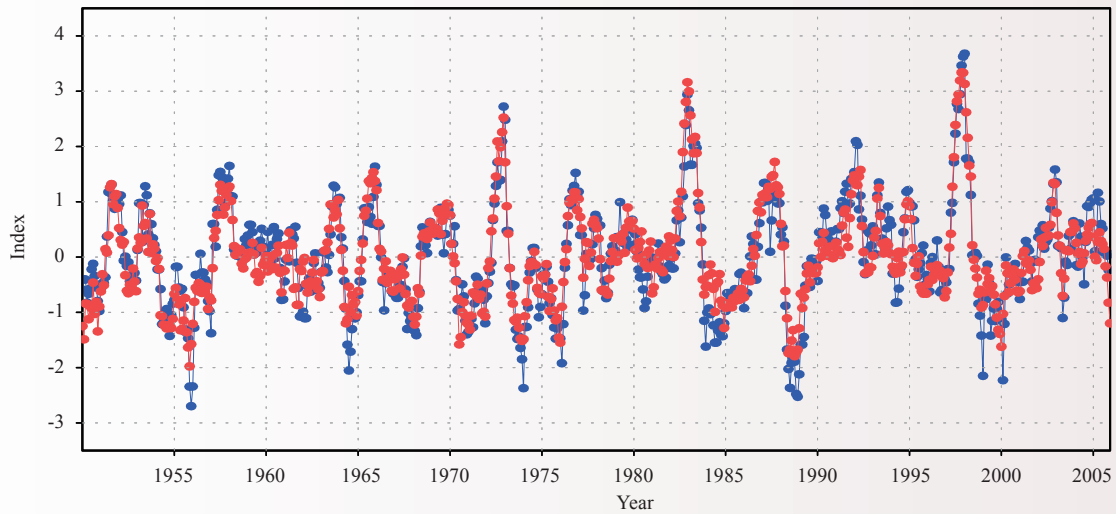
图 11　观测(HadISST，红色)和同化（蓝色）的Nino3海温指数

Fig. 11　Observed (HadISST, red) and assimilated (blue) Nino3 index

图 12　气象科研数据共享平台
Fig. 12　Meteorological scientific and research data sharing platform

Advances in Severe Weather Research

1 Severe weather monitoring technology

1.1 Observation and analysis of microphysical structures of cloud and precipitation over South China

To improve our understanding of the cloud and precipitation properties in South China, the field campaigns were carried out by Chinese Academy of Meteorological Sciences (CAMS). Vertical structures of nonprecipitating and precipitating clouds，3D structures of strong convective precipitations have been observed with X-band phased array radar and X-band polarization radars, a K-band solid-state transmitter cloud radar (CR), a C-band frequency modulated continuous wave (FMCW) vertical pointing radar (CVPR) and a laser ceilometer (CEIL) in Guangdong Province, China. The observational abilities of CR, CVPR radars and CEIL were examined to construct merged cloud-precipitation radar dataset that can be used to analyze statistically the vertical characteristics of clouds and precipitations in South China, including valid rate of observations, cloud-base and cloud-top height estimates and reflectivity distributions (Fig.1). (Liu Liping，Ruan Zhen, Cui Zhehu)

1.2 Integration and operational application of outcomes from radar

(1) The software system of new-generation operational radar data quality control (QC) for radar data assimilation was developed by LaSW, CAMS, in cooperation with the Numerical Weather Prediction Center of CMA, which passed the evaluation organized by Department of Forecasting and Networking of CMA. The radar data QC system for all types of radar in CMA was also developed and used in radar data assimilation. (Wang Hongyan, Liu Liping, Li Feng)

(2) The Wind Profiler Data Quality Control System (WPDQCS) is operated in the Guangzhou Meteorological Bureau to provide support for nowcasting, with its test run in the Meteorological Observation Center of CMA to give the support for GRAPES-MESO data assimilation experiment. It is also operated in the operation system of CAMS to provide support for scientific research (Fig. 2). (Ruan Zhen, Li Feng)

(3) The Beijing Meteorological Bureau dual linear polarization radar processing and nowcasting software systems were developed and used in operational test to realize radar data QC, QPE, hydrological distinguish and nowcasting. (Liu Liping, Hu Zhiqun, Wang Hongyan)

(4) The software systems for squall and convective warning were used in Henan, Zhejiang and Xinjiang electrical power bureaus, in cooperation with Henan electrical power institute. (Liu Liping, Wang Hongyan)

1.3 Field experiment on cloud and precipitation in scientific projects

In the Southern China Monsoon Rainfall Experiment (SCMREX) that was endorsed by the World Meteorological Organization (WMO) as a Research Demonstration Project (RDP) of the World Weather Research Programme (WWRP), and the Third Tibetan Plateau Atmospheric Scientific Experiment (TIPEX-Ⅲ), cloud radar, lidar, X-band phased array radar and C-band dual linear polarization radar were used to observe the microphysical and dynamical structures in clouds and precipitation over the Tibetan Plateau and South China. The vertical motion, cloud water/cloud ice/precipitation/snow contents were documented, the diurnal variations of several important cloud properties were analyzed, including cloud top and base, cloud depth,

cloud cover, number of cloud layers, and their vertical structures, during summertime over the Tibetan Plateau and South China. (Liu Liping, Hu Zhiqun)

2 Research on weather over the Tibetan Plateau

2.1 The effects of surface sensible heat flux (H) and latent heat flux (LE) on the structures of convection and turbulence over the Tibetan Plateau (TP)

Based on results from 11 flux sites during the Third Tibetan Plateau (TP) Atmospheric Scientific Experiment (TIPEX-Ⅲ), land surface parameters and the turbulence characteristics of the atmospheric surface layer over the TP and surrounding regions were analyzed. The large eddy simulations (LES) illustrate that H and LE in the surface layer can have an effect on the structures of convection and turbulence, which also have great impact on the anomalous variations of the liquid water content (LWC) in convective clouds over the TP. The simulations reveal the possible cause of the formation of the special "popcorn clouds" over the TP. (Wang Yinjun, Xu Xiangde)

2.2 Design of a new so-called "interpolation guess" scheme based on the limited automatic sounding observational data on western plateau obtained from the TIPEX-Ⅲ, and its use in data assimilation

A new interpolation scheme of the "interpolation guess" method was designed using the automatic sounding observational data at Shenzha, Gaize, Shiquanhe stations on western plateau from TIPEX-Ⅲ (the Third Tibetan Plateau Atmospheric Scientific Experiment), and more sensitivity experiments were conducted to evaluate the effect on the numerical simulations after all these new data were assimilated into the numerical model. The numerical simulation results indicate that the Threat Score (TS) for the simulated rainfall in the numerical experiments with both the automatic sounding observation only at three stations and with the new data after the "interpolation guess" method has been higher than that in the control experiment without data assimilation, with the improvement of the TS in the experiment with the new method being more obvious than that in the experiment with the original method. (Zhang Shengjun, Xu Xiangde)

2.3 The correlation between Tibetan Convective Systems (TCS) and the hard rain over its downstream regions

A new definition of TCS was introduced to exclude the effects of cirrus and cirrostratus over the Tibet. Based on the new definition, 2032 TCSs were selected and analyzed to study their seasonal variation. The result shows that TCSs play an important role in precipitation over the Tibetan Plateau and its adjacent regions in all four seasons. By analyzing the three-dimensional structure of the water vapor flux, vorticity and divergence prior to and during the heavy rainfall events, the upstream "strong signals" related to heavy rainfall events were revealed. (Hu Liang, Xu Xiangde)

2.4 The use of potential/stream function to analyze the water vapor cycle over the Tibetan Plateau

Based on the understanding of climbing and deflective flows caused by large topography of the Tibetan Plateau (TP) and the "midair heat island" thermal-driven divergence-convergence structure, the kinetic fields were decomposed into stream function and potential function fields. The atmospheric water tower over the TP can be clearly depicted from the water vapor flux and its regional-to-global multi-scale characteristics can be analyzed. The wind vectors of potential function can portrait the regional water vapor fluxes into and out of the TP and their three-dimensional physical diagram. Meantime, the wind vectors of the stream function can anatomically reflect the dynamic structure of the atmospheric circulation, particularly the anticyclonic-

aloft-cyclonic-beneath coupled kinematic structure. With this analysis framework, we examined the dynamic structure caused by the TP topography, its unique atmospheric circulation, and the wave-flow interaction. We further illustrated impact of the dynamic and thermodynamic processes over the TP on the regional-to-global water vapor cycle and the sink and source of the multi-scale transport of water vapor (Fig. 3). (Xu Xiangde)

2.5 The integrated model of moisture transport in heavy rainfall in eastern China

The spatial distribution of summer rainstorm frequency in eastern China is higher in the southeast and lower in the northeast, which is very similar to the distribution of the "staircase" topography. The similarity in the pattern of the three-step staircase topography and the rain bands suggests a strong link between the rainstorm frequency and seasonal migration of Meiyu, moisture transport by monsoonal flow, dynamic and thermodynamic influence of large-scale topography. It is showed that column-integrated moisture transport and moist flow pattern in the summer over eastern China yield great influence on the frequency of extreme rainstorms. (Xu Xiangde)

2.6 The Three-River Headwaters Region moisture sources, pathways and its spatio-temporal structure

The major moisture sources contributed to the Three-River Headwaters Region (TRHR) summer water vapor with relatively short transport timescales (less than 7 days) are mainly originated from the Tibetan Plateau and its northwestern regions, while the moisture transport with longer timescale (8–10 days) could be tracked back from the long-distance oceanic regions, particularly the Bay of Bengal and Arabian Sea. There are two moisture channels: One is related to the moisture located in the southern Indian Ocean crossing the equator nearby the Somalian coastal region; another stems from the central and western Asia (Fig. 4). (Chen Bin).

2.7 Collaborative influences of the Tibetan Plateau and the Pacific/Atlantic on the interannual variations of the land monsoon in the Northern Hemisphere

The Tibetan Plateau (TP) heating can modulate the vertical circulations between the Tibetan Plateau and the Pacific, and therefore regulates the condensation latent heat and dry adiabatic heat over the Pacific, which leads to mid-upper-tropospheric temperature anomalies in situ and ultimately affects the interannual variability of the summer Asian-Pacific Oscillation (APO). The precipitation over the Asian monsoon region was significantly and negatively correlated with that over the mid-latitudes of North America, and was positively correlated with that over the North American monsoon region, constituting an intercontinental contrasting Asian-North American (CANA) precipitation anomaly pattern. The CANA precipitation anomaly pattern was closely related to the land heating of Eurasian (including the Tibetan Plateau) and North America and sea surface temperature (SST) anomalies in the tropical central and eastern Pacific during spring and summer. (Liu Ge, Zhao Ping, Chen Junming)

3 Heavy rainfall research

3.1 Progress of the South China Monsoon Rainfall Experiment

Since 2013, the Heavy Rainfall Research Group at LaSW/CAMS has been leading the South China Monsoon Rainfall Experiment (SCMREX), a unique program for improving heavy rainfall forecasts over South China during the pre-summer rainy season through field campaigns and research on physical mechanisms and convection-permitting modeling, which was endorsed by the World Meteorological Organization (WMO) as a Research Demonstration Project (RDP) of the World Weather Research Programme (WWRP). The SCMREX

RDP (2013–2018) consists of four major components: Field campaign, database management, studies on physical mechanisms of heavy rainfall events, and convection-permitting numerical experiments including impact of data assimilation, evaluation/improvement of model physics, and ensemble prediction. During 1 May–15 June 2016, the SCMREX-2016 intensive observing period (IOP) ran continuously with more portable instruments than those participated in the 2013–2015 IOPs. All the datasets from the operational network and portable instruments have been collected and archived in the SCMREX database with both hardware and data management being upgraded. The SCMREX website (http://scmrex.cma.gov.cn) is also improved in this year with description and images (radar, satellite, and lightning) of major heavy rainfall events during the previous IOPs being added. Moreover, new results are achieved by the studies on physical mechanisms of heavy rainfall, impact of radar data assimilation on QPF, improvement of model cloud microphysics schemes, and development and evaluation of convection-permitting ensemble forecast system. In October 2016, Chief Scientist of SCMREX RDP, Dr. Luo Yali, made a progress report at the WMO Tropical Meteorological Research Working Group Meeting, which was highly praised by the experts at the meeting including the chair of the WMO Monsoon Panel, Prof. Chie-Pei Chang. The progress of SCMREX during 2013–2015 is summarized in a paper that is published in the *Bulletin of American Meteorological Society*. (Luo Yali)

3.2 Studies on heavy rainfall during the pre-summer rainy season

Utilizing the newest, comprehensive observations collected during the SCMREX IOPs, studies by the Heavy Rainfall Research Group suggest that extreme daily rainfall in South China during the pre-summer rainy season was produced by long-lived MCSs with a line alignment of convective cells that favored persistent and large rainfall accumulation over the same region. The characteristics of the extreme-rain-producing MCSs during SCMREX that led to heavy rainfall (duration, organizational patterns, and quasi-stationary behavior) appear to be attributable to the characteristics of the environmental dynamic and thermodynamic conditions during the pre-summer rainy season. Namely, these systems occurred in prevailing low-level southwesterly monsoonal flows providing sufficient moisture, even without the presence of an LLJ, over the complex underlying surfaces in South China (e.g., land/sea contrast, and mountains near the coasts and inland facilitating continuous convective initiation), and within a series of feedbacks from MCSs (i.e., convectively generated cold outflow boundaries where continuous convective initiation usually takes place), as discussed by Wang et al. (2014) and Wu and Luo (2016). As an example, Fig.5 shows how we estimate the depth of a mesoscale cold outflow boundary based on radar observations combined with surface mesoscale analysis. The diurnal cycle of rainfall (DCR) over South China during the pre-summer rainy season is also examined. Three propagating modes accounting for the pre-summer DCR are found: (i) An eastward- or southeastward-propagating mode occurs mostly over southwestern China that is associated with the enhanced transport of warm and moist air from tropical origin and the induced low-level convergence; (ii) A quasi-stationary mode over the east of South China appears locally in the warm sector with weak-gradient flows; (iii) An inland propagating mode occurs during the daytime in association with sea breezes along the southern coastal regions, especially evident throughout the post monsoon-onset period (Fig. 5). (Luo Yali, Bao Xinhua, Jiang Zhina)

3.3 Synoptic analysis of extreme hourly precipitation in China

Synoptic situations associated with extreme hourly precipitation over the extensive eastern China from Hainan Island to Northeast China are investigated using rain gauge data, weather maps, and composite radar reflectivity data, with both objective and subjective approaches to identify the types of synoptic patterns. Seasonal variations of hourly precipitation (0.1 mm h^{-1}) suggest complicated regional features in the occurrence frequency and intensity of rainfall. The 99.9th percentile is thus used as the threshold to define the extreme

hourly rainfall for each station. The extreme rainfall is the most intense over the southern coastal areas and the North China Plain. About 77% of the extreme rainfall records occur in summer with a peak in July (30.4%) during 1981–2013. Nearly 5800 extreme hourly rainfall records during 2011–2015 are classified into four types according to the synoptic situations under which they occur: The tropical cyclone (TC), surface front, vortex/shear line, and weak-synoptic forcing. They contribute 8.0%, 13.9%, 39.1%, and 39.0%, respectively, to the total occurrence and present distinctive characteristics in regional distribution and seasonal or diurnal variations. The TC type occurs most frequently along the coasts of Southeast and South China and decreases progressively toward inland China; the frontal type is distributed relatively evenly in the east of 104°E; the vortex/shear line type shows a prominent center over the Sichuan Basin with two high-frequency bands extending from the center southeastward and northeastward, respectively; the weak-synoptic type occurs more frequently in Southeast, Southwest, and North China, and in the easternmost area of North China. Occurrences of the weak-synoptic type have comparable contributions from mesoscale convective systems and smaller-scale storms with notable differences in their preferred locations. (Luo Yali)

3.4 Characteristics of cloud-to-ground lightning and its relationship with rainfall over central and eastern China

The cloud-to-ground (CG) lightning climatology and its relationship with rainfall over central and eastern China are examined, using 32 million CG lightning flashes data and TRMM (Tropical Rainfall Measuring Mission) measurements during a 6-year period of 2008–2013. Results show substantial spatial and temporal variations of flash density across China. Flash counts are the highest (lowest) in summer (winter) with the lowest (highest) proportion of positive flashes. CG lightning over North China is more active only in summer, whereas in winter CG lightning is more active only in the Yangtze River Valley. The highest CG lightning density exceeding 9 and more than 70 CG lightning days yr^{-1} are found in the northern Pearl River Delta region, followed by the Sichuan Basin, the Yangtze River Delta and the southeastern coast in order. Lower-flash-density days occur over mountainous regions due to the development of short-lived afternoon storms, while higher-flash-density days, typically associated with nocturnal thunderstorms, appear over the North China Plain and Sichuan Basin. The highest CG lightning flashes take place in August whereas monthly convective rainfall peaks in May or July. Flash rates during the warm season are typically maximized in the afternoon hours in coincidence with a convective rainfall peak except for Sichuan Basin and its surrounding mountainous areas where a single late-night convective rainfall peak dominates. Much less lightning activity corresponds to a late night to morning rainfall peak over plains in eastern China due to the increased proportion of stratiform rainfall during that period. (Xia Rudi)

3.5 Characteristics of the temporal and spatial distributions of precipitation over Hainan Island

The causes of the temporal and spatial distributions of precipitation over Hainan Island, including the influences of environmental conditions on the temporal distribution of precipitation and the combined effect of synoptic winds, orography and sea-breeze circulation on the spatial distribution of precipitation, are investigated and discussed, based on the statistical analyses of 5-year high-resolution surface and sounding observations and numerical experiments. The results show that the high humidity and convective available potential energy (CAPE), unstable atmospheric stratification, low free convection level (LFC) and weak vertical wind shear associated with southwesterly during April–September lead to large amounts of precipitation over Hainan Island, along with the beneficial effect of sea-breeze front's (SBF's) convergence tendency under weak synoptic wind conditions. Pronounced precipitation is apt to occur over the leeward side of the mountain under the influences of weak synoptic winds, low mountain and sea-breeze circulation.

Moreover, different propagation features are shown for precipitation depending on different synoptic wind directions. (Liang Zhaoming)

3.6 Analysis of the detailed structure of the squall line over South China

Based on dual-Doppler weather radar retrieved wind, the mechanism and 3D structure of the squall line on 24 April 2007 in Guangdong Province were analyzed. The conceptual model of the squall line was also developed. In the wide trailing stratiform region, the rear-to-front cold inflow enters the squall line below the altitude of 3 km. The storm-relative front-to-rear warm flow enters the squall line from the lower and middle level of the leading edge. Above 7.5 km height, part of the front-to-rear inflow moves forward and part of the inflow slopes gradually into the trailing stratiform region. (Zhou Haiguang)

4 Typhoon research

4.1 The relationship between sea surface temperature and maximum potential intensification rate of tropical cyclones over the North Atlantic

An empirical relationship between sea surface temperature (SST) and the maximum potential intensification rate (MPIR) of tropical cyclones (TCs) over the North Atlantic is developed based on best track TC data and observed SST during 1988–2014. Similar to the empirical relationship between SST and the maximum potential intensity (MPI) of TCs previously documented, results from this study show a nonlinear increasing trend of MPIR with SST. That is the IR showing a general increasing trend with increasing SST as well with a more rapid increasing trend with higher IR when SST is greater than 27 ℃ .The analysis shows that about 29% of Atlantic TCs reach 50% of their MPIR, and only 6% reach 80% of their MPIR at the time when they are at the lifetime maximum intensification rate. Moreover, a TC tends to have a larger intensification rate during its lifetime when it is located in a higher SST region and lower VWS, indicating that SST is not only critical for TC IR but also determines the MPIR. In addition, a theoretical basis for the MPIR has also been provided based on a previously constructed simplified dynamical system for TC intensity prediction, and the theoretical result is well in agreement with the observational fitted MPIR with longer data records over a wide range of SST. (Xu Jing, Wang Yuqing)

4.2 A statistical analysis of the relationship between UTCL and tropical cyclone track and intensity change over Western North Pacific

The geographical and temporal characteristics of upper tropospheric cold lows (UTCLs) and their relationship with tropical cyclone (TC) track and intensity changes over the Western North Pacific (WNP) during 2000–2012 are examined using the best track TC data and global meteorological re-analysis data. An analysis of the two datasets shows that 73% of 346 TCs coexist with UTCLs, and 21% of them coexist with TCs within an initial cut-off distance of 15º, within which interactions could occur. By selecting those co-existed systems within this distance, we find possible influences of UTCLs on TC track and intensity changes, depending on their relative distance and on the sectors of UTCLs where TCs are located. Results show that the impact of UTCLs on TC directional changes are statistically insignificant when averaged within the 15º radius. However, left-turning TCs within 5º distance from the UTCL center tend to occur abrupt turnings. Results also show that TCs seem to interact with an UTCL during their early development stages. Intensifying (weakening) TCs are more distributed in the southern (northern) sectors of UTCLs. In addition, rapid intensifying TCs take place in the east-southeastern and south-southwestern quadrants of UTCLs, whereas rapid weakening cases appear in the western semicircle of UTCLs (Fig. 6). (Li Ying，Wei Na, Zhang Dalin)

5 Lightning research

5.1 Study on the relationship between lightning activity and structure of convective clouds in Qinghai-Tibet Plateau

Based on the observation of the home-grown Total-Sky Cloud Imager, the cloud cover and cloud type over Shigatse are analyzed and found to change with seasons. Meanwhile, the dataset of Precipitation Features (PFs) derived from the observation of TRMM satellite is introduced to study the structures of clouds with lightning and without lightning over the Tibet Plateau. The area of PFs with lightning is an order of magnitude larger than that of the PFs without lightning. The horizontal area of PFs with lightning is generally above 1400 km^2 over the northeastern plateau, while the minimum is below 500 km^2 over the southeast (centered near 29°N, 97°E). Over the plateau, cloud height of PFs with lightning is 2−4 km higher than that of PFs without lightning. The maximum cloud height of PFs with lightning is over southern-central plateau with the value above 12 km, and minimum height is less than 10 km near the southern Tibetan region. The maximum height of 20 dBz radar reflectivity over the plateau is similar and slightly smaller than that over the plain to the south of Himalaya region, but the maximum height of 40 dBz radar reflectivity over the plateau is higher than that over the plain. PFs with lightning over western and northeastern plateau have larger mean lightning density than in other regions. (Zhang Yijun, Zheng Dong, Lü Weitao, Meng Qing, Yang Jun, Yao Wen, Ma Ying, Wang Fei)

5.2 Assimilation of special observation data and research on detecting and forecasting methods for severe thunderstorms

(1) The empirical relationship between flash rate, water vapor mixing ratio and graupel mixing ratio was used to adjust the model relative humidity, which was then assimilated using the three-dimensional variation data-assimilation method in WRF-3DVar system in cycling mode with 10 min intervals. A short-range lightning prediction platform was constructed based on the WRF-Electric model. Two flood season prediction experiments were carried out and the prediction results were preliminarily assessed. The basic scheme which blended the Lightning Nowcasting and Warning System (CAMS_LNWS) and mesoscale numerical weather prediction was designed to improve the 0−12 hour lightning prediction (Fig. 7). (Xu Liangtao, Yao Wen, Zhang Rong)

(2) Based on the comprehensive analysis on the data of radar and lightning from 10 mesoscale convective systems (MCSs), it has been found that the first return stroke currents of stratiform cloud-to-ground (CG) lightning flashes are usually greater than that of convective lightning flashes. Most of stratiform CG lightning flashes strike the ground under the verge of or around the area in stratiform region of MCS, where the reflectivity core (⩾ 30 dBz) locates in the height range of 3−6 km. This characteristic of reflectivity core is consistent with that of brightband. It suggests that the charge structure of the stratiform region with brightband may have an important influence on initiation or propagation of stratiform lightning. This result provides a vital evidence for research of the relationship between stratiform lightning and brightband and a theoretical basis for the development of stratiform CG lightning warning (Fig. 8). (Wang Fei)

5.3 The temporal and spatial relationship between the initial characteristics of lightning and the thunderstorm structure

The location method and technology of lightning Low-Frequency Electric-filed Detection Array (LFEDA), which is running in Guangdong with the aim to detect the lightning activity in three-dimensions, were further

improved. Based on LFEDA, we conducted the lightning observational experiment, obtained good data and then investigated the performance of LFEDA and obtained some preliminary results. The LFEDA shows a fine performance in the location of the triggered lightning flashes (TLFs) which were carried out in the inner of the network of the LFEDA, with the detection efficiency for TLFs and return strokes being 100% and 95%, respectively, and the average location error being 102 m. The combination of the three-dimensional locations of the total lightning during the evolution of thunderstorms with the radar echo also support the reliable performance of LFEDA. In addition, two examples including an intra-cloud lightning and the leader of a cloud-to-ground lightning are exhibited, while some parameters associated with the initial propagation of channels are also counted according to the location data. The analysis proves that LFEDA is capable of describing the three-dimensional channel of lightning to some extent.

Flash initiations within a supercell cluster during 10–11 May 2010 in Oklahoma were investigated based on observations from the Oklahoma Lightning Mapping Array and the Norman, Oklahoma, polarimetric radar (KOUN). The flash initiations at positions dominated by graupel, dry snow, small hail and crystals accounted for 44.3%, 44.1%, 8.0% and 3.0% of the total flashes, respectively. During the tornadic stage of the southern supercell in the cluster, flash initiations associated with graupel occupied the main body, the right flank and the forward flank of the supercell, while those associated with dry snow dominated the outskirts of the adjacent forward anvil, right anvil and rear anvil. The flash initiations associated with small hail were concentrated around the main updraft, particularly toward its front side. Highly dense flash initiations were located in the regions overlying the differential reflectivity (ZDR) arc and right anvil. The average initial height of the flashes decreased gradually from the rear to the front and from the right to the left flanks, while the height range over which initiations occurred reached a maximum at the front of the updraft. The flashes that were initiated in the adjacent forward anvils were the largest on average, followed by those in the regions ahead of the updraft and near the ZDR arc. This study supports the concept of charge pockets and further deduces that the pockets in the right anvil are the most abundant and compact due to the frequent flash initiations, small-sized flashes and thin layers including flash initiations. (Zheng Dong, Zhang Yang, Zhang Yijun, Meng Qing, Zhang Wenjuan, Xu Liangtao, Huang Zhigang)

5.4 Model study on the relationship between the updraft and the charging and discharging processes in thunderstorms

Using a 3D charging-discharging numerical model, the relationship between the updraft and the charging and discharging processes in thunderstorms was analyzed. The results show that the enhancement of updraft restricts the strengthening of lightning activity (here represented by the neutralized charge rate of lightning flashes per minute) while the promoting effect of updraft to lightning activity is still dominant as observations. In the simulation case, the non-inductive charging process with high charging efficiency always occurs within or near the updraft region with the updraft speed less than 20 m s^{-1}. In addition, the height of updraft core agrees with the height of reversion temperature roughly in most of lightning activity. It can be used to separate the regions within which graupel is charged with opposite polarity through the non-inductive charging process. (Wang Fei)

5.5 Dynamical processes and structural evolution in severe thunderstorms

The developments and especially convective initiation (CI) of two local severe storms over the Beijing metropolitan region under unfavorable larger-scale conditions are examined using various observations and high-resolution model simulations. Results reveal that the important roles of the UHI effects, mountain morphology, and convectively generated pressure perturbations in determining the CI location and timing of isolated thunderstorms during the summer months. An analysis of larger-scale environments associated with high rainfall rates and high frequency of cloud-to-ground (CG) lightning flashes (HRHL), high rainfall rates

and low frequency of CG lightning flashes (HRLL), and low rainfall rates and high frequency of CG lightning flashes (LRHL) shows that the upper-level jet with anomaly divergence on its right side and the western Pacific subtropical high were favorable for HRHL and HRLL events. The horizontal wind shear and convective instability in the lower troposphere were important for the three categories of events, but their intensities were the weakest in LRHL events. Front activities related closely only to HRHL events. For events with high lightning activities, the lower atmosphere was warmer and wetter than its surrounding areas. Thunderstorm events with high frequency of flash needed better lifting condition, while HRLL events needed small convective inhibition. LRHL events also needed small 0−6 km vertical wind shear and HRHL events needed large CAPE.

Observational and modeling studies are performed to confirm the types of precipitation particles of lightning initiation, and the associated density, altitude and vertical extent in supercell thunderstorms. A conceptual model was developed to describe the relationship between the characteristics of lightning initiation and vertical structures of the supercell storms. It is also found that the climatology of CG lightning activity with strong or weak electric currents differs significantly in their own characteristics and spatio-temporal structures, depending upon the season and underlying surface conditions. (Zhang Dalin)

5.6 Research of lightning discharge process, development of lightning detection technology and conduction outfield experiment

During Guangdong Comprehensive Observation Experiment on Lightning Discharge (GCOELD), significant progress in success rate of artificial triggered lightning, detailed observations of lighting discharge process, observations of total flash in thunderstorm and research on lightning physical mechanism has been gained. The specific progress is as follows. (1) The numbers and success rate of triggered lightning are 13 and 72%, respectively, both reaching relatively high levels. (2) Continuous interferometer is developed for detailed positioning of lightning channel, and the corresponding system consisting of a three antenna array is set up, which helped to describe the process of lightning discharge in a detailed and high time-resolution way. (3) We have made a further improvement of LFEDA (Low Frequency Electric-field Detection Array), with which, from June to November, acquired different impulse information during intra-cloud lightning, cloud to ground lightning and NBE events in Conghua. By analyzing these acquired data, we made it possible to get a preliminary 3-dimension positioning result for the total flash. Besides, we have investigated several installation sites for LEFDA in the plateau area, and also built 2 substations for testing. (4) A new sight was built for the development of irregular impulse and precursor impulse related to the initiate of leaders; at the same time, the relevance between M-component and continuous current in large charge transfer progress was discovered. (5) We have significantly improved the optical observation ability for the high-speed leader development process and the ability to record the completed electromagnetic radiation field signals of different magnitudes as well. Due to these updates, we revealed the detailed characteristics of leader development process, meanwhile displayed the two basic connection modes for the downward negative leaders and upward connecting leaders in negative cloud to ground flashes (Fig. 9). (Lü Weitao, Zhang Yang, Zheng Dong, Zhang Yijun, Yao Wen, Ma Ying, Huang Zhigang, Xu Liangtao, Qi Qi)

6 Model and reanalysis data

6.1 Research on weather-climate unified model

After the survey of the current international trend of dynamical core development, we selected the icosahedral mesh as the basis of dynamical core development. An icosahedral mesh generator and solvers of

the transport and shallow water equations are developed. A conservative Two-step Shape-Preserving Advection Scheme (TSPAS) is generalized on the icosahedral mesh. Results show that this scheme works well in such an unstructured grid. The performance is comparable to the previous prototypes on the rectangular mesh. For model physical parameterization, a new correlated k-distribution radiation scheme (BCC_RAD) was incorporated to improve the radiation energy imbalance at the top of model atmosphere (TOA). Results show that the TOA residual energy is greatly reduced, and the shortwave cloud radiative forcing over East Asia is also improved by using BCC_RAD scheme. Based on the NCAR CESM model and the coupler CPL7 and replacing the atmospheric and oceanic components, we developed a new coupled system with new atmosphere, ocean, land and ice components, which allow us to master the high-resolution coupled simulation technique. The MPI-M hydrological model was incorporated into the coupled model to achieve the runoff into the ocean, thus close the global water cycle and the model emerges as a complete climate system model. Based on the previous version of the coupled model, we introduced the EnOI-IAU assimilation scheme developed by LASG/IAP to assimilate the observed temperature and salinity profile data (weakly coupled assimilation) and perform decadal climate prediction experiments (Fig. 10−11). (Zhang Yi, Chen Haoming, Rong Xinyao, Li Jian)

6.2　Program for tackling key problems in East Asia regional atmospheric reanalysis data

The system for East Asia regional atmospheric reanalysis data has been built and some preliminary tests were made. Based on the system, long term simulations from June to August in 2014 were accomplished, and a background error (BE) covariance matrix was built based on the simulations. Besides, the new BE was compared with the default BE which is given by the Gridpoint Statistical Interpolation (GSI) system. In addition, the assimilation structure is optimized, and a series of assimilation tests for East Asia regional atmospheric reanalysis data have been launched. In order to show the characteristics of the East Asia regional atmospheric reanalysis data, the key datasets of sounding, GPS/Met, satellite, radar observations, which are not included in the GTS (Global Telecommunication System), were assimilated. A lot of data assimilation experiments were launched by combining the data with field experiments. A whole month experiment was carried out by introducing the data from the third Tibetan Plateau Atmospheric Scientific Experiment (TIPEX-Ⅲ). The cloud microphysical properties over South China have been investigated, and the East Asia regional atmospheric reanalysis data system has been optimized using the observations from the South China Monsoon Rainfall Experiment (SCMREX). (Liang Xudong, Yin Jinfang, Chen Feng, Liu Ying, He Huizhong, Zhou Haibo, Hao Shifeng)

7　Information network support

Upon completion of the CAMS's keystone project "Scientific research data sharing platform", we have integrated the South China Monsoon Rainfall Experiment (SCMREX) data sharing website and the third Tibetan Plateau Atmospheric Scientific Experiment website, in use since the 2016 rainy season. We have also completed more than 10 information security check jobs. Building Intensive website group upgraded and expanded high capacity storage system to improve data service support. We have completed the operational maintenance, management and technical support of the CAMS's information system, ensuring zero security issues (Fig.12). (Gao Mei, Zhang Wenhua, Li Bin, Li Feng, Zhao Shenghua, Zhu Kongju)

气候系统与气候变化
Climate System and Climate Change

气候系统与气候变化研究进展

2016年，气候系统（极地气象）研究所在气候预测理论与方法、气候系统模式研发以及极地气候研究方面获得了显著进展。

1 气候预测理论与方法

1.1 GPCP和CMAP资料在东亚夏季风降水年际变率上的不一致性及其改进方案

揭示了GPCP和CMAP资料在北半球夏季风降水年际变率上的不一致性，提出基于两者算数平均减小该不确定性的方法和理由。GPCP和CMAP降水资料因覆盖全球范围和时间跨度较长而广泛用于气候监测和气候变率研究中。资料对比分析表明，尽管GPCP和CMAP资料均可描述北半球季风区降水的季节循环特征，但两者之间仍然存在明显的绝对误差，这种差异在5—10月的西北太平洋（WNP）季风区最为明显，表现为CMAP资料中WNP季风区夏秋季降水较GPCP资料数据偏多。就气候平均夏季降水的空间分布而言，两套资料的主要差异出现在WNP季风区的海洋上空，以及北非（NAM）和印度（IND）季风区的热带海域，这可能是CMAP资料使用了具有争议的岛屿观测资料。在年际尺度上，GPCP和CMAP资料在北半球五大季风区夏季降水年际变率方面大体一致，但两者在IND和NAF季风区的差异显著。GPCP和CMAP数据的一致性在近几十年逐渐提高，特别是在NAM和IND季风区。使用GPCP和CMAP的算术平均来描述北半球季风区降水的年际变率能够有效降低不同资料间的不确定性，特别是在1979—1997年的IND季风区和1998—2014年的NAF季风区（图1）。（祝从文，刘伯奇）

1.2 东亚夏季风气候季节内振荡的特征和可能成因

该工作证实了东亚夏季风气候季节内振荡（CISO）的存在性，阐明了与CISO位相循环相关主要环流系统的耦合过程和东亚夏季风降水季节内变化的联系。东亚夏季风（EASM）的气候季节内振荡以季风环流的垂向和经向相互作用为特征，与夏季风雨带的季节性北抬相联系。EASM CISO在5—8月最为强盛。采用谐波分析和多变量EOF分析方法，从逐日气候态（1981—2010年平均）风场、降水、非绝热加热以及海温场的季节内变化分析了EASM CISO主模态特征。结果表明，EASM CISO存在的根本原因是东亚地区海陆热力对比对太阳辐射年循环的非对称响应，使得CISO变率中心位于我国东部至西北太平洋上空。在EASM盛行季节，非绝热加热Q1主要由凝结潜热构成，Q1中心位于西北太平洋和东亚地区，因此Q1的水平梯度能够在其中心的东北侧制造负涡度源，其造成的背景上升运动有利于CISO的触发。同时，Q1各成分之间的位相差也能够维持EASM CISO。具体而言，EASM CISO开始于表面感热加热的加强，进而改变大气对流稳定度，调控季风对流及其凝结潜热，而凝结潜热的增加会令地面降温，感热减弱，如此循环往复，构成了EASM Q1的CISO。

多变量EOF结果表明，EASM CISO的前两个主模态的主要特征是850 hPa贝加尔湖附近蒙古气旋、500 hPa西太平洋副高和200 hPa青藏高原上空南亚高压的相互耦合。其中第1主模态表现为上述3个环流系统的同时加强，对应着东亚地区"3极型"降水异常，即梅雨锋位于长江中下游至日本以南，而

东北亚和西北太平洋的降水异常偏少。在 EASM CISO 的第 2 主模态中，蒙古气旋和西太平洋副高加强并向西北方向传播，而南亚高压却异常偏弱，与之对应的是亚洲到西太平洋地区的偶极型降水异常。而 AGCM 试验证明，EASM CISO 的第 1 主模态主要与 SST 对大气环流的强迫作用有关，表现为东亚–太平洋地区逐日 SST 季节变化对大气环流季节演变的驱动作用，但 EASM CISO 的第 2 主模态却无法很好模拟，暗示该模态很可能与大气对 SST 的强迫过程有关（图 2）。（祝从文，刘伯奇）

1.3 南海夏季风爆发年际变化特征及其海温影响因子在1993/1994年前后的年代际差异

揭示了南海夏季风爆发过程的年际变化特征在 1993/1994 年前后存在显著差异，指出春季南印度洋海温和前冬 ENSO 事件分别是 1993/1994 年前后影响南海夏季风建立时间的关键因子。南海夏季风爆发时间具有明显的年际变率。本研究依据南海夏季风爆发期间的动力热力场和环流结构的年际变化，以 1993/1994 年为界，将南海夏季风爆发的年际变化划分为两种不同类型。在 1980—1993 年期间，南海夏季风爆发年际变化的特征是季风降水异常出现在南海北部，伴随着显著的低空纬向风异常，将其定义为"Ⅰ型"爆发，它与副热带环流系统的联系更为紧密。在 1994—2014 年期间，南海夏季风爆发年际变化的特征变为以热带季风对流和高空纬向风异常为主，将其定义为"Ⅱ型"爆发。因此，南海夏季风爆发期间高、低空环流垂直耦合过程在这两个时段也具有明显差异。

影响南海夏季风爆发年际变化两种类型的前期 SSTA 也截然不同，对"Ⅰ型"爆发而言，1983—1993 期间南海夏季风爆发早晚主要受春季南印度洋（40°～20°S，40°～110°E）SSTA 影响，南印度洋暖 SSTA 会导致南海夏季风爆发异常偏晚。这是因为南印度洋暖 SSTA 能够首先造成大尺度经向海平面气压异常，令南印度洋出现低空异常辐合，而低空异常辐散却位于南海地区，随后异常低空反气旋控制着南海北部，产生异常下沉运动，进而减弱南海地区的垂直东风切变和海陆热力对比，最终抑制了南海季风对流的发生，令南海夏季风爆发异常偏晚。对"Ⅱ型"爆发而言，在 1994—2014 期间，前冬 ENSO 事件及其相关的春季热带印度洋 SSTA 是影响南海夏季风爆发迟早的主要海温强迫。前冬暖 ENSO 事件发生后，能够通过"大气桥"造成春季热带印度洋的异常增暖。热带印度洋的异常增暖会激发出热带定常 Kelvin 波，令南海地区对流层中上部平均温度的经向梯度（MTG）减弱，从而推迟了 MTG 由冬到夏季节转换的时间。此外，对流层高层由热带印度洋吹向南海的大尺度东风异常使热带印度洋的上升运动加强，但却令南海南部的上升运动减弱，这将进一步抑制南海季风对流的建立，最终导致南海夏季风爆发异常偏晚。研究结果说明，ENSO 和南海夏季风爆发时间之间的对应关系在 1993/1994 年前后发生了明显改变。这可能是因为在 1993/1994 年之后 La Niña 事件的发生频次明显提高，而这又与 ENSO 事件的年代际调整有关（图 3）。（刘伯奇）

1.4 南亚高压季节变化是南海夏季风爆发的可能前兆信号

研究发现高空南亚高压的季节演变对南海夏季风的爆发具有指示意义，揭示了南海地区跨赤道季风环流建立的动力过程。南海夏季风爆发主要发生在每年的第 28 候（5 月 16—20 日），以往的南海夏季风爆发研究主要基于对流层低层的大气环流和下垫面热状况研究南海夏季风的爆发机理（例如，西太平洋副高的东西移动和局地海温变化的影响）。利用 NCEP/DOE R2 大气再分析资料计算和分析了南海夏季风爆发前后的大气热动力过程，发现南亚高压在第 27 候的向东移动伸入南海上空很可能是导致南海夏季风爆发的主要诱因。第 27～28 候，随着南亚高压的东伸加强，南海上空出现正位涡平流，相应地局地高空上升运动加强，其导致的抽吸作用令低空西太平洋副高开始东撤出南海，季风槽和季风对流逐步建立；随着南海季风对流的不断加强，南亚高压持续东伸发展，与之对应的高空暖中心和近海面暖中心的空间位相叠加，南海地区的对流层温度垂直层结被破坏，从而满足了环流的角动量守恒条件，令季风环流的下沉支能够穿越赤道到达南半球，最终引起了跨赤道的季风经向环流，将南、北半球季风系统相联，南海夏季风最终于第 29 候完全爆发（图 4）。（刘伯奇）

2 气候系统模式研发

2.1 东亚夏季降水结构模拟及其影响因子：2种不同类型大气模式对比

当前气候模式对东亚地区降水模拟存在普遍误差：东南部气候态降水偏少，北部地区气候态降水偏多；模式普遍高估降水频次，低估降水强度；对陆地午后日峰值的模拟普遍提前。研究指出，这些误差并非孤立存在，而是具有一定的内在联系。

研究对比了CAM5和SPCAM5模式的模拟结果，后者可以显式模拟次网格云降水等物理过程。研究指出，与大部分气候模式类似，CAM5具有以上误差特点。其中，CAM5对华南地区午后以16:00—17:00为主的峰值模拟偏早，主要集中在14:00这一午后不稳定最强的时刻。与此对比，SPCAM5缓解了华南地区的降水负偏差问题，降低了平均小时降水频次，提高了降水强度。同时，在以午后降水峰值主导的地区，SPCAM5延迟了降水峰值时刻。

为了明确造成两类模式模拟差异的原因，研究对模式的大尺度变量进行了小时尺度的源汇分析。针对Q1-Qrad的分析指出，SPCAM5在对流加热随时间演变的刻画上具有更明显的倾斜结构。针对Q2的分析指出，SPCAM5对降水峰值前的近地层变干信号具有更明显的表征。这反映了SPCAM5对于午后对流发展的渐进过程，即对流由浅对流至深对流的转换过渡阶段具有更合理的描述。

结合二者结果可以得出以下的物理图像。在CAM5中，每当有午后的不稳定能量出现，模式作出消耗不稳定能量的表现，开始降水，对流无法累积到一定的强度。因此，模式中以频繁的弱降水主导，且降水峰值提前，在气候平均态上表现为降水量偏低。在SPCAM5中，当有午后不稳定能量出现，模式不会立刻产生消耗不稳定能量的行为。模式能够模拟出对流由浅对流发展为深对流的演变阶段。浅对流云的存在使得模式不会快速形成降水，同时有助于不稳定能量的累积。当不稳定能量累积到一定程度时，降水峰值才出现。因此，降水峰值滞后，且峰值时刻降水量增强，降水频次降低，强度提高，在气候平均态上表现为降水量增多。因此，对流由浅至深转化这一过程的合理模拟，使得SPCAM5能够在一定程度上改善东亚地区降水在不同时间尺度上的特征。此外，由于降水峰值时刻对流更强，直接带来的一个副效应是峰值时刻的大尺度上升运动在SPCAM5中更强，这反映了次网格尺度过程对大尺度动力环流的影响。（张祎）

2.2 青藏高原陡峭地形处降水的模拟误差调节

针对大气环流模式在东亚降水模拟存在的一大顽疾"高原南坡陡峭地形区的降水偏差"，本研究发现这一问题对大尺度动力过程更为敏感。研究通过设计一组敏感性试验考察了这一问题。第1组试验为标准AMIP型气候积分的控制试验。第2组试验为敏感性试验，其中，人为的引入了一个与空气散度成正比的水汽散度项。这一项的引入使得空气辐散区的水汽被驱散，辐合区的水汽被堆积，与地形周边的散度效应恰好成对应关系。

通过长期气候积分发现，这一项的引入减少了模式在陡峭高地形区原本高估的降水，增强了模式在低地形区原本低估的降水，对模式在陡峭地形附近的降水误差呈抑制作用。此外，模式整体的降水频次–强度结构亦发生了变化，在陡峭高地形区的降水频次和强度值都有所降低。并且，总降水的主要变化来自于格点尺度降水和水汽含量的改变。这说明大尺度动力因子改变了局地的水汽结构，从而达到改变降水场模拟的结果。在非绝热水汽倾向上，这一水汽散度项表现为对高地形区原始正平流倾向的抑制，而对低地形区原始平流倾向的增加，这与模式气候积分结果相符。

为了能够更好地考察这一水汽散度项对模式的影响，进一步开展了气候模式的短期数值预报试验。该试验通过对模式进行短期的初始化预报构造模式的气候态，以考察短期误差和模式长期气候误差的

联系。研究指出，这一散度项所带来的影响在很短的时间内即形成，是一个快过程变化。由于地形处的空气辐合辐散，高地形处的水汽随着该项的引入被"驱散"，低地形处的水汽随着该项的引入被"补充"。陡峭地形处水汽随大尺度动力因子的改变，影响了模式在该地区的降水特征。这一研究为消除模式在青藏高原地区的模拟误差提供了依据。研究也揭示出大尺度动力因子对降水的影响。（张祎）

2.3　正二十面体大气模式发展：传输与浅水方程求解器

为了适应面向未来的全球高分辨率大气模拟，研究发展了基于正二十面体剖分后形成的球面准均匀网格上的大气模式求解器。球面网格通过对一个规则正二十面体的三角边进行逐次等分所形成，并采用 Voronoi-Delaunay 球面拓扑划分构建为非结构型网格（区别于结构型正二十面体网格，不存在统一的拓扑规则）。求解器采用 Arakawa-C 网格，即质量位于单元格中心，正交预报速度位于单元壁。在罗斯贝半径得以分辨的前提下，C 网格由于对散度模态的模拟优势，非常适合于模拟以散度模态为主导的高分辨率下的大气运动。同时，不同于 Z 网格，C 网格无需求解椭圆方程，避免了全局通信，便于大规模并行。

传输和浅水方程包含了三维静力原始方程的水平部分。首先在正二十面体网格上构造了一个守恒两步保形平流方案（TSPAS），该方案是对 Yu (1994 年)两步保形平流方案在非结构网格上的有限体积推广。通过构造一个合适选取的预估参数，该方案可以灵活选择 Lax-Wendroff 和迎风格式以实现在保持精度的前提下的正定平流传输。本研究还构造了国际上广泛使用的通量纠正格式（FCT），并采用多个球面传输算例（刚体平移测试、变形流场测试等）对比了 TSPAS 和 FCT 方案。结果显示，两种方案都能够很好地实现非结构网格上的正定平流传输，TSPAS 对单调性保持略佳，而 FCT 对信号峰值的保持略佳。本研究还指出了 TSPAS 和 FCT 在构造理念上的差异。

在传输方程的基础上，进一步构建了基于正二十面体 C 网格的球面浅水方程求解器。构造浅水方程，模式应满足一些重要且潜在的物理约束。对于广义形状的非规则 C 网格，其中重要的一点是对与预报风场成正交的科氏力项的近似，以避免切向力产生虚假的能量源汇。采用可严格保持科氏力能量中性的矢量重构算法，以及保证能量转换精确到时间截断误差的基本算子，构造了总能量守恒至时间精度的浅水方程求解器。通过采用多种时间积分方案，证实了这一求解器在能量方面的可靠性。该研究工作作为后续研发奠定了基础。（张祎）

2.4　一种可客观评估模式降水的新方法及其适用性检验

在当前全球大气环流模式分辨率尚不足以分辨云动力尺度云雨演变过程的情况下，由参数化方案计算得到的模式降水只能表征模式格点尺度的平均降水。降水存在极大的时空非均匀性，这使得模式模拟降水与台站观测降水（固定点）和高分辨率卫星反演降水（小网格内的平均情况）难以进行直接比较，这一问题在评估降水小时尺度特征时会更为突出。本研究提出的应用一种新定义的区域降水事件（RRE）方法是客观评估模式对小时尺度降水特征模拟能力的有效手段。为验证该方法的适用性，首先比较了台站观测、小时融合降水产品（CMPA-Hourly）和两套常用卫星产品再现的中国中东部地区暖季（5—9 月）小时降水特征。结果表明，与单站或单点比较不同的是，采用区域降水事件的方法比较不同源资料可以得到基本一致的降水频次与强度的空间分布特征，只是卫星反演降水在量值上与台站观测存在差异。基于单站或单点发现的卫星降水易于高估降水频次而低估降水强度的问题在使用该方法时有显著改进。同时，不同源观测资料均显示出暖季区域降水系数（RRC）分布的南北差异，即长江流域以南 RRC 相对较小，而以北区域则相对较大，表明该方法合理反映了暖季降水特性的区域差异，我国南方地区暖季对流降水频繁，而北方地区系统性的区域性降水更为频繁，这与此前研究的结论亦相一致。从日变化的角度看，卫星反演的降水频次和强度的日变化与台站观测降水也较为一致，基于区域降水事件考察不同资料间差异时未发现卫星资料对午后降水峰值的明显高估。整体而言，融

合降水资料对中国中东部地区小时降水特征的再现要明显优于卫星反演降水。除了不同源资料的一致性外，该方法也能给出不用源资料对降水特性再现的差别。分析发现，在中国中东部地区，代表有限区域内降水空间分布的RRC在夜间至上午达日最大值，表明这一时段区域内降水分布最为均匀。在大部分地区，RRC达到日峰值的时间较区域降水事件强度的峰值时间滞后几个小时，表征了局地对流向层云降水转变的过程。在午后RRC较小，表明局地对流活动频繁，而对午后局地对流探测能力的不同可能是导致不同源资料对午后降水估计存在差异的重要原因之一。由于区域降水事件反映的是有限区域内的降水整体特征，采用该方法对不同源资料进行比较分析时卫星资料高估午后降水的特征不明显，以区域降水事件来分析卫星降水产品小时尺度降水特征亦具有更高的可信度。研究结果表明，区域降水事件是一种可用于比较不同源降水资料小时尺度特征的更合理方法，后续研究将进一步应用该方法评估数值模式模拟的云和降水时空变化特征（图5）。（陈昊明）

3 极地气候研究

3.1 夏季北冰洋中心大气边界层垂直结构与海冰范围变化的关系

最近的研究指出，北极海冰减少加强了北极大气边界层中海–冰–气相互作用，特别是秋季至初冬季海/气热通量的增加和边界层稳定度的下降。1999年以来中国实施了6次北冰洋科学考察。考察期间，开展了对大气垂直结构探测和海–冰–气相互作用的观测试验，使我们对北极浮冰区不同海冰密集度的大气边界层特征有了初步认识。研究指出，北极海冰区的大气逆温层能有效地阻碍大气与冰面之间的热量及物质交换。北冰洋大气边界层可分为稳定型、不稳定型和多层结构等类型，并发现来自高空较强的暖湿气流与冰面近地层冷空气强烈相互作用会形成强风切变和逆温、逆湿过程，从而导致北冰洋高纬度地区的大块海冰破裂。随着北极海冰的持续减少，2008年夏季中国第3次北极科学考察队到达北冰洋85°N海域，第4次北极科学考察队到达北极点附近（88.41°N），2012年第5次和2014年第6次北极科学考察队都到达了80°N以北冰区，使我们得以在北冰洋中心区冰站获取了GPS探空资料，为研究北冰洋高纬度对流层和边界层结构提供了重要基础。Ma等（2011年）和Bian等（2011年）分析了对流层和边界层逆温强度的变化特征，对北冰洋大气层边界层高度的变化特征提出了新认识。本研究利用中国第4～6次北极科学考察队获得的北极探空资料，对比分析北极夏季海冰面积变化对大气边界结构的影响，为研究北极海冰变化对大气环流的影响机理提供观测事实。

为了探索2010、2012和2014年夏季大气垂直结构、边界层高度参数差异的原因，分析了1979—2014年9月1000 hPa和850 hPa温度与海冰范围的变化关系，揭示出新的统计事实和它们的紧密关系，为深入研究北极海冰变化在全球气候变化中的作用提供了重要依据。主要结果如下：

（1）2012年与2010和2014年夏季北冰洋中心区的对流层顶、边界层高度、温度递减率及风速和风向的垂直结构均在1 km以下存在明显差异，2010年和2014年近地面存在明显的逆温结构，2012年逆温层却很少出现，其过程与探测区域周围存在无冰海域和近地层气流较强的混合作用有关。2010和2014年夏季边界层高度与逆温强度呈显著的对数关系，相关系数分别为0.81和0.92，表明逆温强度越强，边界层高度越低。2012年二者对数关系相对离散，相关系数为0.56，边界层高度为690 m，明显高于2010年和2014年的边界层高度，反映了9月海冰范围的年际变化对大气边界层结构有重要影响。

（2）北极大气垂直结构除了受大尺度天气过程的影响外，与海冰覆盖范围的变化有直接关系：北冰洋中心区夏季的海冰面积越大，稳定层结的天气越多；反之对流性的天气增多。通过分析1979—2014年9月北极海冰范围与1000 hPa和850 hPa温度变化的关系，发现近30年北冰洋中心区1000 hPa和850 hPa的温度变化呈显著的升高趋势，变化速率分别为1.3 ℃/10a和0.81 ℃/10a，与海冰范围呈负显著相关，相关数分别为0.83和0.74。结果表明，北极海冰减少，能够引起1000～850 hPa高度的大

气层增温，这是海–冰–气相互作用的动力和热力输送结果。（丁明虎）

3.2 对2008—2013年间南极Dome A 表面物质平衡的再评估

2004/2005年，第21次南极考察在Dome A顶点安装了自动气象站，用于观测该区域的气象参数；2007/2008年，中国第24次南极考察队在Dome A 30 km×30 km区域内布设了49个花杆，用于测量该地区的数字高程、冰流速和表面物质平衡；2010/2011年和2012/2013年分别对各观测站点进行了复测。通过蒙特卡洛模拟，证明局部及区域尺度范围内表面物质平衡至少需要利用12 ～ 20个花杆点建立可靠的估计，因此本研究的观测方案可信度强。通过花杆观测数据计算了该区域的净物质平衡，为（22.9 ± 5.9）kg/（cm²·a），远低于包含Dome C、Dome F和南极点在内的南极冰盖其他地区。结合气象站观测数据利用奥布霍夫–莫宁模型，模拟了该区域的升华和凝华状况，发现Dome A区域的升华损耗为（2.22 ± 0.02）kg/（cm²·a）、凝华损耗为（1.37 ± 0.01）kg/（cm²·a），即大约有14.3%的降雪量通过凝华形式损耗，远高于南极冰盖平均状况，这可能与该区域盛行下沉气流有关，对南极冰盖变化和雪冰芯研究具有重要的指示意义。另外研究发现，由于地形导致的下降风的原因，Dome A西部地区的冰盖雪密度与表面物质平衡要高于其他区域。本研究还建立并分析了Dome A数字高程模型，确认2个山峰穹顶均可以作为东南极冰盖的顶峰，修正了前人的结果。（丁明虎）

3.3 气候模式和地面观测中南极冰盖表面质量平衡的对比

本研究利用3265个多年平均的站点观测结果和29个逐年观测的观测数据对近些年出现的再分析资料和区域气候模式产品（ERA-Interim、JRA-55、MERRA、PMM5、RACMO2.1和RACMO2.3）在南极地区物质平衡的空间分布和年际变率进行检验。

自第1次国际极地年（1957—1958年）以来，世界各国科学家积极参与国际横穿南极科学考察计划（ITASE）和南极物质平衡和海平面研究计划（ISMASS），特别是国际极地年（2007—2009年）的一系列科学计划，对南极冰盖主要流域进行了大量表面物质平衡实地测量，采用的方法主要有花杆、超声高度计（雪深仪），雪坑、冰/雪芯和探地雷达法。Vaughan等 (1999年) 最早对表面物质平衡观测资料进行了编撰，建立了表面物质平衡空间数据库，但是其中包含了很多不可靠的数据，影响了表面物质平衡的空间分析及气候模式结果验证，为此Magand等（2004年)建立了南极积累率实测数据质量控制标尺。基于该标尺，Favier等（2013年）对收集整理的南极物质积累率数据集进行了甄别筛选，在此基础上更新了该数据库。本研究广泛收集了冰芯、雪坑、自动气象站、物质平衡花杆观测资料，特别是国际极地年（2007—2009年）以来的最新研究成果，对Favier等（2013年）编撰的南极冰盖表面物质平衡数据集进一步更新，建立了具有3550个位置观测数据的经质量控制的南极冰盖多年平均表面物质平衡空间数据库。该数据库空间分布极不均匀，南极内陆和海岸许多区域仍然是数据空白区。

ERA-Interim、MERRA、CFSR、JRA-55和NCEP-2模式均能较好地模拟南极冰盖表面物质平衡大尺度空间变化，与实测结果相关系数超过0.75，但是模拟表面物质平衡中尺度变化能力有限，如在昭和站–Dome F断面，中山站–昆仑站断面，兰伯特冰川流域等 。所有这些再分析资料较好地再现了很多海岸区域表面物质平衡梯度，但是其模拟值通常偏高。JRA-25模式显著高估了东南极高原表面物质平衡，而ERA-Interim过低估计了表面物质平衡。总体上来说，由于对边界层潜热通量的高估，NCEP-2过低估计了表面物质平衡。MERRA、JRA-55和CFSR模拟结果与观测值比较一致，但是值得注意的是，所有再分析资料没有包含风吹雪导致的消融过程，说明这3种再分析资料在一定程度上高估了表面物质平衡。

1979—2012年，冰盖尺度上NCEP2、JRA-25、JRA-55、MERRA模拟的表面物质平衡呈显著增加趋势。CFSR和ERA-Interim模拟的表面物质平衡没有显著的变化趋势，这与基于冰芯记录重建的南极冰盖表面物质平衡结果一致。ERA-Interim线性变化趋势显著性水平达不到0.1检验水平的区域最

为广泛。区域尺度上，尽管不同的再分析资料表面物质平衡趋势大小和方向差异显著，但是 NCEP2、MERRA、JRA-25 和 JRA-55 模拟的表面物质平衡在毛德皇后地海岸区域呈异常显著上升趋势，这与该区域的冰芯显示 1989—2007 年积累率呈下降趋势相左。在东南极 70° ～ 170° E 区域内，再分析表面物质平衡变化资料趋势相近，如兰伯特冰川区和威尔克斯地岛中部呈上升趋势，而威尔克斯地岛西部和维多利亚地岛呈下降趋势。需要指出的是，JRA-25 和 NCEP2 在威尔克斯地岛中部过高的上升趋势（＞200 mm/a）令人怀疑。此外，除 ERA-Interim 模式外的 Law Dome 显著上升趋势的再分析表面物质平衡与冰芯记录结果相矛盾。在西南极冰盖，1989—2009 年，再分析表面物质平衡通常呈不显著变化趋势。在艾尔斯渥兹地（Ellsworth Land），ERA-Interim、CFSR、JRA-55 和 MERRA 模拟的表面物质平衡呈上升趋势，这得到了该区域附近 Gomez 冰芯记录的证实。所有再分析资料很好地再现了与罗斯海海冰范围增加有关的威尔克斯地岛表面物质平衡下降趋势。

从格点尺度上线性回归趋势来看，PMM5、RACMO2.1 和 RACMO2.3 模拟的表面物质平衡具有显著性（$p < 0.05$）线性变化趋势的区域都很有限。RACMO2.1 模拟的表面物质平衡显著性变化趋势区域主要集中在毛德皇后地海岸区域和威尔克斯地岛部分区域，而 RACMO2.3 模拟显著变化趋势区域集中在威尔克斯地岛和东南极内陆的部分区域，然而这些显著趋势区域并没有得到冰芯记录结果的证实。1979—2012 年，南极冰盖尺度上 PMM5 和 RACMO2.1 模拟的表面物质平衡没有显著的变化趋势，但是 RACMO2.3 呈显著的下降趋势。29 个具有区域代表性表面物质平衡实测序列与相应的 PMM5、RACMO2.1 和 RACMO2.3 模拟结果的相关分析表明，有 15 个点 RACMO2.3 模拟结果与实测表面物质平衡序列显著相关，而 RACMO2.1 和 PMM5 模拟结果与实测显著相关的点少于 10 个。总的来说，与再分析资料相比，区域气候模式模拟的南极冰盖表面物质平衡年变化趋势可信度不高，这很可能是其内部由于没有同化观测数据限制任由模式自由演化导致的。未来在这些模式长期积分中引入松弛逼近方法或谱逼近方法等进行动力降尺度有望改进模拟表面物质平衡年际变化的能力。（丁明虎）
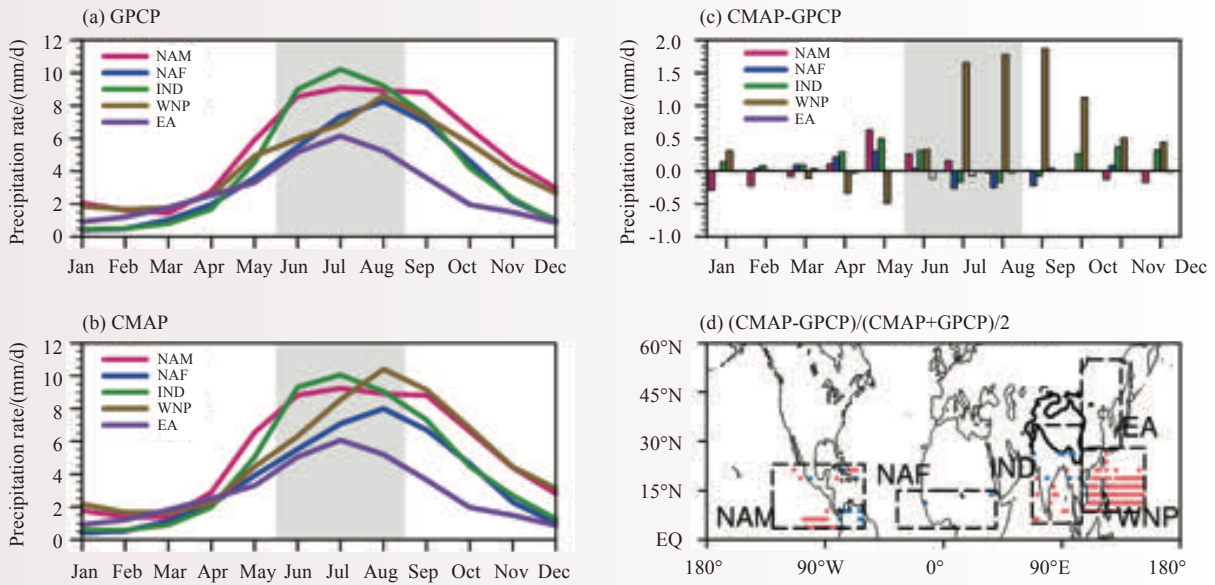
图 1　GPCP（a）和CMAP（b）资料计算的北半球五大季风区气候平均降水的季节循环特征，以及两者季节循环的绝对偏差（c）和两者夏季降水的相对偏差（d）（红点表示＞30%；蓝点表示＜–30%，虚线框表示两者一致的季风区范围，黑色等值线表示1.5 km的青藏高原范围）

Fig. 1　Climatological seasonal cycle of precipitation (1979–2014) calculated based on (a) GPCP and (b) CMAP (unit: mm d^{-1}) products over the five monsoon regions as marked in (d). (c) Absolute difference in the averaged seasonal cycle between the two products (CMAP minus GPCP; unit: mm d^{-1}). (d) Relative difference of the averaged summer precipitation between the two products (0.5 × (CMAP−GPCP) × (CMAP + GPCP)$^{-1}$; red: >30%; blue: <−30%). The black contoured region is the 1.5 km topography of the TP
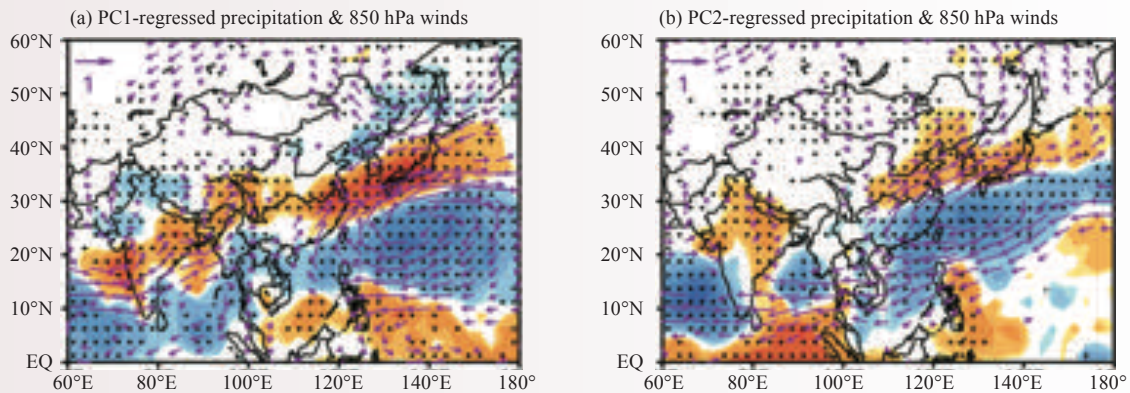
图 2　与东亚夏季风（EASM）气候季节内振荡（CISO）前2个主成分有关的季节内降水（阴影，mm/d，打点区表示通过90%信度检验）和850 hPa风场（矢量，m/s，通过90%信度检验的部分）的回归场

Fig. 2　Regressed intraseasonal anomalies of precipitation (shading, mm d^{-1}; values exceeding 90% confidence level are stippled) and 850 hPa winds (vectors, m s^{-1}; vectors exceeding 90% confidence level are plotted) associated with the first two MV-EOF modes of winds related to EASM CISO
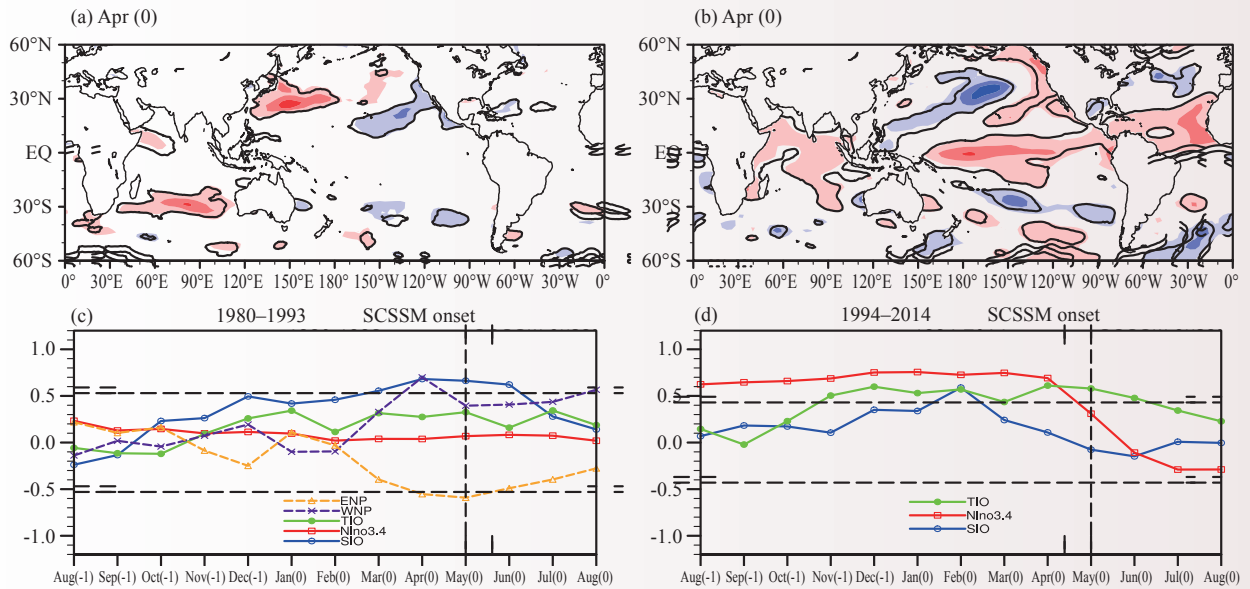
图 3 不同年代影响南海夏季风爆发时间的春季海温关键区（K）(a，b)及其季节变化(c，d) (a，c：1980—1993年；b，d：1994—2014年)

Fig. 3 (a, b) Spring SSTA (K) and (c, d) its seasonal evolution (represented by the correlation coefficient between the regional mean SSTA and the SCSSM onset time) associated with the SCSSM onset time during (a, c) 1980–1993 and (b, d) 1994–2014, respectively
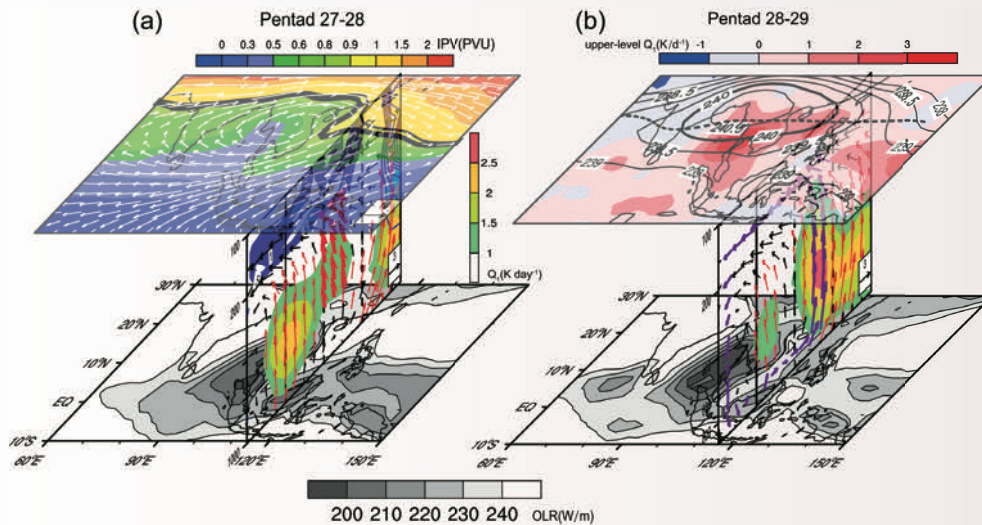
图 4 南海夏季风爆发进程示意：(a)第27～28候（上：360 K等熵位涡（阴影，PVU）和风场（矢量，m/s）；中：非绝热加热（阴影，K/d）、正位涡平流（等值线，10^{-5} PVU/s）和垂直运动（矢量，加粗箭头表示高空上升运动，10^{-2} Pa/s）；下：OLR（W/m²））；(b)第28～29候（上：对流层上部非绝热加热（阴影，K/d）和气温（K）；中：非绝热加热（阴影，K/d）和季风经圈环流（矢量，紫色箭头表示跨赤道季风环流圈，m/s）；下：OLR（W/m²））

Fig. 4 Schematic diagram of the SCSSM onset process. (a) Pentad 27–28 (upper panel: 360 K isentropic potential vorticity (shading, PVU) and winds (vectors, m s^{-1}); middle panel: diabatic heating (shading, K day^{-1}), positive advection of potential vorticity (contours, 10^{-5} PVU s^{-1}) and vertical motion (vectors, heavy ones represent the upper-level ascending, 10^{-2} Pa s^{-1}) over the SCS (averaged along 110°–120°E); low panel: OLR (W m^{-2})). (b) Pentad 28–29 (upper panel: diabatic heating (shading, K day^{-1}) and air temperature (contour, K) in the upper troposphere (averaged bween 400–200 hPa); middle panel: diabatic heating (shading, K day^{-1}) and meridional monsoon circulation (vectors, purple ones are for the cross-equatorial monsoon circulation, m s^{-1}); low panel: OLR (W m^{-2}))
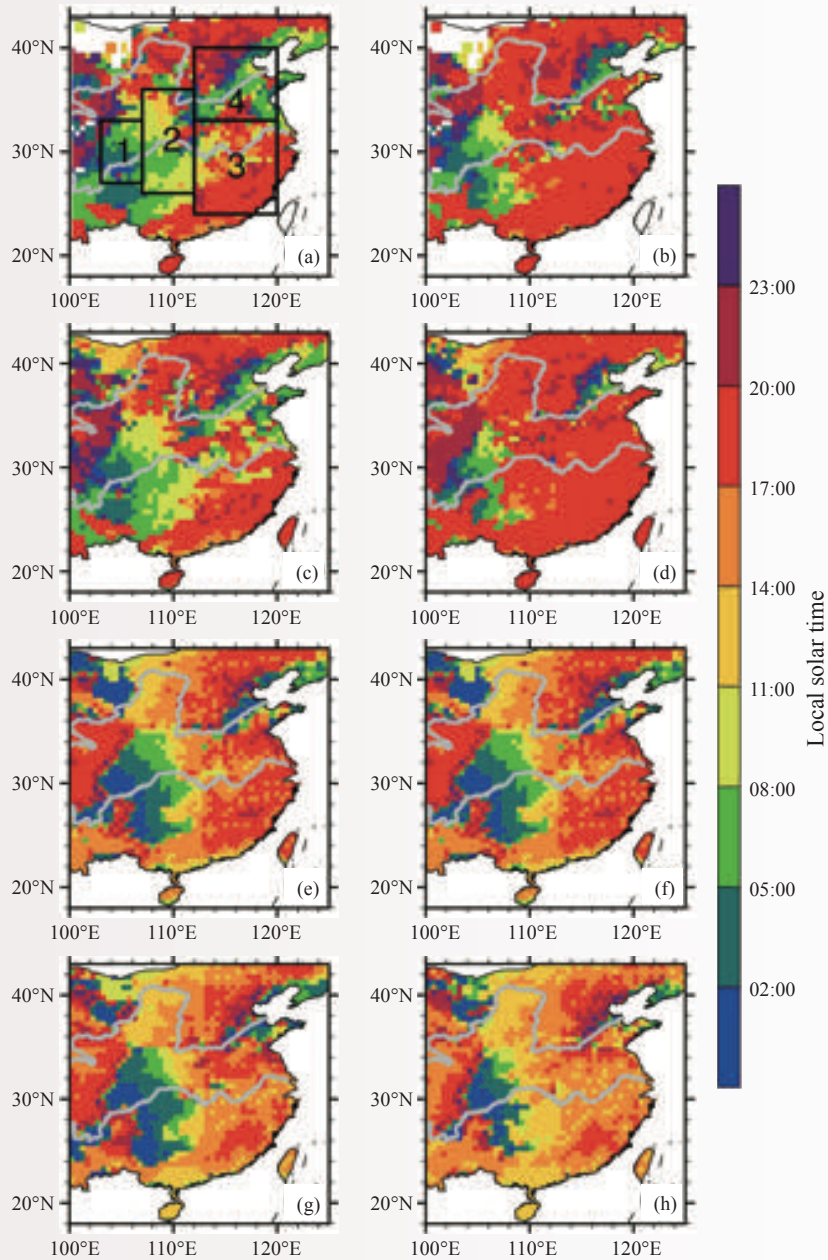
图 5 2008—2013年暖季（5—9月）平均的区域降水事件强度（左）和频次（右）的日峰值位相（当地时间）分布（从上往下依次为台站观测(a～b)，CMPA-Hourly融合降水(c～d)，TRMM 3B42(e～f)和CMORPH(g～h)；灰色实线为长江和黄河的位置）

Fig. 5 The diurnal phase (local solar time) of the 2008−2013 warm season (May−September) mean intensity (left column) and frequency (right column) of RRE from rain gauges (a-b), CMPA-Hourly (c-d), TRMM (e-f) and CMORPH (g-h) products. The locations of the Yellow and Yangtze rivers are marked by gray lines

Progress in Climate System and Climate Change Research

In 2016, the Institute of Climate System (Polar Meteorology) has achieved remarkable improvements in the fields of (1) theory and methodology of climate prediction, (2) development of climate system model, and (3) polar climate.

1 Theory and methodology of climate prediction

1.1 The inconsistency of interannual rainfall variability of boreal summer monsoon between GPCP and CMAP precipitation products and an improvement scheme

This work has revealed the discrepancy between GPCP and CMAP precipitation products in terms of the seasonal and interannual variations of boreal summer monsoon rainfall, and the arithmetic mean of the two products is shown to reduce such uncertainties. GPCP and CMAP precipitation products with global coverage and long record length have been widely used to monitor the climate status and study the climate variability. Our recent work has pointed out that although the GPCP and CMAP products are able to describe the seasonal cycle of rainfall in the boreal summer monsoon region, the absolute error between them is still evident. In particular, the difference in rainfall amount is largest from May to October in the western North Pacific (WNP) monsoon region, presenting more summer and autumn rainfall in the GPCP product. As to the spatial distribution of the climatological mean summer precipitation, the most prominent difference between the two datasets appears over the ocean portion in the WNP, North Africa (NAF) and Indian (IND) monsoon region. It is likely due to the controversial use of atoll gauges over the tropical Pacific in CMAP.

In the interannual timescale, the interannual variabilities of summer precipitation in GPCP and CMAP products are generally consistent over the boreal summer monsoon region, but the evident discrepancy appears over the IND and NAF monsoon regions. The consistency between CMAP and GPCP has increased in the recent decades, especially over the NAM and IND monsoon regions. Further analysis shows that the arithmetic mean of CMAP and GPCP products is an effective method to reduce the uncertainties. The improvement is mostly evident over the IND monsoon region during 1979–1997 and the NAF monsoon region during 1998–2014 (Fig.1). (Zhu Congwen, Liu Boqi)

1.2 The climatological intraseasonal oscillation in the East Asian summer monsoon and its possible mechanisms

The existence of climatological intraseasonal oscillation (CISO) in the East Asian summer monsoon (EASM) has been validated in this work. We have also revealed the CISO-related primary circulations and their coupling process, as well as its association with the EASM precipitation on the intraseasonal timescale.

The climatological intraseasonal oscillation (CISO) of the East Asian summer monsoon (EASM) is characterized by the vertical and meridional interactions of monsoon circulation, with a stepwise northward shift of front-related rain belt during boreal summer, particularly from May to August. To reveal the vertical structure and the internal modes of the EASM CISO, as well as their interaction with the surrounding SSTs, we conducted harmonic and multivariate empirical orthogonal function (MV-EOF) analyses on the climatological daily winds, rainfall, diabatic heating, and SST for the period 1981–2010. The EASM CISO exists not only in diabatic heating, primarily contributed by condensational heating, but also in rainfall and circulation. The

EASM CISO mainly results from the asymmetric response of the land-sea thermal contrast over East Asia to annual solar forcing. As a result, the center of the CISO variability is located over eastern China and the western North Pacific. During the EASM season, the Q1 is mainly associated with condensational heating and is centered over the WNP and East Asia. Thus, the horizontal gradient of Q1 produces a negative vorticity source to the north and east of the Q1 center. The resultant local background ascending motion favors the initiation of the CISO. Moreover, the EASM CISO can also be initiated and maintained by the different phasings of various diabatic heating (Q1) components. Namely, the CISO is initated by changes in surface sensible heat flux, which modulates the atmospheric convective instability, and thus the variations of monsoon convection and the condensational heating. The changes in condensational heating in turn would affect land surface temperature through radiative forcing. This eventually would lead to changes in surface sensible heating flux, and so on.

Results based on the MV-EOF analysis reveal that the first two modes of the EASM CISO are mainly characterized by the coupling of the Mongolian Cyclone (MC) around Lake Baikal at 850 hPa, the WNP subtropical High (WNPSH) at 500 hPa, and the South Asian High (SAH) over the Tibetan Plateau (TP) at 200 hPa. The first leading mode shows a simulteneous enhancement of the MC, WNPSH, and SAH, accompanied by a tripole rainfall anomaly of the strong Meiyu and Baiu fronts around the lower reaches of the Yangtze River and southern Japan, whereas the rainfall was suppressed over northeastern Asia and the WNP. The second leading mode, which indicates the eastward and northwestward propagation of the enhanced MC and WNPSH with the weakened SAH, is associated with a dipole of the rainfall anomaly, with abundant and deficient rainfall over the northeastern and southeastern Asia-Pacific regions, respectively. In this study, we also performed the AGCM simulations forced by daily SST from 1981 to 2010 using the ECHAM5.4 at the resolution of T63L31. The results show that the simulated first CISO leading mode is consistent with the observed, suggesting the critical role of seasonal variations of daily SST in the EASM CISO over the Asia-Pacific region. However, the AGCM runs failed to realistically reproduce the second CISO leading mode. The MC CISO is well reproduced by the AGCM, but the simulated CISO of the WNPSH and SAH is poor compared with the observations likely owing to the lack of feedback of SST to the atmospheric forcing (Fig. 2). (Zhu Congwen Liu Boqi)

1.3 The difference of interannual variation of South China Sea summer monsoon onset and its related SSTs before and after 1993/1994

We have found the distinct differences of interannual variation of South China Sea summer monsoon (SCSSM) onset before and after 1993/1994. It is shown that the SSTA in the southern Indian Ocean in spring and the ENSO in previous winter are key factors in determining the SCSSM onset time before and after 1993/1994, respectively.

Based on their distinct thermodynamic field and circulation structures, we have identified different behaviors of the interannual variability of SCSSM onset in the periods 1980–1993 and 1994–2014. Our results suggest that the interannual variability of the SCSSM onset during 1980–1993 is characterized by rainfall anomalies over the northern SCS and evident anomalous zonal wind in the lower troposphere. This is defined as type-I SCSSM onset, presenting a closer association with subtropical systems. During 1994–2014, the interannual variability of the SCSSM onset is determined by the anomalies of tropical convection and the upper-tropospheric zonal wind, which is herein referred to as type-II SCSSM onset. As a result, the vertical coupling between the upper- and lower-level circulations differs between type-I and type-II SCSSM onsets on the interannual time scale.

The interannual variability of SSTAs in boreal spring is also distinct in the two types of SCSSM onsets. In the type-I SCSSM onset, the interannual variability of the SCSSM onset time is controlled by the spring

SSTAs in the South Indian Ocean (SIO, 40°–20°S, 40°–110°E) during 1980–1993, whereas it is affected by the winter ENSO and spring Tropical Indian Ocean (TIO) SSTAs in the type-II SCSSM onset during 1994–2014, on the interannual time scale. In the 1980–1993 period, the warm SIO SSTAs in spring can delay the SCSSM onset. In this process, the warm SIO SSTAs first produce a large-scale meridional dipole pattern, with anomalous convergence over the SIO and divergence over the SCS in the lower troposphere, bridging via the cross-equatorial flow near 90°E. Then, an anomalous anticyclone forms over the northern SCS, leading to the anomalous descent over the northern SCS and ascent over the land to its north. Subsequently, the vertical easterly shear and meridional land-sea thermal contrast weaken such that they suppress convection associated with the monsoon onset over the SCS and the SCSSM onset is postponed. During the 1994–2014 period, both winter ENSO events and spring TIO SSTAs are closely related to the interannual variability of the SCSSM onset time. A warm ENSO event during winter can induce the warm TIO SSTAs in the following spring via the atmospheric bridge. Subsequently, the meridional temperature gradient (MTG) in the mid- to upper-troposphere weakens over the SCS due to the tropical stationary Kelvin wave stimulated by the warm TIO SSTAs, and this delays the seasonal transition of the MTG from winter to summer. In addition, the anomalous large-scale westerly in the upper troposphere blows from the TIO to the SCS, with the anomalous ascending and descending branches over the TIO and SCS in the tropics, respectively. Consequently, the anomalous descent and weakened zonal easterly shear could suppress convection associated with the monsoon onset over the southern SCS, leading to the late onset of the SCSSM.

The present results also imply an abrupt change in the relationship between ENSO and the timing of the onset of the SCSSM before and after 1993/1994. In fact, the El Niño events of previous winters are followed by a late onset of the SCSSM in both periods, and the closer association between ENSO and the SCSSM onset time and the early SCSSM onset in the recent period after 1993/1994 may be attributed to the more frequent La Niña events, which may be related to the interdecadal adjustment of the ENSO after 1993/1994 (Fig. 3). (Liu Boqi)

1.4 The seasonal evolution of the South Asian High is a possible precursor for the onset of the South China Sea summer monsoon

The seasonal evolution of the South Asian High (SAH) has been suggested to be a precursor for the South China Sea (SCS) summer monsoon onset. We have also revealed the dynamical process that is responsible for the establishment of the cross-equatorial monsoon circulation over the SCS.

The averaged onset time of the SCS summer monsoon (SCSSM) is pentad 28 (16−20 May). Previous studies on the SCSSM onset have focused on the influences of the lower tropospheric circulation and the underlying thermal condition on the SCSSM onset. In the present study, we have used the NCEP/DOE reanalysis data to diagnose the thermal and dynamical processes during the SCSSM onset. It is found that the major incentive for the SCSSM onset is the eastward extension of the SAH to the upper troposphere of the SCS. During Pentad 27−28, the positive potential vorticity advection takes place over the SCS, along with the eastward development of the SAH. Accordingly, the upper-level ascending motion is enhanced, making the low-level western North Pacific subtropical anticyclone to withdraw eastward away from the SCS, followed by the initial formation of the monsoon trough and the onset of monsoon convection. Later, the monsoon convection over the SCS deepens gradually, resulting in the continuous eastward development of the SAH. The near-surface warm SST is overlaid by the upper-level warm center associated with the SAH. Such a thermal configuration implies a destruction of the vertical thermal stratification over the SCS, which satisfies the condition of absolute angular momentum conservation (AMC). As a consequence, the ascending motion over the SCS is able to cross the equator and reaches the Southern Hemisphere, and finally induces the closed cross-

equatorial monsoon circulation that bridges the monsoon systems in the two hemispheres on Pentad 29 after the SCSSM builds up completely (Fig. 4). (Liu Boqi)

2 Development of climate system model

2.1 Comparing simulations and impact factors of precipitation characteristics over East Asia in two different atmospheric models

Current climate models have common biases in simulating precipitation over East Asia. They tend to underestimate the precipitation amount over southeastern China, overestimate the precipitation amount over northern China, and overestimate the precipitation frequency while underestimate the precipitation intensity, and often simulate the afternoon continental precipitation peak too early. These biases are not isolated problems but intimately correlated.

The study compared the CAM5 and Super-Parameterized CAM5 (SPCAM5) simulations of summer precipitation characteristics. SPCAM5 can explicitly simulate cloud and precipitation processes in a GCM's grid column. Results show that CAM5 posesses those aforementioned biases. Especially, over southeastern China, the precipitation peak in CAM5 appears at around 14:00 local solar time, when the unstable condition reaches the maximum. However, in the observation, the precipitation peak occurs at around 16:00–17:00. In contrast, SPCAM5 alleviates the negative precipitation biases over South China, reduces the precipitation frequency while enhances the precipitation intensity. Moreover, over regions dominated by the afternoon precipitation peak, SPCAM5 delays the precipitation peak time by a few hours, closer to observtions.

To figure out reasons for these differences in the model performances, we conducted a source/sink budget analysis by calculating the residuals of large-scale state variables. Results from the Q1-Qrad analysis indicate that SPCAM5 more evidently simulates the progressive evolution of convective heating, which exhibits a tilting structure in the pressure-time transect. The Q2 analysis indicates that SPCAM5 more evidently simulate the drying signal occurring before the intense precipitation starts. These reflect the fact that SPCAM5 better simulate the transition from shallow to deep convection.

Based on the aforementioned analysis, we can draw the following conclusions. In CAM5, when the unstable energy occurs in the afternoon, the model will quickly release the unstable energy through deep convection so as to stabilize the model atmosphere. In this case, precipitation appears quickly in the model and convection cannot be accumulated to certain strength. As a result, the model produces more frequent but less intense rain. In SPCAM5, the model will not instantly remove the unstable energy once the atmosphere becomes unstable. Instead, the model simulates a process in which convection progressively develops from shallow to deep convection. Shallow cumulus clouds inhibit precipitation and help the unstable energy to grow to a higher magnitude. At certain threshold, the precipitation occurs and reaches the maximum at a relatively late stage. Therefore, in SPCAM5, the peak is delayed and accompanied by more intense precipitation. The model atmosphere rains less frequently with higher intensity, and exhibits increased precipitation amount in terms of the climatology. Hence, it is the proper simulation of the transition from shallow to deep convection that helps SPCAM5 to improve the simulations of precipitation characteristics. Meanwhile, because convection becomes more intense near the peak time, a related effect is that the large-scale upward motion becomes stronger during the precipitation peak in SPCAM5. This reflects the impact of sub-grid scale convection on the large-scale dynamics. (Zhang Yi)

2.2 Regulating the precipitation errors along the steep slope of the Tibetan Plateau

A stubborn model bias over East Asia in GCMs, namely, the precipitation errors along the shouthern steep

slope of the Tibetan Plateau, was investigated in this study. Results suggest that this problem is more closely related to the large-scale dynamics. Two contrasting model experiments were designed in this study. The first experiment is a typical AMIP style climate integration. In the second experiment, a moisture divergence term is artificially added to the model's moisture transport equation. With this term added, moisture over the convergent area will be continuously accumulated, while moisture over the divergent area will be gradually removed.

Results show that this additional term well reduces the originally overestimated precipitation amount at the higher part of the steep slope, while enhances the originally underestimated amount at the lower part of the steep slope. Moreover, the entire precipitation frequency-intensity structure was also modulated. The changes in the total precipitation mainly result from the changes in the grid-scale precipitation and moisture contents. This reflects that the large-scale dynamics modulates the local moisture content and regulates the precipitation simulation. By checking the adiabatic moisture tendency, we confirm that this additional term inhibits the original positive moisture advection tendency at the high part, while enhances the tendency at the low part, in accordance with the differences in the simulated precipitaiton climates.

To better understand the impact of this term on the model performance, we conducted numerical weather prediction type experiments. Results show that this term quickly exerts an influence on the precipitation simulation, namely, it is a fast adjustment process. Moisture contents over the higher part are largely removed, while those over the lower part are significantly enlarged. The change of the moisture content influences the precipitation characteristics over the steep slope region. This study offers useful information for suppressing the simulation errors around the Tibetan Plateau. It also reveals the impact of large-scale dynamics on the precipitation simulations. (Zhang Yi)

2.3 Development of an icosahedral atmospheric model: Solvers of transport and shallow water equations

To accommodate the requirement of developing global high-resolution atmospheric models in the future, we are conducting research to solve the atmospheric model equations based on a quasi-uniform mesh obtained from a subdivided icosahedron. The spherical mesh is formed by recursively bisecting each triangular edge of a regular icosahedron. The mesh is further divided into the Voronoi-Delaunay diagram such that an unstructured mesh is achieved. This differs from the structured icosahedral mesh in that there is no uniform topological rule for the grid. The solver utilizes the Arakawa-C staggering grid system, namely, the mass is defined at the cell center and the normal velocity is located at the cell edge. When the Rossby deformational radius can be well resolved, the C-grid system is very suitable for simulating the resultant high-resolution atmospheric motions because of its advantage in depicting the divergent mode. Meanwhile, unlike the Z-grid, a C-grid model does not need to invert an elliptic equation, thus avoiding the massive global communication and favoring the massive parallel computation.

The transport and shallow water equations constitute the horizontal part of a global 3D model. We first built a conservative Two-step Shape-Preserving Advection Scheme (TSPAS). This can be viewed as a finite-volume and unstructured extension of the scheme in Yu (1994). By designing a properly defined pre-integration parameter, this method selects between the Lax-Wendroff and the upwind scheme to maintain a positive definite transport with the minimum loss of numerical accuracy. We also constructed a famous and widely used positive definite transport scheme called "Flux Corrected Transport (FCT)", and compared TSPAS with FCT using various transport experiments. Results show that both schemes fulfill the demand of a positive definite transport. TSPAS retains more monotone solutions and FCT maintains larger maxima of the transported signal. The work also pointed out difference in the designs behind the TSPAS and FCT.

Besides the transport equation, we further constructed a shallow water solver on the icosahedral C-grid. This needs to maintain some important underlying physical constraints. For an irregular C-grid, an important point is to approximate the tangent Coriolis term, which should not be an energy source or sink. We built a shallow water model based on a vector reconstruction algorithm that can rigidly maintain the energetic neutral Coriolis term, and a set of operators that conserve the total energy within the time truncation error. By testing different time integration schemes, we confirmed that the solver perfectly fulfill our requirement. This will be the basis of our further development. (Zhang Yi)

2.4 A new method proposed to objectively evaluate model precipitation and its evaluation using satellite retrieved precipitation

The current advanced global atmospheric model cannot explicitly resolve the evolution of cloud and precipitation at cloud scale. This is because the model simulated precipitation only represents the mean precipitation in the model grid box. Due to the great inhomogeneity of precipitation in nature, it is difficult to objectively compare the grid-box-mean precipitation in the model with rain gauge observed (in a fixed location) or satellite retrieved (in a much high spatial resolution) precipitation. In this study, a new defined method called regional rainfall event (RRE) is proposed to objectively evaluate the model simulated rainfall. To verify the effectiveness of the method, this study compares the hourly characteristics of warm season (May–September) rainfall among rain gauge observations, China Merged Hourly Precipitation Analysis (CMPA-Hourly), and two commonly used satellite products. Results show that the method largely eliminates the differences of rainfall characteristics among different observation measurements over central eastern China.The spatial distribution and diurnal variation of the RRE frequency and intensity are quite consistent among different datasets. All of the datasets present smaller (larger) regional rainfall coefficient (RRC) in south (north) of the Yangtze River. The values of warm season mean frequency and intensity of RRE are also similar compared with these datasets by using RRE, although the TRMM products overestimate the RRE intensity. The diurnal variations of RRE intensity and frequency are also comparable among different datasets, and the overestimation of afternoon peak is not obvious in both TRMM and CMORPH datasets while compared using RRE method. It is found that the spatial spread of rainfall, revealed by RRC, is more uniform during the nocturnal to morning hours over central eastern China. Over most regions in the central eastern China, the RRC reaches the diurnal maximum several hours after the RRE intensity peaks, implying an intermediate transition from convective to stratiform rainfall. In the afternoon, the RRC reaches the minimum, implying that local convections dominate in those hours, which could cause large differences between rain gauge and satellite observations. The RRC reaches the diurnal maximum more frequently in the afternoon in TRMM and CMORPH than in gauge and CMPA-Hourly data, implying the more organized afternoon rainfall systems in satellite products. Despite the similarity among different datasets, the CMPA-Hourly data show great advantages in reproducing gauge-observed mean state and diurnal variations of RREs compared with the TRMM and CMORPH datasets over the central eastern China. This indicates that the CMPA-Hourly dataset is more reliable for analyzing the sub-daily variations while considering the setailed rainfall characteristics as a regional event. Since RRE reflects the whole features of rainfall in a limited region rather in a fixed point or a single grid box, the widely-recognized overestimation of afternoon rainfall in satellite products is not obvious, and the satellite estimates are more reliable in representing sub-daily variation of rainfall in the RRE perspective. This study provides a reasonable method to compare satellite products with rain gauge observations in sub-daily scale, which also have great potential and will be further used to evaluate the spatio-temporal variation of cloud and rainfall in numerical models (Fig. 5). (Chen Haoming)

3 Polar climate research

3.1 Vertical structure of the summer atmospheric boundary layer in the central Arctic Ocean and its relationship with sea ice extent change

The atmospheric vertical structure and changed characteristics of boundary layer parameters, as well as their relationships with sea ice and temperature changes in the central Arctic Ocean (80°–88°N) are presented by adopting the GPS sounding data obtained from the 4–6th Arctic expeditions of China and NCEP (National Centre for Environmental Prediction) reanalysis data. Obvious differences are observed in terms of the tropopause height, the boundary layer height, the temperature inversion, and vertical structure of wind speed and direction in the central Arctic Ocean in summers of 2010, 2012, and 2014. These differences can be explained by the relationships between temperature and changes in sea ice extent in September from 1979 to 2014. In September 2012, the Arctic sea ice extent decreased by 44% with obvious warming. In September 2010 and 2014, it decreased by 22.6% and 17% with an obvious cooling, respectively. A comparison of the two processes shows that sea ice change has a significant influence on the vertical structure of the atmospheric boundary layer. In the recent 30 years, the temperatures at 1000 and 850 hPa in the central Arctic Ocean have displayed an obvious warming trend and are negatively correlated with the sea ice extent. These changes indicate that the continuous reduction of Arctic sea ice will continue the warming of the mid-lower troposphere. (Ding Minghu)

3.2 Re-assessment of recent (2008–2013) surface mass balance over Dome Argus, Antarctica

At Dome Argus, East Antarctica, the surface mass balance (SMB) from 2008 to 2013 was evaluated using 49 stakes installed across a 30 km by 30 km area. Spatial analysis showed that at least 12 and 20 stakes are needed to obtain reliable estimates of SMB at local scales (a few hundred square meters) and regional scales (tens of square kilometers), respectively. The estimated annual mean SMB was (22.9±5.9) kg m^{-2} yr^{-1}, including a net loss by sublimation of (2.22±0.02) kg m^{-2} yr^{-1} and a mass gain by deposition of (1.37±0.01) kg m^{-2} yr^{-1}. Therefore, about 14.3% of precipitation was modified after deposition, which should be considered when interpreting snow or ice core records produced by future drilling projects. The surface snow density and SMB in the western portion of Dome Argus are higher than in other areas. These differences are likely related to the katabatic wind, which is strengthened by topography in this sector. A new digital elevation model (DEM) of Dome Argus was generated, confirming that both peaks of the dome can be considered as the summit of the East Antarctic Ice Sheet. The findings from this study should be valuable for validating SMB estimates obtained from regional climate models and DEMs established using remote-sensing data. (Ding Minghu)

3.3 A Comparison of Antarctic ice sheet surface mass balance from atmospheric climate models and in situ observations

In this study, 3265 multi-year averaged in situ observations and 29 observational records at annual time scale are used to examine the performance of recent reanalysis and regional atmospheric climate model products (ERA-Interim, JRA-55, MERRA, the Polar version of MM5 (PMM5), RACMO2.1, and RACMO2.3) for their spatial and interannual variability of Antarctic surface mass balance (SMB). The simulated precipitation seasonality is also evaluated using three in situ observations and model intercomparison. All products qualitatively capture the macroscale spatial variability of the observed SMB, but it is not possible to rank their relative performance because of the sparse observations at coastal regions with an elevation range from 200 to 1000 m. In terms of the absolute amount of the observed snow accumulation in the interior

Antarctica, RACMO2.3 fits best, while the other models either underestimate (JRA-55, MERRA, ERA-Interim, and RACMO2.1) or overestimate (PMM5) the snow accumulation. Despite underestimated precipitation by the three reanalyses and RACMO2.1, this feature is clearly improved in JRA-55. However, because of changes in the observing system, especially the dramatically increased satellite observations for data assimilation, JRA-55 presents a marked jump in snow accumulation around 1979 and a large increase after the late 1990s. Although precipitation seasonality over the whole ice sheet is common for all products, ERA-Interim provides an unrealistic estimate of precipitation seasonality over the East Antarctic plateau, with high precipitation strongly peaking in summer. ERA-Interim shows a significant correlation with interannual variability of the observed snow accumulation measurements at 28 of 29 locations, whereas fewer than 20 site observations significantly correlate with simulations by the other models. This suggests that ERA-Interim exhibits the highest quality in capturing interannual variability of the observed precipitation. (Ding Minghu)

大气物理与人工影响天气
Atmospheric Physics and Weather Modification

云物理与人工影响天气研究进展

1 科研项目进展

2016年，中国气象局人工影响天气中心承担的各项国家级项目取得重要进展，并申请获得一些新的研究项目，包括国家科技计划重点专项1项，自然科学基金项目3项，气科院基本科研业务费重点项目2项，中国气象局2016年度留学人员科技活动项目择优资助项目1项。承担的重要科研项目主要进展如下。

1.1 机载云粒子测量系统的研究和开发

国家重大科学仪器设备开发专项项目"机载云降水粒子谱仪与成像仪研制"完成了项目的研究任务，并通过了初步验收。项目已按期完成包括云粒子谱仪、云粒子成像仪、降水粒子成像仪样机和软件的研制任务，并进行了一系列仪器基础参数测试、系统优化、环境适应性试验及外场飞行试验。研制仪器已累计进行了60多架次的飞行试验，依据飞行试验结果，进行了反复的性能改进和优化。与国外同类产品的对比试验结果表明，项目研制产品在粒子测量数据方面与国外产品具有较好的一致性。在软件系统研制方面，完成了控制软件的集成开发。项目成果已在吉林、山西等省人工影响天气部门得到应用，取得了良好效果，在国家级重大项目科学试验、人工影响天气业务保障等方面发挥了重要作用。项目成果已初步具备工程化与产业化条件，主要仪器性能指标达到国际同类产品水平。（开放实验室）

1.2 青藏高原云降水物理与大气水循环研究

第3次青藏高原大气科学试验第3课题"青藏高原云降水物理与大气水循环"取得重要进展。2016年度，进一步对2014—2015年度夏季青藏高原科学试验取得的综合探测资料进行深入分析和研究，并开展了数值模拟和卫星反演研究。获取了青藏高原夏季云和降水变化的重要特征。结合飞机观测资料，分析了高原那曲地区上空云降水粒子的微物理特性；开展了青藏高原云底温度、边界层比湿反演校验，开展了模式云微物理过程的检验和验证，建立了基于伽马函数的云滴谱3参数方案。利用MODIS卫星云水气候资料研究了高原云中水分循环特征。（开放实验室）

1.3 其他项目研究进展

（1）行业专项"民机适航性验证自然结冰气象条件研究"，2016年3月在安徽开展飞机结冰气象探测试验，探测到飞机结冰。（区域中心管理办公室，作业指挥与运行中心）

（2）行业专项"南方大范围云系人工增雨作业潜力与作业技术研究"，进行了2015年外场试验资料的处理、微波辐射与探空探测的拟合程度分析，组织开展了FY-2卫星云微物理反演、短时强降水云物理过程分析等。（区域中心管理办公室）

（3）行业专项"人工增雨随机化外场试验和效果检验技术研究"，2016年在吉林、山东、福建、海南4省试验区继续开展了人工增雨随机化外场试验，4个试验区在2016年共获取了32个随机试验样本。（作业指挥与运行中心）

（4）行业专项"层状云人工增雨作业条件识别和效果分析技术"在云降水精细处理和分析技术、

增雨条件和效果监测识别、云降水数值模拟和催化模拟等方面进行了进一步的研究；探索基于多尺度人工增雨概念模型建立的思路和技术方法，建立了华北层状云系作业条件监测识别指标和低涡气旋云系增雨条件模式识别指标；开展了基于扩散传输计算的不同条件下人工增雨作业影响区确定及催化效果物理响应的分析研究，建立了多参量区域动态作业效果物理检验计算方法（K值法），开展了不同条件作业数值模拟试验；发展了云降水精细分析系统（CPAS）核心技术，基于该技术，国家级和河北、河南及山西等试点省建立了先进的人工影响天气（以下简称"人影"）综合分析和指挥平台，同时利用该课题研究成果成功指挥多次飞机增雨作业，取得了作业实效。（作业指挥与运行中心）

（5）基金项目"基于功效分析的非随机化人工增雨作业效果检验最优实用统计方案研究"在前期研究的4种统计检验方案中，针对功效较高的区域历史回归统计检验方案进行了深入研究，研究成果于2016年7月开始在全国人影业务部门推广应用。（作业指挥与运行中心）

（6）多项室内试验课题取得了阶段性研究成果。"北京地区人工消减雾霾试验研究"在消雾霾催化剂和暖云催化剂研究方面取得了阶段性成果。对4种配方燃烧型催化剂、10余种吸湿性稀土物质、2种吸水性高分子粉末、8种粉末表面活性剂和2种液态表面活性剂进行了室内试验研究，对比和筛选高效新型催化剂。同时在吉林敦化进行爆炸型人影弹配方的改进试验。开展了暖云膨胀云室的建设。（开放实验室，装备研发与保障室）

2 科研成果及其推广应用

2.1 人影飞机作业和探测科学试验

东北人影工程建设的2架集成高性能云物理探测和作业飞机，积极参与东北区域和中部、西南、西北等区域飞机增雨作业服务，并且按照中国气象局部署参与了飞机自然结冰探测试验、东北冷涡飞机外场探测试验等科学试验以及G20杭州峰会人工消减雨作业试验等气象服务保障工作。试运行阶段，国家增雨飞机充分发挥了高性能、先进性和跨区域作业的优势，既实现了东北区域人影工程建设目标要求，试运行中探索的运行管理模式也为后续其他区域工程项目建设提供了很好的经验。（区域中心管理办公室）

2.2 人影综合业务系统推广应用

东北人影工程建设的1套区域、省、市、县4级的人影综合业务系统，完整实现了人影5段实时业务功能并建立了区域、省、市县到作业站点的上下协同的业务流程，为构建"横向到边、纵向到底"的人影业务体系提供平台支撑。在完成试点应用后，在东北区域内4个省级、40个市级和15个县级及相关作业点部署业务系统，开展业务试运行。东北区域、4省（区）人员会同国家级团队共同编写《东北区域人影综合业务系统部署工作方案》。以辽宁为第1个全省大范围部署和使用试点，顺利完成全省安装、部署、联调联试。随后依次开展吉林、内蒙古、黑龙江的全省安装部署和联试。同时，该系统部分核心业务功能在宁夏、山西、陕西、河北、江苏等省进行了推广应用。（作业指挥与运行中心）

2.3 人影作业装备弹药物联网管理系统推广应用

编制完成《人工影响天气作业信息格式规范（试行）》和《人工影响天气作业装备与弹药标识编码技术规范（试行）》，并通过减灾司下发全国各人影业务单位执行。

组织建设"人影作业装备弹药物联网管理系统"，开发人影作业装备弹药出厂验收及质量管理系统、人影作业装备弹药信息管理系统、飞机与地面作业信息实时采集监控系统；在贵州、陕西、河南、

北京分别建立不同技术模式的省级应用示范，实现人影作业装备与弹药的全程、规范、自动、实时监控与管理。联合上海物资管理处和国家气象信息中心，完成国家级与示范省级联调联试，对基层指挥作业人员进行操作培训，项目完成后将优选出可用于全国各省市推广的技术模式与系统，提高人影作业安全管理的科技水平和业务现代化程度。（装备研发与保障室，区域中心管理办公室）

2.4 业务技术指南编制及其在省级推广应用

梳理空中云水资源评估和作业效果检验的关键技术方法和思路，编写《云水资源评估技术指南（2016版）》和《人工增雨作业效果检验技术指南（2016版）》，通过专家咨询和评审，已于7月推广至省级人影部门试用。

指导省级人影部门开展效果检验和云水资源评估的本地化释用和关键技术优化。湖北、海南等省根据《云水资源评估技术指南》中的技术方法初步对本省云水资源进行评估释用。编写《云水资源评估物理量输出格式及规范（2016版）》。在河北邢台组织空－地联合云水资源综合观测试验，利用飞机、地基云雷达、激光雷达等探测手段，对云降水长时序加密观测，获取云结构精细监测数据，用于云场诊断等关键技术检验。（作业指挥与运行中心）

2.5 精细化数值模式作业条件预报系统

编写完成人工影响天气模式预报宏观云场检验方案，分别形成国家级和省级检验方案，《人工影响天气模式系统云和降水预报产品省级检验方案(2016版)》，指导各地开展检验工作，形成了人工影响天气保障服务典型个例检验集。

优化CAMS方案，开展了模式人影预报产品的开发。开发了云底高度、云底温度预报产品，利用云雷达、激光雷达、云高仪等观测数据进行产品检验。对WRF_CAMS模式的预报系统进行调试、检验、验收准备；在此基础上形成的云降水显式预报系统（CPEFS_v1.0）已业务化运行。

开展 LAPS-WRF-CAMS同化预报系统应用多个例检验，开展了人影催化模式多个例催化模拟试验。（作业指挥与运行中心）

3 综合外场观测试验

3.1 科学观测外场试验

在安徽池州、安庆地区与商飞集团、上海气象局、安徽气象局合作开展飞机自然结冰探测试验，收集了大量试验数据和资料。自然结冰探测试验开创了国家增雨飞机为国家重大项目建设提供气象保障的先河。

针对黄淮气旋过程云系和降水特征，编制《东北国家级效果检验区东北冷涡云系空－地联合飞机探测与作业科学试验设计方案》和《东北国家级效果检验区东北冷涡云系空－地联合飞机探测与作业科学试验实施方案》，针对黄淮气旋中小尺度垂直结构以及中尺度结构启动了飞机外场观测试验。9月，在南方开展针对积云、层积云的催化及探测试验，作业中采用了冷暖云催化方法。持续开展庐山云雾宏微观特征外场观测研究，5—6月开展了春夏季庐山云雾观测。（人影中心）

3.2 科学试验观测资料分析

针对外场试验，收集和整理了包括飞机、卫星、雷达、探空和地面降水、温压场等综合探测资料，并初步建立了数据库管理系统（飞机综合外场试验数据库管理系统v1.0）。对庐山云雾站的数据库进行了完善，将观测资料进行了整理，并编制数据格式说明。分气溶胶和云探测2个小组对现有飞机观测资料进行整理分析，以及对G20保障的飞机资料进行分析。（作业指挥与运行中心，开放实验室）

4 人工影响天气业务进展

4.1 实施3年行动计划，推进人影业务现代化建设

人影中心成立了实施人影现代化3年行动计划领导小组，编制了《人影现代化行动计划关键任务推进方案》，明确4项关键技术任务和2项技术系统任务，组建由国家级牵头、省级参加的技术团队，组织召开了7次由不同省区市参加的技术交流会，指导各省开展人影关键技术工作，有效促进了全国各地人影工作任务的推进和作业实效的提高。多项3年行动计划工作成果已在全国推广应用。

组织召开第2届全国人工影响天气中心主任会，进一步提高了对人影业务现代化的认识，交流了人影业务现代化的工作经验，展示了人影装备弹药全程监控系统和综合业务系统的阶段成果。

组织开展全国3年行动计划实施情况的中期评估工作。协助全国人影科技咨评委组建评估专家组，对全国各省的自评估报告分别开展实地和书面评估调研，经评估专家组审议，形成最终评审结论。

开展基于卫星、探空和地面观测的云底高度算法研究，并与地基云高仪和激光雷达、云雷达等云底实测资料对比检验，提出并优化云底高度算法，研发云底高度反演产品。升级了基于卫星等综合观测的云特性反演产品，正在中试检验中。

组织北京、河北、内蒙古、辽宁、陕西、贵州、重庆等11个省区市召开"人影作业概念模型和指标体系"交流会，邀请中央气象台首席预报员对各省已有的概念模型及指标体系进行点评，督促各省进行梳理总结。提出了人影作业概念模型和指标体系的分析方法，建立了低槽冷锋类层状云增雨概念模型的建立方法研究。

开展雷达在人影中的应用现状调研，通过典型省调研和全国现状分析，初步编写完成《雷达在人影中应用现状评估及需求分析》报告。（作业指挥与运行中心）

4.2 重大气象服务保障

2016年9月，G20杭州峰会人影保障服务期间，人影中心指导浙江省局编制《人工消减雨作业试验实施方案》；组建由北京、山西、安徽省（市）人影办专家，以及北京大学、中国科学院大气物理研究所、南京大学、南京信息工程大学等院所知名教授或研究员组成的技术支持专家团队，共同把脉指导作业方案设计，配合浙江省气象局圆满完成保障任务。在杭州安装调试云降水精细分析CPAS平台，在北京制作3 km分辨率的云场精细预报作业条件预报、监测预警、方案设计等专报；调派2架国家级增雨机，多次组织实施双机立体作业的演练与实战；开展基于卫星、雷达和雨量等观测资料的多参数动态对比物理检验。G20服务保障让人影中心首次从幕后走到台前，梳理建立了重大活动保障的工作模式，首次实现了人影实时技术流程，是对人影现代化建设成果的一次集中检验。（人影中心）

4.3 国家级人影业务指导和服务工作

面向全国每日发布7类卫星云特征参量监测反演产品和4大类20小类模式预报产品，实时收集全国飞机和地面作业信息。每周制作《未来一周人影作业需求分析》和《全国人影作业信息报》（48期）；每月制作《全国人影作业信息上报质量报》（11期）；收集各省人工影响天气相关业务动态、科技进展、重大服务信息等，每季度编制完成《全国人工影响天气工作动态》（4期）。

针对中部、东北区域增雨作业，甘肃迭部林火，内蒙古草原火灾等服务任务，制作《作业过程预报和飞行计划》6期，组织专题会商近10次，制作发布《人影作业条件潜力预报和飞行预案》专报16期；开展作业条件监测预警，发布预警报10期。

规范人影飞机作业信息编码内容和格式，升级北斗监控系统，完善CPAS指挥平台，实现作业飞机实时监控和跟踪指挥，选取试点省开展业务适用。

开展全国飞机作业方案设计现状调研，初步制定飞机作业方案设计规范。收集全国飞机作业信息，针对重点过程开展合理性分析，制作完成《重大活动人工影响天气效果分析报》模板。编制完成"飞机作业过程分析要点"及2个示例，供各省人影业务单位参考使用。

开展全国人影机载通信和信息传输现状调研，并在调研基础上完善基于北斗监控系统的飞机实时监控和信息传输系统，实现北斗作业飞机地面端跟踪指挥，作业状态的实时显示，目前正在开展省级的试点工作。

在CPAS-WMC V1.0业务平台上，实现了云降水显式预报系统（CPEFS-v1.0）预报产品的显示和综合分析功能，新增组合反射率、云底高度（温度）、雷达回波、温度和高度垂直结构综合图。

与黑龙江、吉林、辽宁、内蒙古4省区人影办制定发布了《东北区域国家高性能增雨飞机试运行管理暂行规定》；人影中心制定发布了《国家高性能增雨飞机飞行作业流程》《指挥岗观测岗和作业岗职责》《新舟60增雨机任务系统操作卡》《飞机增雨和探测飞行基本业务规范》《MA60人工增雨系统操作手册》。通过对这些管理办法和仪器设备操作规程的不断修订完善，逐步提高了国家增雨飞机管理工作的规范化、标准化水平。

分别在北京和陕西阎良举办了云物理探测设备培训班（1期、2期）和机载任务系统培训班。来自中国气象局人影中心、东北区域4省区人影办（中心）和北京、江西、河南、四川、甘肃人影办（中心）的近90人参加了培训。使业务人员全面了解高性能作业飞机任务的组成、功能性能，掌握探测设备的基本结构和工作原理、操作使用，提升系统管理、故障诊断和排除、日常维护、数据质量控制、相关软件使用和管理的能力。

以国家增雨飞机为平台，积极调动科技人员开展内部协作交流，并加强与北京、河南、山西、安徽等省级间业务技术协作和交流，积极吸纳各类人影业务科研人员参与飞机作业探测任务和飞机探测资料应用分析工作，实现对人才培养和科研成果孵化的双丰收。

试运行期间除了多次组织机载任务系统验查与软件改进测试工作外，还结合飞机停靠地省级增雨抗旱需求，抓住有利降水过程，积极开展国家增雨飞机和河南、山西、陕西、安徽和东北区域4省区地方飞机在内的多机联合作业以及空地一体化探测试验，尤其是在G20峰会重大气象服务保障中，利用机载任务系统优势，发挥国家增雨飞机的建设效益，同时积累典型增雨作业和探测个例。

截至12月10日，2架新舟60增雨飞机累计飞行101架次，共计270 h。其中，增雨飞机B-3726累计飞行47架次共122 h，增雨飞机B-3435累计飞行54架次共148 h，2架增雨飞机共经停15个省/市。（作业指挥与运行中心，区域中心管理办公室）

4.4　人影装备安全管理和技术审查

编制完成了《人工影响天气专用技术装备使用许可技术审查办法》。提出增雨防雹高炮和火箭技术性能要求、测试方案。组织编写的行业标准项目"增雨防雹高炮系统技术要求"和"增雨防雹火箭技术要求"已通过人影标委会组织的终审。与上海物管处一起完成《37 mm人工增雨防雹炮弹质量考核试验办法》上报稿；完成《人工影响天气增雨防雹火箭弹考核试验办法》评审。

组织完成了对华云公司"HY-R型增雨防雹燃气炮"技术性能指标的评审工作及"JD-15型37 mm人工增雨防雹炮弹业务试用总结"和"BL-3型66 mm、BL-4型82 mm人工增雨防雹火箭弹业务试用总结"的评审。（装备研发与保障室）

5　人工影响天气工程建设

5.1　新舟60增雨飞机功能验查及系统验收

在2015年验查的基础上，又分别在陕西阎良、河南洛阳和吉林长春，对机载任务系统的催化剂播

撒系统、粒子测量系统、云宏观成像系统、卫星通信系统、任务集成系统5个子系统进行了3次地面和空中的测试与验查。组织专家对卫星通信系统和任务集成系统的软件功能进行了联合测试，引导承建商对系统测试验查过程中发现的问题进行了及时整改。完成了对新舟60增雨飞机的整体功能测试，具备了系统验收的基本条件，正在加快推进系统验收工作。（区域中心管理办公室，装备研发与保障室）

5.2 空中国王增雨飞机改装

完成了空中国王增雨飞机的飞机平台建设，经过2 h试验飞行及试飞项目查验后，飞机平台正式移交给空中国王增雨飞机改装厂（SPEC公司）进行飞机的改装与集成。

审改确定了《高性能增雨飞机改装集成方案》提交SPEC公司进行飞机改装集成。就飞机座椅、飞机采样头安装、CCN进气口、激光雷达安装、气路、集成方案、云宏观摄像位置、焰条焰弹尺寸等设计问题，与SPEC公司多次讨论协商。SPEC公司正在进行机载设备挂载点的改装工作。预计2017年底改装完毕运抵中国。（装备研发与保障室）

5.3 其他区域人影工程

组织完成西北区域人工影响天气项目可研报告的编制及报发改委的前期工作。西北区域人影工程项目得到发改委的批复。组织完成中部区域人影项目可研的编制。组织完成西藏人影基础能力建设可研报告的编制和专家评审。（区域中心管理办公室）

Advances in Cloud Physics and Weather Modification Research

1 Progress in major research projects

In 2016, WMC has made important progresses in research projects. In addition, WMC has successfully applied seven new projects including one key project of national scientific and technological program, three projects of national natural science foundation of China, two key projects of CAMS basic scientific research, and one project for the scientific activities of selected returned overseas professionals in CMA in 2016. The main progresses in research projects of WMC are summarized as follows:

1.1 Research and development of airborne cloud particle measuring system

The research and development project of airborne cloud particle spectrometer and imaging supported by the national key foundation for exploring scientific instrumenthave passed its preliminary acceptance. The project has completed its all research tasks including three probes of cloud particle spectrometer, cloud and precipitation particles imaging as well as the relevant software. A series of experiments including basic parameters of the instruments, system optimization, environmental adaptability and flight tests have been carried out. The airborne measuring system has been improved and optimized according to more than 60 flight tests. The test results show that particle measurement data observed by the instruments are in good consistency with that obtained by foreign products.

The instrument has been successfully used in the Shanxi Weather Modification Office and Jilin Weather Modification Office. Also, it played an important role in national major scientific experiments and operational assurance of weather modification. This instrument can preliminarily be engineered and industrialized, and the major performance indices have achieved the same level of similar foreign products. (Open Laboratory)

1.2 Advances in research of cloud and precipitation processes and atmospheric water cycle over the Tibetan Plateau

Important advances have been made in the research of cloud and precipitation processes and atmospheric water cycle in the project of the Third Tibetan Plateau Atmospheric Scientific Experiment. In 2016, we further investigated the cloud and precipitation processes over the plateau based on the comprehensive experiment data during the summer of 2014–2015, and conducted modeling and satellite retrieval studies. We obtained some important characteristics of cloud and precipitation processes over the plateau. Combing with aircraft measurement over the plateau, we also investigated the cloud microphysical properties in this region. Also, the verification of satellite retrieval of cloud-base temperature and boundary-layer specific humidity has been done. A new cloud spectrum scheme with three parameters based on Gamma Function has been built, and a comparison of the model results with those from the bin model has also been conducted. The water cycle in clouds has been studied based on MODIS cloud water data. (Open Laboratory)

1.3 Research progress in other projects

(1) In March 2016, aircraft icing meteorological experiments were carried out in Anhui Province, aiming to detect aircraft icing. The work was supported by the project of airworthiness verification of civil aircraft under natural icing meteorological condition. (Regional Centre Administration Office, Operation Commanding and Running Centre)

(2) The project of potential and technology of cloud seeding in large-area cloud system of southern China conducted the data processing of field experiment in 2015, and made analysis of the fitting of the microwave radiation and sounding probe, as well as the analyses of cloud microphysical retrieval by the FY-2 satellite and short-term strong precipitation. (Regional Centre Administration Office)

(3) The research project of randomized cloud-seeding field experiment and effectiveness evaluation conducted experiment in Jilin, Shandong, Fujian, Hainan provinces in 2016. The 32 samples of randomized experiments have been collected. (Operation Commanding and Running Centre)

(4) The project of precipitation enhancement and effectiveness evaluation of stratiform clouds conducted further research on the fine processing and analysis of cloud precipitation, rainfall enhancement conditions, recognition of effective monitoring, cloud precipitation numerical simulation and seeding simulation. The multi-scale precipitation enhancement conceptual model and indicators for the cloud seeding condition monitoring of northern stratiform cloud and low vortex cyclone cloud have been established. (Operation Commanding and Running Centre)

(5) The NSFC project of research on the optimal and practical method of non-randomized artificial precipitation further conducted research on the regional historical regression statistical method with better effectiveness. The results have been applied to all the weather modification centers in China since July 1, 2016, which was issued by the Disaster Reduction Division, CMA. (Operation Commanding and Running Centre)

(6) Haze and warm cloud disposal tests have been conducted in cloud laboratory experiment. 4 kinds of formula burning over 10 kinds of rare earth material with good moisture absorption, 2 kinds of water-absorbent polymer powder, 8 kinds of powder surfactant and 2 kinds of liquid surfactants have been tested. (Open Laboratory, Equipment R & D and Support Division)

2 Research achievements and applications

2.1 Two national weather modification aircrafts have conducted many cloud seeding operations and scientific experiments

Two M60 aircrafts integrated with high performance cloud physical detection equipment constructed by northeast weather modification center have actively conducted many cloud seeding services in northeast, central, southwest, and northwest China. The two aircrafts are in the stage of test, these flights and activities have tested all airborne systems and provided important experiences for management and subsequent projects in other areas. (Regional Centre Administration Office)

2.2 Application promotion of weather modification integrated service system

Weather modification integrated service system consisting of four levels covering from region, province, city and county, developed by northeast WMC, has implemented the real-time operation function, set up the collaborative operation process, and built an overall supporting platform.

After the pilot application, a document was issued by Disaster Reduction Division, CMA on July 20, 2016, stating that the system would be deployed and in trial run in the 4 provincial cities, 40 municipal cities and 15 counties, and aslo in business trial run. Deployment Plan on Weather Modification Integrated Service System in Northeast Region has been written by the employees from CMA and provincial bureaus.

Liaoning Meteorological Bureau was the first to deploy and use the system from November 2 to November 19, 2016, which was followed by Jilin, Inner Mongolia, Heilongjiang provinces. Other provinces including Ningxia, Shaan xi, Shanxi, Hebei, Jiangsu have installed the core operation function modules from December 8 to December 27. (Operation Commanding and Running Centre)

2.3 Application promotion of internet-based ammunition management system of weather modification equipment

The Specification of Weather Modification Data Format (Trial Version) and the Specification of Weather Modification Equipment and Ammunition Identification Encoding (Trial Version) have been completed and issued to all WMC.

The Internet-based Ammunition Management System of Weather Modification Equipment, development of the management system of factory acceptance and quality acceptance for weather modification equipment and ammunition, development of the information management system of the weather modification equipment and ammunition and development of the real-time data acquisition monitoring system for aircraft and ground operation's data information have been constructed.

We have demonstrated the application at the provincial level with different technical patterns established in Guizhou, Shaan xi, Henan and Beijing in order to achieve the real-time monitoring and management of the whole process of the weather modification operation equipment and ammunition. United tests of the systems were completed by the national and provincial bureaus with the help of Shanghai bureaus of the equipment and the National Meteorological Information Center. The training to the operation staffs was given. The best technical pattern was selected after the test, which will be promoted to the whole country, aiming to improve the level of the management and modernization. (Equipment R & D and Support Division, Regional Centre Administration Office)

2.4 Completion and promotion of two operation technical guidelines

After combing the key technology method of the cloud and water resource assessment and operation effect tests, documents of Cloud and Water Resource Assessment Technology Guide (2016 Version), and Cloud Seeding Operations Effect Test Technology Guide (2016 Version), which were passed by the review, were issued by the Disaster Reduction Division, CMA and promoted to provincial bureaus for trial application. (Operation Commanding and Running Centre)

2.5 Refined numerical weather forecasting system in operation

Documents for the National Weather Modification Model Forecasting Macro-cloud Field Inspection Method and Provincial Weather Modification Model Forecasting Macro-cloud Field Inspection Method have been completed.

Document of Inspection Method for Cloud and Precipitation Forecast Products was issued on July 1 2016, serving as a guidebook to collect the typical sample test set.

The weather modification products by optimizing the CAMS program and the product test system by using the cloud radar, laser radar, and ceilometer data have been developed. Debugging, testing and acceptance for the WRF_CAMS model forecasting system have been completed. CPEFS_v1.0 system (Explicit Cloud Precipitation Forecast System) was in operation. Experiments of multi-catalytic mode on LAPS-WRF-CAMS assimilation and forecast system were carried out. (Operation Commanding and Running Centre)

3 Field scientific experiments

3.1 Field scientific experiments

Collection of experimental data by carrying out the aircraft icing detection tests with the co-work of commercial aircraft group, Shanghai Meteorological Bureau, Anhui Meteorological Bureau in Chizhou and Anqing, Anhui Province, in March, has been offering the lead role in support for natural icing detection test for

major national construction projects of its kind.

Documents of Design Scheme on Surface-Ground Joint Plane Detection and Operation Scientific Experiments in Northeast National Inspection Area and Implementation Plan on Surface-Ground Joint Plane Detection and Operation Scientific Experiments in Northeast National Inspection Area were made from April to July, which were used for the aircraft outfield observation test based on Huanghuai cyclone small-scale vertical structure and medium-scale structure.

In September, catalytic and observational experiment for cumulus and stratocumulus was carried out, via glaciogenic seeding and warm cloud seeding. Field study of macroscopic and microscopic features of cloud and fog in Lushan was conducted in May and June, 2016. (Weather Modification Centre)

3.2 Analysis for observational data of scientific experiments

Database management system (Aircraft Integrated Field Experiment Database Management System v1.0) has been developed. Comprehensive data including aircraft detection, satellites, radar, sounding and surface precipitation, temperature and pressure have been collected. To improve the database of Lushan cloud and fog station, sorting the observed data, and making the data format instructions have been provided.

Analyses on current historical observational data by plane were done by two teams, namely aerosol and cloud detection teams, respectively. Data collected during the G20 Summit were also analyzed. (Operation Commanding and Running Centre, Open Laboratory)

4 Weather modification operation and service

4.1 Three-year plan for weather modification modernization

We have implemented a three-year plan for weather modification modernization development and set up a member group of Weather Modification Modernization Construction Three-year Plan.

We have completed a document of Weather Modification Modernization Construction Key Task Advanced Programme and made clear 4 key technology tasks and 2 technology system tasks, built a team led by CMA and co-worked with provincial participants. We also instructed the provincial WMC to carry out the key technology work in weather modification, effectively promoted the provincial weather modification work, and applied the results of the Weather Modification Modernization Construction Three-year Plan in the country.

In late October, the Second National Weather Center Director Conference was held, aiming to further enhance the awareness of the weather modification modernization work, and exchange the working experience. The conference also showed progresse in the areas. CMA administrators visited the demo show, making compliment on the IOT applications and excellent design of meteorological information system, which founded the stone for the "Wisdom Weather Modification".

Medium-term assessment of the Three-year Action Plan was done. Results were approved and issued by the Disaster Reduction Division, CMA. Ground and written research were done across the country, with final completion. (Operation Commanding and Running Centre)

4.2 Important weather modification operation services

Implementation plan of artificial rain suppression operation was made during G20 Hangzhou Summit in September, 2016. The scheme was made under the co-work from experts from Beijing, Shanxi, Anhui Province WMC and Peking University, and Institute of Atmospheric Physics, CAS, Nanjing University, Nanjing University of Information Science and Technology, guaranteeing Zhejiang Meteorological Bureau to offer great service for G20 Summit.

The CPAS platform was installed in Hangzhou, the 3 km Fine Forecast of Cloud Field Job Conditions Prediction was issued with monitoring, and program design in Beijing; Two national precipitation aircrafts were deployed for the experiments. Physical inspection of the observation data based on satellite, radar and rainfall was performed; The service for G20 Summit fulfilled the weather modification real-time operation for the first time, which would serve as a milestone. (Weather Modification Centre)

4.3 Operational guidance and service

We have distributed 7 kinds of monitoring inversion products based on satellite cloud parameters and 4 kinds of major categories with 20 sub-category model forecast products on a daily basis; collected real-time national air and ground operation data; made Weekly Weather Modification Requirements Analysis and Weekly National Weather Modification Information Newsletter (48 in total); made Monthly National Weather Modification Information Newspaper (11 in total); made National Weather Modification News each quarter (4 in total); provided cloud seeding for central and northeast regional areas and for the events of Diebu forest fire in Gansu Province and Inner Mongolia grassland fires and other service. We also made Operation Forecast and Flight Plan Report (6 in total), organized 10 video conferences, released Weather Modification Potential Prediction and Flight Plan Reports (16 in total), and issued Early Warning Reports (10 in total).

We also standardized aircraft job data formats, upgraded the Beidou monitoring system, improved the CPAS command platform, achieved real-time monitoring and tracking of command of the operating aircraft, and selected pilot province for trials. We also investigated the National Aircraft Operational Program Design; collected and analyzed national aircraft information; produced the template for Analysis Report on the Effect of Major Weather; completed "Aircraft Operations Analysis" and 2 examples, which was issued on November 16.

We studied the national weather modification airborne communication and information transfer and improved the real-time monitoring and information transmission systems based on Beidou to achieve ground-side track of command, and real-time job status monitor, which was applied to the provincial pilot projects.

In the Precipitation Forecasting System (CPEFS-v1.0), we implemented the function of displaying forecast products and comprehensive analysis, with more modules such as new composite reflectivity and cloud base height (temperature), radar, integrated graphs of temperature and vertical structure.

National airborne cloud seeding trial operation has achieved important progresses. We have made several regulations of aircraft operation management and strengthened the training to improve the operational management level.

Two cloud physical detection equipment training courses and one airborne mission system training course were held in Beijing and Yanliang. We organized training course (phase 1 and phase 2) and airborne mission systems training courses with over 90 participants in Shaanxi. These helped employees to fully understand the composition of operating aircraft with high performance tasks, functional performance, master the basic structure and working principle of detection equipment and operations, and promote system management, fault diagnosis and maintenance, preventative maintenance, data quality control, software usage and management ability.

Based on the airborne cloud seeding aircraft, technological personnel exchanges were held among Beijing, Henan, Shanxi, Anhui and other provincial bureaus. We attracted all weather modification researchers to actively join the aircraft operation missions and aircraft data analysis to achieve the progress in personnel training and scientific research harvest.

We have carried out cloud seeding services and detection experiments with joint efforts in safety and efficiency. According to the guidelines and instructions from CMA, WMC has successfully finished the

airborne cloud seeding system check and software improvement, especially in the effort to co-work with other provinces including Henan, Shanxi, Shaanxi, Anhui and northeastern part of China. We also done such efforts during the G20 Hangzhou Summit.

By December 10, 2016, a number of flights carried out by two M60 precipitation enhancement aircrafts were up to 101, 270 hours in total. For B-3726, flight number was 47 and the total time was 122 hours; for B-3435, the fight number was 54, while the total time was 148 hours, both of which covered 15 provinces/cities. (Operation Commanding and Running Centre, Regional Centre Administration Office)

4.4 Weather modification equipment safety management and technical review

We have finished the report of Weather Modification Special Equipment Licensing Technology Review issued to the WMC and the related factories on June 28. A final review on the industry standard projects－Precipitation Enhancement and Hail Prevention Anti-aircraft Technology Requirement and Precipitation Enhancement and Hail Prevention Rocket Technology Requirement was done. 37 mm Precipitation Enhancement Hail Prevention Shell Quality Assessment Test Method, which was co-worked with Shanghai Property Management Department, has been submitted. Weather Modification Precipitation Enhancement Hail Prevention Shell Quality Assessment Test Method has been completed.

Technical review work on weather modification equipment was done. "HY-R Precipitation Enhancement Hail Prevention Gas Gun Technical Performance Indicators" and "JD-15 Type 37 mm Precipitation Enhancement Hail Prevention Gas Gun Trial Summary" and "BL-3 66 mm, BL-4 82 mm of Precipitation Enhancement Anti Hail Rockets Operation Trial Summary" have been reviewed and all were reported to the Disaster Reduction Division, CMA. National Technology Equipment Maintenance and Catalyst Testing operation was also done. (Regional Centre Administration Office, Equipment R & D and Support Division)

5 Weather modification projects

5.1 M60 aircraft function check and system acceptance

We have promoted M60 aircraft function check and system acceptance work. Three ground and surface test and check for 5 systems including catalyst distributing system, particle measuring system, macroscopic cloud imaging system, satellite communication system and integrated system were done, respectively, in Luoyang (Henan), Yan Liang (Shaanxi) and Changchun (Jilin). Joint test for software functions of satellite communication system and integration system, serving as a guide for the contractors was completed. M60 aircraft overall functional test has been done, which would provide for the progress of the system acceptance. (Regional Centre Administration Office, Equipment R & D and Support Division)

5.2 Cloud-seeding King Air Aircraft platform construction

Cloud-seeding King Air Aircraft platform construction has been completed by late May. After 2 hours test flight and trial flight check, the airplane has been handed over to the Standards Performance Evaluation Corporation (SPEC) for further modification and integration.

Cloud Seeding Airborne Plane with High Performance Modification and Integration Scheme was set before handing over to SPEC. Discussions regarding to aircraft seats, plane sampling head installation, CCN inlet, laser radar installation, gas path and integration solutions, cloud macro camera position, flame size design were held between WMC, CMA and SPEC. Modification work by SPEC in progress is predicted to be shipped back to China by the end of 2017. (Equipment R & D and Support Division)

5.3 Other regional weather modification projects

Northwest Regional Weather Modification Feasibility Study report has been made and submitted to National Development and Reform Commission (NDRC), which was sent to the Disaster Reduction Division, CMA on April 15, 2016. The project was approved by NDRC. Central Weather Modification Feasibility Study Report has been made and submitted to NDRC, which was sent to Disaster Reduction Division, CMA on September 26. Tibetan Weather Modification Foundation Ability Construction Feasibility Study Report has been made and reviewed by experts. (Regional Centre Administration Office)

生态环境与农业气象
Ecological Environment and Agrometeorology

生态环境与农业气象研究进展

1 农业气候资源与农业气象灾害监测预测

1.1 洪涝灾害监测预警与防控关键技术研究

揭示了全国及研究区域农业、玉米、水稻洪涝灾害的时空、风险分布特征，建立玉米、水稻洪涝灾害等级指标11套，分省农业洪涝灾害等级指标10套，玉米、水稻抗涝耐淹形态生理指标3套；研发防洪避灾种植模式3套，制定灾害防控技术规程3项。成果已在湖南、江西、浙江、安徽、广西、重庆、陕西7省（区、市）进行了气象业务应用，制作发布洪涝灾害农业气象专题服务产品、决策服务报告40多期，洪涝预警与减灾服务取得了显著的减灾增产效果。提出了基于灾害风险逆过程分析的等级指标构建方法，突破了基于降水过程的农业、玉米、水稻洪涝灾害等级阈值确定、分省指标可比性等关键技术，为农业灾害实时监测预警评估的业务发展提供了指标支撑。（霍治国）

1.2 重大农业气象灾害立体监测与动态评估技术研究

通过对西南玉米和水稻干旱、南方双季稻低温、黄淮海小麦干热风不同灾害的立体监测与动态评估技术的研究，提出不同农业气象灾害的致灾气象指标和灾害分级指标体系，研发了可在气象业务中应用的基于地面观测、卫星遥感和作物模式相结合的不同灾害的立体监测技术和动态评估的技术方法。上述工作在以下几个方面有所创新：在信息耦合上，集成了地面气象、农业气象、田间小气候观测以及农情、灾情和地理信息等多源信息，向多源信息方向发展；在立体监测和动态评估技术研发上，向模型化、动态化和精细化方向发展；在多源观测资料信息的使用过程中，注重了尺度转换技术。该项目研究解决的农业气象灾害监测与评估中的关键技术是完全针对我国农业生产模式和灾害对象，具有明显的地域性和现实性等特点；同时该研究也是针对气象和农业部门的业务需求和决策服务需求而展开的。因此，本项目的实施可显著地提高我国农业气象灾害的监测和评估能力。（赵艳霞）

1.3 重大农业气象灾害预测预警关键技术研究

揭示了气候变暖背景下南方双季稻低温灾害突变、发生趋势、等级风险、综合风险的地理分布特征，提出了预测预警的风险分区方法；建立了南方双季稻低温灾害预测预警指标与技术体系，≥5天预警、≥1个月预测的准确率在80%以上；开发了精细化土壤墒情预报系统，实现了自动调用资料、自动运行、自动生成产品等功能；利用改进后的作物模拟模型对区域农业干旱进行模拟验证，将模型分别采用链接遥感技术和不链接遥感技术2种方式模拟区域农业干旱，并将其模拟结果与基准值进行对比。结果表明，引入遥感信息后，作物干旱模型对区域农业干旱的模拟能力明显提高。研究成果已在相关省级农业气象业务服务中推广应用，提升了农业气象灾害预测预警的时效性、准确率。（刘建栋）

1.4 重大农业气象灾害风险评价与管理关键技术研究

针对我国典型地区农业干旱、洪涝、低温冷害等农业气象灾害发生频繁、影响严重且目前尚无有效风险评价技术的状况，选择东北、华北和长江中下游地区主要粮食产区的主要农作物为研究对象，

基于多种技术集成的风险分析方法，从农业气象灾害风险研究入手，以农作物为中心，从土壤–作物–大气连续体出发，提出了基于灾害形成机理的农业气象灾害风险综合评价理论；构建了农业气象灾害静态和动态风险相耦合的评价与风险图绘制技术、多种农业气象灾害风险综合评价与区划技术及农业气象灾害风险预警技术；编制了主要粮食产区的农业气象灾害风险图谱；研制了农业气象灾害风险分析与评价系统；提出了农业气象灾害综合风险管理技术对策体系。主要研究成果在吉林、河北等省的气象、农业等相关部门推广应用，取得了良好效果，为农业防灾减灾提供了必要的理论依据和技术支撑。（王春乙）

1.5　基于遥感信息与气温的夏玉米土壤水分估算模型

土壤水分是土壤–植被–大气连续体的一个重要组分，是决定陆地生态系统水分状况的关键因子，也是作物的水分供应库。为估算站点尺度不同深度的土壤水分，基于能量平衡方程和水分亏缺指数（WDI），提出了基于地面遥感信息（植被指数 NDVI 和下垫面温度）和气温估算土壤相对湿度（WR）方法。利用 2014 年中国气象局固城生态与农业气象试验站夏玉米水分控制试验资料验证表明，该方法可以有效估算不同深度的土壤相对湿度，其中对 0 ～ 10 cm 土壤水分估算精度最高，决定系数达 90%；对 0 ～ 20 cm 到 0 ～ 50 cm 土壤水分估算的平均相对误差均在 15% 以内，相对均方根误差均在 20% 以内。（周广胜）

1.6　玉米干旱致灾临界气象条件及其监测预警技术

基于试验资料和相关研究资料的综合分析，初步阐明了作物在干旱和其他气候变化关键因子相互作用下，叶片气孔导度、水分利用率和生长相互协调的响应和适应机制。基于项目观测试验资料分析了在不同生育期干旱发生发展过程中玉米的光合生理和叶绿素荧光参数变化特征以及复水的影响。拔节期开始水分控制的玉米，控水 2 周后 SPAD、g_s、E 显著下降，但叶绿素荧光参数（Φ_{PSII}、Fv'/Fm'）无显著下降；抽雄期开始水分控制的玉米，控水 1 周后光合特征参数就发生显著下降，且抽雄期干旱导致的光合速率下降速度大于拔节期；在复水干旱解除后，光合能力虽有一定程度的恢复，但仍没有达到其对照的水平。对同一叶片全生育期的观测资料分析表明，Asat、g_s、E 随着生育期（即叶片的叶龄）的进展呈下降趋势、SPAD 呈先升后降趋势，且干旱处理的玉米各参数的下降比对照大；而同一叶片的叶绿素荧光参数（Φ_{PSII}、Fv'/Fm'）在水分充分条件（对照）下呈现较为平稳的波动，4 种干旱处理没有导致荧光参数的显著下降，并在干旱后复水的情况下比对照有明显升高。这表明，随着叶片生长发育的进程，其光合系统 II（PSII）的耐旱性可能有所增加。

利用土壤湿度观测资料对气象干旱指标等级重新划分。首先采用线性内插法得到站点逐日土壤相对湿度序列（1992—2010 年）；分别分析玉米生长季内水分胁迫下（各发育阶段土壤相对湿度低于对应阶段玉米发生干旱时的土壤相对湿度上限值）的逐日平均土壤相对湿度与平均 MCI 指数之间的关系，建立 MCI 指数与土壤相对湿度的关系模型；根据观测资料确定了玉米不同生育期气象干旱指数的上限。将以上结果初步在业务系统中实现，在气象灾害风险管理系统中建设了玉米影响评估模块，该系统可以实时计算玉米干旱累计指数：同一发育阶段期间各干旱过程逐日值的累加，即当 MCI 小于上限时，干旱指数开始累加；不同发育阶段及全生育期干旱累积指数计算方法为各发育阶段累加值与历史上该时段干旱对产量影响的影响系数乘积之和。该系统 2016 年 9 月 30 日全国玉米干旱累积指数的分析结果显示，玉米气象干旱主要分布在东北的西部、内蒙古东部以及湖北、安徽、江苏、四川等地（图 1）。（周莉）

1.7　植物适应未来气候变化的自我防御机制

对贝加尔针茅进行相对长期（42 d）的增温（正常、增温 4 ℃）和水分变化（降水增加 15%、正常、

降水减少15%）模拟试验结果表明，在相对长的暖干气候条件下，贝加尔针茅的光合作用主要受非气孔限制调控，尽管光能利用效率和光合作用速率减弱，但自我防御机制使贝加尔针茅有能力维持正常的生长活动。（周广胜）

1.8　北方冬小麦精细化土壤墒情和灌溉预报技术及其应用

完善了农田土壤水分和灌溉预报数据集，其中北方冬小麦区的逐日气象资料和自动土壤水分资料扩展到2016年7月31日。进一步深入研究了遥感作物水分亏缺指数反演方法。分析了Ångström-Prescott公式中a、b系数的年代际变化，确定了研究区域以及中国各大区域1961—2010年各年代逐月a、b系数参考值。以冬小麦生长机理、农田土壤水分平衡方程为根据，以本项目各种试验资料为依托，在前期冬小麦农田水量平衡简化模型和精细化逐日多层土壤墒情和灌溉预报模型研究和3个省级冬小麦精细化土壤墒情和灌溉预报系统本地化试用基础上，初步构建了国家级冬小麦精细化土壤墒情和灌溉预报系统程序。利用项目科研成果和3个省级冬小麦精细化土壤墒情和灌溉预报系统业务平台，分别在河北、山东、河南省发布了一些服务产品，为农业等部门灌溉决策提供了有价值的参考信息（图2）。（毛飞）

1.9　海南冬季瓜菜气象灾害风险区划

基于海南省各市县1971—2010年3—5月不同持续少雨日数的发生频率及其过程降水量，开展了辣椒春季干旱人工控制试验。试验采用均匀组合设计，设置持续干旱日数（10、15、20、25、30、35、40、45、50 d）和补水量（0、2、4、6、8、10、12、14、16 mm）2因素9水平处理，测定不同处理下的不同深度（10、20、30、50、100 cm）土壤湿度，分析不同处理对辣椒死苗率、生理特性和产量的影响。试验结果表明，辣椒死苗率与20 cm土壤相对湿度和持续干旱日数显著相关，与补水量相关性不大。随着持续干旱日数的增加，辣椒净光合速率、蒸腾速率和气孔导度均呈下降趋势，辣椒相对产量损失呈明显加重趋势。构建了基于持续干旱日数的辣椒春季干旱等级指标，经历史灾情验证，与实际发生情况相吻合。为开展辣椒春季干旱监测预警业务服务提供了指标和方法支持。（霍治国）

1.10　1961—2015年中国潜在蒸散时空变化特征与成因

基于全国552个气象站点1961—2015年逐日气象数据，利用Penman-Monteith公式得到各站点逐日蒸散量（ET_0），以全国和各干湿气候区为研究单元，从年、季节和年代际尺度分析ET_0的时空分布特征及其变化成因。结果表明：我国年平均ET_0为621～1733 mm，在年、年代际尺度表现为干旱区ET_0最高、半干旱区和湿润区次之、半湿润区最低；季节尺度上，ET_0的空间分布存在明显差异，且夏季ET_0最高、春秋季次之、冬季最低。我国年平均ET_0以–0.52 mm/a的速率递减，该下降趋势在1972年存在突变现象；干旱区和湿润区大部分站点ET_0呈减小趋势，且干旱区减小速率较大；而在半干旱区和半湿润区，ET_0呈增加和减小趋势的站点数大致相当。研究表明，近55年我国ET_0呈减少趋势主要是由风速减小、日照时数降低和水汽压微弱增加共同导致的。（王培娟）

1.11　基于冬小麦水分胁迫试验的干旱监测指数构建

借助中国气象科学研究院大型人工水分控制试验场，于2013—2014年和2014—2015年的冬小麦生长期内，分别种植当地冬小麦主栽品种"河农6425"和"郯麦98"，对其进行3个水分胁迫处理，同时设置1个对照，研究不同水分胁迫条件对冬小麦生长发育的影响。根据水量平衡方程，计算不同水分胁迫和对照条件下冬小麦全生育期的实际蒸散量（ET_a），以对照条件下的实际蒸散作为作物标准蒸散（ET_c），构建冬小麦全生育期干旱监测指数（$CDMI=1–ET_a/ET_c$），并结合不同水分胁迫条件下冬小麦减产率和CDMI的关系，划分干旱等级。本研究建立的干旱监测指数以标准蒸散为参照，与基于潜在蒸散的干旱监测指数相比，能够真正地反映农作物的干旱程度，可为我国华北冬麦区干旱监测提供客观依据。（王培娟）

1.12　西南地区水稻洪涝等级指标构建及风险分析

为全面评估水稻洪涝的综合风险，基于自然灾害系统理论和农业气象灾害风险评估方法，利用西南地区（重庆、四川、贵州和云南）193个气象站1961—2012年逐日降水资料、396个县（市）1981—2012年水稻产量、面积资料和17个农气站点水稻生育期数据，以及西南地区数字高程（DEM）数据，构建区域水稻洪涝灾害致灾因子危险性、承灾体暴露性、孕灾环境敏感性和区域抗灾能力指数，以及综合风险评价模型，对西南地区水稻洪涝进行风险分析与区划。结果表明：（1）水稻不同生育阶段洪涝等级风险概率分布存在明显的地区差异，洪涝危险性表现为移栽分蘖期＞拔节孕穗期＞抽穗成熟期；全生育期高、次高危险区主要分布于云南南部和东北部、贵州南部，以及四川的成都、眉山和德阳地区。（2）基于不同时间序列的水稻相对暴露率明显波动，水稻生产承灾体高、次高暴露区主要集中在四川东北部和重庆地区；孕灾环境高、次高敏感区主要位于云南北部、四川南部和贵州东南部地区；水稻洪涝低抗灾能力区主要位于贵州。（3）西南地区水稻洪涝综合风险呈由中部向四周递增的趋势，高、次高风险区主要位于贵州南部、云南南部和四川东北部地区，低风险区位于重庆南部和云南北部地区（图3）。（杨建莹）

1.13　冬前和春季灌溉对华北冬小麦影响的研究

通过在灌溉越冬水（80/150 mm）和不灌溉越冬水条件下，春季气温分别稳定通过0 ℃、3 ℃、7 ℃和10 ℃时进行春季第1水灌溉的多年田间模拟试验，探讨了冬前和春季灌溉对华北冬小麦生长发育和籽粒产量的影响，以揭示华北冬小麦适宜的灌溉方式和灌溉时间。结果表明，无越冬水灌溉条件下，冬后气温稳定通过0 ℃时进行春季第1水灌溉能够缓解冬季干旱，使冬小麦春季有效茎数增加，对有效穗数和产量增加作用显著；越冬水灌溉条件下，春季气温稳定通过7 ℃时进行春季第1水灌溉能够减少关键生育期的连续干旱时间，有利于冬小麦产量增加。越冬水量的大小（80 mm和150 mm）对冬小麦产量的影响不显著。春季第1水对冬小麦的生长发育至关重要，无春季第1水灌溉条件下，冬小麦减产平均达32.2%。因此，为达到冬小麦的稳产高产和节水灌溉目的，无越冬水灌溉条件时，应选择在春季气温稳定通过0 ℃时进行春季第1水灌溉；有越冬水灌溉条件时应适量灌溉，并选择春季第1水在气温稳定通过7 ℃时灌溉。（刘涛）

1.14　荒漠草原土壤呼吸对水热变化的响应机制

利用开路式土壤碳通量测量系统，基于2011—2012年野外观测资料，针对陆地碳源汇评估中的土壤呼吸，在荒漠草原开展不同水热条件下土壤呼吸的变化研究及其控制机制研究。结果发现，荒漠草原生长季的土壤呼吸显著大于非生长季。非生长季，土壤呼吸的差异主要是由增温处理引起的，土壤呼吸与土壤温度呈显著的指数相关（$R^2 = 0.74$，$p < 0.01$）。在生长季，根系呼吸（21.9%）对荒漠草原土壤呼吸的贡献率远低于异氧呼吸（78.1%），土壤有机碳、土壤含水量、根系生物量、微生物量是影响土壤呼吸的主要因素，其中，0 ～ 10 cm土壤有机碳是土壤呼吸最重要的影响因子，土壤含水量对土壤呼吸的间接贡献率最高。基于生长季不同水热条件下荒漠草原土壤呼吸对其影响最大的4个因子的响应关系，建立了土壤呼吸的响应模型（$R^2 = 0.67$，$p < 0.01$）。（刘涛）

1.15　基于遥感方法的黄淮海平原冬小麦耗水特征及用水结构研究

利用2011—2012年气象数据、遥感影像（MODIS）、地表能量平衡方程模型（SEBA）和地面农作物信息，结合农田水分平衡方程，对2011—2012年冬小麦生长季内有效降水量、农田灌溉量、实际耗水量和农田水分损失进行了估算，并采用调研的灌溉量数据对估算结果进行对比验证。结果表明，灌溉量估算值与实际值间有较好的相关性（$R^2 = 0.79$）；冬小麦生长前期，降水能满足70%以上的农田耗水；＞90%冬小麦灌浆期耗水依靠灌溉；黄淮海区域灌溉量高值区域位于西部山前平原水浇地区，灌

溉均值为412.76 mm；区域冬小麦耗水量与灌溉量成正相关（$R^2 = 0.68$，$p < 0.01$）。（杨建莹）

2 农业对气候变化的响应与适应

2.1 1961年以来中国农业气象灾害演变规律及其灾损评估

气候变暖背景下中国极端气候事件呈增加趋势，气候将变得暖时更暖、旱时更旱、涝时更涝。农业干旱灾害发展呈面积增大和频率加快趋势，且北方旱灾影响明显高于南方；冬小麦涝渍呈增加趋势且生育后期灾害强度增加更明显；水稻高温热害增加趋势明显且重度灾害显著增加，低温冷害总体呈减少态势，但近30年低温阴雨呈增加趋势；霜冻害总体呈减少趋势但局部地区有加重趋势。农业气象灾害的演变趋势、强度和类型已经发生显著变化，使得当前针对农业气象灾害开展种植制度调整的避灾农业面临二次避灾风险，严重威胁到国家粮食安全、生态文明建设和精准扶贫。（周广胜）

2.2 中国草地生态系统固碳现状、速率、机制和潜力研究

基于野外4000多个调查点和TEM模型，利用气候、海拔、土壤和植被数据，以月为时间步长对中国草地生态系统的碳密度、储量空间分布及动态变化进行了模拟；估算了全国草地生态系统的碳储量；绘制了中国草地土壤和植被碳密度的空间分布图，揭示了其空间分布特征；定量描述了气候和人类共同作用下，1960年代以来中国草地碳密度的时空变化幅度及区域差异；模拟了未来气候情景下中国草地碳收支动态。主要创新点是针对一套参数TEM模型空间模拟精度不高的问题，提出了基于草地生态型的"分区域参数化率定方案"，建立了适合中国草地的TEM模型参数系列，为准确监测和评估全国草地生态系统碳收支、NPP、GPP等提供了基础。（汲玉河）

2.3 气候变化背景下青稞安全气象保障关键技术研究

在A2和B2气候情景下，西藏太阳能资源虽然有略微降低的趋势，但其仍为世界上太阳能资源最丰富的地区之一。无论A2还是B2气候情景下，西藏地区的太阳能资源总体的时间分布格局没有发生明显改变，均表现为冬季最小、夏季最大；但是其变化幅度在各月份上差异明显，总体表现为夏季增加，而其他季节则相对降低。气候变化背景下西藏全年降水总体上表现为增加趋势，但其仍为世界上降水量较少的地区之一。降水的年内分布仍相当不均，冬季最小、夏季最大，且夏季降水增加明显；空间上自东向西逐渐减小的分布格局亦没有发生改变，但西部降水较东部降水增加更为明显。气候变化背景下的增温效应有益于青稞产量提高，但产量的空间分布特征基本保持不变。目前青稞产量高值区在未来气候变化背景下增值更大，换言之，目前适宜区更加适宜青稞产量提高。（刘建栋）

2.4 基于APSIM模型识别气候变化对北方地区主要旱地作物产量的影响

通过优化常用的农作物模拟模型（APSIM），识别北方春小麦和春玉米关键发育期和产量对气候变化的响应。研究表明，APSIM模型在内蒙古、甘肃、黑龙江、吉林、辽宁等北方地区有较好的适用性。1961—2010年内蒙古春小麦潜在产量总体呈降低的变化趋势，平均值为3561 kg/hm²，其中20世纪80年代潜在产量最高，达3681 kg/hm²，21世纪初最低，为3433 kg/hm²。区域间差异明显：近50年内蒙春小麦潜在产量分布由中间向东部和西部呈条带状逐渐增加，且在3个区域中，西部麦区潜在产量最大，中部麦区最小。影响内蒙春玉米生育期的主要气象因子是最高温度，其次是最低温度，太阳辐射、降水和潜在蒸散对春玉米生育期的影响效果一样。影响春玉米产量的主要气象因子依次为最高温度、最低温度、降水、太阳辐射和潜在蒸散（图4）。（赵俊芳）

2.5 不同积温模型对东北春玉米不同阶段积温的稳定性评价

基于东北地区春玉米品种"丹玉13""龙单13""东农248"和"四单19"生长发育资料和气象观

测资料，分别拟合了沈国权、高亮之和殷新佑非线性积温模型参数，对3种积温模型模拟结果进行比较和稳定性评价，并与常用积温法计算的结果对比。对常用积温法、沈国权非线性积温模型、高亮之非线性积温模型、殷新佑非线性积温模型4种方法进行稳定性分析的结果表明，自出苗到成熟的全生育期，3种非线性积温模型均优于常用积温法，表现出更好的稳定性。在出苗–拔节阶段，4种方法在"丹玉13"品种的稳定性一致，而"龙单13""东农248"和"四单19"3个品种的常用积温法略逊于3种非线性积温模型；拔节–抽雄阶段是稳定性最差的阶段，无论哪个品种，在此阶段的变异系数均最大；在抽雄–成熟阶段，4种方法的稳定性差别不大。研究结果可为东北春玉米发育期预报和产量预报等工作提供理论依据和技术支持。（郭建平）

2.6　气候变化对东北区农业气候资源的影响

系统分析了气候变化情景下东北主要农业气候资源的时空特征。1961—2099年期间，热量资源整体为南高北低，未来热量资源明显增加，东北地区年均温度呈升高趋势，中排放情景（RCP4.5）和高排放情景（RCP8.5）下分别升温约2 ℃和3 ℃，≥ 10 ℃初日提早3 ～ 4 d，初霜日推迟2 ～ 6 d，导致可能生长季延长4 ～ 10 d；温度的升高与生长季的延长使得积温大幅增加，截至21世纪末，增幅分别达400 ℃·d和700 ℃·d。水资源呈增加趋势，但变化较少。热量资源变化速率有明显变化，高排放情景下增温速率更快，东北地区未来有暖湿趋势。以温度升高为代表的气候变化在东北地区对农业生产具有一定的积极影响，生长季的延长和积温的增加使得农作物可利用热量资源更加丰富，原有因受到热量资源限制的不可种植区域将会减少，可种植区域扩大；种植品种得到改善，原来种植早熟品种区域可由中晚熟品种代替，晚熟品种种植面积进一步扩大，如晚熟玉米积温需要达到3000 ℃·d，由原有松嫩平原北扩至大兴安岭附近，甚至在辽宁的部分地区可种植一年两熟制作物。（郭建平）

2.7　大气CO_2浓度升高和增温影响作物需水量变化机理研究

在2013—2015年试验基础上，2016年分析了增温和CO_2浓度升高环境下小麦水分利用效率变化及其与需水量和产量的耦合变化机理。分析结果表明，增温和CO_2浓度升高对于项目需水量变化具有叠加复合影响效应。增温提高了小麦群落和冠层温度，促进能量流动和水分循环，增加了小麦植株蒸腾和株间蒸发量，增加了小麦日需水量。CO_2浓度升高导致叶片气孔导度降低、减少叶片蒸腾速率，有助于提高水分利用效率。另外，CO_2浓度升高的肥效作用有利于提高小麦产量。综合来看，增温和CO_2浓度升高增加了小麦需水量，提高了水分利用效率。需水量增加有助于提高小麦产量。在未来增温和CO_2浓度升高环境下，通过热量资源和CO_2的不断增加和转入，小麦需水量、水分利用效率和产量三者是处于正反馈耦合机制中。（俄有浩）

2.8　北方农牧交错区退耕地植被演替调控机制研究

以空间代替时间的样带调查方法，研究北方农牧交错区退耕地植被演替过程，从相对宏观的角度揭示自然环境因子对退耕地植被演替的调控机制。针对项目设定的研究目标，在山西–宁夏农牧交错带进行了野外样带调查工作。重点收集了农牧交错区典型生态系统0 ～ 500 cm土壤深度的土壤湿度、质地、养分含量，以及植被盖度、生物量、物种等信息。鉴于降水、气温等气象因素具有较大的时空波动性，拟从更稳定的土壤干层、土壤质地、地貌等环境信息，结合气候因素识别出制约中国北方生态系统空间分布、群落演替的关键因素，研究生态系统的环境适应性及耐受气候变化的弹性。此外，采集了树木年轮数据，以配合研究北方生态系统对气候变化响应与适应。（汲玉河）

2.9　增温与CO_2浓度升高对冬小麦处理和品质的影响

2015/2016年生长季试验观测到的发育期、株高、单株生物量和密度的影响结果与前2年基本一致，穗粒数减少仍然是导致减产的根本原因，不同的是该试验季复合处理的小穗数减少达到显著水平，

穗粒数减少主要归因于小穗数下降。对连续3年试验的籽粒粗蛋白、粗脂肪、粗纤维和粗淀粉测定结果进行了统计分析，在复合处理条件下，冬小麦籽粒的蛋白质含量均有增加，其中2年表现为显著增加，而淀粉、脂肪和纤维含量均没有规律性的变化。冬小麦叶片全氮含量从拔节期至开花期有逐渐减少的趋势，但在各发育阶段对照与复合处理的叶片全氮含量没有显示出显著性差异，在各发育阶段对照与复合处理的叶片有机碳含量也没有显著性的差异。（谭凯炎）

2.10 我国小麦品种改良对物候的影响

利用农业气象观测数据分析了我国小麦品种改良对物候的影响。结果表明，春小麦品种变化造成不同发育阶段间的热量单位有所增加，出苗－成熟期每年增加3.5 ℃的热量单位。对不同地区的比较发现，西藏、内蒙古和新疆地区春小麦品种变化对物候的影响较大，对不同发育期间的热量单位多为正效应。我国冬小麦品种变化对播种到出苗、出苗到停止生长、停止生长到返青、拔节到抽穗、乳熟到成熟期间热量单位的影响趋势不明显，而对返青到拔节、抽穗到乳熟期间热量单位有正效应。其中，青海、西藏、福建和新疆地区冬小麦品种变化对物候的影响仍较大，对不同发育阶段的热量单位多为正效应（图5）。（马玉平）

2.11 冬小麦发育期主要影响因子作用的量化及对产量影响的模拟

收集了华北平原47个农业气象观测站1986—2010年冬小麦的发育期资料和同期的逐日平均气温数据，利用基于3基点温度（T_b为0 ℃，T_{opt}为22 ℃，T_{max}为32 ℃）的双线性发育期模型，以1986—1988年的平均品种状态对发育期模型进行参数化，随后模拟1986—2010年间的返青－抽穗期与抽穗－成熟期，并计算模拟误差随时间的变化趋势。品种更替使冬小麦返青－抽穗日数总体呈增加趋势，但趋势不明显，且存在显著的区域差异，其中平原南部、北部日数略有缩短，而中部及山东东部增加较明显。品种变化使抽穗－成熟期日数呈显著增加趋势，平原南部增加尤其明显，平原中部和东西北部增加不明显，有些区域甚至还略有缩短。本研究表明，品种变化对发育期的影响，随发育期的不同而不同，在不同的区域也有不同的表现。在研究未来气候变化对发育期的影响时，如果能考虑到这种区域差异，将有助于降低模拟的不确定性（图6）。（邬定荣）

2.12 应用统计模型模拟气候变化对玉米产量的影响及不确定性研究

多模式的集合是处理不确定性的有效方法。研究考虑由IPCC第5次评估报告的8个全球气候模式和3个排放情景（RCP2.6/4.5/8.5）组成的24个气候模式数据代表气候输出不确定性，与应用Bootstrap方法产生100组参数的2个统计模型代表的作物模型内部参数不确定性相结合，以辽宁省本溪、吉林省长岭、黑龙江省海伦农气站为研究地点，量化评估了2个未来时段（2010—2039年和2040—2069年）相对于1976—2005年基准时段玉米产量的影响及不确定性。研究结果表明，未来2个时段玉米产量降低均不足5%。应用方差分析法，量化了单一不确定性来源对最终集合产量综合不确定性结果的影响，如气候模式结构和排放情景的不确定性、作物模型参数的不确定性。研究结果表明，气候情景的不确定性对最终结果的不确定性影响，要大于作物模型参数不确定性所带来的影响；增加的集合产量方差表明未来气候变化背景下产量模拟的不确定性增加。（张祎）
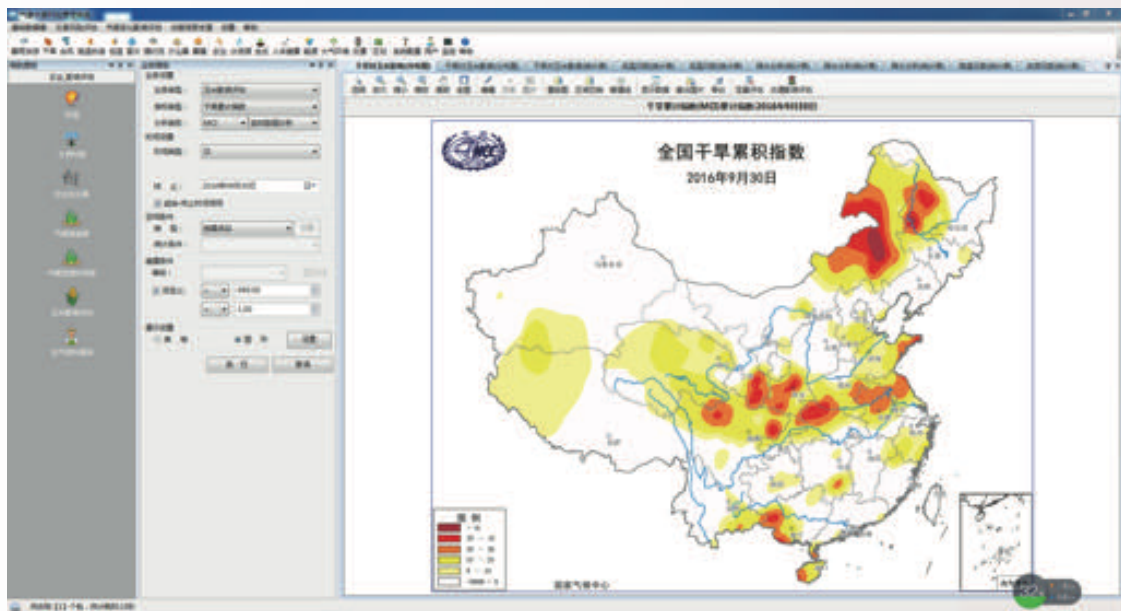
图 1　玉米气象干旱业务系统界面
Fig. 1　The operational system of maize meteorological drought
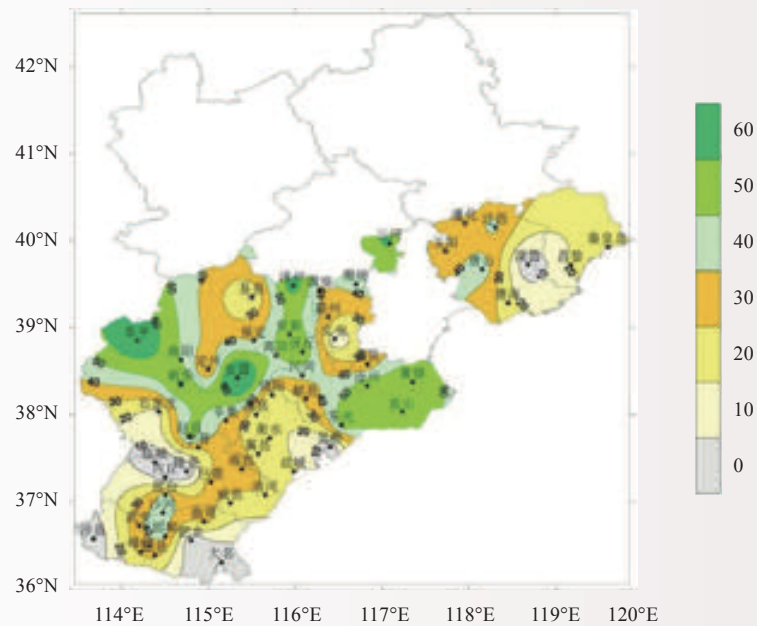
图 2　2016年河北省冬小麦开花、灌浆期灌溉量（m³/亩，1亩 = 0.0667 hm²）预报
Fig. 2　Irrigation forecast of winter wheat flowering and filling stage in Hebei Province in 2016
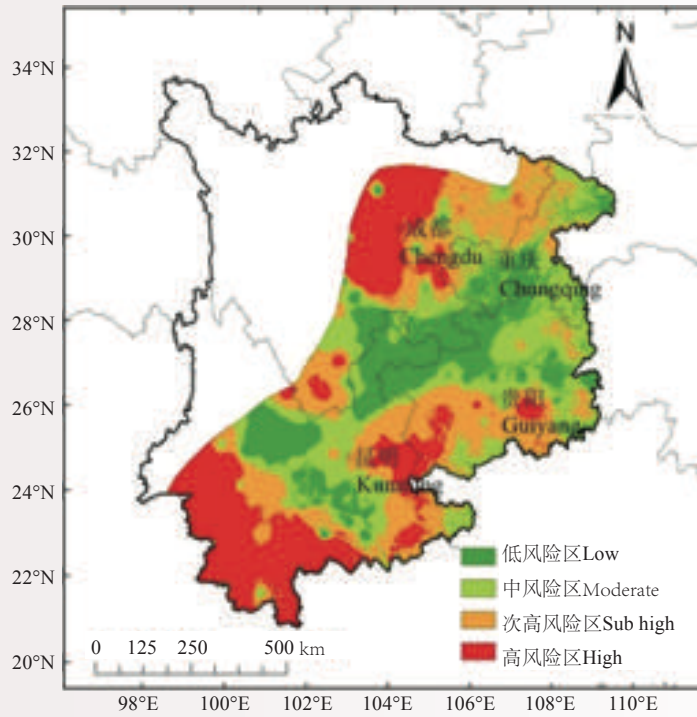
图 3　西南地区水稻洪涝综合风险等级空间分布
Fig. 3　Spatial distribution of integrative risk of rice flood in Southwest China
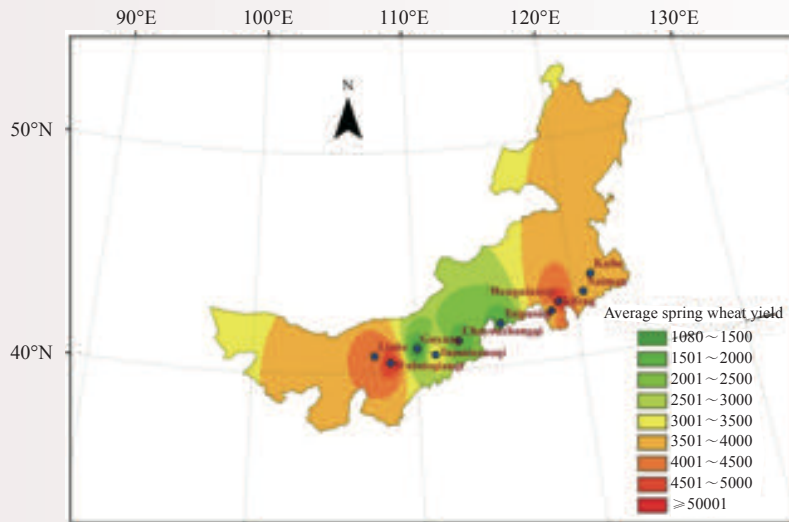
图 4　1961—2010年内蒙古春小麦产量平均分布
Fig. 4　Average distribution of spring wheat yield in Inner Mongolia from 1961 to 2010
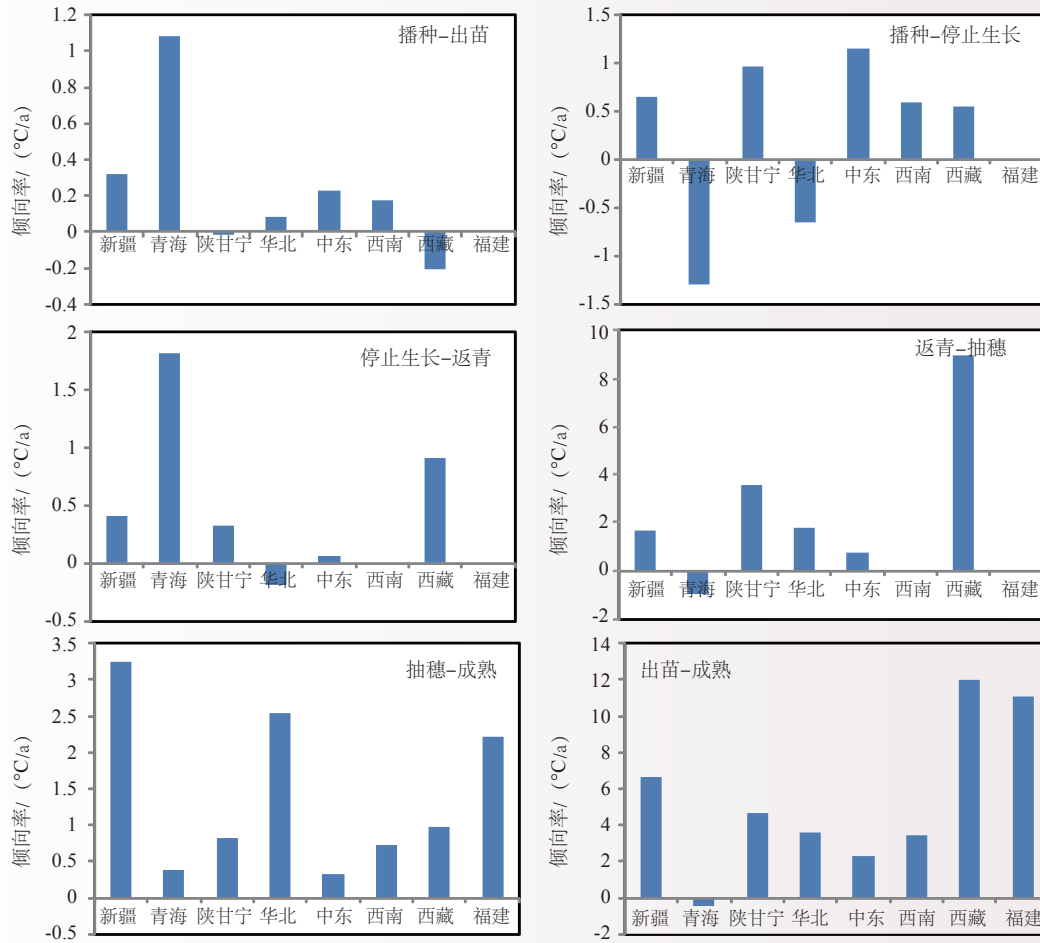
图 5   我国不同地区冬小麦品种变化影响不同发育阶段间热量单位的倾向率

Fig. 5   The tendency rate of the heat unit in different developmental periods affected by the variation of winter wheat varieties in different regions (Xinjiang, Qinghai, Shanganning, North China, Central and East China, Southwest China, Xizang and Fujian) in China
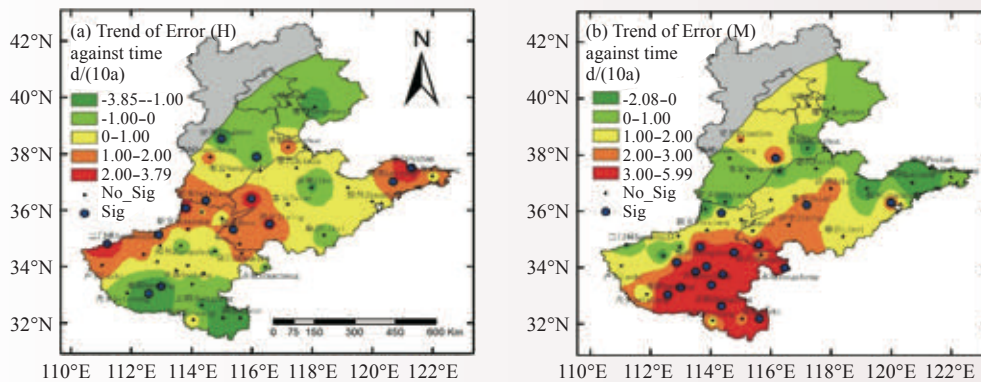
图 6   1986—2010年冬小麦抽穗期、成熟期模拟误差趋势空间分布（Error(H)为抽穗期模拟误差；Error(M)为成熟期模拟误差；Sig表示在0.05水平上差异显著；No_Sig表示在0.05水平上差异不显著）

Fig. 6   The spatial distribution of the simulation error trends in heading (H) and maturity (M) stages during 1986–2010. Sig denotes significant at 0.05 significance level and No_Sig means not significant at 0.05 significance level

Progress in Ecological Environment and Agrometeorology Research

1 Agroclimatic resources and agrometeorological disasters forecasting and early warning

1.1 Research on flood disaster monitoring and early warning and prevention and control key technology

The results of this project revealed the temporal and spatial distribution characteristics of agriculture, corn, and rice flood disasters in the whole country and in the study area. Eleven sets of corn and rice flood disaster level indicators and ten sets of provincial agriculture flood disaster level indicators were built. Three sets of waterlogging and flood tolerance physiological indicators were established. Three sets of flood control and disaster prevention in cropping model farming and cultivation integrated technology were developed. Three sets of disaster prevention and control of technological processes were constructed. The results have been used for meteorological business applications in Hunan, Jiangxi, Zhejiang, Anhui, Guangxi, Chongqing, Shaanxi seven provinces (district and city). It made and published more than forty special service products and decision-making service reports of floods and agricultural weather. Flood warning and disaster reduction service achieved a significant efficiency of disaster reduction and production increase. This project put forward the construction method of level indicators based on the inverse risk analysis of disaster risk, resolved the key technologies of the flooding level threshold of agricultural flooding, maize and rice flooding, and the comparability of provincial indicators which are based on precipitation process, and provided indicators to support the development of real-time monitoring and forecasting of agricultural disaster. (Huo Zhiguo)

1.2 Techniques of the 3D monitoring and the dynamic assessment of key agrometeorological disasters

To study the 3D monitoring and the dynamic assessment of the dry-hot wind for winter wheat in Huang-huai-hai areas, cold damage for double cropping rice in southern China and agricultural drought in Southwest China, we established meteorological indicators and a grading system for the above agrometeorological disasters, and developed the 3D monitoring and the dynamic assessment techniques which are based on ground observations, remote sensing and crop models and are applied to meteorological operation. The work has some innovations in the following aspects: (1) information coupling is developed into a diversified development, which integrated ground meteorological, agrometeorological, farmland small-scale, agricultural situation and disasters, and geographic data; (2) the 3D monitoring and the dynamic assessment have been oriented to modeling, dynamic and refined analysis; (3) the transformation technology of spatial scale is emphasized in the process of multi-source information use. The key monitoring and assessment techniques, which are totally tailored to Chinese agricultural production and disasters, are highly regional and practical, taking into account the operational service needs of the meteorological and agricultural sectors. The implementation of the research findings can significantly improve the monitoring and assessment of agrometeorological disasters in China. (Zhao Yanxia)

1.3 Prediction of the key agro meteorological disasters in China

Impacts of the low temperature stress on double-rice growth in southern China, including its abrupt

change, trends, grade risk and the characteristics of the spatial distribution of the integrated risk, were revealed in the study, based on which methods on the risk zoning for prediction was presented. Prediction index and systematic technology were also established to forecast low temperature impacts on double rice growth in southern China, with the prediction accuracy as high as 80% at the temporal scales of either 5 days or one month. Detailed soil moisture can also be obtained by a successfully established prediction system, with functions such as automatic data input, operation and product-generation. The improved crop growth model was used to simulate the regional agro-drought in North China Plain. Coupled with the remote sensing technology, the calibrated crop model showed obvious advantage in regional agro-drought prediction, which was identified by the comparison between the simulation results and the base line values. All of the relevant achievements have been applied in the provincial agrometeorological services, leading to an improved prediction of the agrometeorological disaster with higher accuracy. (Liu Jiandong)

1.4 Risk assessment and management technology for major agrometeorological disasters

According to the situation of the frequent agrometeorological disasters such as drought, flood and chilling disasters happened in typical areas in China with severe effects, and the lacks of effective risk assessment technology, the main crops of the major agricultural regions in Northeast China, North China, and the Middle and Lower Reaches of the Yangtze River were selected, based on multi-technology integrated risk analysis methods and the risk study of agrometeorological disasters, centered on crops and started from the continuum of the soil-plant-atmosphere, finally the integrated assessment theory of agrometeorological disaster risk based on the formation mechanism of disaster was proposed. The technologies of assessment coupling static and dynamic risk of agrometeorology disasters, risk mapping, integrated assessment and regional assessment of multi-disasters and early warning were formed. Besides, risk maps of agrometeorological disasters in major crops producing area were made. Agrometeorological disaster risk analysis and evaluation system was developed. Moreover, a countermeasure system of agrometeorological disasters integrated risk management technology was proposed. The extension and application of our main research achievements had good effects on relevant departments of Jilin, Hebei and other provinces which provided the necessary theoretical basis and technical supports for agricultural disaster prevention and mitigation. (Wang Chunyi)

1.5 Soil moisture estimation method based on both remote sensing and air temperature in a summer maize ecosystem

Soil moisture is an important component of the soil-vegetation-atmosphere continuum (SPAC), which is a key factor determining the water status of terrestrial ecosystems, and is also the main sources of water supply for crops. In order to estimate soil moisture at different soil depths at a station level, based on the energy balance equation on the earth and the water deficit index (WDI), a soil moisture estimation model was established on the hypothesis that evapotranspiration deficit ratio (i.e., WDI) depends linearly on soil relative humidity. Thus, the soil moisture could be estimated in terms of the remote sensing data (the normalized difference vegetation index (NDVI) and surface temperature (T_s)) and the ground observations (air temperature T_a). The soil water estimation model was validated based on the data from the drought process experiment on summer maize (*Zea mays* L.) in response to different irrigation treatments carried out during 2014 at Gucheng Eco-agrometeorological experimental station (39°08'N, 115°40'E) of China Meteorological Administration. The model was used to estimate soil relative humidity at different soil depths (0–50 cm) in terms of the parameters from the genetic algorithm and nonlinear programming algorithm. The results indicate that the soil water estimation model developed in this study is able to evaluate soil relative humidity at different soil depths in the summer maize, and the hypothesis is reasonable that evapotranspiration deficit ratio (i.e., WDI) depends linearly on soil relative humidity. It was shown that the estimation accuracy of 0–10 cm surface soil moisture

was the highest ($R^2 = 0.90$). The correlation of the estimated and measured soil relative humidity in deeper soil layers (up to 50 cm) could pass the significance test at the level of 0.0001 with the RMAEs less than 15% and the PRMSEs less than 20%. Results from this study could provide a reference for drought monitoring and irrigation management. (Zhou Guangsheng)

1.6 Critical meteorological conditions in maize response to drought disaster and the monitoring and pre-warning technology

Based on the integrations on the experimental data and relevant studies, the response and adaptive mechanism under the combinations of drought and other key factors of climatic change were elucidated preliminarily in terms of the coordinative changes between leaf stomatal conductance (g_s), water use efficiency (WUE), and plant/leaf growth. Based on the measurement and experimental data of the present project, the changes in photosynthetically physiological process and chlorophyll fluorescence and their responses to drought and rewatering were examined in maize plants subjected to drought at different growth and development stages. Leaf relative chlorophyll concentration (SPAD meter readings), g_s, and transpiration rate (E) significantly decreased in two weeks after withholding water at jointing, but the chlorophyll fluorescence parameters including actual quantum yield of PSII primary photochemistry in the light-adapted state (Φ_{PSII}), maximum quantum yield of PSII primary photochemistry in the light-adapted state (F_v'/F_m') remained stable. The photosynthetic capacity traits significantly decreased in one week after withholding water at tasseling, and the leaf net photosynthetic rate decreased more due to drought stress during tasseling than during jointing. Based on the measurements on the same leaves during their entire growth periods, the photosynthetic capacity was restored to some extent, but not reaching the level of the control treatment. Light-saturated photosynthetic rate (A_{sat}), g_s, and E trended to decrease; SPAD values increased first, then decreased. In addition, there were greater declines in various parameters under drought relative to the control treatment. The changes in chlorophyll fluorescence parameters (Φ_{PSII}, F_v'/F_m') of the same leaves remained relatively stable with the leaf growth at amply watering condition. Meanwhile the chlorophyll fluorescence parameters did not decrease significantly under the four drought treatments, even obvious increases in the corresponding parameters occurred after rewatering when the maize plants experienced the drought stress. It is indicated that the drought tolerance of the photosystem II (PSII) may be enhanced with maize leaf growth and development.

Based on the soil moisture observational data, a new criterion of drought intensity for Drought Index, MCI, was given. Firstly, the daily relative humidity time-series (1992–2010) at a certain site was obtained by linear interpolation. Secondly, a statistic model was established based on the relationship between MCI index and soil relative humidity. Then, based on the observed data, the upper limit of meteorological drought index of maize at different growth stages was determined. A "drought impact on maize assessment module" was constructed in the operational system of "meteorological disaster risk management system" based on the above results. The system can be used to evaluate the drought effects on maize. Figure 1 shows the results of the maize drought accumulation index on September 30, 2016. The maize meteorological drought was mainly distributed in the western part of Northeast China, eastern Inner Mongolia and Hubei, Anhui, Jiangsu and Sichuan (Fig.1). (Zhou Li)

1.7 New finding on self-photoprotection mechanism of plant adapting to future climate change

We examined the photosynthetic responses of *Stipa baicalensis* to relatively long-term exposure (42 days) to the predicted elevated temperature and water availability changes to determine the mechanisms through which the plant would acclimate to future climate change. Two thermal regimes (ambient and +4 °C) and three irrigation levels (partial, normal and excess) were used in environmental control chambers. The gas exchange parameters, light response curves and A/C_i curves were determined. The elevated temperature

and partial irrigation reduced the net photosynthetic rate due to a limitation in the photosynthetic capacity instead of the intercellular CO_2 concentration. Partial irrigation decreased Rubisco activation and limited RuBP regeneration. The reduction in V_{cmax} increased with increasing temperature. Excess irrigation offset the negative effect of drought and led to a partial recovery of the photosynthetic capacity. Although its light use efficiency was restricted, the use of light and dark respiration by *Stipa baicalensis* was unchanged. We concluded that nonstomatal limitation was the primary reason for photosynthesis regulation in *Stipa baicalensis* under relatively long-term climate change conditions. Although climate change caused reductions in the light use efficiency and photosynthetic rate, a self-photoprotection mechanism in *Stipa baicalensis* resulted in its high ability to maintain normal live activities. (Zhou Guangsheng)

1.8 Fine soil moisture and irrigation forecasting technologies for winter wheat in northern China and their application

The data set of soil moisture and irrigation forecast was improved. The daily meteorological data and automatic soil moisture data in northern winter wheat region in the data set extended to July 31, 2016. The remote sensing inversion methods of crop water deficit indices were studied further. The decadal changes of the *a* and *b* coefficients in ÅngstrÖm-Prescott formula were analyzed. The *a* and *b* coefficients of month by month for different ages from 1961 to 2010 in the study area and major regions of China were given. Based on growth mechanism of winter wheat, soil water balance equation, various test data, the previous research of the simplified models of water balance in winter wheat field and the fine daily multi-layer soil moisture and irrigation forecast models and the localization trial of three provincial fine soil moisture and irrigation forecasting systems of winter wheat, a national fine soil moisture and irrigation forecasting system software was constructed initially. Using the project research results and three provincial fine soil moisture and irrigation forecasting system service platforms, a number of service products were released and provided valuable reference information for agriculture and other departments in Hebei, Shandong and Henan provinces (Fig. 2). (Mao Fei)

1.9 Meteorological disaster risk zoning of melon & vegetables in Hainan Province

Based on the occurrence frequency and process precipitation of different dry or less rainy days in March to May from 1971 to 2010 in Hainan cities and counties, the spring drought artificial control experiment was carried out. The experiment was conducted with uniform combination design of continuous drought days (10, 15, 20, 25, 30, 35, 40, 45, 50 days) and the amount of water supply (0, 2, 4, 6, 8, 10, 12, 14, 16 mm): 2 factors 9 level treatments, the determination of different treatments under different depth of soil (10, 20, 30, 50, 100 cm), the effects of different treatments on the seedling death rate, physiological characteristics and yield of pepper were analyzed. The results show that the rate of dead paprika seedlings was significantly correlated with soil relative moisture at depth 20 cm and continuous drought days, and little correlated with irrigations. With the increase of continuous drought day duration, net photosynthetic rate, transpiration rate and stomatal conductance of paprika decreased and relative yield loss increased significantly. Grades index of spring drought disaster for paprika was constructed, the drought disaster index for paprika fitted well the actual drought disaster situation and could help provide strategies for monitoring and precaution against drought disaster for paprika. (Huo Zhiguo)

1.10 Temporal and spatial variation characteristics of potential evapotranspiration in China during 1961—2015

The spatio-temporal distribution characteristics of evapotranspiration (ET_o) on the national and four climatic regional scales were analyzed at annual, seasonal and decadal scales, respectively, and the reasons of

the spatio-temporal pattern for ET_o were analyzed based on Penman-Monteith method and daily meteorological data at 552 meteorological station in China from 1961 to 2015. Results show that the average annual ET_o is about 621–1733 mm in China. The regions with the highest ET_o mainly distribute in the arid region, while the areas with lower ET_o concentrate in the semi-arid, humid and semi-humid regions at both 55-year average and different decadal scales. The spatial distributions of ET_o are different in the seasonal scale. ET_o is the highest in summer, followed by spring and autumn, and the lowest in winter. Temporally, the average annual ET_o decreases at a rate of –0.52 mm/a from 1961 to 2015, and the decreasing trend has a mutation phenomenon in 1972. Although there is an increasing trend since the last decade of the twentieth, the mutation year was not detected with the M-K method. The change trend of ET_o is different in different climate regions. ET_o in most sites showed a decreasing trend in arid region and humid region, and the number of meteorological stations with decreasing rate in arid region is more than that in humid region. In semi-arid and semi-humid regions, the number of sites is roughly equivalent to the increasing or decreasing trend for ET_o. ET_o at more than 85% of the sites in China was mainly affected by wind speed and sunshine time. Studies have shown that the decreasing trend of ET_o in nearly 55 years was mainly caused by the decrease of the wind speed, the reduction of sunshine time and the slight increase of vapor pressure. (Wang Peijuan)

1.11 Construction of drought monitoring index based on the winter wheat water stress experiment

Aiming to study the effects of different irrigation treatments on the growth and development of winter wheat, the field experiment was conducted with local predominant variety to simulate three water stresses, i.e., persistent severe drought, moderate drought, and mild drought, during the whole growth period of winter wheat over 2013–2014 (variety: Henong 6425) and 2014–2015 (variety: Yanmai 98) using the large-scale artificial water control field at the Gucheng ecological-meteorological experimental station in North China Plain. Based on water balance equation, the actual evapotranspiration of winter wheat under different water stresses (ET_a) and CK conditions (ET_c) were computed. Furthermore, a crop drought monitoring index (CDMI) which can reflect the degrees of water demands and deficits was built based on ET_a and ET_c. The thresholds of CDMI were determined referring to the yield reduction of winter wheat under different persistent water stresses, and further constructed a drought monitoring index system of winter wheat during the whole growth period. Compared to the traditional drought monitoring index based on potential evapotranspiration, the CDMI based on ET_c can reflect drought degree more objectively and reasonably, which can be served as a method to monitor the drought of winter wheat in North China Plain. (Wang Peijuan)

1.12 Flood risk assessment and zoning for rice in Southwest China

As the main crop in Southwest China (Sichuan, Chongqing, Guizhou and Yunnan provinces), rice is widely accepted to be seriously threatened by the flood disaster. Agro-flood risk analysis is helpful for improving the ability of regional disaster management and reducing potential flood risk. In this study, the rice flood risk was analyzed and zoned using the integrated rice flood risk assessment model including hazard, exposure, sensitivity, and flood prevention and mitigation, and based on the daily rainfall data in 193 meteorological stations from 1961 to 2012, rice production data in 396 counties including plant and yield data from 1981 to 2012, the phenophase data of rice from 17 agrometeorological stations and geographic data in Southwest China. The results indicate that flood hazard risk probabilities variated with phenophase and hazard level. High flood hazard risk happened in transplanting-tillering stage, followed by jointing-booting and tasselling-maturity stages. High-risk areas of flood hazard in the whole rice growth stage was detected to be located in southern and northeastern Yunnan, southern Guizhou, and Chengdu, Meishan and Deyang in Sichuan Province. High and sub-high exposure zones were mainly located in the northeastern part of Sichuan Province and Chongqing. Subsequently, high and sub-high sensitive zones were mainly found in the northern

Yunnan Province, southern Sichuan Province and southeastern Guizhou Province. Low flood prevention and mitigation zones were located in parts of Guizhou. Finally, the high and sub-high zones for the integrated rice flood risk were detected in the northeastern Sichuan Province, southern Guizhou Province and southern part of Yunnan Province, while southern Chongqing and northern Yunnan were recognized with low rice flood risk (Fig. 3). (Yang Jianying)

1.13 Effects of winter and spring irrigation on winter wheat in North China

A field simulation experiment about irrigation of the first springing water (FSW) at different air temperatures (0, 3, 7, and 10 °C) in 3 years was designed under the preconditions of the irrigation of overwintering water (OWW) (80/150 mm) and no OWW. We explored the effects of OWW and FSW irrigation on growth and grain yield, and tried to find appropriate irrigation patterns and schemes of winter wheat in the North China Plan (NCP). The results show that FSW irrigation could relieve winter drought in air temperature stability through 0 °C under no OWW irrigation, which increased effective stalk number in spring, effective panicle number and grain yield significantly. The time of continuous drought in key growth stages could be reduced by FSW irrigation in air temperature stability through 7 °C under OWW irrigation, which increased grain yield significantly. We found no significant relationship between the amount (80 mm and 150 mm) of OWW irrigation and grain yield. Meanwhile, FSW was essential to the growth of winter wheat: there was an average reduction of 32.2% on grain yield under no FSW irrigation. Therefore, in order to ensure a stable and high yield of winter wheat and water-saving irrigation in the NCP, we should irrigate FSW in air temperature stability through 0 °C under no OWW irrigation and irrigate FSW in air temperature stability through 7 °C under proper amount of OWW irrigation. (Liu Tao)

1.14 The response mechanism of soil respiration on grassland desert hydrothermal change

A warming treatment and a control, and three watering levels were applied using a free air temperature increase facility with open soil carbon flux measurement system. R_s was measured throughout the year, and soil nutrition properties and microbial biomass carbon were determined over the growing season. R_s rates were significantly higher during the growing season than during the non-growing season. However, the warming treatment led to a marked increase in R_s in winter. Soil temperature and R_s were described by an exponential function with a Q_{10} of 1.92 ($R^2 = 0.74$, $p < 0.01$); and root respiration (21.9%) was lower than heterotrophic respiration (78.1%). Soil organic carbon, soil moisture, root biomass, and soil ammonium-N were determined to be driving R_s during the growing season. The most important factor was soil organic carbon content in the 0–10 cm soil layer, with soil moisture showing little direct effect on R_s. Using the four most critical factors of soil respiration under hydrothermal conditions in the growing season, we established a model describing the responses of R_s to environmental change ($R^2 = 0.67$, $p < 0.01$). Soil environmental variables including temperature, moisture, nutrition status, root growth, and soil microbial activity might co-regulate soil carbon emission, which would be considered critical in assessing the carbon balance under climatic change in arid areas. (Liu Tao)

1.15 Estimating water use patterns in winter wheat using remote sensing in Huang-Huai-Hai Plain

Each water use component of winter wheat in Huang-Huai-Hai (3H) Plain from 2011 to 2012, including effective precipitation (PP_{eff}), irrigation water applied (IWA), actual evapotranspiration (ET_a) and on-farm water losses (F), was calculated at both temporal and spatial scales, integrating meteorological data, MODIS, SEBAL (Surface Energy Balance Algorithm for Land) model and the water balance equation. There was a clear relationship between survey- and model-values of IWA ($R^2 = 0.79$), indicating the applicability of the model-based method in IWA estimation. Precipitation in the 3H Plain provided >70% of total water use at the

early stage of winter wheat. However, over 90% of crop water use depended on IWA at the grain filling stage. A high-IWA belt for the whole growing stage in winter wheat was mainly observed in basin-irrigable land and dry land, with average IWA = 412.76 mm. Water consumption in the winter wheat period represented a significant relationship with irrigation ($p < 0.01$) in 3H Plain, with R^2 of 0.68. (Yang Jianying)

2 Response and adaptation of agriculture to climate change

2.1 Assessment of agrometeorological disasters and yield losses in China since 1961

Since 1961, the extreme climate events in the whole nation showed an increasing trend. China's climate exhibited warm becomes warmer and dry becomes drier, together with more floods under the climate change. Both the area and occurrence frequency of the national agricultural drought disaster also showed an increasing trend, and the drought showed an increasing trend from south to north. The occurrence frequency of waterlogging in winter wheat showed an increasing trend, and the intensity of the disaster increased more obviously in the late growth stage. The high temperature heat damage of paddy rice showed a significant increasing trend, and the severe disasters increased significantly. The chilling damage showed a decreasing trend, but in the recent 30 years, low temperature and rainy injury showed an increasing trend. The frost damage generally decreased, but the local area has aggravated the trend. The changes in evolution trend, intensity and types of agro meteorological disasters have taken place. As a result, the agricultural layout at present, together with the countermeasures for the food security and the ecological civilization construction as well as poverty alleviation, should be adjusted in order to adapt to the changing agrometeorological disasters. (Zhou Guangsheng)

2.2 Research on status quo, rate, mechanism and potential of carbon sequestration in grassland ecosystem in China

Based on more than 4 thousand survey points and TEM model, the carbon density, spatial distribution and dynamic change of grassland ecosystem in China were simulated with monthly time step, using climate, elevation, soil and vegetation data. The carbon storage of grassland ecosystem in China was estimated. The spatial distribution pattern of soil carbon density in Chinese grassland was drawn, and its spatial distribution characteristics were revealed. The spatial and temporal variation of carbon density of grassland in China and its regional differences since 1960s were quantitatively described. Carbon budget in China under the future climate scenarios was simulated. The main innovation is to solve the problem that the spatial precision of TEM is not high based on a set of parameters. A parameterization scheme was presented according to grassland ecology zone, and a series of TEM model parameters suitable for Chinese grassland were established, which could provide a basis for monitoring and evaluating carbon budget, NPP, GPP, etc. (Ji Yuhe)

2.3 Key technology on the agrometeorological service for highland barley production under climate change scenarios

The solar radiation resource will reduce slightly under both A2 and B2 climate change scenarios over the Tibetan Plateau, while it would still be/retain the region with the most abundant solar resource in the world. Temporal distribution pattern of the solar radiation will have no obvious change under both A2 and B2 scenarios, with the minimum in winter and maximum in summer. However, the monthly variation in the solar radiation will change clearly, increasing in summer and decreasing in other seasons. Trends in the total annual precipitation will increase under climate change scenarios, yet it will still be referred to as the less-precipitation area in the world. Seasonal precipitation will become even more inhomogeneous, with minimum

in winter and maximum in summer, revealing an increase in precipitation simultaneously. The general spatial distribution pattern of precipitation, with precipitation decreasing from east to west spatially, will witness no marked change under climate change scenarios, but increase in precipitation will become more obvious in the western than in the eastern part of the Tibetan Plateau. Increase in temperature will have positive impacts on the enhancement of highland barley yields under climate change scenarios, but the main features in the spatial distribution of highland barley yields will basically remain unchanged. Higher enhancement of the highland barley yield will occur in the current high-yield regions. In other words, under climate change conditions in the future, the greater enhancement of the highland barley can be expected/envisaged in the current optimum regions for highland barley growth. (Liu Jiandong)

2.4 Identifying the effects of climate change on the yield of main dryland crops in the northern China based on APSIM crop model

The responses of key growth stages and yield of spring wheat and spring maize to climate change in the northern China were identified based on the optimized APSIM crop simulation model. The results show that the APSIM model had a good applicability in Inner Mongolia, Gansu, Heilongjiang, Jilin, Liaoning and other northern regions. The potential yield of spring wheat in Inner Mongolia decreased from 1961 to 2010, with an average of 3561 kg/hm^2. In particular, the potential yield of spring wheat was the highest in the 1980s (3681 kg/hm^2) and the lowest in the 2010s (3433 kg/hm^2). There were significant differences among regions. Over the past 50 years, the potential yield of spring wheat in Inner Mongolia increased gradually from the middle region to the east and the west regions. Among the three regions, the potential yield of spring wheat was the highest in the western region and was the smallest in the middle wheat region.

The main meteorological factors influencing the key growth stages of spring maize in Inner Mongolia were the maximum temperature, followed by the minimum temperature. The effects of solar radiation, precipitation and potential evapotranspiration on the growth stages of spring maize were the same. The key meteorological factors affecting the spring maize yield were the maximum temperature, the minimum temperature, precipitation, solar radiation and potential evapotranspiration (Fig. 4). (Zhao Junfang)

2.5 The stability assessment of different accumulated temperature model on accumulated temperature in different stages of spring maize in Northeast China

Based on the growth data of 4 spring maize varieties "Danyu 13" "Longdan 13" "Dongnong 248" "Sidan 19" and the meteorological data in Northeast China, the model parameters of Shen Guoquan's, Gao Liangzhi's and Yin Xinyou's nonlinear accumulated temperature models were fitted, respectively. The stability of accumulated temperature of simulated results from different nonlinear models were compared and evaluated. They were also compared with the results of the commonly accumulated temperature model. The results of Shen Guoquan's, Yin Xinyou's, Gao Liangzhi's nonlinear accumulated models and the commonly accumulated temperature model showed that the stability of accumulated temperature from the three nonlinear models are better than the commonly accumulated temperature model from emergence to maturity. From seedling to jointing stage, the stability of accumulated temperature from the four models are uniform for "Danyu 13", but the three nonlinear models are slightly better than the commonly accumulated temperature model for "Longdan 13" "Dongnong 248" "Sidan 19". The stability of the accumulated temperature from the jointing to tasseling stage is the worst stage, because the coefficient of variation in this stage is the biggest for each of varieties. From the tasseling to maturity stage, the stability of the accumulated temperature is almost not different in the four models. The results provide a theoretical basis and technical support for the development of spring maize in Northeast China. (Guo Jianping)

2.6　Effects of climate change on agricultural climate resources in the northeast region of China

The temporal and spatial characteristics of major agroclimatic resources in the northeast region of China were systematically analyzed. During the period of 1961–2099, the heat resource is more abundant in the southern region than in the northern region, and the heat resource shows a significant increasing trend in the future. The average annual temperature in the northeast region of China will rise by about 2 °C and 3 °C in median emission scenarios (RCP4.5) and high emission scenarios (RCP8.5), respectively. The first day of over 10 °C will appear 3–4 days earlier. The first frost date will delay by 2–6 days. Therefore, the potential growth season may increase by 4–10 days. The accumulated temperature will be enriched because of temperature rising and growth season extending. By the end of this century, the accumulated temperature will increase by 400 °C·d and 700 °C·d in median emission scenarios and high emission scenarios, respectively. Water resource shows a weaker increasing trend. There are significant changes in the heat resource change rate, and high emission scenario corresponds to a faster warming. There is a warming trend in the future in the northeast region of China. The temperature rising in the northeast region of China has a positive impact on agricultural production. The heat resource that can be used by crop will be more abundant because of growth season extending and accumulated temperature increasing. The original no-planting area due to heat resource restrictions will be reduced, and the planting area will be expanded. The planting varieties will be improved, the region planting early maturing varieties can be replaced by late maturing varieties, and the late maturing varieties planting area will be further expanded. As such, the late maturing maize needs the accumulated temperature to reach 3000 °C·d, the planting area will extend from the original Songnen Plain to the Greater Khingan Range. Even double crops a year may occur in some areas in Liaoning. (Guo Jianping)

2.7　On the effects of CO_2 concentration elevation and temperature rising on crop water requirement

Based on the experiments during 2013–2015, the changes in wheat water use efficiency and the coupling mechanism correlation with water requirement and yield under the background of elevation in atmospheric carbon dioxide concentration and increase in air temperature in future were analyzed. The results show that the individual effects of increase in air temperature and elevation in atmospheric carbon dioxide concentration on wheat water requirement and wheat growth are additive. The increased air temperature lifted the temperature in wheat canopy and communities, eventually accelerated energy flow and hydrological cycle within the wheat field. As a result, the daily water requirement has rose through increase in transpiration from wheat plant and evaporation between plants. The elevated CO_2 also led to reduced leaf stomatal conductance and net photosynthetic rate, resulting in higher water use efficiency. In addition, the CO_2 fertilization effect has promoted wheat yield increase. On the integrative view, the elevation in atmospheric carbon dioxide concentration and increase in air temperature have increased the wheat water requirement, resulting in higher water use efficiency. The increased water requirement in turn has contributed to wheat yield increase. In the future, the more agricultural thermal resources and atmospheric CO_2 imported in the wheat eco-system will induce increased wheat water requirement, and further the higher yield and WUE, leading to a positive feedback circulatory eco-system. (E Youhao)

2.8　Study on the regulation mechanism of vegetation succession of abandoned farmland in farming-pastoral zone in northern China

In this work, the vegetation succession process of abandoned farmland in farming-pastoral zone in northern China was studied using a space-for-time substitution method by transect sampling. The regulation mechanism of natural environmental factors on vegetation succession in abandoned farmland was revealed from a relatively macro perspective.

According to the research objectives of the project, the field transect survey was carried out in Shanxi-Ningxia agro-pastoral ecotone. Soil moisture content, soil texture and nutrient content at soil depth of 0–500 cm, as well as vegetation coverage, biomass, species and other information in the typical ecosystem of agro-pastoral ecotone were collected. In view of the greater temporal and spatial variability of rainfall, temperature and other meteorological factors, the more stable environmental information such as soil dry layer, soil texture, geomorphology as well as climatic factors will be used to select the key factors restricting the spatial distribution and community succession of ecosystem to explore the environmental adaptability and tolerance to climate change in northern China. In addition, tree ring data were also collected and will be used to study the response and adaptation to climate change of the northern ecosystem. (Ji Yuhe)

2.9 The impact of elevated temperature and CO_2 concentration on winter wheat yield and grain quality

During 2015–2016 winter wheat growing season, the third year of the manipulative experiment under elevated temperature and CO_2 concentration using OTC and infrared heaters was conducted. The data for phenology, plant height, stem density and dry biomass per plant obtained in this year produced results essentially in agreement with those in previous two years. The root cause of yield decline was still the reduction of grain number per ear, which was mainly attributed to the significant reduction of spikelet number in this year. Meanwhile the data of grain quality and leaf carbon and nitrogen contents measured in the 3 consecutive years were analyzed. The results show that crude protein in winter wheat grain under the combined treatment slightly increased, but the contents of fat, fiber and starch in grain were not significantly influenced. No significant differences in nitrogen and organic carbon contents in winter wheat leaves were found between the combined treatment and control over growing stages, although a tendency of decline of nitrogen content in winter wheat leaves from jointing stage to flowering stage likely existed. (Tan Kaiyan)

2.10 Effects of wheat varieties improvement on phenology in China

The effects of wheat varieties improvement on phenology were analyzed using the agrometeorological observation data in China. The results show that there is an increase in heat units at different developmental stages caused by varieties change. The heat unit from emergence to maturity increased by 3.5 °C/a. A comparison of different regions indicates that the variation of spring wheat varieties in Tibet, Inner Mongolia and Xinjiang has a great influence on the phenology. Most of them are positive effects on heat unit in different developmental periods. The change of winter wheat varieties has no obvious effect on heat unit during sowing to emergence, emergence to stop growth, stop growth to turn green, jointing to heading and milk to maturity while positive effect on heat unit during turning green to jointing and heading to milky. The effect of winter wheat variety on phenology is still large in Qinghai, Tibet, Fujian and Xinjiang. The effects are mostly positive on heat unit in different developmental periods (Fig. 5). (Ma Yuping)

2.11 Quantification of impacts of the main influencing factors in the growing period of winter wheat and simulation of the impact on production

Winter wheat phenological observation and daily average temperature data were collected from 47 agricultural meteorological observation stations in the North China Plain (NCP) during 1986–2010. A bilinear phenology model, which is based on three-base-point temperature (T_b was set to 0 °C; T_{opt}, 22 °C; T_{max}, 32 °C), was used to detect the impact of cultivar shift on phenology. Parameters of the phenology model were calculated and validated by the state of average varieties during 1986–1988. The durations from turning green to heading (T-H) and heading to maturity (H-M) during 1986 to 2010 were simulated and the trends of the simulation errors over years were calculated. Generally, duration of T-H increased by cultivar shift, but few of the trends

are statistically significant. The trends are varied substantially at different stations. The days of T-H in the southern and northern plain were slightly shortened, while in central area and eastern Shandong, it increased significantly. Cultivar shift increased the duration of H-M significantly, especially in the southern plain, but no so obvious in the other areas, though it was slightly shortened in some areas. This study shows that the effects of cultivar shift on phenology were different in different development stages and regions. In the studies regarding the effects of future climate change on phenology, the uncertainties of the results will be reduced if this spatio-temporal difference of the impacts was considered (Fig. 6). (Wu Dingrong)

2.12 Using statistical model to simulate the impact of climate change on maize yield with uncertainties

The multi-model ensemble method is an effective way to deal with uncertainties. 24 climate projections consisting of the combinations of eight GCMs and three emission scenarios representing the climate projections uncertainty, and two crop statistical models with 100 sets of parameters in each model representing parameter uncertainty within the crop models, were employed to evaluate the impact of climate change on maize yield at three locations (Benxi, Changling, and Hailun) across Northeast China (NEC) in the periods 2010–2039 and 2040–2069, taking 1976–2005 as the baseline period. The results of ensemble simulations showed that maize yield reductions were less than 5% in both future periods relative to the baseline. To further understand the contributions of individual sources of uncertainty, such as climate projections and crop model parameters in ensemble yield simulations, variance decomposition was performed. The results indicate that the uncertainty from climate projections was much larger than that contributed by crop model parameters. The increased ensemble yield variance revealed the increasing uncertainty in the yield simulation in the future periods. (Zhang Yi)

大气成分与大气化学
Atmospheric Composition and Atmospheric Chemistry

大气成分和大气化学研究进展

1   大气成分及相关特性变化的观测研究

1.1   对气温在雾霾−人体健康效应中的再评估

探讨了雾霾−人体健康影响中的不同季节效应。首先，敏感人群健康风险随着雾霾级别的增加而增加；其次，不同的疾病风险，季节/气温对它们的修饰是不同的。春季，雾霾对呼吸道疾病人群的影响最大，而夏季和冬季，心血管疾病的人群受到的影响最大。此外，因为雾霾具有滞后效应和累积效应，所以在一个持续几天的雾霾事件中，人群的健康风险也有一定的累积。由于来源和粒径分布的不同，不同季节可吸入细颗粒物对健康的影响差异，反映了可吸入细颗粒物的理化特性。夏季，气温可以作为独立的一个环境因子刺激人体，而在冬季则只是作为颗粒物理化特性的一个指引。（李怡）

1.2   2014—2015年中国主要城市大气污染特征及其与气象条件的关系

2013年1月开始中国环境监测总站开始面向社会发布实时的全国主要城市空气质量数据，为研究全国尺度的大气污染状况研究提供了数据支撑。尽管已有研究分析了中国城市大气污染时空分布特征，但多尺度气象条件对中国城市大气污染的影响及这种影响的空间差异还不清楚。利用2014—2015年全国31个省会城市6项污染物（CO、NO_2、O_3、PM_{10}、$PM_{2.5}$和SO_2）小时浓度数据分析了中国主要城市的大气污染特征及其与多尺度气象条件的关系。单一的气象要素很难系统地描述气象条件对大气污染的影响，采用小波分解−人工神经网络（WT-ANN）方法建立统计模型，利用解释方差量化了不同地区气象条件对污染物浓度逐日变化的贡献。研究发现，2014年6项污染物年平均浓度为1.2 mg/m^3、42.2 μg/m^3、49.0 μg/m^3、109.8 μg/m^3、63.7 μg/m^{3}和32.6 μg/m^3。2015年大部分城市污染物浓度明显降低（O_3除外），CO、NO_2、PM_{10}、$PM_{2.5}$和SO_2平均浓度下降5.3%、4.9%、11.4%、12.0%和21.5%，而O_3平均浓度增加7.4%。$PM_{2.5}$作为首要污染物出现的比率最高，其次依次为PM_{10}、O_3、NO_2、SO_2和CO。WT-ANN模拟结果显示，气象条件是驱动污染物浓度逐日变化的主要因子，多尺度气象条件在大部分城市对污染物浓度的解释方差超过70%。2015年有利扩散的天气形势比率有所减少，而不利扩散的天气形势比率有所增加，说明2015年中国主要城市空气质量的改善主要与污染物减排有关。（何建军）

1.3   我国不同背景地区新粒子生成事件的特征及其对云凝结核的影响

在华北区域本底站上甸子、华中地区泰山站和长三角本底站临安开展了3 ～ 800 nm气溶胶数谱和新粒子生成事件的研究。3 nm颗粒物的成核速率在上甸子、泰山和临安分别是6.3，3.7和5.8个/（cm^3·s），增长速率分别为3.6、6.0和6.2 nm/h。新粒子生成事件的对比研究结果表明，在长三角地区有更强的低挥发有机蒸汽的源和更强的凝结汇。在我国背景区域观测到的新粒子生成事件和国外其他背景站点相比，有较高的凝结汇、成核速率和增长速率。凝结汇和成核速率可以高达国外站点的10倍左右，而增长速率可以高出1 ～ 2倍。在新粒子生成事件天气中，云凝结核数浓度可以增加2 ～ 6倍。并且较国外其他背景站点而言，新粒子生成事件对于我国大气中云凝结核数浓度的影响要更显著（图1）。(沈小静)

1.4 2015年阅兵期间减排对气溶胶数谱和新粒子生成事件的影响

为保障2015年阅兵期间良好的空气质量，北京及周边省市于8月20至9月3日实施了高强度的减排措施。本研究对比了2015年阅兵期间和2008年奥运期间的污染物减排情况和同期其他年份（2010—2013年）非减排情况下气溶胶数谱的差异。结果表明，阅兵期间气溶胶积聚模态颗粒物数浓度有显著下降，PM_1质量浓度降低了60% ～ 90%。颗粒物浓度的下降还与气象要素有关，阅兵期间来自南部的污染气团只有14%，而在同期其他年份，污染气团能达到60%。在阅兵期间，共观测到6次新粒子生成事件，频率较非减排期间高，但是成核速率和增长速率较非减排期间低。通过对比凝结汇、气态硫酸、辐射和相对湿度发现，上甸子地区控制新粒子生成的首要因素是凝结汇，其次是气态硫酸的浓度(图2)。（沈小静）

1.5 气溶胶光学–辐射特性地基观测研究

针对2015年12月华北严重雾霾过程开展了气溶胶光学–辐射特性研究，水汽含量增加有利于雾霾发展加剧；雾霾期间有大量细粒子吸湿增长为粗模态；评估了客观因素对气溶胶光学特性的误差贡献；临近站点之间的AAOD、SSA相关性较AOD低的原因可能与局部大气扩散和气溶胶类型（吸收性黑碳和棕碳）差异有关（图3 ～ 4）。（车慧正）

1.6 不饱和有机酸在矿物气溶胶表面非均相反应的机理及动力学研究

非均相反应在大气中起着重要作用，其可以改变大气气溶胶组分从而造成空气污染。然而不饱和有机酸作为一类重要的挥发性有机物，其非均相反应的机理和动力学过程仍然不清楚。在我们的研究中，利用努森池反应器–四极杆质谱和漫反射红外光谱原位模拟了大气典型不饱和有机酸（丙烯酸和甲基丙烯酸）在典型矿物气溶胶表面的非均相反应。首次获取了该非均相反应的一系列真实摄取系数，并估算了大气中不饱和有机酸的非均相反应寿命。另外，结合漫反射红外光谱仪技术，同时检测了反应过程中气溶胶表面产物变化，解析了反应通道。结果表明，不饱和有机酸在矿物气溶胶表面的非均相反应是其大气去除的一种重要途径。尤其是在重污染天气下，此非均相反应可以促使挥发性有机物在气溶胶表面的转化，在气溶胶表面生成羧酸盐等二次有机物，直接改变气溶胶表面组分。（吴玲燕）

1.7 兰州冬季不同化学物种对细颗粒物污染的贡献

兰州冬季亚微米气溶胶质量浓度以90 μg/m³为分界线，分成"低浓度"和"高浓度"2个区域。硫酸盐、硝酸盐、铵盐和氯化物在低浓度区域均呈现单调递增，甚至接近线性增长的特点，而在高浓度区，这些物种的浓度均开始下降。对有机物种而言，一次有机气溶胶（POA，包括BBOA、CCOA、HOA和COA）和二次有机气溶胶（SOA，包括OOA1、OOA2）的变化趋势明显不同。在低浓度区，POA和SOA均呈现增长的趋势，但增长速率不同，而在高浓度区，二者变化趋势正好相反，即POA在高浓度区不断增长，而SOA则增长缓慢甚至呈现下降趋势。这些观测结果说明，兰州有机气溶胶中一次有机气溶胶占有主导地位，尤其在亚微米气溶胶浓度偏高时段贡献更加明显，兰州一次排放是细颗粒物的主要污染源，并且在高浓度污染事件中起着举足轻重的作用。（张养梅）

1.8 华北平原夏季强化观测

光化学污染问题在我国一些地区越来越突出，尤其是在华北平原，成为迫切需要与霾污染一同解决的大气环境问题。光化学污染是以高浓度臭氧、过氧乙酰硝酸、二次气溶胶等为主要特征污染类型，对人体健康、农业与林业产量等均有负面影响。中国气象科学研究院区域大气污染与光化学团队长期关注这类问题，已通过一些项目开展了多年研究。在环保公益专项（编号201509002）经费的支持下，团队于2016年6月13至7月31日再次在华北平原开展了强化观测。试验期间，团队在河北饶阳县和山

东德州市2个站点同步开展了臭氧及其前体物以及气溶胶的观测。本次试验按计划完成了既定观测任务，取得了大量宝贵观测资料，为后期综合分析和模拟研究打下了良好的基础。（徐晓斌）

1.9 灰度仪测量的夏季华北平原黑碳垂直廓线

黑碳（BC）气溶胶是可见光的最强吸收成分，具有很强的气候效应。2014年夏季在华北平原农村饶阳气象站现场观测中，采用系留汽艇对BC垂直廓线进行了测量。本工作首次对BC垂直分布随混合层的演变进行了研究，对67条有效测量廓线获得了包括混合高度（H_m）和混合层BC浓度（C_m）及自由对流层BC浓度（C_f）等要素。H_m在清晨时段通常低于0.2 km，随着湍流增强而迅速上升，在傍晚时分达到最大。在晴朗的夏日，混合层顶可发展到1 km以上高度，而在阴天却维持在较低高度。日落后混合层塌陷，逐步形成温度的夜间边界层。混合层BC浓度C_m的最高和最低值分别出现在清晨和下午时段。白天时段的BC基本上均匀地分布于混合层，而在混合层之上却显著下降。整个现场观测期间C_m在1.12～14.49 μg/m³范围波动，平均为(5.16 ± 2.49) μg/m³。与一些城市地区例如意大利米兰和中国上海的测量结果接近。傍晚后的BC逐步在近地面积累，并形成随高度指数变化的分布。与H_m和C_m的较大变化相反，C_f在日内基本不变，在清洁条件下大约为地面浓度水平的10%，在污染的情况下接近地面浓度的50%。BC垂直分布的直接测量有助于更准确地评估其直接辐射强迫，并且可改进区域气溶胶光化特性的遥感反演。（徐晓斌）

1.10 中国瓦里关全球大气本底站地面臭氧长期趋势及影响因素Ⅰ：总趋势与特征

对流层臭氧是重要大气氧化剂，同时也是温室气体和大气污染物。臭氧浓度上升可影响大气氧化性、气候、人体健康和植物生长。因此，臭氧本底水平的长期趋势是环境和气候变化评估非常需要的信息。迄今为止，这样的信息只能在欧洲和北美一些代表性站点获得，在我国和许多发展中国家极为缺乏。我国青藏高原东北角的瓦里关全球大气本底站（36°17′N，100°54′E，海拔3816 m）自1994年起就开展了地面臭氧的长期观测。本工作对1994—2013年的数据进行了系统分析，对地面臭氧的变化特征、长期趋势和影响因素进行研究，并已经在2篇论文中归纳发表，其中本文主要关注地面臭氧总体的日变化、季节变化和长期趋势。为取得可靠的臭氧趋势，采用Mann-Kendall趋势检验法和Hilbert-Huang变换（HHT）对臭氧长期观测资料进行了分析。研究表明，瓦里关的山–谷风效应在该站臭氧的昼夜变化中起重要作用，导致夜间高值和白天低值。山–谷风既有日变化也有季节变化，利用这种特征首次定义了与季节相关的白天和夜间时段，并用于趋势计算中的数据选取。计算结果表明，瓦里关地面臭氧白天和夜间的总体趋势分别为（0.24 ± 0.16）×10⁻⁹/a和（0.28 ± 0.17）×10⁻⁹/a；最大的夜间增长出现在秋季（（0.29 ± 0.11）×10⁻⁹/a），其次分别是春季（（0.24 ± 0.12）×10⁻⁹/a）、夏季（（0.22 ± 0.20）×10⁻⁹/a）和冬季（（0.13 ± 0.10）×10⁻⁹/a）。HHT谱分析识别出了4个阶段，具有不同增长趋势，其中最大增长出现于2000年5月和2010年10月前后。HHT分析还揭示了瓦里关地面臭氧时间序列中存在着2～4年、7年和11年等周期变化信号。本研究成果可用于气候和环境变化评估以及化学–气候模式的验证（图5）。（徐婉筠）

1.11 北京大气颗粒物中真菌气溶胶对有机碳的贡献

真菌气溶胶是大气颗粒物的重要组成部分，也会对大气颗粒物中的有机碳（OC）产生贡献。为了摸清北京大气颗粒物中真菌气溶胶对OC的贡献，本研究在清华大学和密云设置采样点，分别代表城区和郊区，采集PM₂.₅和PM₁₀，对真菌气溶胶分子示踪物甘露糖醇进行分析测试。结合单个真菌气溶胶中分子示踪物含量的转换系数f甘露糖醇（0.49×10⁻³ ng/个）以及分子示踪物的质量浓度，获得北京地区全年真菌气溶胶的数浓度，再应用单个真菌气溶胶中平均含碳量经验常数f_{oc} = 13 ± 2.3 PgC/个，估算出北京城区PM₂.₅和PM₁₀中真菌气溶胶OC年均浓度分别为（0.3 ± 0.2）μgC/m³和（0.8 ± 0.7）μgC/m³，及

其对OC贡献的年均水平分别为（1.2±0.7）%和（3.5±3.7）%。真菌气溶胶对OC的贡献呈现了明显的季节变化特征，随夏、秋、春、冬而递减。夏季北京市区和郊区PM$_{10}$中真菌气溶胶对OC的贡献分别高达（7.3±3.3）%和（14.1±10.5）%。因此，需要在更多人口密集城市地区的研究，才能更好地了解大气中真菌气溶胶的浓度水平、季节变化特征以及对有机气溶胶的贡献。(梁林林)

1.12 大气环境容量系数A值频率曲线拟合及其应用

在用A值法确定大气环境容量的研究中，给出了大气环境容量系数的理论定义、特性及其累积频率曲线的PⅢ型拟合，同时证明该系数也可定义为空气自洁指数。以北京为例探讨了不同重现期的大气环境容量系数在不同控制区面积、时段所对应的容量及其相应空气质量的关联。按1951—2014年的气象数据计算的北京百年一遇的年均A值为4.47，而百日一遇的日均A值仅为0.23。研究结果表明，大气环境容量系数的频率分析或可成为大气环境管理中的一个重要工具。(王郁)

1.13 污染源减排与气象要素对2014年"APEC蓝"的影响

"APEC蓝"这个名词被官方及各种媒体用来描述2014年APEC会议期间（11月5—11日）北京蓝蓝的天空。通常情况，那段时间北京污染比较严重。滑动t检验方法研究出2014年北京"APEC蓝"窗口的准确时间为11月1—14日，北京及其周边地区空气质量大为改善，PM$_{2.5}$、PM$_{10}$、SO$_2$和NO$_2$浓度都明显减少，尤以PM$_{10}$最为明显。小波分析和多尺度相关等方法分析显示11月1—6日和11—13日是减排措施与气象场的共同作用，而7—10日则主要是减排的作用。（汪萍）

2 大气成分模式的发展应用及大气成分的影响研究

2.1 东亚夏季风系统对未来人为气溶胶及其前体物排放减少的响应

利用包含了气溶胶直接、半直接和间接效应的气溶胶–气候耦合模式，结合一个中低温室气体排放水平的情景（RCP4.5），研究了东亚夏季风系统对21世纪末人为气溶胶及其前体物排放减少的响应。结果表明，2000—2100年气溶胶减少造成东亚季风区夏季平均大气顶和地表全天净短波辐射通量分别增加3.9 W/m^{2}和4.0 W/m^2。辐射场的变化导致热力场、动力场和水循环的改变。气溶胶减少增加了东亚夏季海陆表面热力性质对比，导致东亚季风区夏季850 hPa风场产生明显的西南和南风距平，且引起东亚副热带急流位置北移，从而增强了东亚夏季风环流。季风的增强造成东亚季风区夏季平均降水增加10%。（王志立）

2.2 人为气溶胶排放减少对将来极端气候的影响

利用一个地球系统模式的集合模拟结果，分析了在人为气候变化情景下气溶胶排放的减少对中国和全球极端温度和降水的影响。结果表明，在RCP8.5情景下，减少的气溶胶排放极大地增强了温室气体增加导致的增暖效应，使得极端气候明显增加。在2031—2050（2081—2100）年，气溶胶减少引起的中国区域平均极端温度和极端降水的增加分别占到其总增加的23%（14%）和32%（30%）以上。气溶胶减排引起的极端气候变化具有明显的区域差异。研究还表明，21世纪全球平均表面温度每度增暖下全球极端降水的变化强烈依赖于排放情景中的强迫成分，其中气溶胶强迫造成的极端降水随增暖的增加率明显大于温室气体强迫的影响。如果未来采用较低的温室气体排放路径，气溶胶强迫将对极端降水的增加起到关键作用。（王志立）

2.3 气溶胶推迟午后降水现象研究

利用珠江三角洲地区长期的PM$_{10}$、云地闪电、SO$_2$、NO$_2$、降水等小时观测数据，研究了大气主

要污染物与降水日变化之间的关系。降水日变化峰值发生前，气溶胶有抑制降水的趋势；峰值后，气溶胶有促进降水的趋势。在污染条件下，珠江三角洲地区全天累计发生正闪（PCG）约占所有闪电的30%，是全球陆地正常平均气候态下的3倍；且1400～1500 LT以后，气溶胶有促进闪电多发的趋势。利用WRF数值模式，发现气溶胶污染条件下模式能很好地再现降水日变化特征，而在清洁条件下，降水明显提前。这表明气溶胶有推迟降水的作用。同时，通过关闭模式的直接辐射效应模块发现，降水也会显著提前，表明气溶胶辐射效应在气溶胶推迟降水过程中发挥了不可忽视的作用。因此，我们提出了气溶胶辐射效应(ARI)与气溶胶云微物理效应（ACI）在白天不同时刻相互竞争导致降水推迟的新机制（图6～7）。（郭建平）

2.4 基于多源主被动卫星数据的气溶胶对中国东部地区不同云垂直结构的影响机制研究

以往的研究工作很少研究不同云的垂直结构对气溶胶的响应。本项目围绕该方向主要取得了如下2项重要突破：（1）利用2008—2010年3个暖季（5—9月）星载云雷达数据，研究中国东部不同地区的积云、对流云、云层云等不同云类型的垂直概率分布特征，结合地基能见度观测，首次给出了中国东部人类活动密集区气溶胶对不同类型云在不同高度上存在间接效应的观测证据，并指出气溶胶对对流云的上部存在促进作用，这种促进作用是以下层云发展受抑制为代价的，这个观测结果印证了气溶胶对对流云降水的促进作用理论(Invigoration Effect)。（2）成功分离下对流层稳定度(LTS)以及垂直风速等气象条件对气溶胶云相互作用的影响。（郭建平）

2.5 基于探空数据构建的中国边界层高度气候数据集

边界层是地气系统物质交换的主要场所，对云降水系统的发生发展过程具有重要意义。目前我国缺乏大范围长期的边界层高度观测数据，现有的边界层高度信息主要来自零星的个别加强试验的观测反演结果和来自国外的再分析资料2个渠道。本项目利用2011—2015年全国120个探空站02:00、08:00、14:00、20:00（北京时）探空观测温度、湿度、风等秒级精细廓线数据，通过改进的整体理查森算法，成功反演一套覆盖我国不同地区不同季节的边界层高度气候数据集。考虑到夏季是降水多发期，首次给出了夏季我国大范围的边界层高度日变化空间分布。云对边界层发展的影响在不同时次有显著的差异，其中14:00点的云盖对边界层发展起到明显的抑制作用。同时，发现我国大部分站点的边界层高度与地面气压和近地面稳定度呈负相关，而与近地面风速和气温呈正相关。（郭建平）

2.6 2013年1月重霾污染过程中国地区气溶胶短期辐射影响及其地区差异研究

采用WRF-CMAQ-SES2离线耦合模式系统模拟了2013年1月重霾污染过程中国地区气溶胶对地面辐射的短期影响效应及其地区差异。结果表明：（1）经过地面实测PM_{10}和$PM_{2.5}$浓度订正后，气溶胶模拟浓度较接近于实测值，显著减小了气溶胶模拟的不确定性；（2）采用上述不确定性较小的气溶胶垂直廓线资料模拟的总辐射和直接辐射更接近于实测辐射值；（3）2013年1月重污染过程气溶胶对总辐射、直接辐射的削减值介于-200～-100 W/m^2，其短期影响可达气溶胶长期气候效应的2个量级；（4）由于气溶胶化学组成的地区差异导致气溶胶的短期辐射影响程度自北向南呈减小趋势，其中霾污染较重的京津冀地区气溶胶对辐射的影响最大，另外即使在相同的气溶胶浓度状况下，气溶胶对辐射的影响亦存在南北差异。（程兴宏）

2.7 本底站和城区站CO浓度变化特征和源贡献

采用FLEXPART大气扩散模式结合清单的模拟方法，通过与2010年北京上甸子大气本底站和城区海淀宝联站的CO观测浓度的比较，研究了北京地区CO浓度变化特征，并统计分析了各类排放源的贡献差异。研究结果表明，上甸子站和宝联站CO模拟浓度与观测浓度的变化趋势基本一致，相关系数分别优于0.74和0.45；与观测值相比，2个站模拟浓度值偏低，模式对观测浓度峰值模拟能力有限。利

用不同源清单模拟获得的同一站点CO浓度值相近，但交通、工业、民用等分类排放源对CO模拟浓度的贡献差异明显。与INTEX-B2006 清单相比，利用MEIC2010排放清单模拟的宝联站交通与工业排放贡献的占比小、民用排放占比大；而上甸子站交通排放贡献的占比小，民用与工业排放的贡献占比大。因此，利用FLEXPART模式结合清单的模拟方法对CO浓度具有较好的模拟能力，可以较为准确地反映区域大气本底站和城区站CO浓度的变化特征；各类排放源对模拟浓度的贡献不仅受到测站所在地的局地排放源影响，更与影响测站的印痕区域的排放源密切相关。（程巳阳）

2.8 伴随模式在追踪污染事件重点源区中的应用

利用GRAPES-CUACE气溶胶伴随模式，对2015年11月27日至12月2日北京市一次高浓度$PM_{2.5}$污染过程进行敏感性分析，显示了伴随模式在追踪重点排放源区及关注敏感排放时段等方面的优越性。研究表明，本次污染事件所关注的北京市$PM_{2.5}$峰值浓度是北京市本地排放源和周边省市排放源共同作用的结果。从累积敏感系数来看，目标时刻前23 h 内，本地源贡献占主导，$PM_{2.5}$峰值浓度对本地排放源响应迅速；目标时刻前5 h，本地源对峰值浓度的贡献达到最大，逐时敏感系数峰值为9.4 μg/m³。周边源贡献表现为周期性波动，逐时敏感系数在目标时刻前9 h、29 h 和43 h，出现3次峰值，分别为6.66 μg/m³、6.24 μg/m³ 和1.74 μg/m³，伴随着偏南风，周边源在目标时刻前1 ～ 57 h 内持续不断地向北京市输送污染物，不同距离的周边源对目标时刻$PM_{2.5}$峰值浓度的影响时段和程度不一样，目标时刻前72 h 内，北京、天津、河北及山西排放源对目标时刻$PM_{2.5}$峰值浓度的累积贡献比例分别为31%、9%、56%及4%。从逐时敏感系数来看，天津源贡献的主要时段为目标时刻前1 ～ 33 h，逐时敏感系数峰值出现在目标时刻前9 h，为2.1 μg/m³；山西源贡献的主要时段为目标时刻前17 ～ 33 h，逐时敏感系数峰值出现在目标时刻前27 h，为0.71 μg/m³；河北源贡献的主要时段为目标时刻前1 ～ 57 h，逐时敏感系数呈现周期性波动，出现3次峰值，分别为4.55 μg/m³、5.31 μg/m³、1.59 μg/m³（图8 ～ 10）。（安兴琴）
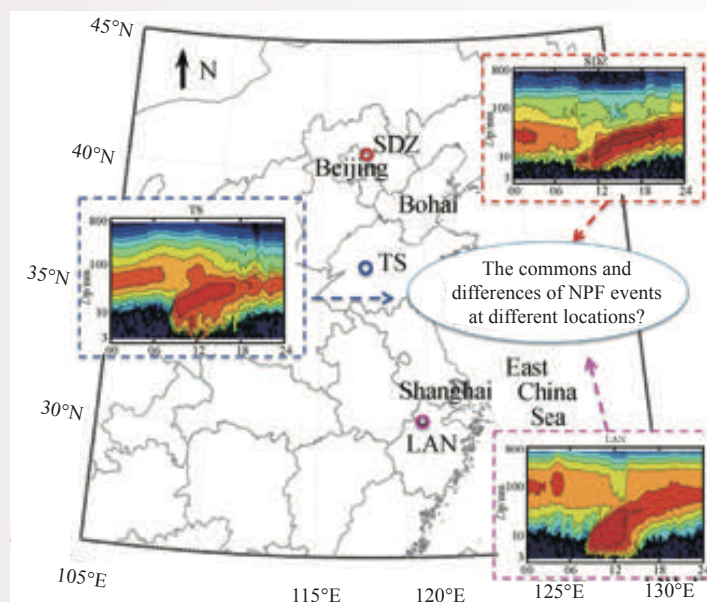
图 1 我国不同背景地区的新粒子生成事件
Fig. 1 New particle formation events at different rural sites in China
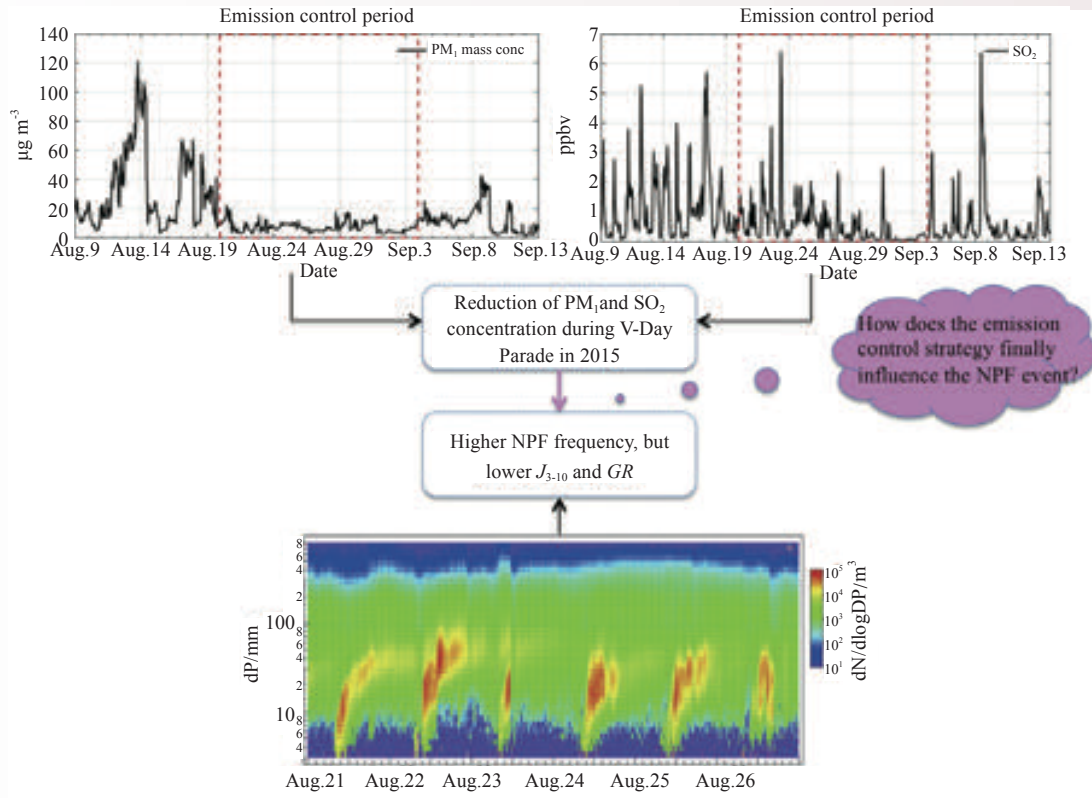
图 2　2015年阅兵期间污染物减排对新粒子生成事件的影响

Fig. 2　The influences of emission control on new particle formation events during China's V-Day parade in 2015
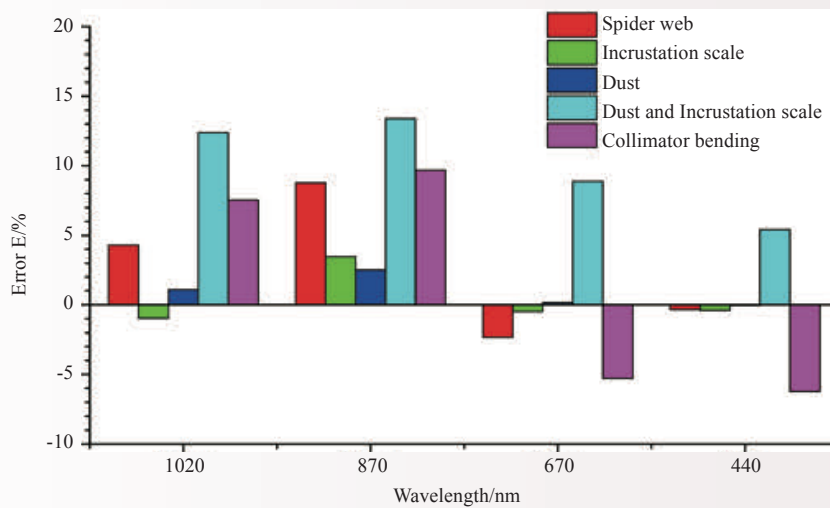
图 3　不同因子对气溶胶光学特性观测的影响

Fig. 3　Errors in retrieving aerosol optical properties by various factors
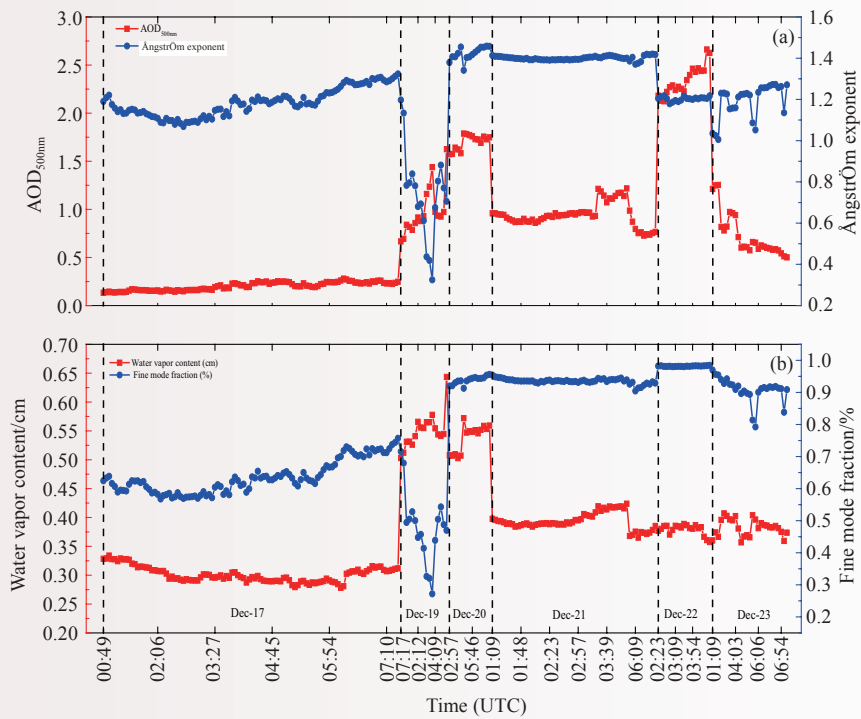
图 4 雾霾期间气溶胶光学特性变化

Fig. 4 Variations of aerosol optical properties during heavy haze episodes in Beijing
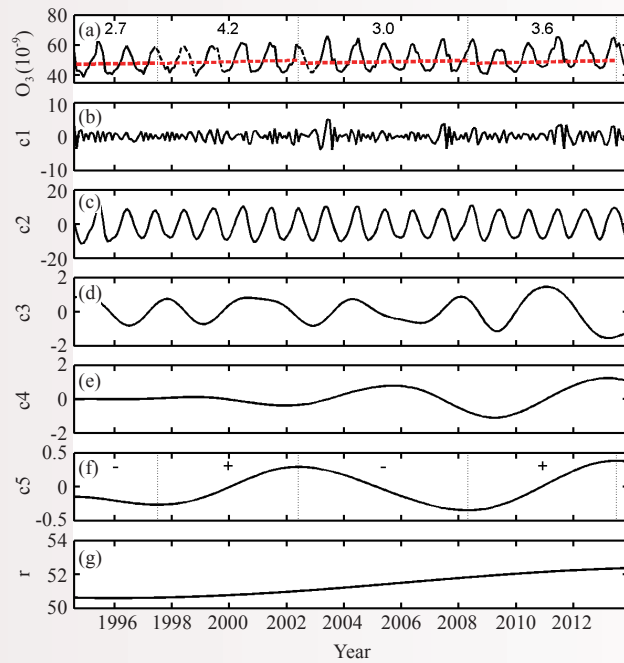
图 5 1994—2013年瓦里关地面臭氧月平均浓度（a虚线为内插值）、c1～c5模态函数（b～f）以及残差（g）（（a）中的时间段根据c5的斜率来确定，红色虚线为Kendall趋势，响应数值为Kendall变率（10^{-9}/a））

Fig. 5 The monthly averaged ozone concentrations at WLG from 1994 to 2013 (dashed lines in (a) denote interpolated data) and its intrinsic mode functions c1–c5 (b–f) and its residue (g). The time segments in (a) were determined by the slope of c5. The red slashed lines are the Kendall's trends and the numbers are the Kendall's slope (in 10^{-9} a^{-1})
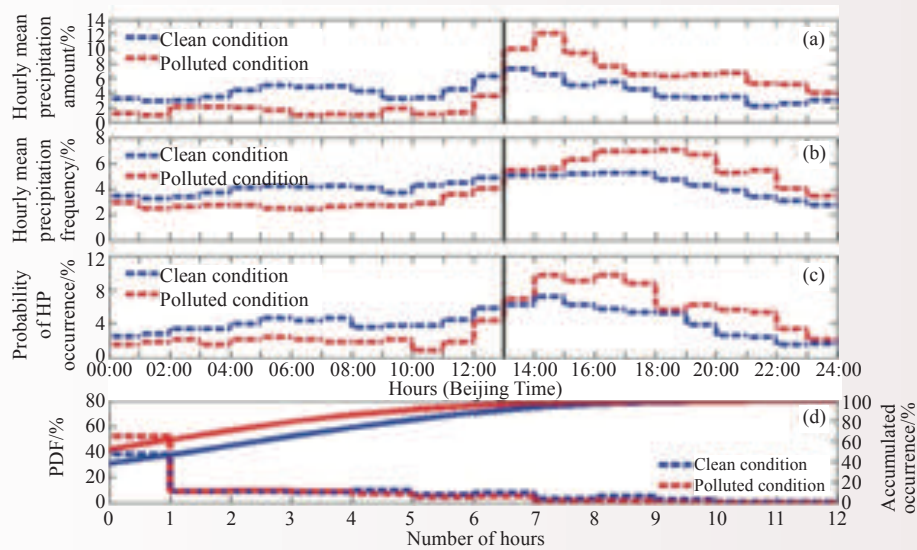
图 6 基于2008－2012年5个暖季（5－9月）长期时空匹配的小时气溶胶和降水数据得到的污染和清洁条件下降水强度、降水频次以及强降水频次的日变化

Fig. 6 Diurnal variation of precipitation intensity, precipitation frequency, and heavy precipitation frequency under polluted and pristine conditions based on collocated hourly aerosol and rain gauge data for the warm seasons during the period of 2008–2012
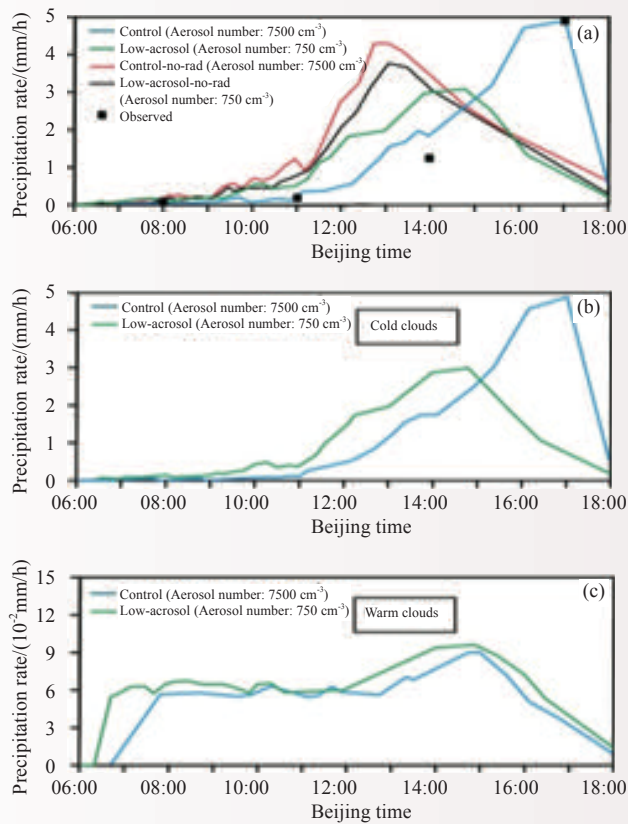
图 7 WRF模式模拟的不同气溶胶浓度以及气溶胶辐射效应考虑与否条件下的所有降水(a)、冷云降水（b）以及暖云降水（c）系统日变化结果

Fig. 7 The diurnal cycles of the WRF simulated precipitation (a), precipitation formed in warm clouds (b), and cold clouds (c) under various aerosol concentrations with or without aerosol radiative effects
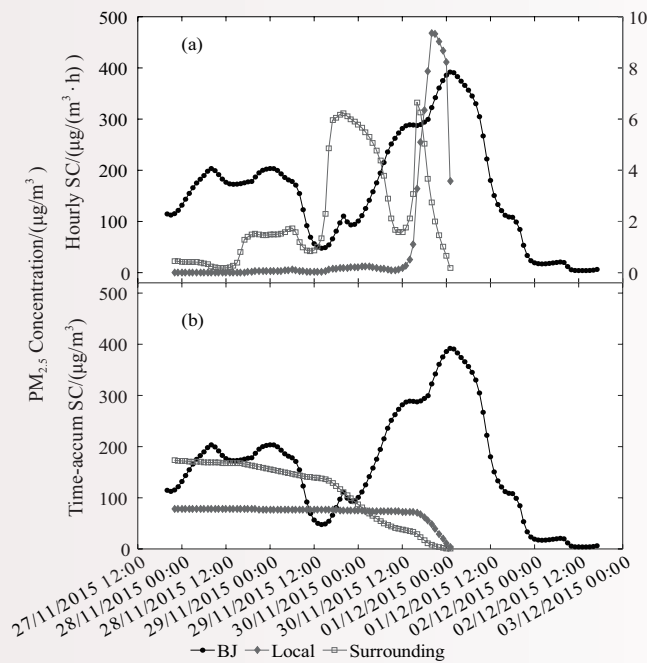
图 8　本地源及周边源逐时（a）和时间累积（b）敏感系数序列

Fig. 8　Time series of hourly (a) and temporally-cumulated (b) sensitivity coefficients of local and surrounding emissions
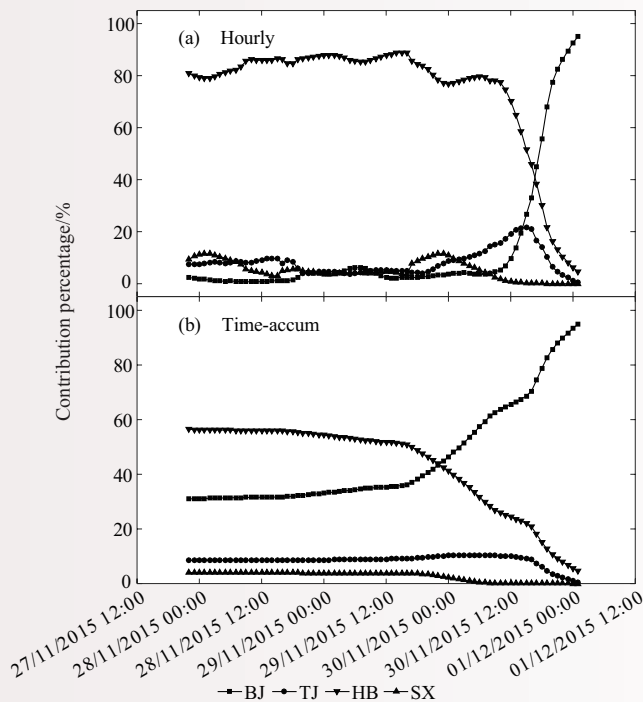
图 9　北京（BJ）、天津（TJ）、河北（HB）及山西（SX）排放源对目标时刻（2015年12月1日01:00）PM$_{2.5}$峰值浓度逐时（a）与时间累积（b）贡献百分比序列

Fig. 9　Percentage variation of hourly (a) and temporally-cumulated (b) contributions of Beijing, Tianjin, Hebei and Shanxi emissions to the PM$_{2.5}$ peak concentration at the target time (i.e., 01:00 1st Dec. 2015)
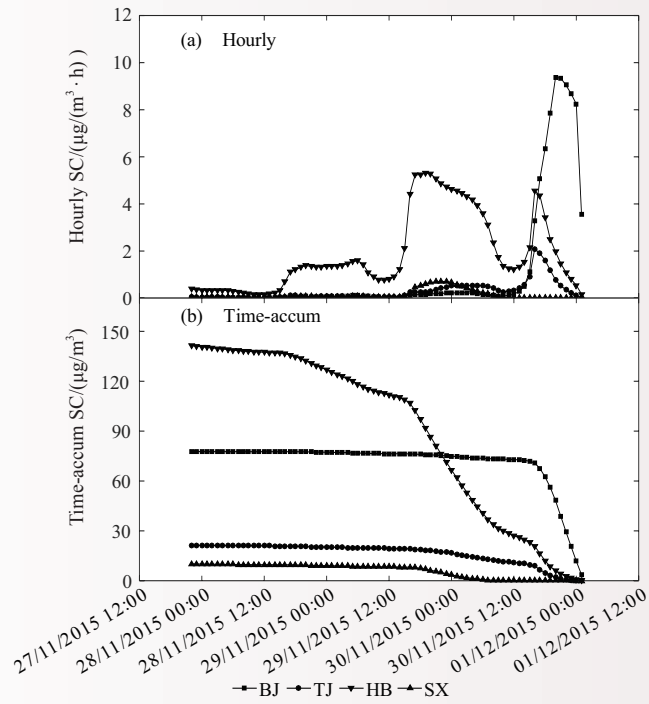
图 10　北京（BJ）、天津（TJ）、河北（HB）及山西（SX）排放源逐时(a)与时间累积(b)敏感系数序列
Fig. 10　Time series of hourly (a) and temporally-cumulated (b) sensitivity coefficients for Beijing, Tianjin, Hebei and Shanxi emissions, respectively

Progress in Atmospheric Composition and Atmospheric Chemistry Research

1 Observational studies of atmospheric composition and related properties

1.1 Reassessing the effects of temperature enhancement under haze environment on human mortality

We studied the haze impact on human health during different seasons. Results indicate significant (p < 0.05) associations between haze intensity and relative health risks (RHRs) of all-cause, cardiovascular, and respiratory mortalities for some sensitive human groups, and increased haze intensity could increase the RHR of mortality, ranging between 1.5%–7.0% on different lagging days. No significant association was observed for genitourinary, digestive, or metabolic diseases. The cumulative effects of haze during a 6-day lag of cardiovascular, respiratory, and all-cause mortalities were in the mortality range of 2%–11%. The lag and cumulative effects differ under cold and warm seasons. We found significant seasonal modification in the associations: The enhanced effects of haze on respiratory diseases in spring, on all-cause mortality in spring and winter, and on cardiovascular mortality in summer and winter. We conclude that air temperature appears to be a unique factor in associating haze and mortality in summer but an indication for the physical property of fine particles. (Li Yi)

1.2 Air pollution characteristics and their relation to meteorological conditions during 2014–2015 in major Chinese cities

Since January 2013, the real-time hourly averaged concentrations of six pollutants (i.e., CO, NO_2, O_3, PM_{10}, $PM_{2.5}$ and SO_2) based on air quality monitoring stations in major Chinese cities have been released to the public. This provides a good opportunity to publicize nationwide temporal and spatial pollutant characteristics. Although several studies systematically investigated the temporal and spatial trends of pollutant concentrations, the relation between air pollution and multi-scale meteorological conditions and their spatial variations on a nationwide scale remain unclear. A single meteorological parameter could not reflect the overall relation between meteorological conditions and air pollution. A combination of multi-scale meteorological conditions using the ANN model combined with wavelet transformation is a useful method to study this complex relationship. This study analyzes the air pollution characteristics and their relation to multi-scale meteorological conditions during 2014–2015 in 31 provincial capitals in China. Results show that the annual average concentrations of the six pollutants were 1200, 42.4, 49.0, 109.8, 63.7, and 32.6 μg m^{-3} in 2014, which decreased 5.3%, 4.9%, 11.4%, 12.0% and 21.5% for CO, NO_2, PM_{10}, $PM_{2.5}$ and SO_2, respectively, but increased 7.4% for O_3 in 2015. The highest rate of a major pollutant over China was $PM_{2.5}$ followed by PM_{10}, O_3, NO_2, SO_2 and CO in that order. Meteorological conditions were the primary factor determining day-to-day variations in pollutant concentrations, accounting for more than 70% of the variance of daily average pollutant concentrations over China. Meteorological conditions in 2015 were more adverse for pollutant dispersion than in 2014, indicating that the improvement in air quality was caused by emission controls. (He Jianjun)

1.3 Key characteristics of new particle formation events at three background sites and their influences on cloud condensation nuclei

Long-term continuous measurements of particle number size distributions with mobility diameter sizes

ranging from 3 to 800 nm were performed to study new particle formation (NPF) events at Shangdianzi (SDZ), Mt. Tai (TS), and Lin'an (LAN) stations representing the background atmospheric conditions in the North China Plain (NCP), Central East China (CEC), and Yangtze River Delta (YRD) regions, respectively. The mean formation rate of 3-nm particles was 6.3, 3.7, and 5.8 $cm^{-3}s^{-1}$, and the mean particle growth rate was 3.6, 6.0, and 6.2 $nm\ h^{-1}$ at SDZ, TS, and LAN, respectively. The NPF event characteristics at the three sites indicate that there may be a higher source of low volatile vapors and higher condensational sink of pre-existing particles in the YRD Region. The formation rate of NPF events at these sites, as well as the condensation sink, is approximately 10 times higher than some results reported at rural/urban sites in western countries. However, the growth rates appear to be 1–2 times higher. Generally, the cloud condensation nuclei (CCN) number concentration can be enhanced by approximately a factor of 2–6 on these event days. NPF events have also been found to have greater impact on CCN production in China at the regional scale than in the other background sites worldwide (Fig.1). (Shen Xiaojing)

1.4 Influences of emission control on particle number size distribution and new particle formation during China's V-Day parade in 2015

Temporary restricted emission control strategies were conducted to ensure high air quality for China's V-Day parade (20 August–3 September 2015) in Beijing and nearby cities. In this study, the particle number size distributions during this period and the 8–23 August 2008 Olympics period are compared to those occurring during the same period without restricted emission control in 2010–2013 (20 August–3 September). Results show significant reductions in the accumulation mode particle number concentration in 2015, with the PM_1 mass concentration decreased by 60%–90%. The alleviating PM_1 concentration might be attributed partly to some weather conditions, based on a back-trajectories analysis showing that the southerly polluted air mass accounted for 14% of the total back trajectories in 2015, whereas it contributed to approximately 60% in the other years. During the control period in 2015, six new particle formation (NPF) events were observed, with higher frequencies but lower formation and growth rates than those during the same period in 2010–2013. A comparison of the condensation sink (CS), sulfuric acid, solar radiation and relative humidity between the different years indicated that the CS determines mostly the NPF occurrence and then the concentration level of precursor vapors participating in the NPF event at Shangdianzi station (Fig. 2). (Shen Xiaojing)

1.5 Aerosol optical-radiative properties from ground-based measurements

Aerosol optical properties based on ground and satellite data retrievals during a serious haze episode in December 2015 over Beijing were studied. Results show that high relative humidity could accelerate haze development, and that ample fine particles could grow into large particles through hygroscopic processes. Errors in retrieving aerosol optical properties from sunphotometer measurements of CARSNET due to a variety of objective factors were analyzed. Results indicate that lower correlations of AAOD with SSA than AOD between two nearby urban sites in Beijing could be attributed to differences in diffusive conditions and aerosol types (e.g., black carbon and brown carbon) (Fig. 3–4). (Che Huizheng)

1.6 Mechanisms and kinetics of heterogeneous reactions of unsaturated organic acids on α-Al_2O_3 and $CaCO_3$

Heterogeneous reactions play a vital role in determining the evolution of atmospheric aerosols, especially air pollution. However, their mechanisms and kinetics involving unsaturated organic acids, as an important volatile organic compound, still remain elusive. In this work, the heterogeneous uptake of two representative atmospheric unsaturated organic acids on mineral aerosols including α-Al_2O_3 and $CaCO_3$ were investigated using a Knudsen cell reactor and an in situ Diffuse Reflectance Infrared Fourier Transform Spectrometry

(DRIFTS) reactor. The corresponding reaction pathways were proposed after analyzing the DRIFTS spectral features. In addition, the initial uptake coefficients of unsaturated organic acids and their heterogeneous fate were obtained for the first time. Our results suggest that heterogeneous reactions on α-Al_2O_3 and $CaCO_3$ can be important sinks for acrylic acid and methacrylic acid, as well as possible contributors to the organic coating found on atmospheric aerosols, especially under high-polluted events. (Wu Lingyan)

1.7 Contributions of various chemical species to fine particle pollutants in winter in Lanzhou

The NR-PM_1 mass concentrations are separated into "lower" and "higher" than 90 μg m^{-3} mass loading ranges during wintertime in Lanzhou. Results show monotonic and almost linear increases in sulfate, nitrate, ammonium and chloride, with increasing PM loading in the higher mass loading range, but began to decrease in the lower mass loading range. Significantly different trends of variations were found between POA species (i.e., BBOA, CCOA, HOA, COA, and total POA) and SOA species (i.e., OOA1, OOA2, and total SOA). That is, both the POA and SOA species had increasing trends but with various rates in the lower mass loading range. However, inversed variation trends were observed between the POA and SOA species in the higher mass loading range. The POA species increased dramatically in the higher mass loading range, while the SOA species showed slow increasing or even decreasing in the higher mass loading range. The POA dominated SOA in most of the sampling time and even became more dominant with increased SOA mass fraction in NR-PM_1. These results reveal that primary emissions are the major sources of fine PM in Lanzhou and they play an important role in building up high PM pollution during wintertime. (Zhang Yangmei)

1.8 Summer intensive field campaign in the North China Plain

Photochemical pollution has become severer in some regions in China, particularly in the North China Plain (NCP). It is urgently needed to solve this atmospheric environment problem along with haze pollution. Photochemical pollution is characterized as high ambient concentrations of ozone, peroxyacetyl nitrate (PAN) and secondary aerosols, which have adverse impacts on human health, crop growth and forest productivity. The Regional Air Pollution and Photochemistry (RAPP) team at CAMS has paid close attention to such problems through several research projects for many years. With the funding of an Environmental Protection Public Welfare Scientific Research Project (grant no. 201509002), the team conducted another intensive field campaign in the NCP during the period of 13 June–31 July 2016, with ozone and its precursor gases as well as aerosols observed at Raoyang (a rural site in Hebei) and Dezhou (a urban site in Shandong). The team successfully completed the planned measurements and collected many valuable data, which will facilitate the future integrated analyses and model validations. (Xu Xiaobin)

1.9 Vertical profiles of black carbon measured by a micro-aethalometer in summer in the North China Plain

Black carbon (BC) is a dominant absorber in the visible spectrum and a potent factor in climatic effects. Vertical profiles of BC were measured using a micro-aethalometer attached to a tethered balloon during the Vertical Observations of trace Gases and Aerosols (VOGA) field campaign in summer 2014 at a semirural site in the North China Plain (NCP). The diurnal cycle of BC vertical profiles along with the evolution of the mixing layer (ML) was investigated for the first time in the NCP region. Statistical parameters including identified mixing height (H_m) and average BC mass concentrations within the ML (C_m) and in the free troposphere (C_f) were obtained for a selected dataset of 67 vertical profiles. H_m was usually lower than 0.2 km in the early morning and rapidly rose thereafter due to strengthened turbulence. The ML height was peaked in the late afternoon, at more than 1 km on sunny days in summer, but with much lower values on cloudy days. The ML collapsed near the sunset, followed by the formation of a stable nocturnal boundary layer (NBL).

Accordingly, the highest and lowest C_m were found in the early morning and the afternoon, respectively. In the daytime, BC was almost uniformly distributed within the ML but it decreased significantly above. C_m ranging from 1.12 to 14.49 μg m^{-3} with an averaged value of (5.16±2.49) μg m^{-3} were observed during the field campaign, which are comparable with observations in many polluted urban areas such as Milan in Italy and Shanghai in China. As evening approached, BC gradually built up near the surface and declined exponentially with height. In contrast to the large variability found both in H_m and C_m, C_f stayed relatively unaffected throughout the daytime. C_f was less than 10% of the ground level under clean conditions, while it amounted to half of the ground level in some polluted cases. In situ measurements of BC vertical profiles have an important implication for accurately estimating direct radiative forcing by BC and improving the retrieval of aerosol optical properties by remote sensing in this region. (Xu Xiaobin)

1.10 Long-term trends of surface ozone and its influencing factors at the Mt Waliguan GAW station, China Part I: Overall trends and characteristics

Tropospheric ozone is an important atmospheric oxidant, greenhouse gas and atmospheric pollutant. Increased ozone concentrations could affect the atmospheric oxidation capacity, climate, human health and vegetation growth. Therefore, determination of the long-term trends of baseline ozone is highly desirable for environmental and climate change assessment. So far, studies on the long-term trends of ozone at representative sites are available mainly for European and North American sites. Corresponding studies are lacking for China and many other developing countries. Measurements of surface ozone were carried out at a baseline Global Atmospheric Watch (GAW) station in the north-eastern Tibetan Plateau region (Mt Waliguan, 36°17′N, 100°54′E, 3816 m a.s.l.) for the period of 1994–2013. To uncover the evolutional characteristics, long-term trends and influencing factors of surface ozone at this remote site in western China, a two-part study was carried out, with this one focusing on the overall characteristics of diurnal, seasonal and long-term variations and the trends of surface ozone. To obtain reliable ozone trends, we performed the Mann-Kendall trend test and the Hilbert-Huang Transform (HHT) analysis on the ozone data. Our results confirm that the mountain-valley breeze plays an important role in the diurnal cycle of surface ozone at Waliguan, resulting in higher ozone values during the night and lower ones during the day, as was previously reported. Systematic diurnal and seasonal variations were found in mountain-valley breezes at the site, which were used to define season-dependent daytime and nighttime periods for trend calculations. Significant positive trends in surface ozone were detected for both daytime ((0.24±0.16) ×10^{-9}/a) and nighttime ((0.28±0.17) ×10^{-9}/a). The largest nighttime increasing rate occurred in autumn ((0.29±0.11) ×10^{-9}/a), followed by spring ((0.24±0.12) ×10^{-9}/a), summer ((0.22±0.20) ×10^{-9}/a) and winter ((0.13±0.10) ×10^{-9}/a). An HHT spectral analysis identified four different stages with different positive trends, with the largest increase occurring around May 2000 and October 2010. The HHT results suggest that there were 2–4 a, 7 a and 11 a periodicities in the time series of surface ozone at Waliguan. Results obtained in this study may be used to assess climate and environment changes and to validate chemistry-climate models (Fig. 5). (Xu Wanyun)

1.11 Contributions of fungal spores to organic carbon in ambient aerosols in Beijing, China

Fungal spores are ubiquitous components of atmospheric aerosols and contributors to organic carbon (OC) in ambient aerosols. To better understand the contributions of fungal spores to OC in Beijing, China, ambient concentrations of the molecular tracers for fungal spores, i.e., mannitol in PM_{10} and $PM_{2.5}$ were measured at an urban site (Tsinghua University) during a year, while observations of PM_{10} at a rural site (Miyun) were conducted during a late spring and a summer. With the conversion coefficient of the averaged mannitol per spore ((0.49 ± 0.20) Pg), the year-round number concentrations of fungal spores were obtained. Using a conversion factor of 13 PgC spore-1, the annual averaged concentrations of spore-OC in $PM_{2.5}$ and PM_{10} at

the THU site were observed at (0.3 ± 0.2) µgC m^{-3} and (0.8 ± 0.7) µgC m^{-3}, respectively, while the respective contributions of spore-OC to total OC were (1.2 ± 0.7) % and (3.5 ± 3.7) %. The seasonal trend of fungal contribution to OC (from the highest to lowest levels) was: summer, autumn, winter and spring. During the summer season, the contribution of fungal spores to OC was observed at a high level at the rural site $((14.1 \pm 10.5)$ %), compared to the urban site $((7.3 \pm 3.3)$ %). Thus, more studies are needed to better understand the spatial, temporal and size distributions of fungal OC contributions to atmospheric aerosols in populated areas. (Liang Linlin)

1.12 The cumulative frequency curving fitting of atmospheric capacity A-coefficient and its application

The definition, characteristics and type P Ⅲ fitting of the cumulative frequency curve of the atmospheric capacity coefficient are obtained with the A-value approach. Results show that the so-obtained A-coefficient can be served as an air-self-cleaning Index. The relationship between the air quality and the environmental capacity coefficient under various recurrence periods is studied for several control areas and periods. Based on the meteorological observations obtained in Beijing from 1951 to 2014, we found an average annual A-value of 4.27 for a hundred of recurrence years and an average daily A-value of 0.23 for a hundred of recurrence days. Results indicate that the frequency analysis of atmospheric capacity coefficient can be an important tool for atmospheric environment management. (Wang Yu)

1.13 APEC-Blue Skies due to emission reduction and favorable meteorological conditions

The term APEC Blue has been used by official news and other medias in China since the Asia-Pacific Economic Cooperation (APEC) Summit held in Beijing during 5–11 November 2014. That is, clear-sky duration detected by moving t-test appeared during the APEC period, which was unusual for the heavily polluted city of Beijing. Observations show that blue window corresponds to low air pollution with respect to $PM_{2.5}$, PM_{10}, SO_2, and NO_2 under restricted emission-control measures implemented in and near Beijing, especially PM_{10}. Statistical investigations using wavelet and multi-scale correlation analysis revealed that the blue window resulted from both strong northerly winds and emission reductions. These two factors played an important role in producing "cleaning air" on 1–6 and 11–13 November, whereas the emission reduction became more important in reducing pollutant during 7–10 November. (Wang Ping)

2 Model development and implementation, the impacts of atmospheric compositions on climate, weather, and human health

2.1 Response of the East Asian summer monsoon system to future reductions in emissions of anthropogenic aerosols and their precursors

The response of the East Asian summer monsoon (EASM) system to reductions in the emission of anthropogenic aerosols and their precursors at the end of the 21st century projected by Representative Concentration Pathway (RCP) 4.5 is studied using an aerosol-climate model with aerosol direct, semi-direct, and indirect effects included. Results show that the summer mean net all-sky shortwave fluxes averaged over the East Asian monsoon region (EAMR) at the TOA and surface increase by 3.9 and 4.0 Wm^{-2}, respectively, due to the reductions of aerosols in 2100 relative to 2000. Changes in radiation affect local thermodynamic and dynamic processes and the hydrological cycle. The decreases of aerosols lead to increases in contrast to land-sea surface temperature over the EAMR, southwest and south winds at 850 hPa over eastern and southern China and the surrounding oceans, and the northward movement of the East Asian subtropical jet,

thus strengthening the EASM. In turn, the enhancement of the EASM causes a 10% increase in summer mean precipitation averaged over the EAMR. (Wang Zhili)

2.2 The effect of reduction in anthropogenic aerosol emissions on projected climate extremes

This study investigates the effect of reduced aerosol emissions on projected temperature and precipitation extremes in China and globe under the anthropogenic climate change scenario using the ensemble simulations from an Earth System Model. The reduced aerosol emissions under the Representative Concentration Pathway 8.5 (RCP8.5) scenario magnify the warming effect due to greenhouse gases (GHG), thus leading to significant increases in climate extremes. The reduced aerosols contribute to more than 23% (14%) and 32% (30%) of the total increases in temperature and precipitation extremes averaged over China during 2031–2050 (2081–2100), respectively, under the RCP8.5 scenario. There are great regional differences in changes of climate extremes caused by the aerosol reduction. Results also show that the increased rate of precipitation extremes with global mean surface warming in the 21st century depends on the compositions of radiative forcing. The increased rate caused by aerosol forcing is significantly larger than that caused by GHG forcing. The aerosol forcing in the coming decades can play a critical role in inducing changes in precipitation extremes if a lower GHG emission pathway is adopted. (Wang Zhili)

2.3 An observational and modeling analysis of precipitation and lightning delays by air pollution over the Pearl River Delta

Given the radiative and microphysical effects of aerosols on the development of convective clouds, an observational and modeling analysis of aerosol concentrations was conducted to reveal if the overall aerosol effects would have any discernible impact on the diurnal variations of precipitation and lightning. For this purpose, daily PM_{10} data were categorized as clean, medium, or polluted. Heavy precipitation and lightning were found to occur more frequently later in the day under polluted conditions than under clean conditions. An analysis of the diurnal variations in several meteorological factors such as air temperature, vertical velocity, and wind speed reveals that the influence of aerosol radiative and microphysical effects serve to suppress and enhance convective activity, respectively. Although the effects of aerosol particles on the heavy precipitation can be discerned throughout the daytime, it is not possible to separate their radiative and microphysical influences from those of atmospheric dynamics and thermodynamics. WRF simulations were carried out to identify mechanisms controling the precipitation and lightning under the influences of aerosols. Results show that during the first 8 h period, aerosols acting as a radiation absorber suppress deep convection and precipitation by inducing greater radiative heating and stability. Lesser convection and precipitation occur under polluted conditions than under clean conditions. Due to the suppressed convection, the depletion of convective energy decreases, which in turn boosts the level of stored energy after this period. The boosted level of stored energy enables updrafts to be strong enough to transport a greater amount of cloud liquid to the freezing level and above under polluted conditions than under clean conditions. This in turn induces greater freezing-related latent heating, buoyancy and thus stronger convection, and results in the transition from lower precipitation rates during the first 8 h period to higher precipitation rates during the later 4 h period under polluted conditions than under clean conditions (Fig. 6–7). (Guo Jianping)

2.4 A CloudSat perspective on the cloud climatology and its association with aerosol perturbations in the vertical over eastern China

Although considerable effort has been paid to investigating aerosol-cloud interactions from space, only a few studies have examined the response of vertical cloud structure to aerosol perturbations. A three-dimensional cloud climatology of eight different cloud types identified from the CloudSat Level 2 cloud products during

the warm season (May to September) of 2008–2010 over eastern China was first analyzed. Using visibility as a proxy for cloud condensation nuclei, in combination with satellite-observed radar reflectivity, normalized contoured frequency by altitude diagrams of the differences in cloud radar reflectivity (Z) profiles under polluted and clean conditions were constructed. Results show that Z tends to be inhibited for shallow cumulus clouds (shallow Cu) and enhanced in the upper layers for deep cumulus (deep Cu), nimbostratus (Ns), and deep convective clouds (DCC) under polluted conditions. Overall, an analysis of the modified center of gravity (MCOG) and cloud top height (CTH) also pointed to a similar aerosol effect, except for the non-significant changes in MCOGs and CTHs in deep Cu. The impacts of environmental factors such as lower tropospheric stability and vertical velocity are also discussed for these types of clouds. Although consistent aerosol-induced elevations in MCOGs and CTHs for Ns and DCC clouds are observed, the meteorological influences cannot be completely ruled out, which merits further studies. (Guo Jianping)

2.5 A climatology of the planetary boundary layer height in China derived from radiosonde and reanalysis data

The important roles of the planetary boundary layer (PBL) in climate, weather and air quality have long been recognized, but little is known about the PBL climatology in China. Using the fine-resolution sounding observations made across China and reanalysis data, we conducted a comprehensive investigation of the PBL in China from January 2011 to July 2015. The PBL height (PBLH) is found to be generally higher in spring and summer seasons than that in fall and winter. A comparison of seasonally averaged PBLHs shows, on average, good agreement, despite the pronounced inconsistence in some regions. The PBLHs derived from three- or four-times-daily soundings in summer tend to peak in the early afternoon, and the diurnal amplitude of the PBLH is higher in the northern and western regions of China than that in the other regions. An investigation of the meteorological influences on the annual cycle of the PBLH shows that the PBLH at most sounding sites is negatively correlated with surface pressures and lower tropospheric stability, but positively correlated with near-surface wind speeds and temperatures. In addition, clouds tend to suppress the PBL development, particularly in the early afternoon. This indicates that meteorology plays a significant role in the PBL processes. The key findings from this study lay a solid foundation for us to gain a deep insight into the roles of the PBL in determining the air pollution, weather and climate of China. (Guo Jianping)

2.6 Short-term aerosol radiative effects and their regional differences during heavy haze episodes in January 2013 in China

Short-term direct effects of aerosols on surface shortwave radiation and their regional differences during the heavy haze episodes in January 2013 in China are investigated using the offline Weather Research and Forecasting (WRF) - the Community Multiscale Air Quality (CMAQ) - radiative transfer scheme (SES2) model system. The aerosol concentrations are first generated using the WRF-CMAQ model simulations and then corrected based on the observed concentrations of PM_{10} and $PM_{2.5}$. The atmospheric profile data produced by the WRF model and the corrected aerosol concentrations are used as inputs to the SES2 model to calculate the global horizontal irradiance (GHI) and direct solar irradiance (DIR) at the surface for a period of heavy haze episodes in January 2013 in China. The effects of aerosol on the GHI and DIR at the surface are then analyzed. The modeled radiation is evaluated against the observations, showing some improvement due to the use of corrected aerosol concentrations. The shortwave radiative effects of aerosols are determined by differences between the model calculations with and without the inclusion of aerosols. Results show that the short-term aerosol radiative impacts during heavy haze days are very large, ranging between 100 and 200 W m^{-2} that are about two orders of magnitude greater than that of the long-term climate impacts. The aerosol concentrations have a large spatial variation with the highest concentration occurring in the areas of Beijing-Tianjin-Hebei,

which causes a large difference in the radiative effect nationwide. In addition to the total concentration, aerosol compositions also vary from the north to south in China, leading to a significant difference in radiative effect even when the total aerosol concentration is the same at two locations. (Cheng Xinghong)

2.7 Evolution characteristics of and source contribution to CO concentration at the background and urban stations

The FLEXPART atmospheric diffusion model simulations, given emission inventory, have been used to study the evolution characteristics of CO concentrations in Beijing by comparing with the observed CO concentrations at Shangdianzi (SDZ) atmospheric background and Baolian (BL) urban stations in 2010. Meanwhile, various source emission contributions to their CO concentrations were statistically analyzed. Results show similar variations of the simulated CO concentrations to the observed values at SDZ and BL, with the correlation coefficients of greater than 0.76 and 0.45 between the simulation and observations, respectively. The simulated values were lower than the observed, which could be attributed to the limited ability of the model in reproducing CO peaks. The simulated CO concentrations remain similar, when using different source emissions at the same sites, but the contributions of specific classifications differ distinctly. For example, using the emission inventories of MEIC2010 versus INTEX-B2006, the contribution ratios of transportation and resident at both sites were less and greater, respectively, whereas the contribution ratio of industry was less at BL, but greater at SDZ. Therefore, the FLEXPART model simulation for a given emission inventory is an effective tool to study CO concentrations, and their evolution characteristics at the atmospheric background and urban stations. Contributions of emission sources were not only affected by local emissions but also determined by source emissions in the footprint area of measurement stations. (Cheng Siyang)

2.8 An application of an adjoint model to tracking influential haze source areas of pollution episodes: A case study of a pollution episode in Beijing in December 2015

An aerosol adjoint module of the atmospheric chemical modeling system GRAPES-CUACE (Global-Regional Assimilation and Prediction System coupled with the CMA Unified Atmospheric Chemistry Environment) was used to perform a sensitivity analysis of a high concentration $PM_{2.5}$ pollution episode (November 27–December 2, 2015) in Beijing. Results illustrate the superiority of the adjoint model in tracking influential haze source areas and sensitive emission periods. It was found that the peak $PM_{2.5}$ concentration at the target time in Beijing was the collective effects of local and surrounding emissions in this air pollution episode. An analysis of the temporally cumulated sensitivity coefficients indicates that local emissions played a primary role within 23 hours ahead of the target time. In addition, the peak $PM_{2.5}$ concentration responded rapidly to local emissions, with a maximum hourly contribution of 9.4 μg m^{-3} around 5 hours prior to the target time. Contributions from surrounding emissions exhibited a pattern of periodic fluctuation, and their three peak values of hourly sensitivity coefficients appeared around 9, 29 and 43 hours ahead of the target time, with values of 6.66, 6.24 and 1.74 μg m^{-3}, respectively. Air pollutants from the surrounding emissions were continuously transported to Beijing within 1–57 hours ahead of the target time by southerly winds. It was also found that the impacts of different surrounding emissions on the peak $PM_{2.5}$ concentration in Beijing varied, depending upon their influencing time periods and degrees. The accumulative contributions of Beijing, Tianjin, Hebei and Shanxi emissions accounted for 31%, 9%, 56% and 4%, respectively, within 72 hours ahead of the target time. An analysis of the hourly sensitivity coefficients indicates that the main contribution time periods of Tianjin, Shanxi and Hebei emissions were 1–33, 17–33 and 1–57 hours prior to the target time, respectively. The peak values of hourly sensitivity coefficients of Tianjin and Shanxi emissions were 2.1 and 0.71 μg m^{-3} around 9 and 27 hours ahead of the target time, respectively, while those of Hebei emissions appeared a periodic fluctuation with three peak values of 4.55, 5.31 and 1.59 μg m^{-3}. (Fig. 8–10). (An Xingqin)

2016年1月7—8日，气科院2015年度学术年会在北京召开。来自中国气象局8个专业研究所、省气象局、高校、国家级业务单位的专家学者针对气象科技前沿问题和气象业务的关键技术及有关成果进行了交流研讨。年会邀请陈大可院士、张人禾院士、贺克斌院士、谈哲敏教授、段晚锁研究员分别做了特邀报告。年会还设立了灾害性天气、农业气象、气候、大气成分和城市气象、人工影响天气5个分会场，100多位科研人员参加了学术交流。

On 7–8 January 2016, the 2015 Annual Academic Meeting of CAMS was held in Beijing. Experts and scholars from the eight specialized institutes as well as the provincial meteorological services of CMA, universities and colleges, and national-level operational institutions attended the meeting and held discussions on cutting-edge issues of meteorological science and technology, key technologies in meteorological operation, as well as relevant outcomes. Scientists including Academicians Chen Dake, Zhang Renhe, He Kebin, Prof. Tan Zhemin and Researcher Duan Wansuo were invited to deliver themed reports. The Annual Meeting also covered topics on severe weather, agrometeorology, climate, atmospheric composition and urban meteorology, and weather modification in five sub-sessions, which were attended by over 100 research staff carrying out academic exchanges.
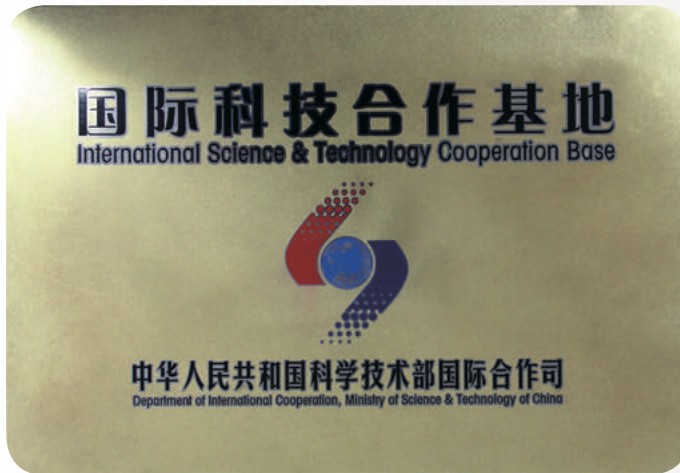
2016年1月19—21日，国家科技部召开全国国际科技合作基地座谈会。会上公布了2015年度评估中获得优秀的国际科技合作基地名单。在参评和检查的359家国际科技合作基地中，气科院"气象科学国际科技合作基地"以前20名的优异成绩位列"优秀"名单中。

On 19–21 January 2016, the Ministry of Science and Technology (MOST) held the discussion on National Bases of International Scientific and Technological Cooperation, during which the list of those outstanding bases elected in the year 2015 was announced. Among the 359 candidated bases that participated in peer review and supervised selection process, CAMS' International Scientific and Technological Cooperation Base in Atmospheric Sciences won the title of Outstanding Base, ranking in the top 20 bases.

2016年1月23日，国家重点基础研究发展计划（973计划）"登陆台风精细结构的观测、预报与影响评估"项目2015年度学术年会在北京召开。各课题负责人汇报了已取得的研究成果和未来工作计划。咨询专家组、项目专家组、各课题负责人及骨干成员50余人参加了会议。项目首席科学家端义宏研究员主持了会议。

On 23 January 2016, the 2015 Annual Academic Meeting of National Basic Research Program of China (973 Program), "Observation, Forecasting and Impact Assessment of Landing Typhoons Fine-scale Structures" was held in Beijing. All task team leaders reported on the achieved research outcomes as well as future work plans. Over 50 members attended the meeting, including those from the expert advisory group, project expert group, task team leaders and cadres, etc. Dr. Duan Yihong, Project Chief Scientist, presided over the meeting.

2016年3月1日，中国气象局人工影响天气中心在北京召开了国家人影飞机业务试运行工作研讨会，河南、河北、山西、安徽、山东、陕西6省人影部门和四川三星通航公司主要负责人参加了会议。会议商定，3—4月在上述6省抓住有利天气过程，开展新舟60增雨飞机的增雨作业。中国气象局人工影响天气中心副主任王晓辉主持了会议。

On 1 March 2016, CMA Weather Modification Centre (WMC) held the Workshop for National Weather Modificaiton Aircrafts Test Operation, which was attended by heads of the provincial weather modification centres including Henan, Hebei, Shanxi, Anhui, Shandong and Shaanxi, as well as head of the Sichuan Sanxing Shipping Corporation. It was agreed upon during the meeting that rainfall enhancement by Modern Ark 60 aircrafts should be implemented in the above six provinces in March and April, taking advantage of the weather conditions. Mr. Wang Xiaohui, Deputy Director-General of WMC, presided over the meeting.

2016年3月9日，中国气象科学研究院与黑龙江省气象局在北京签署了合作协议。双方希望通过在科技、人才、资源等方面的合作，共同为国家防灾减灾和粮食安全做贡献。气科院院长端义宏、黑龙江省气象局局长杨卫东等参加签约仪式。

On 9 March 2016, CAMS and Heilongjiang Provincial Meteorological Service signed Cooperation Protocol in Beijing. Both sides expressed the desire to jointly contribute to disaster prevention and mitigation and food security of the country through cooperation in science and technology, talents development as well as resources. Dr. Duan Yihong, President of CAMS, and Mr. Yang Weidong, Director-General of Heilongjiang Provincial Meteorological Service, as well as other relevant staff, attended the signing ceremony.

2016年3月12日，国家自然科学基金重点项目"青藏高原陆面过程参数化的不确定性及其对高原地–气耦合作用的影响"启动会在京召开。气科院院长端义宏、吴国雄院士和徐祥德院士等项目专家组成员、项目全体研究人员及研究生参会。项目负责人气科院"千人计划专家"陈飞教授汇报了项目实施方案。

On 12 March 2016, the launching meeting of a key project of the National Natural Science Foundation of China (NSFC), "Uncertainties in Land-Surface Modeling over the Tibetan Plateau and Their Impacts on Land-Atmosphere Interactions" was held in Beijing. The meeting was attended by project group members including Dr. Duan Yihong, CAMS President, Prof. Wu Guoxiong, Academician from Chinese Academy of Sciences (CAS) and Dr. Xu Xiangde, Academician from Chinese Academy of Engineering (CAE), etc. as well as the entire project research staff and graduate students. The Project Leader, Prof. Chen Fei reported on the implementation plan, who is a CAMS scientist of the Chinese Government's Recruitment Program of Global Experts (known as "the Thousand Talents Plan").

2016年3月18日，气科院院长端义宏主持召开灾害天气国家重点实验室换届重组动员大会，中国气象局科技与气候变化司司长罗云峰出席并讲话，气科院全体在职职工参会。实验室主任梁旭东介绍了实验室整改方案。他表示，实验室将进一步明确科学任务，面向国际科技前沿，开展灾害天气形成机理以及监测与预测有关的理论、方法和关键技术研究。

On 18 March 2016, CAMS President, Dr. Duan Yihong presided over the

Reorganization Meeting of State Key Laboratory on Severe Weather (LaSW) for change of office term. The Director-General of CMA Department of Science & Technology and Climate Change, Dr. Luo Yunfeng attended and addressed the meeting while the entire CAMS staff participated in the meeting. The Director of LaSW, Dr. Liang Xudong, introduced the reorganization plan, in which he expressed the dedication of LaSW in further explicitly identifying its scientific tasks, facing the international scientific frontiers and conducting researches in relevant theories, methodologies and key techniques regarding the mechanism of severe weather as well as its monitoring and prediction.

2016年4月21日，中国气象科学研究院与南京信息工程大学联合组建的"资料同化研究和应用联合中心"及"次季节–季节研究联合中心"揭牌仪式和工作交流会在南京信息工程大学举行。南京信息工程大学蒋建清校长出席，气科院赵平副院长代表端义宏院长出席并与南京信息工程大学周伟灿副校长共同为两个中心揭牌。

On 21 April 2016, the Joint Centre of Data Assimilation Research and Application as well as the Joint Centre of Subseasonal to Seasonal Research established jointly by CAMS and NUIST (Nanjing University of Information Science & Technology) held the inauguration ceremony as well as the experience sharing discussion at NUIST. NUIST President, Prof. Jiang Jianqing and CAMS Vice President, Prof. Zhao Ping, on CAMS President Duan Yihong's behalf, attended the activities, during which Prof. Zhao Ping and NUIST Vice President, Prof. Zhou Weican together launched the inauguration of the two centres.
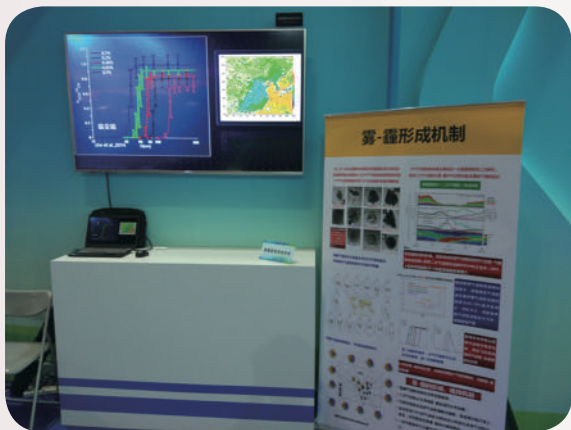
2016年6月1—7日，以"创新驱动发展，科技引领未来"为主题的国家"十二五"科技创新成就展在北京展览馆举行。气科院研发的雾–霾数值预报系统(CUACE/Haze-fog)科研成果参加了展会。

On 1–7 June 2016, the Exhibition of S & T Innovative Outcomes for the National 12th Five-Year Plan was held at Beijing Exhibition Center, with the theme of "Innovation Drives Development; Science and Technology Lead the Future". The haze-fog NWP system (CUACE/Haze-fog) developed by CAMS, was exhibited.

2016年6月8日，中国气象局副局长宇如聪一行深入气科院对重点工作进行调研，端义宏院长主持了调研会。宇如聪一行听取了气科院改革、灾害天气国家重点实验室整改、第3次青藏高原大气科学试验、天气气候一体化模式等进展汇报后，与气科院相关负责人及专家进行了座谈和交流。

On 8 June 2016, CMA Deputy Administrator, Dr. Yu Rucong, with his colleagues visited CAMS to survey on the key working assignments of CAMS, which was presided over by CAMS President, Dr. Duan Yihong. Dr. Yu listened to the progress reports on CAMS reform, LaSW reorganization, the Third Tibetan Plateau Atmospheric Scientific Experiment, research on Weather-Climate Unified Model and exchanged thoughts with CAMS leaders as well as experts.

2016年6月15日，"东亚区域大气再分析"项目实施方案论证会在北京召开。会议由国家气象科技创新工程第三方专家章国材研究员主持。项目首席科学家梁旭东研究员汇报了实施方案，经讨论专家组一致同意通过"东亚大气再分析"项目实施方案，并给出了完善实施方案的意见和建议。

On 15 June 2016, the discussion for the project implementation plan of "Regional Atmosphere Reanalysis for East Asia" was held in Beijing, which was presided over by Dr. Zhang Guocai, a third-party expert from the National Project of Meteorological Science and Technology Innovation. The Project Chief Scientist, Dr. Liang Xudong reported on the implementation plan, which was unanimouly agreed upon by the expert group after discussion. The expert group also presented advice and suggestions for improving the plan.

2016年6月24日，由气科院牵头的国家重大科学仪器设备开发专项"机载云降水粒子谱仪与成像仪研制"项目初步验收会议在北京召开。验收专家组认为，该项目在机载云降水粒子谱仪与成像仪国产化研制、测试及应用推广等方面取得了重要成果，填补了我国机载云降水粒子测量系统的空白，改变了该设备长期依赖进口的局面。

On 24 June 2016, the special project of the National Key Scientific Instrument and Equipment Development, "Development of Spectrometer and Imager for Airborne Cloud Precipitation Particle", which was led by CAMS, held its preliminary project checking-up in Beijing. The checking-up expert group considered that this project had achieved significant outcomes in the made-in-China research & development, test running and popularized application of the spectrometer and imager for airborne cloud precipation particles. Such project was also considered to have filled the gap in measurement system of airborne cloud precipation particles in China, which has changed the situation of dependence on the import of such equipement over many years.

2016年6月29日，深圳市气象局局长王延青一行7人访问气科院，就城市气象灾害研究与城市气候服务等攻关问题与气科院专家座谈，端义宏院长主持了座谈会。双方希望在灾害预警、资料融合应用等方面开展合作。

On 29 June 2016, a seven-member group led by Ms. Wang Yanqing, Director-General of Shenzhen Meteorological Service, visited CAMS and discussed with CAMS experts on key technical issues such as urban meteorological disasters research and urban climate service, etc. The discussion was presided over by CAMS President, Dr. Duan Yihong. Both sides expressed their desire to cooperate in disasters warning, data integration application, etc.

2016年8月5日，气科院灾害天气国家重点实验室组织召开了"我国龙卷风强度等级标准"制定专家咨询会。会议由气科院科技处处长张义军主持。实验室主任梁旭东介绍了国际上龙卷风强度等级标准，以及我国龙卷风强度等级标准研究方案。与会专家围绕标准制定流程、标准框架结构和关键科学问题进行了深入研讨。

On 5 August 2016, CAMS LaSW organized and held the Expert Advisory Meeting on Standard-Setting of Tornado Intensities in China, which was presided over by Dr. Zhang Yijun, Director of CAMS Science and Technology Division. The Director of LaSW, Dr. Liang Xudong, introduced the international classification standards for tornado intensities, as well as the research plan for classification standards for tornado intensities in China. In-depth discussions were conducted among the experts focusing on standard setting-up process, its framework as well as relevant key scientific issues.

2016年9月，气科院王志立作为通信作者和共同第1作者发表于《地球物理快报》上的论文"极端降水对温室气体和气溶胶辐射强迫的敏感性"入选了《自然》期刊（2016年，537卷，7620期）"研究亮点"栏目。王志立等的研究表明，21世纪全球平均表面温度每度升高下极端降水的变化强烈依赖于排放情景中的强迫成分，其中气溶胶强迫将对极端降水的增加起到关键作用。该成果对全球应对气候变化、制定减排策略等具有重要科学意义。

The paper "Sensitivity of Precipitation Extremes to Radiative Forcing of Greenhouse Gases and Aerosols" by Wang Zhili of CAMS (the corresponding and joint first author) was published in the journal *Geophysical Research Letters* in September 2016 and selected to the Research Highlights column of journal *Nature* (2016, 537 (7620)). Wang et al. (2016) indicated that the change of precipitation extremes per degree of surface warming in the 21st century markedly depends on the composition of radiative forcing in different emissions scenarios. The aerosol forcing leads to a larger increased rate than GHG forcing by a factor of 2 to 4 for various precipitation extremes indices. The aerosol forcing in the coming decades can play a critical role in inducing change in precipitation extremes if a lower GHG emission pathway is adopted. This study has implications for policy-making on global response to climate change and mitigation strategies.

2016年9月，第5届邹竞蒙气象科技人才奖评选结果揭晓，气科院罗亚丽研究员喜获该奖。罗亚丽研究员主要从事暴雨、强对流等灾害性天气研究工作，主持和参加了多项国家级科研项目。目前担任WMO世界天气研究计划（WWRP）研究发展项目（RDP）"华南季风降水试验"（SCMREX）首席科学家，2013年入选首批中国气象局科技领军人才。

In September 2016, result of the Fifth Zou Jingmeng Award for S & T Talents in Meteorology was announced and Dr. Luo Yali, CAMS Researcher, was awarded. Dr. Luo has been engaged in severe weather research such as rainstorm, strong convection, etc, who has led or participated in several national-level research projects. She is also the Chief Scientist of the South China Monsoon Rainfall Experiment (SCMREX), a Research and Development Programme (RDP) in WMO World Weather Research Programme (WWRP).
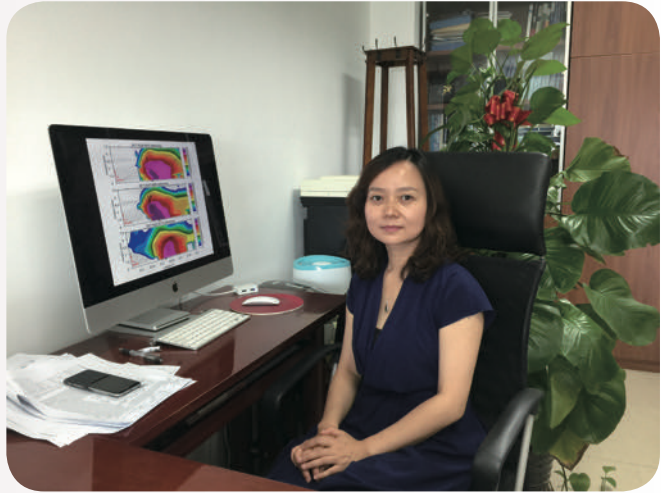
2016年7月11至9月26日，气科院彭浩和张通参加了中国第7次北极考察，获取了走航过程中大气化学成分（如温室气体、一氧化碳、臭氧和黑碳）的观测数据，同时在长期冰站上开展了21次GPS探空气球观测，并架设了1个漂流自动气象站，以期获取北极地区大气边界层和海冰表面的各气象要素（温、湿、压、风）的变化特征。

On 11 July–26 September 2016, Peng Hao and Zhang Tong from CAMS participated in the Seventh-Chinese National Arctic Research Expedition (CHINARE). They have obtained on course the atmospheric chemistry observation data such as greenhouse gases, carbon monoxide, ozone and black carbon. They also released 21 GPS sounding balloons at a long-term ice station and set up one floating Automatic Weather Station (AWS) to obtain various features of meteorological elements including temperature, humidity, pressure and wind speed of the atmospheric boundary layer and sea-ice surface in the Arctic.

2016年9月28日，"天气气候一体化模式关键技术"攻关任务专家论证会在北京召开。该攻关任务由气科院牵头实施，围绕天气气候一体化模式研发面临的大气模式动力框架、东亚区域大气物理过程参数化、无缝隙预报预测等方面的关键科学和技术问题开展前瞻性攻关研究。以吴国雄院士为组长的论证专家组肯定了该任务方案，同时对方案的实施提出了建设性的意见。

On 28 September 2016, the expert discussion on the CAMS-led key task of "Weather-Climate Unified Model Key Technologies" was held in Beijing. The task focuses on proactive research on key scientific and technological issues of research on Weather-Climate Unified Model such as dynamic framework of atmospheric model, parameterization of atmospheric physical process, seamless forecast and prediction, etc. The expert group which was headed by Prof. Wu Guoxiong, Academician of CAS, unanimously approved the task plan and raised advice and suggestions for the implementation of the plan.

在2016年9月24—30日于葡萄牙召开的第33届国际雷电防护会议（ICLP）上，气科院张义军研究员获得了ICLP科学委员会奖。张义军研究员长期从事雷电监测、预警和防护领域的研究工作，提出了新型全闪电三维探测技术的研发思路和技术路线，创建了雷击机理试验平台并推进了野外雷击防护测试试验的发展，上述工作为我国雷电防护理论和试验水平的提高做出了重要贡献。

During the 33rd International Conference on Lightning Protection (ICLP）held on 24–30 September 2016 in Portugal, Dr. Zhang Yijun, CAMS Researcher, won the ICLP Scientific Committee Award. Dr. Zhang Yijun has been engaged in the research of lightning monitoring, warning and protection. He has put forward the development concept and technical roadmap for the new-generation three-dimensional detection technique of full lightning and also established lightning strike mechanism test platform as well as promoted the development of field lightning protection experiment. The above-mentioned work has made great contribution to the improvement of theory and experiment quality of lightning protection in China.

2016年10月24日，由气科院牵头承担的科技部国家重点研发专项"云水资源评估研究与利用示范"启动会在北京召开。项目聚焦云水资源（水凝物）及其变化规律，将对如何合理开发云水资源并同陆地水资源长期耦合利用展开研究。中国气象局副局长许小峰，中国科学院院士周秀骥、丑纪范、吕达仁，中国工程院院士李泽椿、许健民、丁一汇、徐祥德，以及相关领域专家和项目组成员90多人出席会议。会议由副院长李集明主持。

On 24 October 2016, the launching meeting for National Key Research Project of MOST, "Research and Application Demonstration of Cloud-Water Resource Assessment", was held in Beijing. This research project focuses on cloud-water resource (hydrometeor) as well as its variation pattern and carries out studies on how to make good use of cloud and water resources combining the coupled application of water resources on the land. The meeting was presided over by CAMS Vice President, Mr. Li Jiming and attended by over 90 members including CMA Deputy Administrator, Dr. Xu Xiaofeng; CAS Academicians, Zhou Xiuji, Chou Jifan, Lü Daren and NAE Academicians, Li Zechun, Xu Jianmin, Ding Yihui, Xu Xiangde, etc; as well as experts from related areas and project staff.

2016年10月29日，在全国人工影响天气中心主任会议期间，中国气象局局长郑国光，副局长矫梅燕参观了在中国气象局科技大楼展示的人工影响天气综合业务系统和物联网系统，与在场专家针对人影火箭、炮弹信息化处理等问题进行了热烈讨论，并对未来人影业务现代化发展提出了要求。

On 29 October 2016, during the National Meeting of Directors for Weather Modification Centres, CMA Administrator, Dr. Zheng Guoguang and Deputy Administrator, Prof. Jiao Meiyan, paid a visit to the weather modification integrated operation system and internet of things system exhibited at CMA S & T building. They had heated discussions on information processing of weather modification rockets and shells, etc. with experts at the meeting, and also presented requirements for future modernization of weather modification operations.

2016年11月4—5日，由中国气象科学研究院与英国林肯大学等合作申请的科技部中英国际合作重点项目"基于高分雷达遥感和快中子水分传感技术发展近实时的高时空分辨的区域土壤湿度监测方法"学术研讨会暨项目启动会在北京召开。林肯大学的Simon Pearson、Richard Turner，亚伯大学的George Petropoulos，以及英国生态与水文中心的Jonathan G. Evans 4位专家以及气科院、南京信息工程大学等30多位科研人员参加研讨会。房世波研究员主持了会议。

On 4–5 November 2016, the academic workshop i.e. launching meeting of MOST China-UK joint Key Project, "Synthesis of Remote Sensing and Novel Ground Truth Sensors to Develop High Resolution Soil Moisture Monitoring", jointly applied by CAMS and UK University of Lincoln as well as other institutions, was held in Beijing. Over 30 experts and research staff attended the meeting, including four UK experts as Simon Pearson and Richard Turner from University of Lincoln, George Petropoulos from Aberystwyth University and Centre for Ecology and Hydrology (CEH) and research staff from CAMS, NUIST, etc. The meeting was presided over by Dr. Fang Shibo, CAMS Researcher.

2016年11月9—10日，气科院灾害天气国家重点实验室与中国气象局成都高原气象研究所在四川成都联合召开了"全国青藏高原科学试验学术交流会"。会议围绕青藏高原及周边资料融合技术、青藏高原陆面与边界层物理过程等5方面议题进行了交流。吴国雄院士、徐祥德院士、张人禾院士等专家应邀做大会特邀报告，"第3次青藏高原大气科学试验——边界层与对流层观测"项目首席科学家赵平研究员在大会上介绍了该项目的最新进展。

On 9–10 November 2016, CAMS LaSW and CMA Chengdu Institute of Plateau Meteorology jointly held the Academic Meeting of National Tibetan Plateau Scientific Experiment in Chengdu, Sichuan Province. The meeting focused on five agenda items including integration techniques for data of Tibetan Plateau and surrounding areas, surface and boundary layer physical processes of Tibetan Plateau, etc. CAS Academicians, Prof. Wu Guoxiong, Prof. Zhang Renhe and NAE Academician, Dr. Xu Xiangde delivered invited presentations. "The Third Tibetan Plateau Atmospheric Scientific Experiment—Boundary Layer and Troposphere Observation" Project Chief Scientist, Prof. Zhao Ping, introduced the updates of the project on the meeting.

2016年11月13—14日，"中国农业资源与区划学会农业灾害风险专业委员会2016年学术年会暨会员代表大会"在海南省琼海市召开。会议围绕农业灾害风险科学的理论和方法等7个方面进行了交流与讨论。会议上，气科院霍治国研究员当选为农业灾害风险专业委员会第一届理事会理事长。来自气科院、中国农业大学、浙江大学等高校以及各省气象局等单位的130余名代表参加了会议。

On 13–14 November 2016, the 2016 Annual Academic Meeting, i.e. Member Conference for Specialized Committee on Agricultural Disasters Risk of the Chinese Society of Agricultural Resources and Regional Planning was held in Qionghai, Hainan Province. The meeting held exchanges and discussions with focus on scientific theories and methods of agricultural disasters risk. CAMS Researcher, Dr. Huo Zhiguo was elected as Chairperson of the First Council of Specialized Committee on Agricultural Disasters Risk. Over 130 representatives attended the meeting, including those from CAMS, China Agricultural University, Zhejiang University and provincial meteorological services.

东亚的降水模拟预测问题长久以来是数值模式面临的一大困难。气科院张祎和陈昊明博士利用当前先进的多尺度模拟系统，针对东亚降水模拟问题进行了全面深入的研究。研究指出，模式中降水的负偏差、高频次、低强度的降水结构以及午后降水峰值出现时刻过早等问题，存在着内在的联系。其系统性原因在于模式普遍对午后对流发展的渐进过程模拟欠佳。该研究成果发表于Journal of Climate 杂志，并被美国多尺度模拟中心（CMMAP）列为2016最新研究进展。

Simulation and prediction of precipitation over East Asia have long been a main obstacle for weather and climate numerical models. Drs. Zhang Yi and Chen Haoming of CAMS thoroughly studied the precipitation

观测（OBSCMO，TRMM）和模拟（CAM5，SPCAM5）的东亚子区域降水频次–强度关系分布
Observed (OBSCMO, TRMM) and simulated (CAM5, SPCAM5) precipitation frequency-intensity structures over a sub-domain of East Asia.

simulation problem based on a state-of-the-art multiscale modelling framework. This work pointed out that negative precipitation biases, high-frequency-low-intensity precipitation structures and earlier peaks of later afternoon precipitation, are tightly connected. The fundamental issue is that models cannot well simulate the gradual transition stage of convection development. This work is published by *Journal of Climate*, and is highlighted by Centre for Multiscale Modelling Atmospheric Process in 2016.

2016年12月21日，中国气象局大气化学重点开放实验室召开了第3届学术委员会会议。实验室主任徐晓斌介绍了本年度中国气象局对部门重点实验室2012—2015年度工作评估的情况，重点汇报了实验室本年度主要工作进展与成果，与会委员们肯定了实验室过去几年的工作成绩，对实验室未来发展提出了中肯建议。

On 21 December 2016, CAMS Key Open Laboratory on Atmospheric Chemistry held its Third Meeting of the Academic Committee. Director of the laboratory, Dr. Xu Xiaobin reported on CMA's assessment result of its key laboratory for the period of 2012–2015 conducted in 2016, with a highlight of the working progress and outcomes of the laboratory in 2016. The committee members appraised the achievements of the laboratory over the past few years and presented pertinent suggestions for its future development.

2016年12月20—21日，气候系统研究所在北京召开了"2016年度次季节–季节气候预测理论和方法"研讨会。会议围绕东亚季风区季节内振荡特征、持续性高温或严寒事件成因与机制、短期气候预测新方法和新技术等方面进行了深入交流。中国科学院大气物理研究所、北京大学、北京师范大学和国家气候中心等单位的多位专家应邀到会指导。

On 20–21 December 2016, the 2016 Workshop on Theories and Methodologies of Subseasonal-

to-seasonal Climate Prediction was held in Beijing by Institute of Climate System, CAMS. The workshop focuses on the features of intraseasonal oscillations in East Asia monsoon region, the causes and mechanisms of persistent heat wave or extreme cold events, the novel methods and techniques of short-term climate prediction, etc. Several experts, from Institute of Atmospheric Physics, Chinese Academy of Sciences (IAP/CAS), Peking University, Beijing Normal University and CMA National Climate Centre, etc, were invited to attend this workshop and give guidance.

2016年12月21日，河南省气象局局长赵国强一行3人到气科院调研。端义宏院长主持接待。院党委副书记、纪委书记李慧参加调研。双方就科研成果转化和应用、共同防灾减灾以及进一步完善气科院河南分院建设方案进行了研讨。

On 21 December 2016, Director-General of Henan Provincial Meteorological Service, Mr. Zhao Guoqiang, together with two of his colleagues, visited CAMS and they were met by CAMS President, Dr. Duan Yihong, Deputy Secretary of CAMS CPC Committee as well as Secretary of Discipline Inspection Commission, Mr. Li Hui and other CAMS colleagues. The two sides discussed about research outcomes transfer and application, joint disasters prevention and mitigation, as well as further improvement of construction plan for CAMS sub-branch in Henan Province, etc.

2016年12月26日，天气气候一体化模式关键技术攻关团队2016年度学术年会在北京召开，团队首席研究员周天军、李建、梁旭东及来自气科院、中国科学院大气物理研究所、南京信息工程大学等的团队成员和张大林教授等特邀专家参加会议。会议围绕一体化模式研发如何与大型外场观测试验，以及东亚区域再分析等工作结合进行了深入讨论。

On 26 December 2016, the key research team of Weather-Climate Unified Model held its 2016 Annual Academic Meeting in Beijing. The Chief Scientist of the team, Drs. Zhou Tianjun, Li Jian and Liang Xudong, team members from CAMS, IAP/CAS and NUIST, specially invited experts including Prof. Zhang Dalin, attended the meeting and conducted in-depth discussions with focuses on how the unified model should be combined with large-scale field observation experiment and East Asia region reanalysis.

2016年，气科院获中国气象学会大气科学基础研究成果奖1项（宇如聪，李建，陈昊明），四川省科技进步一等奖1项（徐祥德，张胜军，陈斌等），第33届国际雷电防护会议（ICLP）科学委员会奖1项（张义军），海洋工程科学技术奖一等奖1项，以及2016年邹竞蒙气象科技人才奖1项（罗亚丽）。

In the year of 2016, CAMS won an Award for Fundamental Research Outcome in Atmospheric Sciences granted by Chinese Meteorological Society (Yu Rucong, Li Jian, Chen Haoming); a First Prize of Science &Technology Advancement awarded by Sichuan Province (Xu Xiangde, Zhang Shengjun, Chen Bin, etc.); a Scientific Committee Award of the 33rd International Conference on Lightning Protection (Zhang Yijun); a First Prize of Ocean Engineering Science &Technology; and a Zoujingmeng Award for Talents in Meteorological Science and Technology (Luo Yali).

2016年，气科院获得专利6项（关立友，苏正军(2项)，姚雯，杨俊，姚波等），软件著作权6项（姚展予，王亚强(2项)，杨建莹，程已阳，姚雯等）。

In the year of 2016, CAMS won 6 patents (Guan Liyou, Su Zhengjun (2 patents), Yao Wen, Yang Jun, Yao Bo, etc.) and 6 software copyrights (Yao Zhanyu, Wang Yaqiang (2 copyrights), Yang Jianying, Cheng Siyang, Yao Wen, etc.)

2016 年新项目
New Projects in 2016

课题名称 Title	项目类别 Project/Fund	执行期间 Duration	负责人 Principal Investigator
植物对地质封存二氧化碳泄漏的耐受机理研究 The vegetation tolerance mechanism to carbon dioxide leakage from CCS	基金委：青年科学基金项目 NSFC：youth program	2017—2019	张雪艳 Zhang Xueyan
中国东北样带与以色列北南降水梯度生态系统的干旱生理调节与弹性 Physiological adjustments and resilience to drought in ecosystems across Northeast China transect and the Israel north-south precipitation gradient	基金委：国际（地区）合作与交流重点项目 NSFC：key program, International cooperation and exchange project	2017—2020	周广胜 Zhou Guangsheng
应用三维完全 Stokes 冰流模型诊断模拟东南极 Lambert-Amery 冰川流域系统的热力学特征 Diagnostics and simulation of the thermodynamic features of the Lambert-Amery Glacier Drainage System, East Antarctica, using a three dimensional full stokes ice sheet model	基金委：青年科学基金项目 NSFC：youth program	2017—2019	张通 Zhang Tong
中国华北雷暴降雪动力和云微物理机制的模拟研究 Simulation of the dynamical and microphysical mechanism of the thundersnow in North China	基金委：青年科学基金项目 NSFC：youth program	2017—2019	徐良韬 Xu Liangtao
云雷达功率谱密度数据识别高原云相态方法研究 Cloud phase classification method using cloud radar powder density data over the Tibet Plateau	基金委：青年科学基金项目 NSFC：youth program	2017—2019	庄薇 Zhuang Wei
东亚-太平洋遥相关和欧亚遥相关对江淮持续性极端降水的影响机理 Mechanisms of persistent precipitation extremes in the Yangtze-Huai River Valley triggered by both East Asia-Pacific teleconnection and Euro-Asia teleconnection	基金委：青年科学基金项目 NSFC：youth program	2017—2019	陈阳 Chen Yang
全球陆面碳、水通量模拟误差的量化和归因 Quantification and attribution of errors in simulated carbon and water fluxes from land surface	基金委：青年科学基金项目 NSFC：youth program	2017—2019	李剑铎 Li Jianduo
基于地面雷达资料对青藏高原那曲地区夏季对流云时空分布和垂直结构特征的研究 Characteristics of temporal-spatial distribution and vertical structure of summer convective clouds over Naqu over the Tibetan Plateau based on surface radar dataset	基金委：青年科学基金项目 NSFC：youth program	2017—2019	汪会 Wang Hui
北京地区持续性大雾的微物理结构观测研究 Observational study on microphysical structure of persistent fog in Beijing region	基金委：青年科学基金项目 NSFC：youth program	2017—2019	郭丽君 Gu Lijun

课题名称 Title	项目类别 Project/Fund	执行期间 Duration	负责人 Principal Investigator
ENSO 与气候平均态的相互作用——基于海气耦合模式的数值模拟研究 Interaction between ENSO and the climatological mean state—based on the numerical simulations of coupled models	基金委：青年科学基金项目 NSFC：youth program	2017—2019	华莉娟 Hua Lijuan
层云闪电的发生和发展与回波亮带关系的研究 Study on the relationship between the initiation and propagation of stratiform lightning and the brightband of radar reflectivity	基金委：青年科学基金项目 NSFC：youth program	2017—2020	王飞 Wang Fei
闪电初始阶段特征与雷暴结构的时空配置关系 Space-time relationships between lightning initiation characteristics and thunderstorm structures	基金委：面上项目 NSFC：general program	2017—2020	郑栋 Zheng Dong
产生地面大风的华南强对流系统中小尺度精细结构和演变的相控阵天气雷达观测研究 High-temporal resolution X band phased-array Doppler observation of severe convective fine structure and evolution with gale force wind in South China	基金委：面上项目 NSFC：general program	2017—2020	刘黎平 Liu Liping
初生对流的地基综合观测和微波辐射模拟研究 Study on ground-based comprehensive observations and microwave radiation simulation of convective initiation	基金委：面上项目 NSFC：general program	2017—2020	杨俊 Yang Jun
双台风相互作用对中国极端降水的影响 Impacts of binary tropical cyclones on extreme precipitations over mainland of China	基金委：面上项目 NSFC：general program	2017—2020	任福民 Ren Fuming
热带气旋过台湾岛后路径偏折与结构变化的机理研究 Study on the mechanism of track deflection and structural changes of tropical cyclones after crossing Taiwan Island	基金委：面上项目 NSFC：general program	2017—2020	徐晶 Xu Jing
东亚季风区季节内振荡的年际变化及其对中国东部夏季降水异常的影响 Interannual variations of intraseasonal oscillation and its impact on summer rainfall over eastern China	基金委：面上项目 NSFC：general program	2017—2020	齐艳军 Qi Yangjun
地形强迫对中国东部降水气候分布的影响研究 The effect of topographic forcing on rainfall distribution over Eastern China	基金委：面上项目 NSFC：general program	2017—2020	宇如聪 Yu Rucong
高分辨率观测和放射性 C-14 分析技术的含碳气溶胶源识别研究 The source identification of carbonaceous aerosol by high resolution measurement and carbon-14 technology	基金委：面上项目 NSFC：general program	2017—2020	张养梅 Zhang Yangmei

课题名称 Title	项目类别 Project/Fund	执行期间 Duration	负责人 Principal Investigator
我国背景区域关键气溶胶光学参数及其对辐射强迫影响研究 Study of key aerosol optical parameters and their effects on radiative forcing at background sites	基金委：重点项目 NSFC：key program	2017—2020	孙俊英 Sun Junjing
不同气候背景条件下气溶胶对云雾滴谱特征影响机制的观测研究 Observational study on the impacts of aerosol on cloud and fog droplet spectrum characteristics over different climate conditions	基金委：重点项目 NSFC：key program	2017—2020	段婧 Duan Jing
国际理论物理中心气溶胶与云相互作用学术活动 Academic activities on aerosol-cloud interactions at the International Centre for Theoretical Physics (ICTP)	基金委：国际（地区）合作与交流项目 NSFC：international cooperation and exchange project	2016—2016	徐良韬 Xu Liangtao
基于高分雷达遥感和快中子水分传感技术，发展近实时的高时空分辨率的区域土壤湿度监测方法 Synthesis of remote sensing and novel ground truth sensors to develop high resolution soil moisture monitoring mothed	基金委：国际（地区）合作与交流重点项目 NSFC：key program, international cooperation and exchange project	2016—2019	房世波 Fang Shibo
青藏高原水汽"源汇"结构的多尺度变化及其对区域降水影响研究 The multi-scale variability of the moisture source-sink over the Tibetan Plateau and its effects on the precipitation over its surrounding areas	基金委：面上项目 NSFC：general program	2017—2019	陈斌 Cheng Bin
大气环流模式对青藏高原陡峭地形区降水模拟的改进研究 Study on improving the simulation of precipitation over the steep edge of the Tibetan Plateau	基金委：重点项目 NSFC：key program	2017—2020	李建 Li Jian
青藏高原大气动力、热力过程对中国东部大气污染时空变异影响的机理 The effects of atmospheric dynamics and thermodynamic processes over the Tibetan Plateau on the spatial and temporal variation of air pollution in eastern China and the associated mechanisms	基金委：重点项目 NSFC：key program	2017—2020	徐祥德 Xu Xiangde
云水资源评估研究与利用示范 Study on cloud water resources assessment and demonstration of utilization	科技部：重点研发专项 MOST：key program	2016—2020	周毓荃 Zhou Yuquan
北京市霾污染条件下 PAN 的变化特征及其源汇研究 The variation characteristics and formation mechanism of PAN under hazy conditions in Beijing	科技部：重点研发专项（青年项目） MOST：key program	2016—2020	徐婉筠 Xu Wanyun

课题名称 Title	项目类别 Project/Fund	执行期间 Duration	负责人 Principal Investigator
我国大气重污染累积与天气气候过程的双向反馈机制研究 Feedback mechanism linking heavy aerosol pollution, weather, and climate	科技部：重点研发专项 MOST：key program	2016—2020	张小曳 Zhang Xiaoye
珠三角不同典型陆面背景下重污染过程大气污染物与低层气象要素垂直结构及其时空演变研究 Study of vertical structures and temporal-spatial evolution of atmospheric pollutants and meteorological parameters of lower atmosphere during heavy pollution process in the Pearl River Delta	科技部：重点研发专项 MOST：key program	2016—2020	孙俊英 Sun Junjing
亚洲现代风尘排放的源汇模式和迁移机制 Source-sink mode and transportation mechanism of modern Asian dust emissions	科技部：重点研发专项 MOST：key program	2016—2020	车慧正 Che Huizheng
华南前汛期暖区特大暴雨的发生发展机理及其可预报性 The mechanism and predictability of a warm-sector convective system producing torrential rain during pre-rainy season in South China	教育部：留学回国人员专项 MOE：scientific research foundation for returned overseas Chinese scholars	2016—2018	黄龄 Huang Ling
基于主被动卫星遥感的云上沙尘气溶胶直接气候效应研究 Study on the above-cloud dust aerosol direct radiative forcing using active and passive satellites	教育部：留学回国人员专项 MOE：scientific research foundation for returned overseas Chinese scholars	2016—2018	徐慧 Xu Hui

MOST：Ministry of Science and Technology（科技部）

NSFC：Natural Science Foundation of China （国家自然科学基金）

MOE：Ministry of Education（教育部）

人才培养
Education and Training

2016年5月，气科院成立了由25人组成的第10届学位评定委员会，徐祥德院士为委员会主席，端义宏院长和周广胜副院长为副主席。6月7日学位委员会讨论通过了2016届毕业研究生学位授予，9月13日讨论确定了2016年博士生导师和硕士生导师的遴选名单。

In May 2016, CAMS established its Tenth Diploma Conferring Committee consisting of 25 members, with Xu Xiangde, Academician of Chinese Academy of Engineering, as the Chair of the Committee, DuanYihong and Zhou Guangsheng, CAMS President and Vice President, as the Deputy Chairs. On 7 June, the Committee discussed and approved the conferring of Graduate Degree for graduates of 2016 while on 13 September, confirmed the candidate list of tutors for PhD and Master graduates.

2016年6月，科技部印发了《关于公布2015年创新人才推进计划入选名单的通知》，气科院成功入选国家创新人才培养示范基地，本批次全国共有34家单位入选。气科院入选国家

创新人才培养示范基地，将为继续推进青年骨干人才、科技创新领军人才、重点领域创新团队的培育和建设提供重要的平台。

In June 2016, Ministry of Science and Technology of China (MOST) released "the Announcement of Candidates for Innovation Talents Promotion Plan in 2015" by which CAMS was successfully nominated as a Demonstrative Training Base of Innovation Talents, among the overall 34 bases over the whole country. Being elected as a base of innovation talents training, CAMS will continue to provide the important platform for advancing the development of young cadres, scientific and technological innovation talents as well as innovation teams in key areas.

在中国气象局和中国地质大学（武汉）合作协议的框架下，气科院与中国地质大学（武汉）签订了共建"大气科学菁英班"协议，气科院科研人员将全程参与中国地质大学（武汉）大气科学专业本科生的教学和培养工作，这对于提高气科院研究生生源质量有重要意义。2016年10月9日，中国地质大学（武汉）首届大气科学菁英班举行了开学典礼。

Under the framework of the Cooperation Protocol between China Meteorological Administration and China University of Geosciences (Wuhan), CAMS signed with China University of Geosciences (Wuhan) the Agreement for Joint Establishment of Elite Class in Atmospheric Science. According to such agreement, CAMS research staff will be fully involved in the teaching and development of atmospheric science undergraduates at China University of Geosciences (Wuhan), which is of great significance to the improvement of CAMS graduate students' quality. On 9 October 2016, University of Geosciences (Wuhan) held the School Opening Ceremony for First Elite Class in Atmospheric Science.

2016年，气科院共招收硕士研究生45人、博士研究生18人，进站博士后5人；毕业硕士44人、博士7人。目前在学研究生221人，其中硕士研究生134人，博士研究生70人，在站博士后17人。

2016年6月24日，气科院2016届毕业生毕业典礼在北京举行。在毕业典礼上颁发了2016年度奖学金，包括华风优秀研究生奖、华风优秀研究生导师奖，华云研究生优秀成绩奖、华云优秀毕业生奖、华云优秀学生干部奖等。

In 2016, 45 Master Degree Candidates, 18 Doctoral Candidates and five Post Doctors were recruited by CAMS while 44 got Master Degree and seven received PhD Degree. At present, there are altogether 221 graduates at CAMS, among whom 134 are Master Degree Candidates, 70 are Doctoral Candidates and 17 are Post Doctors.

On 24 June 2016, the Graduation Ceremony for CAMS Graduates of 2016 was held in Beijing, during which a number of awards were conferred, including the Annual Scholarship of 2016, Huafeng Prize for Outstanding Graduates, Huafeng Prize for Outstanding Supervisors, Huayun Prize for Excellent Performance of Graduates, Huayun Prize for Outstanding Graduates, and Huayun Prize for Outstanding Student Cadres, etc.

2016年8月7—12日，由气科院主办的全国大气科学领域优秀大学生暑期学校在北京举行。暑期学校聘请张大林、龚山陵、张义军、沈学顺、郭建平和李建6位专家为学生授课，暑期学校校长周秀骥院士与学生进行了座谈并为学员颁发了毕业证书。期间，还组织学生参观了中央气象台、北京市观象台和固城生态与农业气象试验站等地。

On 7–12 August 2016, Summer School for Outstanding Undergraduates in Atmospheric Science over the Country hosted by CAMS was held in Beijing. Six CAMS experts were invited to give lectures for the Summer School, including Prof. Zhang Dalin, Prof. Gong Shanling, Dr. Zhang Yijun, Dr. Shen Xueshun, Dr. Guo Jianping and Dr. Li Jian. Head of the Summer School, Dr. Zhou Xiuji who is an Academician of Chinese Academy of Sciences, had discussions with the students and conferred them graduation certificates. During the Summer School, visits were also organized to the Central Meteorological Observatory (CMA National Meteorological Centre), Beijing Meteorological Observatory as well as Gucheng Ecological and Agri-Meteorological Integrated Observation Experiment Station, etc.

合作与交流
Cooperation and Communication

2016年3月15日，美国国家大气研究中心（NCAR）王薇研究员访问灾害天气国家重点实验室并做了题为"WRF模式的最新进展"的学术报告。报告主要介绍了WRF模式在新的云量计算方案等5个方面的改进。报告由气科院千人计划专家陈飞教授主持。

On 15 March 2016, Ms. Wang Wei, research fellow from US National Center for Atmospheric Research (NCAR), visited CAMS State Key Laboratory on Severe Weather (LaSW) and delivered the presentation titled "Recent Enhancements in WRF Model", in which enhancements of WRF Model in five aspects, including cloud computing scheme, were introduced. The presentation was presided over by Prof. Chen Fei, Scientist of the Chinese Government's Recruitment Program of Global Experts (known as "the Thousand Talents Plan").

2016年3月23日，美国国家大气研究中心（NCAR）刘志权博士受邀到气科院进行学术交流并做了题为"我国大气再分析计划与进展"的学术报告。刘志权博士结合全球大气再分析系统的发展状况，重点介绍了中国全球大气再分析系统的研究计划，以及中国全球再分析资料与东亚区域大气再分析资料研究的相互关系。梁旭东研究员主持了报告会。

On 23 March 2016, Dr. Liu Zhiquan from NCAR paid an invited visit to CAMS and delivered the presentation titled "the Atmospheric Reanalysis Program of China and Its Progress". On the basis of development of the global atmospheric reanalysis system, Dr. Liu highlighted the research plan of global atmospheric reanalysis system in China, as well as the correlation between the global reanalysis data of China and research of atmospheric reanalysis data of East Asia. The presentation was presided over by Dr. Liang Xudong, CAMS Researcher.

2016年4月20日，韩国首尔市气象厅厅长Nam Jae-Cheol一行5人访问了气科院。端义宏院长与Nam Jae-Cheol厅长就未来双方合作内容及方式进行了交流。随后韩国代表团一行参观了大气化学重点开放实验室，王亚强副所长向来宾介绍了实验室在大气成分基础观测、实验室分析、环境模式建立及应用等方面的情况。

On 20 April 2016, a five-member delegation headed by Director-General of KMA (Korea Meteorological Administration)'s Seoul Regional Meteorological Office, Dr. Nam Jae-Cheol, visited CAMS. The President of CAMS, Dr. DuanYihong met and exchanged with Dr. Nam on future cooperation content and modalities between the two institutions. After the meeting, the KMA delegation visited the CAMS Key Laboratory on Atmospheric Chemistry and Dr. Wang Yaqiang, Deputy Director of the Laboratory, introduced the Laboratory's observation, analysis, the development and application of environment numerical models, etc.

2016年5月12日，印度尼西亚气象、气候和地球物理局（BMKG）教育和培训中心主任Herizal率领印度尼西亚气象代表团一行7人参观了大气化学重点开放实验室。王亚强副所长向来宾介绍了气科院在大气成分基础观测、实验室分析、环境模式建立及应用等方面的研究现状。

On 12 May 2016, a seven-member delegation headed by Mr. Herizal, Director of Education and Training Centre, the Agency for Meteorology, Climatology and Geophysics of the Republic of Indonesia (BMKG), visited CAMS Key Laboratory on Atmospheric Chemistry. Dr. Wang Yaqiang, Deputy Director of the Laboratory, introduced the observation and analyses of atmospheric compositions, the development and application of environment numerical models, etc.

2016年5月30日，阿拉伯联合酋长国（简称阿联酋）国家气象和地震中心（NMSC）代表团访问了中国气象局人工影响天气中心。郭学良副主任向来宾介绍了人工影响天气中心的科研和业务情况。阿方人员介绍了阿联酋的气象站、国家雷达网以及人工增雨科学研究项目等情况。双方就人工影响天气研究进行了深入交流讨论。

On 30 May 2016, the delegation from the National Centre of Meteorology and Seismology (NMSC), United Arab Emirates (UAE), visited CMA Weather Modification Centre (WMC). Dr. Guo Xueliang, Deputy Head of WMC, introduced scientific research and operation of the Centre. The NMSC delegation introduced meteorological stations, national radar network and precipitation enhancement research programs, etc. in UAE. In-depth discussions about weather modification research were held.

2016年6月28日，尼泊尔农业发展部下属气候相关灾害适应能力建设项目处处长ShibNandan Prasad Shah先生一行9人访问中国气象局人工影响天气中心。人工影响天气中心副主任郭学良向来宾介绍了我国人工影响天气管理、科研业务的总体情况，以及人工影响天气中心的主要工作。双方就人工增雨、人工消减雨作业等进行了技术交流。

On 28 June 2016, a nine-member delegation visited CMA Weather Modification Centre (WTC), which was headed by Mr. ShibNandan Prasad Shah, Division Head of Capacity Building for Climate Disasters Response, Nepal Ministry of Agricultural Development (MoAD). Dr. Guo Xueliang, Deputy Head of WMC, briefed on weather modification management, scientific research and operation in China, as well as the main responsibilities of WMC. Technical exchanges on rain enhancement, dispersal and mitigation were conducted.

2016年7月5日，美国Aerodyne Research有限公司副总裁、气溶胶和云化学中心主任Douglas Worsnop博士应邀访问气科院并做了题为"气溶胶质谱测定方法：从1 nm到1μm"的精彩报告。报告会由大气成分研究所孙俊英研究员主持，来自气科院大气成分研究所和气候系统研究所以及中国气象局数值预报中心的有关科研人员及研究生听取了报告。

On 5 July 2016, Dr. Douglas Worsnop, Vice President of Aerodyne Research Inc, USA as well as Head of Center for Aerosol and Cloud Chemistry, was invited to visit CAMS and delivered an attractive presentation titled "Mass Spectrometry of Atmospheric Aerosol: 1 nanometer to 1 micron". The seminar was presided over by Dr. Sun Junying, who is from CAMS Institute of Atmospheric Composition. Research staff and graduate students from CAMS Institute of Atmospheric Composition and Institute of Climate Systems as well as Numerical Weather Prediction Center of CMA attended this seminar.

2016年7月13日，法国国家气象研究中心的Jean-Louis Roujean教授和美国科罗拉多州立大学的刘术艳博士访问了气科院，分别做了题为"极端天气事件中微波集成检索系统（MIRS）的应用"和"MSG气溶胶和太阳辐射卫星产品反演与验证"的学术报告，并与气科院相关科研人员围绕气溶胶、降水卫星产品的不确定性以及应用前景进行了热烈讨论。大气成分研究所郭建平研究员主持了报告会。

On 13 July 2016, Prof. Jean-Louis Roujean from Centre National de la Recherche Meteorologique (CNRM) of France and Dr. Liu Shuyan from Colorado State University of US visited CAMS and gave academic presentations titled "The MIRS Application for Extreme Weather Events" and "Solar Radiation and Aerosol Products from MSG: methods and validation" respectively. The two experts also conducted in-depth and heated discussions with CAMS research staff on the uncertainty of aerosoland precipitation satellite products as well as application prospects. The presentation was presided over by Dr. Guo Jianping, Researcher from CAMS Institute of Atmospheric Composition.

2016年7月14日，美国农业部农业研究中心水文与遥感实验室Martha Anderson等一行4人访问气科院。代表团在生态环境与农业气象研究所副所长王培娟陪同下参观了固城生态与农业气象实验站，随后在气科院与相关科研人员进行了学术交流。Martha Anderson和Feng Gao研究员分别做了题为"基于数据融合方法监测从田块到全球尺度的农作物蒸散和水分胁迫"和"基于时空信息融合技术监测作物长势"的报告，2个报告提供了很好的农业气象灾害监测方法及思路。

On 14 July 2016, a four-member delegation from Hydrology and Remote Sensing Laboratory, Agricultural Research Service, United States Department of Agriculture led by Martha Anderson visited CAMS. The delegation paid a visit to Gucheng Ecological and Agri-Meteorological Integrated Observation Experiment Station in the accompany of Wang Peijuan, Deputy Director of CAMS Institute of Ecological Environment and Agricultural Meteorology and after the visit, exchanged with CAMS research staff on academic issues. Dr. Martha Anderson and Dr. Feng Gao gave presentations titled "Monitoring ET and Crop Stress at Field to Global Scales Using Data Fusio" and "Spatial and Temporal Information Fusion for Crop Condition Monitoring" respectively, which provided thought-provoking methods for agrometeorological disasters monitoring.

2016年7月18日，欧洲中期天气预报中心（ECMWF）主任Florence Rabier一行3人在中国气象局国际司周恒司长陪同下访问气科院。院长端义宏向来宾简要介绍了气科院概况，科技处于飞副处长做了第3次青藏高原大气科学试验进展报告，大气成分研究所王亚强所长介绍了气科院雾–霾数值预报模式。随后端义宏院长带领ECMWF代表团参观了大气化学重点开放实验室。

On 18 July 2016, a three-member delegation from European Centre for Medium-range Weather Forecast (ECMWF) led by its Director, Dr. Florence Rabier, visited CAMS accompanied by Mr. Zhou Heng, Director-General of CMA Department of International Cooperation. Dr. Duan Yihong, CAMS President, briefed on CAMS work and Yu Fei, Deputy Director of CAMS Science and Technology Division, introduced the progress of the Third Tibetan Plateau Atmospheric Scientific Experiment. Dr. Wang Yaqiang, Deputy Director of CAMS Institute of Atmospheric Composition, introduced CAMS' fog-haze NWP model, after which the ECMWF delegation visited the CAMS Key Laboratory on Atmospheric Chemistry accompanied by Dr. Duan Yihong.
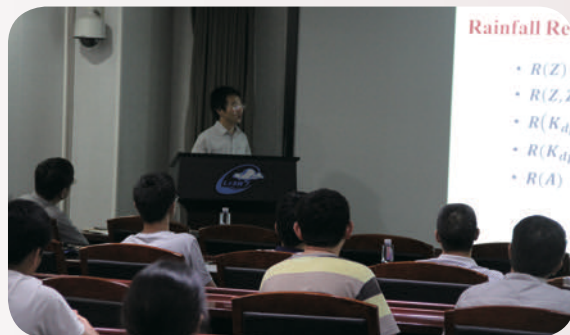
2016年7月12日，美国科罗拉多州立大学电子和计算机工程学院V. Chandrasekar教授和陈浩南博士应邀访问气科院，分别做了题为"高分辨率极化雷达网的降水粒子分类和降雨估测"和"双偏振雷达的现状：从系统到应用"的学术报告。Chandrasekar教授介绍了双偏振雷达的主要特性、优势及其应用。陈浩南博士介绍了Dallas-Fort Worth高分辨率城市气象雷达网的观测及其应用。灾害天气国家重点实验室副主任吕伟涛主持了报告会。

On 12 July 2016, Prof. V. Chandrasekar and Dr. Chen Haonan from School of Electronic and Computer Engineering, Colorado State University, paid an invited visit to CAMS and delivered presentations titled "Hydrometeor Classification and Rainfall Estimation with High-Resolution Polarimetric Radar Network" and "Current State of Dual-Polarization Radar: from System to Applications" respectively. Prof. Chandrasekar introduced the features, advantages and applications of dual-polarization radars and Dr. Chen Haonan introduced the observation and application of Dallas-Fort Worth high-resolution urban meteorological radar network. Dr. Lü Weitao, Deputy Director of LaSW, presided over the presentation.

2016年7月13日，日本情报通信研究院（NICT）Toshio Iguchi教授和大阪大学Tomoo Ushio教授应邀访问气科院，分别做了题为" TRMM卫星PR降水雷达和GPM卫星DPR雷达介绍： PR/DPR算法发展历程"和"国际空间站全球闪电测量以及相控阵天气雷达的发展"的学术报告，实验室吕伟涛副主任主持了报告会。Toshio Iguchi教授详细介绍了卫星雷达资料在台风、龙卷等灾害性天气预警预报中的应用。Tomoo Ushio教授介绍了日本闪电探测方面的现状以及国际空间站闪电观测计划等。

On 13 July 2016, Prof. Toshio Iguchi from National Institute of Information and Communications Technology (NICT) and Prof. Tomoo Ushio from Osaka University, Japan, paid an invited visit to CAMS. The two professors delivered presentations titled "Understanding of TRMM/PR and GPM/DPR: History of PR/DPR Algorithms Development" and "Global Lightning and Sprite Measurements from International Space Station (GLIMS) and Development of the Phased Array Weather Radar" respectively. Dr. Lü Weitao, Deputy Director of LaSW, presided over the presentation. Prof. Toshio Iguchi introduced in detail the application of satellite and radar data in the warning and forecasting of severe weathers such as typhoon, tornado, etc and Prof. Tomoo Ushio introduced current status of lightning detection in Japan as well as lighting observation plans of international space stations.

2016年7月29日，美国德州农工大学大气科学系和化学系张人一教授访问气科院大气成分研究所并做了题为"城市细颗粒物的形成和机理：进展和挑战"的学术报告。报告由孙俊英研究员主持，与会人员与张教授就气溶胶与气候、极端天气的关系等问题进行了热烈讨论。

On 29 July 2016, Prof. Zhang Renyi from School of Atmospheric Sciences as well as School of Chemistry, Texas Agricultural and Mechanical University, visited CAMS Institute of Atmospheric Composition and delivered the presentation titled "The Formation and Mechanism of Urban Fine Particulate Matter: Progress and Challenges". The seminar was presided over by Dr. Sun Junying, and heated discussions were conducted between Prof. Zhang and participants on the correlation of aerosol with climate, extreme weather events, etc.
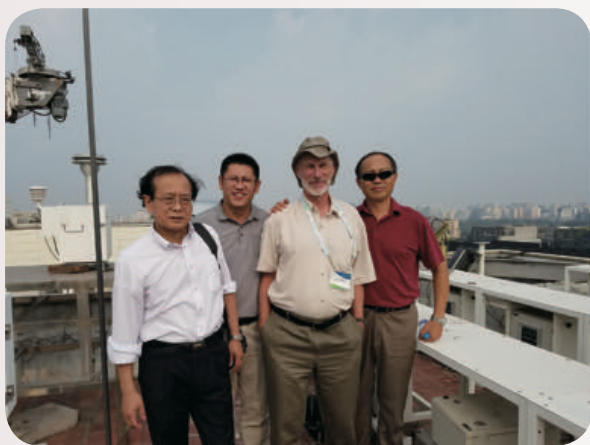
2016年8月3日，美国NASA戈达德航天中心(GSFC)的Brent Holben博士和日本地球观测中心(EORC)的Teruyuki Nakajima教授应邀访问气科院，分别做了题为"全球气溶胶监测网3.0版气溶胶光学厚度滤云方案和质量控制"和"基于日本温室气体观测卫星和葵花8号卫星遥感气溶胶新方法"的学术报告。大气成分研究所副所长车慧正研究员主持了报告会。报告结束后，两位来宾参观了大气化学重点开放实验室，并就中国气溶胶遥感观测网(CARSNET)未来的发展给出了宝贵的建议。

On 3 August 2016, Dr. Brent Holben from NASA's Goddard Space Flight Center and Prof. Teruyuki Nakajima from Japan's Earth Observation Research Center (EORC) were invited to visit CAMS Institute of Atmospheric Composition, and delivered academic presentations titled "AERONET Version 3 Database AOD Cloud Screening and Quality Controls" and "A new Aerosol Remote Sensing with GOSAT/CAI and Himawari-8 Satellite-Borne Imagers" respectively. The presentation was presided over by Dr. Che Huizheng, Deputy Director of CAMS Institute of Atmospheric Composition. After the presentation, the two experts visited Atmospheric Chemistry Laboratory and provided constructive advice on the future development of China's Aerosol Remote Sensing Network (CARSNET).

2016年8月4日，美国国家大气研究中心（NCAR）的Michael Barlage博士访问气科院灾害天气国家重点实验室并做了题为"用于改进WRF季节性预测的简单作物模型的发展和评估"的学术报告。实验室主任梁旭东研究员主持了报告会。预测农作物产量是WRF模型的未来发展方向之一，Michael Barlage博士介绍了一个简单的农作物模型WRF-Crop及其应用效果。

On 4 August 2016, Dr. Michael Barlage from US National Center for Atmospheric Research (NCAR) visited CAMS State Key Laboratory on Severe Weather (LaSW) and delivered the presentation titled "Development and Evaluation of a Simple Crop Model for WRF Seasonal Forecast Improvement". Dr. Liang Xudong, Director of LaSW presided over the presentation. With crop yield prediction being a developing trend of WRF model in future, Dr. Michael Barlage introduced a simple WRF-Crop model and its application effect.

2016年8月11日，美国国家环境预报中心（NCEP）的刘舜博士访问气科院灾害天气国家重点实验室并做了题为"WSR-88D雷达与闪电同化资料在NCEP的业务应用"的学术报告。报告全面介绍了雷达与闪电资料在NCEP的业务应用情况，特别是美国WSR-88D雷达网偏振升级改造后，对雷达数据的质量控制有了明显的提升，改进了中小尺度强对流天气预报。报告会由实验室主任梁旭东研究员主持。

On 11 August 2016, Dr. Liu Shun from National Center for Environmental Prediction (NCEP) visited CAMS State Key Laboratory on Severe Weather (LaSW) and delivered the presentation titled "Assimilation of WSR-88D Radar Data and Lightning Data at NCEP". The presentation covered comprehensive application of radar data and lightning data in NCEP operation, in particular the improved forecast for small to meso-scale strong convective weather with much stronger radar data quality control after the upgraded reconstruction of US WSR-88D polarized radar network. The presentation was presided over by Dr. Liang Xudong, Director of LaSW.

2016年8月19日，澳大利亚联邦科学与工业研究组织（CSIRO）的郑邦友博士访问气科院生态环境与农业气象研究所并做了题为"谷物对未来气候的适应：用作物模型和基因模拟方法探索其复杂性"的学术报告，气科院生态环境与农业气象研究所房世波研究员主持了报告。郑邦友博士主要介绍了APSIM模型、建模数据的删选及模型的验证等问题。

On 19 August 2016, Dr. Zheng Bangyou from Commonwealth Scientific and Industrial Research Organization (CSIRO) visited CAMS Institute of Ecological Environment and Agricultural Meteorology and delivered the presentation titled "Adaptation of Cereals to Future Climate: Exploring Complexity Using Crop Model and Genetic Simulation", which was presided over by Dr. Fang Shibo, Resercher from Institute of Ecological Environment and Agricultural Meteorology. In his presentation, Dr. Zheng Bangyou mainly covered APSIM model, selection of modeling data as well as model verification, etc.

2016年8月30日，美国俄克拉何马大学风暴分析与预报中心（CAPS）刘成思博士到气科院灾害天气国家重点实验室进行学术交流并做了题为"ARPS-En3DVar与ARPS-EnKF同化系统在雷达资料同化中的比较"的学术报告。报告会由实验室主任梁旭东研究员主持。

On 30 August 2016, Dr. Liu Chengsi from Center for Analysis and Prediction of Storms (CAPS), University of Oklahoma, visited CAMS State Key Laboratory on Severe Weather (LaSW) and delivered the presentation titled "Comparison between Assimilation Systems of ARPS-En3DVar and ARPS-EnKF in Radar Data Assimilation", which was presided over by Dr. Liang Xudong, Director of LaSW.
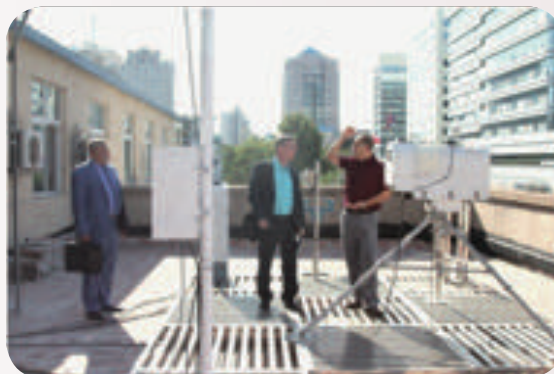
2016年9月5日，俄罗斯联邦水文气象与环境监测局计算中心主任谢尔盖•鲁波夫一行8人在国际司胡晓平副处长陪同下参观气科院大气化学重点开放实验室和云雾物理环境重点开放实验室。大气成分研究所副所长王亚强向来宾介绍了气科院大气成分的基础观测、预报模式的发展及应用的情况，人工影响天气中心苏正军副研究员介绍了实验室人工影响天气科研仪器设备和应用现状。

On 5 September 2016, an eight-member delegation from the Computing Centre of Federal Service for Hydrometeorology and Environmental Monitor, Russian Federation (Roshydromet) led by Dr. Sergey Lubov visited CAMS Key Laboratory on Atmospheric Chemistry and CMA Key Laboratory for Cloud Physics and Weather Modification, accompanied by Mr. Hu Xiaoping, Deputy Director for Bilateral Cooperation from CMA International Cooperation Department. Dr. Wang Yaqiang, Deputy Director of CAMS Institute of Atmospheric Composition, introduced the observation of atmospheric compositions, the development and application of prediction models, etc. Dr. Su Zhengjun from WMC introduced the research equipment of CMA Key Laboratory for Cloud Physics and Weather Modification and its application.

2016年9月13日，美国劳仑斯利弗莫尔国家实验室郑雪博士访问气科院灾害天气国家重点实验室并做了题为"利用外场观测数据识别CAM（Community Atmosphere Model）模式在洋面大气边界层云模拟中的缺陷"的报告。他介绍了其所在团队利用亚速尔群岛的站点观测数据对CAM模式及其更新版本进行的对比和验证情况。报告会由实验室副主任徐晶博士主持。

On 13 September 2016, Dr. Zheng Xue from the US National Laboratory of Lawrence Livermore visited CAMS State Key Laboratory on Severe Weather (LaSW) and delivered the presentation titled "Using Field Observations to Identify Deficiencies in the Community Atmosphere Model (CAM) Simulations of Marine Boundary Layers Clouds", in which he introduced the inter-comparison and calibration of the observation data from Azores collected by his team with that of CAM model as well as its updated version. The presentation was presided over by Dr. Xu Jing, Deputy Director of LaSW.

2016年11月9日，英国气象局Kalli Furtado博士访问气科院灾害天气国家重点实验室并做了题为"基于对流尺度模拟改进英国气象局统一模式的微物理参数化方案"的学术报告。Kalli Furtado博士介绍了英国气象局对流尺度模拟的研究现状和进展。实验室罗亚丽研究员主持了报告会。

On 9 November 2016, Dr. Kalli Furtado from UK Met Office (UKMO) visited CAMS State Key Laboratory on Severe Weather (LaSW) and delivered the presentation titled "Using Convective-Scale Simulations to Improve Microphysics Parameterization in the Met Office Unified Model", in which he introduced the current status and progress of convective scale modeling at UKMO. The presentation was presided over by Dr. Luo Yali, Researcher from LaSW.

2016年11月15日，美国强风暴实验室（NSSL）张芃菲博士应邀访问气科院灾害天气国家重点实验室，做了题为"衰减率在双线偏振雷达降水估测中的应用"的学术报告。报告会由刘黎平研究员主持，实验室科研人员以及研究生参加了报告会。

On 15 November 2016, Dr. Zhang Pengfei from US National Severe Storms Laboratory (NSSL), paid an invited visit to CAMS State Key Laboratory on Severe Weather (LaSW) and delivered the presentation tilted "Utilization of Specific Attenuation for Dual Polarimetric Radar QPE", which was presided over by Dr. Liu Liping, Researcher from LaSW. Research staff and graduate students from LaSW attended the presentation.

2016年12月23日，美国佐治亚理工学院的王劲峰博士访问气科院灾害天气国家重点实验室并做了题为"基于最大熵输出理论的地球大气能量与水分交换的模拟"的学术报告。王劲峰博士详细介绍了他发展的新的通量计算方案——最大熵输出法验证情况。气科院副院长赵平研究员主持了报告会。

On 23 December 2016, Dr. Wang Jinfeng from US Georgia Institute of Technology (GIT) visited CAMS State Key Laboratory on Severe Weather (LaSW) and delivered the presentation titled "Modeling Earth-Atmosphere Exchange of Energy and Water Using Maximum Entropy Production Theory", in which Dr. Wang gave a detailed introduction on the verification of Maximum Entropy Production Methods as his newly developed flux calculation scheme.The presentation was presided over by Prof. Zhao Ping, CAMS Vice President.

2016年12月23日，美国犹他大学大气科学系蒲朝霞教授访问气科院灾害天气国家重点实验室并做了题为"资料同化：天气与气候既独立又相互协同的科学"的学术报告。蒲朝霞教授指出资料同化是独立、合作性的天气、气候研究，并提出了"大数据"同化概念，介绍了资料同化的应用领域及优势。报告会由气科院千人计划专家张大林教授主持。

On 23 December 2016, Prof. Pu Zhaoxia from US University of Utah visited CAMS State Key Laboratory on Severe Weather (LaSW) and delivered the presentation titled "Data Assimilation: An Independent and Collaborative Science for Weather and Climate Studies", in which she pointed out that data assimilation was both independent and cooperative research in weather and climate and raised the assimilation concept of "Big Data", with an introduction of application areas and advantages of data assimilation. The presentation was presided over by Prof. Zhang Dalin, Scientist of the Chinese Government's Recruitment Program of Global Experts (known as "the Thousand Talents Plan").

2016 年出版物
Publications in 2016

作者 Author (rank)	题名 Title	出版物名/出版社 Publication name or Publisher	年，卷（期） Year, Volume (Issue)	备注 Notes
An Xingqin	Development of an adjoint model of GRAPES-CUACE and its application in tracking influential haze source areas in North China	Geoscientific Model Development	2016，9(6)	SCI
An Xingqin (2nd)	Model assessment of atmospheric pollution control schemes for critical emission regions	Atmospheric Environment	2016，124	SCI
Che Huizheng (2nd)	Analysis of the error in retrievals of aerosol optical properties from sunphotometer measurements of CARSNET due to a variety of objective factors	Atmosphere	2016，7(1)	SCI
Che Huizheng (2nd)	Investigation of the optical properties of aerosols over the coastal region at Dalian, Northeast China	Atmosphere	2016，7(8)	SCI
Che Huizheng (2nd)	Aerosol optical properties over Beijing during the World Athletics Championships and Victory Day military parade in August and September 2015	Atmosphere	2016，7(4)	SCI
Che Huizheng (2nd)	Aerosol optical properties based on ground and satellite retrievals during a serious haze episode in December 2015 over Beijing	Atmosphere	2016，7(5)	SCI
Che Huizheng (2nd)	The variation in visibility and its relationship with surface wind	Theoretical and Applied Climatology	2016，15(2)	SCI
Che Huizheng (3rd)	Spatial distribution and temporal variation of aerosol optical depth in the Sichuan Basin, China, the recent ten years	Atmospheric Environment	2016，147	SCI
Che Huizheng (3rd)	A 20-year simulated climatology of global dust aerosol deposition	Science of the Total Environment	2016，557-558	SCI
Che Huizheng, et al.	Calibration of the 936 nm water-vapor channel for the China aerosol remote sensing NETwork (CARSNET) and the effect of the retrieval water-vapor on aerosol optical property over Beijing, China	Atmospheric Pollution Research	2016，7(5)	SCI
Chen Bin, et al.	Climatology of wintertime long-distance transport of surface-layer air masses arriving urban Beijing in 2001–2012	Atmospheric Environment	2016，151	SCI
Chen Fei	Assessing uncertainties in the Noah-MP ensemble simulations of a cropland site during the Tibet Joint International Cooperation program (JICA) field campaign	Journal of Geophysical Research-Atmospheres	2016，121(16)	SCI
Chen Haoming, et al.	A new method to compare hourly rainfall between station observations and satellite products over central-eastern China	Journal of Meteorological Research	2016，30(5)	SCIE

作者 Author (rank)	题名 Title	出版物名/出版社 Publication name or Publisher	年，卷（期） Year, Volume (Issue)	备注 Notes
Chen Yang, et al.	Mechanisms for concurrent low-latitude circulation anomalies responsible for persistent extreme precipitation in the Yangtze River Valley	Climate Dynamics	2016，47(3)	SCI
Chen Yueli	Preliminary studies on the dynamic prediction method of rainfall-triggered landslide	Journal of Mountain Science	2016，13(10)	SCIE
Ding Minghu	Re-assessment of recent (2008–2013) surface mass balance over Dome Argus, Antarctica	Polar Research	DOI: 10.3402/polar.v35.26133	SCI
Ding Minghu (2nd)	A comparison of Antarctic ice sheet surface mass balance from atmospheric climate models and in situ observations	Journal of Climate	2016，29(14)	SCI
Ding Minghu (2nd)	Structure of summer atmospheric boundary layer in the center of Arctic Ocean and its relation with sea ice extent change	Science China: Earth Science	2016，59(5)	SCI
Fang Shibo (2nd)	Correlative analysis of the relationship between changes in surface solar radiation and haze pollution (atmospheric turbidity index) in Beijing from 1961 to 2011	Global NEST Journal	2016，18(1)	
Fang Shibo (2nd)	Lichen elemental composition distinguishes anthropogenic emissions from dust storm input and differs among species: Evidence from Xilinhot, Inner Mongolia, China	Scientific Reports	2016，6	SCI
Fang Shibo (3rd)	Use of the lichen *Xanthoria manchurica* in monitoring atmospheric elemental deposition in the Taihang Mountains, Hebei, China	Scientific Reports	2016，6	SCI
Fang Shibo, et al.	Changing trends and abrupt features of extreme temperature in Mainland China from 1960 to 2010	Atmosphere	2016，7(2)	SCI
Fang Shibo, et al.	Change in temperature extremes and its correlation with mean temperature in mainland China from 1960 to 2015	International Journal of Climatology	DOI: 10.1002/joc.4965	SCI
Gao Wenhua	Coupling spectral-bin cloud microphysics with the MOSAIC aerosol model in WRF-Chem: Methodology and results for marine stratocumulus clouds	Journal of Advances in Modeling Earth Systems	2016，8(3)	SCI
Gao Wenhua	A study of cloud microphysics and precipitation over the Tibetan Plateau by radar observations and cloud-resolving model simulations	Journal of Geophysical Research-Atmospheres	2016，121(13)	SCI
Guo Jianping	The diurnal cycle of $PM_{2.5}$ and its association with MODIS AOD over China: Implications for $PM_{2.5}$ remote sensing	Environmental Pollution	2016，12(1)	

作者 Author (rank)	题名 Title	出版物名/出版社 Publication name or Publisher	年，卷（期） Year, Volume (Issue)	备注 Notes
Guo Jianping (2nd)	Planetary boundary layer height from CALIOP compared to radiosonde over China	Atmospheric Chemistry and Physics	2016，16(1)	SCI
Guo Jianping (2nd)	On the influence of the diurnal variations of aerosol content to estimate direct aerosol radiative forcing using MODIS data	Atmospheric Environment	2016，141	SCI
Guo Jianping (2nd)	Delaying precipitation by air pollution over Pearl River Delta. Part 2: Model simulations	Journal of Geophysical Research-Atmospheres	2016, 121(19)	SCI
Guo Jianping (2nd)	A CloudSat perspective on the cloud climatology and its association with aerosol perturbation in the vertical over East China	Journal of the Atmospheic Sciences	2016，33(1)	SCI
Guo Jianping, et al.	The climatology of planetary boundary layer height in China derived from radiosonde and reanalysis data	Atmospheric Chemistry and Physics	2016，16(20)	SCI
Guo Jianping, et al.	Impact of various emission control schemes on air quality using WRF-Chem during APEC China 2014	Atmospheric Environment	2016，140	SCI
Guo Jianping, et al.	Three-dimensional structure of aerosol in China: A perspective from multi-satellite observations	Atmospheric Research	2016，178-179	SCI
Guo Jianping, et al.	Delaying precipitation and lightning by air pollution over the Pearl River Delta. Part I: Observational analyses	Journal of Geophysical Research-Atmospheres	2016, 121(11)	SCI
Guo Xueliang (2nd)	Mesoscale numerical simulation study of warm fog dissipation by salt particles seeding	Advances in Atmospheric Sciences	2016，33(5)	SCI
Hou Qing,et al.	Assessment of resident's exposure level and health economic costs of PM_{10} in Beijing from 2008 to 2012	Science of the Total Environment	2016，563-564	SCI
Hu Liang	The seasonal variation of Tibetan convective systems: Satellite observation	Journal of Geophysical Research-Atmospheres	2016, 121(10)	SCI
Huo Zhiguo (2nd)	Monitoring and forecasting winter wheat freeze injury and yield from multi-temporal remotely sensed data	Intelligent Automation and Soft Computing	2016，22(2)	SCI
Huo Zhiguo (2nd)	Estimating leaf SPAD values of freeze-damaged winter wheat using continuous wavelet analysis	Plant Physiology and Biochemistry	2016，98	SCI
Li Jianduo	Quantification and attribution of errors in the simulated annual gross primary production and latent heat fluxes by two global land surface models	Journal of Advances in Modeling Earth Systems	2016，8(3)	

作者 Author (rank)	题名 Title	出版物名/出版社 Publication name or Publisher	年，卷（期） Year, Volume (Issue)	备注 Notes
Li Ying(2nd)	A statistical analysis of the relationship between upper-tropospheric cold low and tropical cyclone track and intensity change over the Western North Pacific	Monthly Weather Review	2016，144(5)	SCI
Liang Linlin	Seasonal variations and source estimation of saccharides in atmospheric particulate matter in Beijing, China	Chemosphere	2016，150(1)	SCI
Liu Boqi(2nd)	The East Asian subtropical summer monsoon: Recent progress	Journal of Meteorological Research	2016，30(2)	SCIE
Liu Boqi,et al.	A possible precursor of the South China Sea summer monsoon onset: Effect of the South Asian high	Geophysical Research Letters	2016，43(20)	SCI
Liu Boqi,et al.	Two types of interannual variability of South China Sea summer monsoon onset related to the SST anomalies before and after 1993/94	Journal of Climate	2016，29(19)	SCI
Liu Ge,et al.	Effect of tropical Indian Ocean thermal condition during preceding winter on summer high temperature anomalies over the southern Yangtze River Valley	International Journal of Climatology	DOI: 10.1002/joc.4932	SCI
Liu Liping (2nd)	Toward understanding the properties of high ice clouds at Naqu site over the Tibetan Plateau using ground-based active remote sensing measurements obtained during a short period in July 2014	J. Appl. Meteor. Clim.	2016，55(5)	SCI
Liu Tao,et al.	Effects of warming and changing precipitation rates on soil respiration over two years in a desert steppe of northern China	Plant and Soil	2016，400(1)	SCI
Liu Ying,et al.	The structure and development of an extratropical cyclone over northeastern Asia	SOLA	DOI: 10.2151/sola.2016-050	SCI
Liu Yu	Skewness of cloud droplet spectrum and an improved estimation for its relative dispersion	Meteorology and Atmospheric Physics	2016，128(2)	SCI
Luo Yali(2nd)	Mesoscale observational analysis of lifting mechanism of a warm-sector convective system producing the maximal daily precipitation in China mainland during pre-summer rainy season of 2015	Journal of Meteorological Research	2016，30(5)	SCIE
Luo Yali(2nd)	Impact of assimilating wind profiling radar observations on convection-permitting quantitative precipitation forecasts during SCMREX	Weather and Forecasting	2016，31(4)	SCI
Luo Yali,et al.	Ground-based radar reflectivity mosaic of Meiyu precipitation systems over the Yangtze River-Huaihe River basins	Advances in Atmospheric Sciences	2016，33(11)	SCI

作者 Author (rank)	题名 Title	出版物名/出版社 Publication name or Publisher	年，卷（期） Year, Volume (Issue)	备注 Notes
Luo Yali,et al.	Synoptic situations of extreme hourly precipitation over China	Journal of Climate	2016，29(24)	SCI
Lü Junmei, et al.	Teleconnection patterns impacting on the summer consecutive extreme rainfall in central-eastern China	International Journal of Climatology	DOI: 10.1002/joc.4923	SCI
Lü Weitao (2nd)	High-speed video observations of the fine structure of a natural negative stepped leader at close distance	Atmospheric Research	2016，178-179	SCI
Lü Weitao (3rd)	From pixels to patches: A cloud classification method based on a bag of micro-structures	Atmospheric Measurement Techniques	2016，9(2)	SCI
Lü Weitao, et al.	Two basic leader connection scenarios observed in negative lightning attachment	High Voltage	2016，1(1)	EI
Ma Jianzhong (2nd)	MAX-DOAS measurements and satellite validation of tropospheric NO_2 and SO_2 vertical column densities at a rural site of North China	Atmospheric Environment	2016，133	SCI
Ma Ying,et al.	A vision-based precipitation sensor for detection and classification of hydrometeors	IEEE Sensors Journal	2016，16(11)	SCI
Peng Xindong (2nd)	Improvement of the Mellor-Yamada-Nakanishi-Niino planetary boundary layer scheme based on the observational data in China	Boundary-Layer Meteorology	2016，160(7)	SCI
Peng Xindong (2nd)	A wind power forecasting system based on the WRF model and Kalman filtering over a wind-farm in Japan	Journal of Renewable Sustainable Energy	2016，8(1)	SCI
Rong Xinyao (3rd)	Seasonal predictability of sea surface temperature anomalies over the Kuroshio Oyashio Extension Low in summer and High in winter	Journal of Geophysical Research: Oceans	2016，121(9)	SCI
Shen Xiaojing, et al.	Particle climatology in central East China retrieved from measurements in planetary boundary layer and in free troposphere at a 1500-m-high mountaintop site	Aerosol and Air Quality Research	2016，16	SCI
Shen Xiaojing, et al.	The influence of Asian dust outflow on particle microphysical and optical properties at Mt.Tai in central East China	Atmospheric Environment	2016，143	SCI
Shen Xiaojing, et al.	Key features of new particle formation events at background sites in China and their influence on cloud condensation nuclei	Frontier Environment Science & Engineering	2016，10(5)	SCI
Shen Xiaojing, et al.	The influence of emission control on particle number size distribution and new particle formation during China	Science of the Total Environment	2016，573	SCI
Shi Xiaohui (2nd)	Spatio-temporal characteristics of extreme precipitation events during 1951–2011 in Shandong, China and possible connection to the large scale atmospheric circulation	Stochastic Environmental Research and Risk Assessment	2016，30(5)	SCI

作者 Author (rank)	题名 Title	出版物名/出版社 Publication name or Publisher	年，卷（期） Year, Volume (Issue)	备注 Notes
Wang Donghai (2nd)	Improving numerical experiments on persistent severe rainfall events in southern China using spectral nudging and filtering schemes	Quarterly Journal of the Royal Meteorological Society	2016, 142(701)	SCI
Wang Fei,et al.	Characteristics of cloud-to-ground lightning strikes in the stratiform regions of mesoscale convective systems	Atmospheric Research	2016, 178-179	SCI
Wang Gaili	Evaluation and correction of quantitative precipitation forecast by storm-scale NWP model in Jiangsu, China	Advances in Meteorology	2016, 1-13	SCI
Wang Gaili	A quantitative comparison of precipitation forecasts between the storm-scale numerical weather prediction model and auto-nowcast system in Jiangsu, China	Atmospheric Research	2016, 181	SCI
Wang Hong (2nd)	The impacts of different PBL schemes on the simulation of $PM_{2.5}$ during severe haze episodes in the Jing-Jin-Ji region and its surroundings in China	Advances in Meteorology	2016, 1-15	SCI
Wang Peijuan (3rd)	Influences of leaf-specular reflection on canopy BRF characteristics: A case study of real maize canopies with a 3-D scene BRDF model	IEEE Transactions on Geoscience and Remote Sensing	DOI: 10.1109/TGRS.2016.2598442	
Wang Ping, et al.	Inverse modeling of black carbon emissions over China using ensemble data assimilation	Atmospheric Chemistry and Physics	2016, 16(2)	SCI
Wang Ping, et al.	"APEC Blue" association with emission control and meteorological conditions detected by multi-scale statistics	Atmospheric Research	2016, 178-179	SCI
Wang Yaqiang (2nd)	Outlier flag: A tool for scientific data quality control by outlier data flagging	Journal of Open Research Software	2016, 4(1)	
Wang Yaqiang (3rd)	Regional prediction of carbon isotopes in soil carbonates for Asian dust source tracer	Atmospheric Environment	2016, 142	SCI
Wang Zhili (2nd)	Sensitivity of precipitation extremes to radiative forcing of greenhouse gases and aerosols	Geophysical Research Letters	2016, 43(18)	SCI
Wang Zhili (3rd)	A modeling study of effective radiative forcing and climate response due to tropospheric ozone	Advances in Atmospheric Sciences	2016, 33(7)	SCI
Wang Zhili (3rd)	The updated effective radiative forcing of major anthropogenic aerosols and their effects on global climate at present and in the future	International Journal of Climatology	2016, 36(12)	SCI
Wang Zhili, et al.	Projected response of East Asian summer monsoon system to future reductions in emissions of anthropogenic aerosols and their precursors	Climate Dynamics	2016, 47(5)	SCI
Wang Zhili, et al.	The effect of future reduction in aerosol emissions on climate extremes in China	Climate Dynamics	2016, 47(9)	SCI

作者 Author (rank)	题名 Title	出版物名/出版社 Publication name or Publisher	年，卷（期） Year, Volume (Issue)	备注 Notes
Wei Ting	Developed and developing world contributions to climate system change based on CO_2, CH_4 and N_2O emissions	Advances in Atmospheric Sciences	2016，33(5)	SCI
Wei Ting	Quantitative estimation of the climatic effects of carbon transferred by international trade	Scientific Reports	2016，6	SCI
Wei Ting (2nd)	Variations in large-scale tropical cyclone genesis factors over the western North Pacific in the PMIP3 last millennium simulations	Climate Dynamics	2016，47(1)	SCI
Wei Ting (2nd)	A new consumption-based accounting model for greenhouse gases from 1948 to 2012	Journal of Cleaner Production	2016，133(1)	SCI
Wei Ting (2nd)	Enhanced intensity of global tropical cyclones during the mid-Pliocene warm period	PNAS	2016，113(46)	SCI
Wei Ting, et al.	Variations in temperature-related extreme events (1975–2014) in NY-Ålesund, Svalbard	Atmospheric Science Letters	2016，17(1)	SCI
Wu Bingyi, et al.	Summer Arctic dipole wind pattern affects the winter Siberian high	International Journal of Climatology	2016，36(2)	SCI
Wu Lingyan	Mechanism and kinetics of heterogeneous reactions of unsaturated organic acids on α-Al_2O_3 and $CaCO_3$	ChemPhysChem	2016，17(21)	
Wu Lingyan (3rd)	Temperature dependence of the heterogeneous uptake of acrylic acid on Arizona test dust	Journal of Environmental Sciences	2016，7(12)	
Xiao Dong, et al.	Responses of the summer Asian-Pacific zonal thermal contrast and the associated evolution of atmospheric circulation to transient orbital changes during the Holocene	Scientific Reports	2016，6	SCI
Xu Jing(2nd)	Bayesian geoadditive modelling of climate extremes with nonparametric spatially varying temporal effects	International Journal of Climatology	2016，36(12)	SCI
Xu Jing, et al.	The relationship between sea surface temperature and maximum intensification rate of tropical cyclones in the North Atlantic	Journal of the Atmospheric Sciences	2016，73(12)	SCI
Xu Liangtao, et al.	The role of dynamic transport in the formation of the inverted charge structure in a simulated hailstorm	Science China: Earth Science	2016，59(7)	SCI
Xu Wanyun, et al.	Long-term trends of surface ozone and its influencing factors at the Mt. Waliguan GAW station, China—Part 1: Overall trends and characteristics	Atmospheric Chemistry and Physics	2016，16(10)	SCI
Xu Xiangde (2nd)	The upstream "Strong Signals" of the water vapor transport over the Tibetan Plateau during a heavy rainfall event in the Yangtze River Basin	Advances in Atmospheric Sciences	2016，33(1)	SCI

作者 Author (rank)	题名 Title	出版物名/出版社 Publication name or Publisher	年，卷（期） Year, Volume (Issue)	备注 Notes
Xu Xiangde (2nd)	Extreme precipitation events in East China and associated moisture transport pathways	Science China: Earth Science	2016，59(9)	SCI
Xu Xiaobin (3rd)	Vertical profiles of black carbon measured by a micro-aethalometer in summer in the North China Plain	Atmospheric Chemistry and Physics	2016，16(8)	SCI
Yang Jianying, et al.	Indicator-based evaluation of spatio-temporal characteristics of rice flood in Southwest China	Agriculture, Ecosystems and Environment	2016，230	
Yang Jun, et al.	A total sky cloud detection method using real clear sky background	Atmospheric Measurement Techniques	2016，9	SCI
Yang Yuanqin, et al.	PLAM—a meteorological pollution index for air quality and its applications in fog-haze forecasts in North China	Atmospheric Chemistry and Physics	2016，16(1)	SCI
Zhai Panmao (3rd)	Impact of urban land-use change in eastern China on the East Asian subtropical monsoon: A numerical study	Journal of Meteorological Research	2016，30(2)	SCI
Zhai Panmao, et al.	The strong El Niño in 2015/2016 and its dominant impacts on global and China	Journal of Meteorological Research	2016，30(3)	SCI
Zhang Guo, et al.	Assessing uncertainties in the Noah-MP ensemble simulations of a cropland site during the Tibet Joint International Cooperation program (JICA) field campaign: Uncertainty in Noah-MP simulations	Journal of Geophysical Research-Atmospheres	2016，121(16)	SCI
Zhang Renhe (2nd)	Interannual variation of the wintertime fog-haze days across central and eastern China and its relation with East Asian winter monsoon	International Journal of Climatology	2016，36(1)	SCI
Zhang Renhe (2nd)	The relationship between soil moisture and LAI in different types of soil in central eastern China	Journal of Hydrometeorology	2016，17(11)	SCI
Zhang Ruonan, et al.	Climatology and interannual variability of the wintertime snow cover over China	International Journal of Climatology	DOI: 10.1002/joc.4599	
Zhang Shengjun (2nd)	A study on the mechanism of rapid weakening of typhoon Xangsane (0020) over the East China Sea	Journal of Tropical Meteorology	2016，22(3)	SCIE
Zhang Tong, et al.	Temperate ice layer found in the upper area of Jima Yangzong Glacier, the headstream of Yarlung Zangbo River	Science Bulletin	2016，61(8)	SCI
Zhang Xiaoye (2nd)	Characterization and parameterization of aerosol cloud condensation nuclei activation under different pollution conditions	Scientific Reports	2016，6	SCI
Zhang Yang, et al.	Simultaneous optical and electrical observations of "chaotic" leaders preceding subsequent return strokes	Atmospheric Research	2016，170	SCI

作者 Author (rank)	题名 Title	出版物名/出版社 Publication name or Publisher	年，卷（期） Year, Volume (Issue)	备注 Notes
Zhang Yang, et al.	Characteristics and correlation of return stroke, M component and continuing current for triggered lightning	Electric Power System Research	2016，139	SCI
Zhang Yangmei(2nd)	Characterization of particle number size distribution and new particle formation in an urban environment in Lanzhou, China	Journal of Aerosol and Science	2016，103(1)	SCI
Zhang Yi,et al.	Impact of moisture divergence on systematic errors in precipitation around the Tibetan Plateau in a general circulation model	Climate Dynamics	2016，47(9)	SCI
Zhang Yi,et al.	Comparing CAM5 and superparameterized CAM5 simulations of summer precipitation characteristics over continental East Asia: Mean state, frequency-intensity relationship, diurnal cycle, and influencing factors	Journal of Climate	2016，29(3)	SCI
Zhang Yi,et al.	Using statistical model to simulate the impact of climate change on maize yield with climate and crop uncertainties	Theoretical and Applied Climatology	DOI: 10.1007/s00704-016-1935-2	SCI
Zhang Yijun (2nd)	Influence of the ground potential rise on the residual voltage of low-voltage surge protective devices due to nearby lightning flashes	IEEE Transactions on Power Delivery	2016，31(2)	SCI
Zhang Yijun, et al.	A review of advances in lightning observations during the past decade in Guangdong, China	Journal of Meteorological Research	2016，30(5)	SCI
Zhao Junfang (3rd)	Study on spring wheat yield change of Inner Mongolia in time and space based on APSIM model	ICADME	DOI: 10.2991/icadme-16.2016.79	EI
Zhao Junfang (3rd)	Potato plant image detection based on deep learning	ICADME	DOI: 10.2991/icadme-16.2016.74	EI
Zhao Junfang, et al.	Coincidence of variation in potato yield and climate in northern China	Science of the Total Environment	2016，573	SCI
Zhao Junfang, et al.	Drought monitoring based on TIGGE and distributed hydrological model in Huaihe River Basin, China	Science of the Total Environment	2016，553	SCI
Zhao Ping (3rd)	Relative roles of land- and ocean-atmosphere interactions in Asian-Pacific thermal contrast variability at the precessional band	Scientific Reports	2016，6	SCI
Zhao Ping, et al.	Summer precipitation anomalies in Asia and North America induced by Eurasian non-monsoon land heating versus ENSO	Scientific Reports	2016，6	SCI
Zheng Dong	Characteristics of flash initiations in a supercell cluster with tornadoes	Atmospheric Research	2016，167	SCI
Zheng Dong (2nd)	Characteristics of the two active stages of lightning activity in two hailstorms	Journal of Meteorological Research	2016，30(2)	SCIE

作者 Author (rank)	题名 Title	出版物名/出版社 Publication name or Publisher	年，卷（期） Year, Volume (Issue)	备注 Notes
Zheng Dong, et al.	Climatology of lightning activity in South China and its relationships to precipitation and convective available potential energy	Advances in Atmospheric Sciences	2016，33(3)	SCI
Zheng Dong, et al.	Climatological comparison of small- and large-current cloud-to-ground lightning flashes over southern China	Journal of Climate	2016，29(8)	SCI
Zheng Xiangdong (3rd)	Validation of Aura MLS retrievals of temperature, water vapour and ozone in the upper troposphere and lower-middle stratosphere over the Tibetan Plateau during boreal summer	Atmospheric Measurement Techniques	2016，9(8)	SCI
Zhong Lingzhi, et al.	Application of the Doppler weather radar in real-time quality control of hourly gauge precipitation in eastern China	Atmospheric Research	2016，172-173	SCI
Zhou Chunhong, et al.	Improving aerosol interaction with clouds and precipitation in a regional chemical weather modeling system	Atmospheric Chemistry and Physics	2016，16(1)	SCI
Zhou Guangsheng (2nd)	Climate-associated distribution of summer maize in China from 1961 to 2010	Agriculture, Ecosystems and Environment	2016，232	
Zhou Guangsheng (2nd)	Possible impact of climate change on the quality of apples from the major producing areas of China	Atmosphere	2016，7(9)	SCI
Zhou Guangsheng (2nd)	Forest litterfall and its composition: A new dataset of observational data from China	Ecology	2016，97(5)	SCI
Zhou Guangsheng (2nd)	Does precipitation mediate the effects of elevated CO_2 on plant growth in the grass species Stipagrandis?	Environmental and Experimental Botany	2016，131	
Zhou Guangsheng (2nd)	Detection of photosynthetic performance of Stipabungeana seedlings under climatic change using chlorophyll fluorescence imaging	Frontiers in Plant Science	2016，6	
Zhou Guangsheng (2nd)	Sensitive indicators of zonal Stipa species to changing temperature and precipitation in Inner Mongolia grassland, China	Frontiers in Plant Science	2016，7	
Zhou Guangsheng (2nd)	Effects of changing precipitation and warming on functional traits of zonal Stipa plants from Inner Mongolian grassland	Journal of Meteorological Research	2016，30(3)	SCIE
Zhou Guangsheng (2nd)	Spatio-temporal dynamic simulation of grassland carbon storage in China	Science China: Earth Science	2016，59(10)	SCI
Zhou Guangsheng (2nd)	A self- photoprotection mechanism helps Stipa baicalensis adapt to future climate change	Scientific Reports	2016，6	SCI

作者 Author (rank)	题名 Title	出版物名/出版社 Publication name or Publisher	年，卷（期） Year, Volume (Issue)	备注 Notes
Zhou Guangsheng (2nd)	Elevated CO_2 can modify the response to a water status gradient in a steppe grass: From cell organelles to photosynthetic capacity to plant growth	BMC Plant Biology	2016，16(1)	
Zhou Guangsheng (2nd)	Nitrogen cycles in terrestrial ecosystems: Climate change impacts and mitigation	Environmental Reviews	2016，24(2)	
Zhou Haiguang	Wind structure of a subtropical squall line in China: Results from Dual-Doppler radar data	Advances in Meteorology	2016，18	SCI
Zhu Congwen (2nd)	Discrepancies in boreal summer monsoon rainfall between GPCP and CMAP products during 1979–2014	Atmospheric and Oceanic Science Letters	2016，9(3)	
Zhu Congwen (2nd)	The cooperative impacts of the El Niño-Southern Oscillation and the Indian Ocean Dipole on the interannual variability of autumn rainfall in China	International Journal of Climatology	2016，36(4)	SCI
Zhu Congwen (2nd)	Coupling modes of climatological intraseasonal oscillation in the East Asian summer monsoon	Journal of Climate	2016，29(17)	SCI
Zhu Congwen (3rd)	A novel way to detect correlations on multi-time scales, with temporal evolution and for multi-variables	Scientific Reports	2016，6	SCI
Zuo Zhiyan (2nd)	Prediction skill and predictability of Eurasian snow cover fraction in the NCEP climate forecast version 2 reforecasts	International Journal of Climatology	2016，36(12)	SCI
Zuo Zhiyan (3rd)	Contributions of anthropogenic and external natural forcings to climate changes over China based on CMIP5 model simulations	Science China: Earth Science	2016，59(3)	SCI
Zuo Zhiyan, et al.	Influence of soil moisture in eastern China on East Asian summer monsoon	Advances in Atmospheric Sciences	2016，33(2)	SCI

作者 Author (rank)	题名 Title	出版物名/出版社 Publication name or Publisher	年，卷（期） Year, Volume (Issue)	备注 Notes
安兴琴（第 2）	北京地区颗粒物健康效应研究——沙尘天气、非沙尘天气下颗粒物（$PM_{2.5}$、PM_{10}）对心血管疾病入院人次的影响	中国环境科学	2016，36（8）	EI
蔡淼（第 2）	一次浅对流云人工消云试验的飞机和卫星观测研究	科技与创新	2016，6（6）	
车慧正（第 2）	2010—2012 年我国西北地区沙尘个例气溶胶特征分析	气象与环境科学	2016，39（2）	
陈斌	拉格朗日水汽源诊断方法在三江源区的应用	应用气象学报	2016，27（6）	
陈悦丽	降雨型滑坡的集合预报模型及其初步应用的试验研究	大气科学	2016，40（3）	
程巴阳等	本底站和城区站 CO 浓度变化特征和源贡献	中国环境科学	2016，36（10）	EI
程兴宏	基于 CMAQ 模式和自适应偏最小二乘回归法的中国地区 $PM_{2.5}$ 浓度动力–统计预报方法研究	环境科学学报	2016，36（8）	
程兴宏	2013 年 1 月华北地区重霾污染过程 SO_2 和 NO_x 的 CMAQ 源同化模拟研究	环境科学学报	2016，36（2）	
程兴宏（第 2）	太阳辐射预报滚动订正方法研究	气象科技	2016，44（1）	
党娟等	一次降水性层积云系的微物理特征分析	高原气象	2016，35（6）	
党娟等	三七炮弹碘化银成核率的检测	应用气象学报	2016，27（2）	
端义宏（第 2）	超强台风"威马逊"（2014）云微物理特征的模拟与对比分析	气象学报	2016，74（5）	
俄有浩等	长江中下游地区暴雨特征及洪涝淹没风险分析	生态学杂志	2016，35（4）	
房世波（第 2）	农业干旱遥感监测指数及其适用性研究进展	科技导报	2016，34（5）	
房世波（第 2）	NDVI 与气候因子关系在不同时间尺度上的结果差异	遥感学报	2016，20（3）	
房世波（第 2）	中国卫星遥感气溶胶研究进展	能源环境保护	2016，30（1）	
郭建平	农业气象灾害监测预测技术研究进展	应用气象学报	2016，27（5）	
郭建平（第 2）	基于江西地区多卫星数据的气溶胶立体分布研究	大气与环境光学学报	2016，11（5）	
郭建平（第 2）	西藏改则地区雨季上对流层／下平流层大气垂直结构观测研究	气象学报	2016，74（5）	
郭建平（第 2）	全球热带海洋地区降水季节变化的 TRMM 卫星观测研究	科学通报	2016，61（1）	SCI
郭建平（第 2）	我国东北地区玉米冷害风险评估	应用气象学报	2016，27（3）	
郭建平（第 2）	不同积温模型的稳定性评估——以东北春玉米为例	生态学杂志	2016，35（10）	

作者 Author (rank)	题名 Title	出版物名/出版社 Publication name or Publisher	年，卷（期） Year, Volume (Issue)	备注 Notes
郭建平等	2001—2012 年青藏高原积雪覆盖率变化及地形影响	高原气象	2016，35（1）	
郭学良（第2）	北京 2009—2013 年期间持续性大雾的类型、垂直结构及物理成因	大气科学	2016，40（2）	
郭学良（第2）	南海季风区冰相相变潜热对中尺度对流云和降水影响作用的数值模拟研究	气候与环境研究	2016，21（6）	
郭学良（第2）	辽宁地区不同降水云系雨滴谱参数及其特征量研究	大气科学	2016，40（6）	
郭学良（第2）	我国冰粒降水天气的观测特征统计分析	大气科学学报	2016，39（3）	
郭学良（第2）	青藏高原那曲地区夏季对流云结构及雨滴谱分布日变化特征	科学通报	2016，61（15）	SCI
何建军	气象条件和污染物排放对兰州市冬季空气质量的影响	高原气象	2016，35（6）	
胡志群（第2）	C 波段偏振雷达数据预处理及在降水估计中的应用	高原气象	2016，35（1）	
霍治国（第2）	鲜食玉米形态特征、生理特性及产量对淹水的响应	玉米科学	2016，24（3）	
霍治国（第2）	早稻灌浆期淹水对剑叶理化特性及产量和品质的影响	中国水稻科学	2016，30（2）	
霍治国（第2）	基于生育时段的湖南省早稻洪涝等级指标及时空变化特征	生态学杂志	2016，35（3）	
霍治国（第2）	南方双季稻低温灾害等级预测	生态学杂志	2016，35（4）	
霍治国（第2）	基于 Fisher 判别的南方双季稻低温灾害等级预警	应用气象学报	2016，27（4）	
霍治国（第2）	气候变暖背景下南方早稻春季低温灾害的发生趋势与风险	生态学报	2016，36（5）	
霍治国（第2）	海南番茄春季干旱灾害等级指标	热带气象学报	2016，32（5）	
汲玉河	安徽省森林碳储量现状及固碳潜力	植物生态学报	2016，40（4）	
李建（第2）	青藏高原东南缘低层风场垂直结构与变化特征	高原气象	2016，35（3）	
李英（第2）	初夏孟加拉湾风暴活动期间青藏高原大气环流的异常特征	热带气象学报	2016，32（4）	
李英（第2）	台湾地形诱生中尺度系统对台风 Meranti（1010）迅速加强影响的数值研究	大气科学	2016，40（6）	
刘伯奇（第2）	非绝热加热对 6 月东北冷涡形成演变的影响及其可能机制	气象与环境学报	2016，32（6）	

作者 Author (rank)	题名 Title	出版物名/出版社 Publication name or Publisher	年，卷（期） Year, Volume (Issue)	备注 Notes
刘伯奇（第2）	当前重大厄尔尼诺事件对我国春夏气候的影响	中国科学院院刊	2016，2（1）	
刘舸（第2）	2013 年我国南方持续性高温天气及副热带高压	大气科学	2016，40（5）	
刘恒毅等	闪电起始过程时空特征的宽带干涉仪三维观测	应用气象学报	2016，27（1）	
刘黎平	垂直指向的 Ka 波段云雷达观测的 0 ℃层亮带自动识别及亮带的特征分析	高原气象	2016，35（3）	
刘黎平（第2）	多部 X 波段天气雷达测量偏差分布及组网拼图结果分析	高原气象	2016，35（3）	
刘黎平（第2）	云雷达联合微波辐射计反演混合性降水层云液态水含量的方法研究	暴雨灾害	2016，35（1）	
刘黎平（第2）	雨滴谱仪网数据在雷达定量降水估测中的应用	暴雨灾害	2016，35（2）	
刘黎平（第2）	雨滴谱的变化对降水估测的影响研究	高原气象	2016，35（1）	
刘涛等	华北地区冬小麦灌溉制度及其环境效应研究进展	生态学报	2016，36（19）	
刘卫国等	2014 年春季华北两次降水过程的人工增雨催化数值模拟研究	大气科学	2016，40（4）	
刘煜（第3）	青藏高原沙漠化对东亚沙尘气溶胶的敏感性模拟分析	高原气象	2016，35（3）	
楼小凤	气溶胶对北京地区云和降水影响的模拟研究	地理研究	2016，35（10）	
楼小凤等	一次降雹过程的系列催化模拟研究	应用气象学报	2016，27（2）	
罗亚丽（第2）	不同边界层参数化方案和陆面过程参数化方案对一次梅雨锋暴雨显式对流模拟的影响分析	热带气象学报	2016，32（5）	
吕伟涛（第2）	基于线支持区域的闪电通道识别算法	应用气象学报	2016，27（6）	
吕伟涛（第2）	基于闪电先导随机模式对不同连接形态的模拟	应用气象学报	2016，27（3）	
马建中（第2）	华北平原固城站 NO_2 对流层柱浓度变化特征	应用气象学报	2016，27（3）	
马玉平（第3）	气候变化和人类活动对三江源地区植被生产力的影响	冰川冻土	2016，38（3）	
马玉平等	黄淮海地区夏玉米对干旱和涝渍的生理生态反应	干旱地区农业研究	2016，34（4）	
毛飞等	1961—2010 年中国 Ångström-Prescott 系数时空变化特征	气象与环境科学	2016，39（1）	

作者 Author (rank)	题名 Title	出版物名/出版社 Publication name or Publisher	年，卷（期） Year, Volume (Issue)	备注 Notes
南素兰（第2）	中国季风区大气降水同位素的季节尺度环流效应	第四纪研究	2016，36（3）	
牛涛	华北地区雾和霾天气环流特征聚类分析	气候与环境研究	2016，21（5）	
牛涛	大气相对湿度资料融合及融合湿度精度检验——基于 2013 年 1 月我国中东部地区卫星和探空相对湿度数据	气候与环境研究	2016，21（1）	
齐艳军等	1998 年夏季长江流域大气季节内振荡的结构演变及其对降水的影响	大气科学	2016，40（3）	
任福民（第2）	超强台风"丹娜丝"对 1323 号强台风"菲特"极端降水的作用	气象	2016，42（2）	
任福民（第2）	CMIP5 模式集合对中国区域性低温事件的模拟与预估	气候变化研究进展	2016，12（5）	
任福民（第3）	1980—2014 年中国台风大风和台风极端大风的变化	气候变化研究进展	2016，12（5）	
任福民（第3）	孟加拉湾和阿拉伯海热带气旋活动双峰型差异及可能成因	热带气象学报	2016，32（3）	
阮征（第2）	雨滴谱仪与风廓线雷达反射率对比试验	气象	2016，42（1）	
阮征（第2）	垂直探测雷达对北京地区夏季降水分类统计	高原气象	2016，35（3）	
阮征（第2）	FMCW 技术在气象雷达中的应用及青藏高原云探测	现代雷达	2016，38（3）	
阮征（第2）	风的空间不均匀分布对风廓线雷达数据质量影响研究	热带气象学报	2016，32（2）	
阮征（第2）	C-FMCW 雷达对江淮降水云零度层亮带探测研究	应用气象学报	2016，27（3）	
阮征（第2）	风廓线雷达数据质量影响因子及处理算法	应用气象学报	2016，27（2）	
阮征（第2）	激光雨滴谱仪测速误差对雨滴谱分布的影响	应用气象学报	2016，27（1）	
沈小静等	北极黄河站秋季气团传输影响下大气气溶胶数谱分布特征	冰川冻土	2016，38（3）	
苏京志等	全球变暖趋缓研究进展	大气科学	2016，40（6）	
孙俊英等	大气气溶胶散射吸湿增长特性研究进展	气象学报	2016，74（5）	
王东海（第2）	秦巴山区云垂直结构分析	成都信息工程大学学报	2016，31（5）	
王东海（第2）	卫星微波观测资料在混合同化中的应用	气象与环境科学	2016，39（3）	
王东海（第2）	FY2E 辐射资料的直接同化试验研究	热带海洋学报	2016，32（3）	

作者 Author (rank)	题名 Title	出版物名/出版社 Publication name or Publisher	年，卷（期） Year, Volume (Issue)	备注 Notes
王东海（第2）	粒子下落末速度和粒子谱形参数对降水模拟影响的数值研究	大气科学	2016，40（4）	
王东海（第2）	夏季风爆发前后中国区域对流层顶高度变化特征	应用气象学报	2016，27（4）	
王飞等	上升运动核心区与霰粒子非感应起电区关系的模拟研究	高原气象	2016，35（3）	
王红艳（第2）	三维变分方法反演风场的效果检验	高原气象	2016，35（4）	
王红艳等	新一代天气雷达降水估算的区域覆盖能力评估	高原气象	2016，35（6）	
王宏（第2）	山东一次 $PM_{2.5}$ 污染过程的模拟特征	气候与环境研究	2016，21（3）	
王瑛	华北地区不同类型站点挥发性有机物的光化学臭氧生成潜势研究	中国科技成果	2016，17（23）	
王瑛（第2）	华北农村夏季大气甲醛浓度变化特征	环境科学研究	2016，29（8）	
王郁（第2）	大气环境容量系数 A 值频率曲线拟合及其应用	中国环境科学	2016，36（10）	EI
温敏（第2）	两次引发辽宁暴雪过程低涡的动力发展机制	气象	2016，42（4）	
邬定荣（第2）	华北平原冬小麦主要发育阶段日数对温度的敏感性分析	中国农业气象	2016，37（4）	
吴玲燕	大气二次有机气溶胶非均相反应过程模拟	中国科技成果	2016，17（15）	
武炳义等	从 2011/2012 和 2015/2016 年冬季大气环流异常看北极海冰以及前期夏季北极大气环流异常的作用	气象学报	2016，74（5）	
徐良韬等	台风莫拉菲（2009）登陆前后电荷结构演变的模拟研究	气象学报	2016，74（6）	
徐祥德（第2）	中国东部夏季暴雨极端事件与水汽输送相关流型特征	中国科学：地球科学	2016，46（8）	
徐祥德（第2）	应用谱逼近方法模拟 2008 年初南方持续性降水过程及其水汽通道周期特征分析	大气科学	2016，40（3）	
徐祥德（第3）	风云静止卫星资料在一次暴雨云分析中的应用	热带气象学报	2016，32（1）	
徐晓斌	中国霾和光化学污染观测研究进展	应用气象学报	2016，27（5）	
杨建莹等	西南地区水稻洪涝灾害风险评估与区划	中国农业气象	2016，37（5）	
姚文清（第3）	基于南海夏季风季节内振荡的降水延伸期预报试验	应用气象学报	2016，27（3）	
姚展予（第2）	一次火箭人工增雨作业雷达回波响应探讨	气象科技	2016，44（6）	

作者 Author (rank)	题名 Title	出版物名/出版社 Publication name or Publisher	年，卷（期） Year, Volume (Issue)	备注 Notes
姚展予（第2）	一次飑线过程的雨滴谱特征研究	气象学报	2016，74（3）	
姚展予（第2）	江淮对流云人工增雨作业效果检验个例分析	气象	2016，42（2）	
尹金方（第3）	双线偏振雷达资料在数值模式中的应用：模拟器的构建	气象学报	2016，74（2）	
宇如聪等	中国大陆日降水峰值时间位相的区域特征分析	气象学报	2016，74（1）	
翟盘茂等	江淮流域持续性极端降水及预报方法研究进展	应用气象学报	2016，27（5）	
张果等	东亚区域陆面过程方案 Noah 和 Noah-MP 的比较评估	气象	2016，42（9）	
张人禾等	中国冬季积雪特征及欧亚大陆积雪对中国气候影响	应用气象学报	2016，27（5）	
张人禾等	中国土壤湿度的变异及其对中国气候的影响	自然杂志	2016，38（5）	
张阳（第2）	人工触发闪电先驱电流脉冲波形特征及模拟	应用气象学报	2016，27（6）	
张义军等	雷暴闪电放电活动对电离层影响的研究进展	应用气象学报	2016，27（5）	
张义军等	广东野外雷电综合观测试验十年进展	气象学报	2016，74（5）	
赵俊芳（第2）	我国"镰刀弯"地区春玉米种植的气候适宜性与调整建议	应用生态学报	2016，27（12）	
赵俊芳等	华南地区龙眼寒害灾损风险评估	应用生态学报	2016，27（2）	
赵艳霞（第2）	五个常见日太阳总辐射模型在华北地区的有效性验证及分析	中国农业气象	2016，37（5）	
郑栋（第2）	北京和广州地区云闪初始击穿电场变化特征	气象与环境科学	2016，39（3）	
郑栋（第2）	青藏高原闪电和降水气候特征及时空对应关系	应用气象学报	2016，27（4）	
周广胜（第2）	1961—2013 年东北三省玉米低温冷害强度的时空分布特征	气象科学	2016，36（14）	
周广胜（第2）	中国富士苹果种植的气候适宜性研究	气象学报	2016，74（3）	
周广胜（第2）	1961—2010 年内蒙古草原植被分布和生产力变化	生态学报	2016，36（15）	
周广胜（第2）	基于地面遥感信息与气温的夏玉米土壤水分估算方法	应用生态学报	2016，27（6）	
周广胜（第2）	基于光合产物动态分配的玉米生物量模拟	应用生态学报	2016，27（7）	
周广胜（第2）	1961—2013 年东北三省玉米低温冷害频率的时空动态研究	气象学报	2016，74（3）	

作者 Author (rank)	题名 Title	出版物名/出版社 Publication name or Publisher	年，卷（期） Year, Volume (Issue)	备注 Notes
周广胜（第2）	中国草地碳储量时空动态模拟研究	中国科学：地球科学	2016，10	
周广胜（第2）	中国天然林凋落物量的空间分布及其影响因子分析	中国科学：生命科学	2016，11	
周广胜（第2）	中国橡胶种植北界	生态学报	2016，36(5)	
周广胜（第3）	内蒙古草原火的时空动态特征研究	草业学报	2016，25(4)	
周广胜等	城市内涝防治需充分预估气候变化的影响	生态学报	2016，36(16)	
周广胜等	适应气候变化的国际行动和农业措施研究进展	应用气象学报	2016，27(5)	
周莉（第2）	盘锦芦苇沼泽的土壤冻融特征	湿地科学	2016，14(3)	
周凌晞（第2）	北京上甸子站大气 CO_2 及 $\delta^{13}C$（CO_2）本底浓度观测研究	环境科学	2016，37(4)	